Preparation, Characterization and Applications of Kaolin Based Low Cost Ceramic Membranes

Thesis submitted in partial fulfillment of the requirements for the degree of

DOCTOR OF PHILOSOPHY

by

D. Vasanth

Department of Chemical Engineering
Indian Institute of Technology Guwahati
Guwahati - 781039, India

PREPARATION, CHARACTERIZATION AND APPLICATIONS OF KAOLIN BASED LOW COST CERAMIC MEMBRANES

Vasanth Dhakshinamoorthy

Preparation, Characterization and Applications of Kaolin Based Low Cost Ceramic Membranes

Thesis submitted in partial fulfillment of the requirements for the degree of

DOCTOR OF PHILOSOPHY

by

D. Vasanth
Roll No.: 09610715

Department of Chemical Engineering
Indian Institute of Technology Guwahati
Guwahati - 781039, India

March, 2014

Dedicated To

V. Dhakshinamoorthy

Department of Chemical Engineering
Indian Institute of Technology Guwahati
Guwahati - 781039, India

CERTIFICATE

This is to certify that the thesis entitled **"Preparation, Characterization and Applications of Kaolin Based Low Cost Ceramic Membranes"** being submitted by ***D. Vasanth*** for the award of PhD degree has been carried out under our guidance and supervision. The work documented in this thesis has not been submitted to any other University or Institute for the award of any degree or diploma.

(Dr. G. Pugazhenthi)
Associate Professor
Department of Chemical Engineering
Indian Institute of Technology Guwahati
Guwahati - 781039, India.

(Dr. Ramgopal V. S. Uppaluri)
Professor
Department of Chemical Engineering
Indian Institute of Technology Guwahati
Guwahati - 781039, India.

Acknowledgements

Doing an experimental Ph.D. requires significant help from several people, without whose contributions it would be very difficult to carry out the necessary tasks. I am highly thankful to several people who have helped me in different ways for the completion of my research work.

First, I wish to express my sincere and heartfelt thanks to **Dr. G. Pugazhenthi** and **Prof. Ramagopal V. S. Uppaluri**, for providing me continuous inspiration and guidance throughout the entire course of work I am highly indebted to both of them for providing me suggestions, constructive inspiration and constant encouragement throughout the tenure of the thesis. **Dr. G. Pugazhenthi** enabled me to develop thoughts for meticulous research planning and execution of the research work. It has been a great privilege to work with him and I sincerely appreciate his flexibility and openness to deal with specific issues of my research work. Through him I have learnt how to write a journal article and improve its quality, which have substantially contributed to the writing of my Ph.D. thesis. I would like to also thank him for his patience and amicable nature. I am highly grateful to **Prof. R. Uppaluri** for his continuous support and interesting discussions that encouraged me to have the freedom to focus upon specific issues. The numerous brain storming sessions during the project meetings with him were very useful in enriching my analytical power. I have received significant support from **Prof. R. Uppaluri** for the grammatical corrections of my Ph.D. thesis and I will also try to acknowledge for the time management skills I have learnt from Prof. R. Uppaluri with respect to technical, communication and writing skills. All in all, it is an enriching experience for improving my communication and writing skills under his able guidance.

Second, I sincerely thank my doctoral committee members **Dr. Mahuya De, Dr. Chandan Das**, Department of Chemical Engineering, and **Dr. K. Pakshirajan,** Department of Biotechnology. Their constructive and coherent suggestions have contributed enormously to enhance the quality of my research.

Third, I express my heartfelt thanks to faculty members of the Department of Chemical Engineering for their kind cooperation during my stay in the department. I am also thankful to all present and ex-staff members and scientific officers of the Chemical Engineering Department for their genuine help during my entire research period.

I am thankful to the **Central Instruments Facility** of IIT Guwahati for allowing me to carry out **Scanning Electron Microscopy** analysis on my own**,** which has been very important in this research work. In this regard, I should acknowledge the help provided by **Mr. Kula Kamal Senapati**, Scientific Officer, Central Instruments Facility, IIT Guwahati. He taught me how to use the SEM instruments, and take images at various critical conditions of the sample. I am also thankful to the **Central Workshop** of IIT Guwahati for providing me the experimental setup facilities which was very much essential in my research work.

Special thanks to **Mr. Kanchapogu Suresh and Mr. Emani Sriharsha** for their help and co-operation in my research work. I was fortunate enough to get excellent lab mates like, **Kellothu Suresh**, **Manish Kamal, Ashim Kumar Basumatary** and **Vinoth Kumar** for their friendly support and timely assistance whenever needed.

Vasanth Dhakshinamoorthy

Abstract

Compared to polymeric membranes, ceramic membranes have excellent combinations of mechanical, chemical and thermal stability, longer shelf life, good cleaning/defouling properties and capability to withstand against organic solvents. Amongst various types of ceramic membranes, kaolin based ceramic membranes are promising due to their lower raw material and sintering costs. Several applications exist for ceramic membrane technology and in these the wastewater treatment application is highly relevant as it has the potential to encourage the industrial and economic competitiveness of kaolin based low cost ceramic membranes.

This work addresses the preparation, characterization and application of kaolin based low cost ceramic membranes. Various characterization techniques such as particle size distribution (PSD), thermogravimetric (TG), X-ray diffraction (XRD), scanning electron micrograph (SEM), flexural strength, corrosion resistance, water permeability and solvent permeability analysis have been conducted to evaluate the membrane characterization parameters. Depending upon the achieved set of characterized parameters for different fabricated membranes, important wastewater treatment applications such as treatment of oil-water emulsion, separation of *E. Coli.* bacteria from synthetic solution have been studied using microfiltration operation and chromium (VI) removal has been studied using adsorption-microfiltration process. Finally, one of the ceramic membranes has been utilized as a support to fabricate LTA zeolite composite membranes and has been investigated for the ultrafiltration of bovine serum albumin (BSA) protein solution.

With emphasis upon uni-axial dry compaction method for ceramic membrane fabrication and in-situ hydrothermal method for LTA zeolite composite membrane fabrication, the originality and uniqueness of the technical content presented in this Ph.D. thesis is outlined as follows:

a) Identification of inorganic raw material compositions (kaolin, quartz, calcium carbonate, sodium carbonate, boric acid and sodium metasilicate) to achieve microfiltration range low cost ceramic membranes with diverse membrane characterization parameters.

b) Comparatively similar or better membrane performance characteristics (dead end membrane flux and rejection) for the separation of oil-water emulsion and bacteria (*E. coli*) solution.

c) Identification of adsorption (yeast) and microfiltration (ceramic membrane) combination process for the efficient removal of chromium (VI) from its aqueous solution.

d) Cross flow microfiltration of oil-water emulsion using kaolin based low cost ceramic membranes.

e) Fabrication of LTA zeolite composite membranes for application towards ultrafiltration processes.

During the early research, three ceramic membrane supports A1 – A3 were prepared using an identified new composition of precursors and simple uniaxial compaction method. The membrane morphologies varied from an average pore size and porosity of 2.48 – 4.46 µm and 44 – 27 %, respectively. Amongst these membranes, A2 membrane prepared at a sintering temperature of 950 ^{o}C possessed optimal combinations of

characterization parameters such as mechanical strength (28 MPa), average pore size (3.07 µm) and porosity (38 %).

In order to further reduce the membrane pore size, novel raw material compositions have been identified to achieve three distinct microfiltration membranes B1 – B3 (average pore size and porosity of 1.06 – 2.22 µm and 45 – 34 %, respectively). Amongst these, B1 membrane possessed optimal characterization parameters (34 MPa mechanical strength, 45 % porosity and 1.06 µm average pore size). During MF of oil-water emulsions, the B1 membrane provided a good separation performance of dead end flux and rejection of 7.23×10^{-5} m^3/m^2s and 85 %, respectively at a feed concentration and pressure of 250 mg/L and 69 kPa, respectively. Similarly, during the carried out MF studies for the separation of bacteria, the B1 membrane provided a dead end MF flux and rejection of 1.23×10^{-4} m^3/m^2s and 99 %, respectively for a feed concentration and pressure of 6×10^5 CFU/mL and 69 kPa, respectively. For the identified adsorption-MF process using baker's yeast, the B1 membrane provided an excellent dead end MF optimal flux and rejection of 2.07×10^{-5} m^3/m^2s and 94 %, respectively at a Cr (VI) feed concentration, yeast concentration, pH and applied pressure of 100 mg/L, 10 g/L, 1 and 207 kPa, respectively.

Eventually, a further reduction in the membrane morphology has been targeted with the addition TiO_2 to B1 composition. Subsequently, in addition to B1, sub-micron range MF membranes C1 and C2 were fabricated and all have been tested for dead end and cross flow microfiltration of oil-water emulsions. For membranes B1, C1 and C2, the average porosity and pore diameter varied from 45, 41 and 39 % and 1.06, 0.90 and 0.35 µm, respectively. During dead end MF experiments, C1 was identified as a best membrane for

the treatment of oily wastewater which provided an oil rejection and permeate flux of 96 % and 6.5×10^{-5} m^3/m^2s, respectively, at a lower applied pressure of 69 kPa.

During cross flow MF conducted at various combinations of pressure differentials (69 – 345 kPa) and circulation rates (2.78 – 13.9×10^{-7} m^3/s) and feed concentration for 100 mg/L, the membrane C1 provided optimal oil rejection and permeate flux of 87 % and 5.54×10^{-5} m^3/m^2s at a pressure and cross flow rate of 207 kPa and 13.9×10^{-7} m^3/s, respectively. Amongst standard fouling models, cake filtration provided best fitness to represent the flux decline data for all the membranes.

The LTA zeolite composite membranes D1 – D4 fabricated with in-situ hydrothermal method using B1 ceramic support possessed an average pore size and porosity of 215 – 76 nm and 30 – 23%, respectively. The pure water permeability of the membranes D1 – D4 varied from 1.22×10^{-7} – 1.19×10^{-8} m^3/m^2s kPa. For the D4 membrane, the optimal flux and rejection values of 4.54×10^{-7} m^3/m^2s and 80 %, respectively were obtained at a pH and pressure of 2.5 and 207 kPa, respectively for the separation of bovine serum albumin (BSA)

Amongst all membranes, it has been identified that membranes A2, B1, C1 possessed optimal characterization parameters or/and provided optimal performance for various applications. Based on the retail cost of the raw materials, the fabrication cost of A2, B1 and C1 membranes has been estimated to be 49.4, 49.2 and 50 $\$/m^2$, respectively. With these experimental observations and theoretical observations, the thesis anticipates to serve as a useful guide and reference for the implementation of kaolin based ceramic membranes in process industries for wastewater treatment applications.

Contents

List of Tables

List of Figures

Abbreviations

BSA	bovine serum albumin
CFU	colony forming unit
Cr	chromium
CVD	chemical vapour deposition
DPC	diphenyl carbazide
E. coli	escherichia coli
EtOH	ethanol
IPA	isopropyl alcohol
LRV	log reduction value
LTA	linde type-A
MF	microfiltration
MtOH	methanol
MW	molecular weight
MWCO	molecular weight cut-off
NF	nanofiltration
o/w	oil-in-water
PAN	polyacrylonitrile
PTFE	polytetrafloroethylene
PUF	polymer enhanced ultrafiltration
PV	pervaporation
PVA	Polyvinyl alcohol
RBAO	reaction bonded aluminum oxide
TMAOH	tetramethylammonium hydroxide
UDMH	unsymmetrical dimethyl hydrazine
UF	ultrafiltration
USEPA	united states environmental protection agency

Notations

A	effective membrane area (m^2)
C_f	concentration of oil, bacteria, chromium (VI) and BSA in the feed (mg/L, CFU/mL, mg/L and mg/L)
C_p	concentration of oil, bacteria, chromium (VI) and BSA in the permeate (mg/L, CFU/mL, mg/L and mg/L)
d_i	nore diameter of i^{th} pore
d_s	pore diameter
d_{XRD}	crystallite size (nm)
F	load at the fracture point (kN)
J	permeate flux (m^3/m^2s)
J_0	intitial permeate flux (m^3/m^2s)
J_v	water flux (m^3/m^2s)
K	shape constant
k_b	complete pore blocking model constant in Eq. (5.3) (1/s)
k_c	cake filtration model constant in Eq. (5.6) (s/m^2)
k_i	intermediate pore blocking model constant in Eq. (5.5) (1/m)
k_s	standard pore blocking model constant in Eq. (5.4) ($s^{0.5}/m^{0.5}$)
L	span length (mm)
L_h	hydraulic permeability (m^3/m^2s kPa)
l	pore length (mm)
n	number of pores
ΔP	trans-membrane pressure (kPa)
R	rejection (%)
r_l	pore radius (µm)
t	filtration time (s)
t_s	thickness of the sample (mm)

V	volume of permeate sample (m^3)
v_{mem}	volume of membrane (m^3)
W_1	weight of the dry membrane (g)
W_2	weight of the wet membrane (g)

Greek letters

ε	porosity of the membrane (dimensionless)
ρ_{water}	density of water (Kg/m^3)
σ_{fl}	flexural strength (MPa)
μ	viscosity (cP or kPa s)
τ	tortuosity factor
λ	CuKα radiation wavelength (Å)
β	full-width at half-maximum (Radians)
θ	diffraction angle (deg.)
σ	surface tension (mN/m)

Chapter 1:

Introduction and Literature Review

Chapter 1

Introduction and Literature Review

This chapter presents a brief summary of the basic fundamentals, terminologies and applications of membrane technology along with the basis of the problem chosen in this work. State of art on the preparation, characterization of ceramic and ceramic - ceramic composite membrane and their applications have been elaborately discussed. Based on the state of art on the membrane preparations and their applications for the treatment of oil-in-water emulsions and removal of bacteria, chromium metal and bovine serum albumin from their aqueous solutions, the objectives of the thesis have been summarized. Finally, the organization of the present work has been presented.

1.1 Background

Ongoing trends to globalize world economy requires enhanced input, processing and output in several process industries such as petroleum, petrochemical, chemical, food, and metallurgical industries etc. Driven with technological inventions, process industries intend to accommodate process variations in the form of novel technologies, process intensification and advanced separation technologies. These efforts are targeted to minimize waste production and cost and maximize energy efficiency. Process flow sheets constitute primarily reactors and separators in which the separation technology offers several exciting opportunities for research and innovation. Apart from well-established separation technologies such as distillation, absorption and adsorption technologies in industrial processing schemes, novel technologies such as ion-exchange, membrane

technology etc., have received significant attention due to their cost effectiveness and scalability to achieve medium and compact process systems.

Membrane technology involves utilizing a membrane polymeric/ceramic material that facilitates the separation of few or more constituents by the application of suitable driving force (pressure, concentration etc.) across the membrane. Amongst several novel technologies, membrane technological applications established in industrial schemes include air separation, hydrogen recovery from refinery gas streams, desalination of sea and brackish water and wastewater treatment. From a materials perspective, membrane technology market is dominated with the application of inexpensive polymer membranes and ceramic membranes are gradually receiving attention both in terms of research as well as industrial applications.

1.2 Ceramic membranes

Despite having significant number of applications in the process industries, polymeric membranes suffer with the basic limitation of lower combinations of chemical, mechanical and thermal stability. Industrial process schemes produce several intermediate streams which need to be pre-processed to undergo processing with polymeric membrane technology. For instance, to minimize membrane fouling, feed stock pH needs to be altered. Similarly, hot streams are cooled to 25 – 50 ^{o}C to safeguard the shelf life of polymeric membranes, as these membranes are heat sensitive.

Opposed to polymeric membranes, ceramic membranes provide higher combinations of chemical, mechanical and thermal stability.

Table 1.1: A summary of ceramic and polymeric membrane properties.

Desired Feature	**Ceramic membranes**	**Polymeric membranes**
Shelf Life	10 – 15 years typically in several installed cases with a minimal shelf life of 5 – 10 years.	12 – 18 months lower life span.
High temperature operability	Resistance to high temperature (350 – 500 ^{o}C).	Not possible. Operability in the low temperature range (25 – 50 ^{o}C).
High pressure operability	Designed for pressures up to 30 bars.	Polymeric membranes generally do not withstand high pressures due their lower mechanical strength .
Chemical stability	Stable in organic solvents, oxidants, and hydrocarbons.	Lower chemical stability in several chemicals and solvents.
Applicability to pH	Applicability to wider pH ranges (0.5 – 14).	Narrow applicable range of pH.
Susceptibility to biological attacks	More stable in biological attacks such as fungus, bacteria and virus etc.	Polymeric membranes are susceptible to biological attacks and particularly to fungal contamination.
Regeneration	Enhanced ease of cleaning and (chemical or steam) sterilization.	Cleaning is quite difficult. Acidic cleaning is not advisable.
Cost	Higher cost. About 500 – 2000 \$/m^2	Comparatively low cost than ceramic membranes (225 –350 \$/m^2).
Brittleness	They are brittle in nature.	They are not highly brittle.
Scale up	Difficult due to complex fabrication processes.	Easy as films can be scaled up easily.

This is due to the fact that ceramics membranes are fabricated at high sintering temperatures, which are well above the temperatures that exist for various intermediate streams in the process industries. Further, ceramic membranes can be subjected to rigorous cleaning schemes due to their higher corrosion and fouling resistance. In addition, the mechanical strength of a ceramic matrix is bound to be higher than that of the polymeric film due to the inherent properties of the materials. Various primary inorganic materials that can be used to fabricate inorganic membranes include alumina, zirconia and glass. A comparative summary of ceramic and polymeric membranes is presented in Table 1.1.

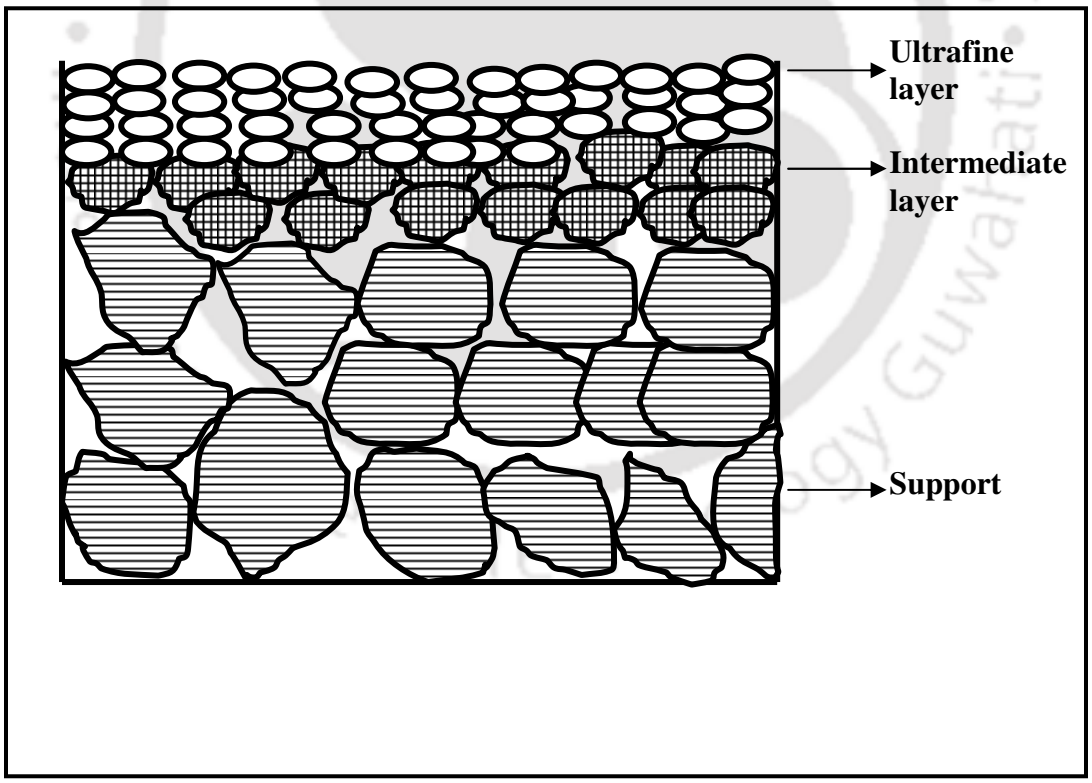

Figure 1.1: Typical cross sectional morphology of a ceramic membrane.

1.3 Ceramic membrane preparation methods

The fabrication of a ceramic membrane primarily consists of two phases namely the fabrication of ceramic support that provides mechanical resistance to the filtered medium and achieving a selective skin or top layer. Depending upon the pore size, the skin layers play an active role in ultrafiltration (UF) and nanofiltration (NF) processes. Fig. 1.1 illustrates the typical cross-sectional morphology of a ceramic membrane. This includes a macroporous support layer, mesoporous intermediate layer and a microporous skin layer. Further details with respect to the fabrication of these layers is presented as follows.

1.3.1 Support formation

A ceramic support is fabricated by casting inorganic powder into desired shape and subsequent consolidation of the green substrate by sintering. The fabrication process for the ceramic support consists of four sequential steps namely:

a) Choice of appropriate inorganic raw materials.

b) Preparation of ceramic power/paste.

c) Membrane casting.

d) Consolidating or firing (heat treatment).

A brief overview of these steps is presented as follows.

a) Choice of appropriate inorganic raw materials

The morphological properties of various raw material precursors influences the porosity (or structural density) and pore size of the ceramic support and is therefore an important parameter to achieve membranes with desired attributes. The structural density of the

support increases with decreasing grain size of the raw materials. Similar variation exists for the pore size. Typically, the ratio of grain to pore size is strongly dependent on the shape of the particles and is about 2.5. In order to facilitate the coating of a homogeneous thin layer on the support, the pore size of the skin layer must be adaptable with the grain size of the layer on which it is to be deposited. The presence of large pores on the internal surface of channels could lead to penetration of the skin layer grains into the support which will give raise to defects such as pinholes and cracks in the membrane morphology. The structural density of the membrane must be sufficient enough to ensure excellent mechanical resistance. On the other hand, lower structural density offers higher transport resistance for fluid through the support. Therefore, tradeoffs exist for the optimization of grain size to achieve acceptable combinations of mechanical and hydraulic resistance. In addition, various combinations of raw materials can be used to target the variation in grain size. Thereby, additional variations in pore size distributions can be achieved after sintering.

b) Preparation of ceramic powder/paste

During the paste preparation step, the ceramic powder is usually mixed with the solvent (water) and organic additives (Burggraaf 1996) to induce plastic properties to the prepared paste. The plasticity of the paste enables flexibility to shape the ceramic structure without cohesion. Another desired effect of the organic additives is to increase the unfired material strength during the shaping and drying steps which enables the elimination of defects such as cracks. Typical organic additives used during the paste preparation include binders, plasticizers, lubricants and deflocculants. Plasticizers induce

plastic properties to the paste. Generally, viscous and wetting polymers are used as plasticizers. Lubricants such as glycerin assist the paste to slide in the extrusion apparatus. By controlling the surface charge of the particles, deflocculants avoid powder agglomeration by steric effect. Moreover, mixing and pugging are also important steps in paste preparation. Mixing is an essential step to obtain good dispersion and perfect homogeneity by the even distribution of constituents. Similarly pugging is necessary to obtain paste. During pugging, the progressive addition of water to the powder mixture leads to achieving a high viscous paste. The powder preparation procedure is very simple in comparison to that of the paste preparation. During the powder preparation step, the powder is usually mixed in a mixer or ball mill with suitable binders. Subsequently, the powders are sieved with a suitable screen (30 – 40 mesh).

c) Membrane casting

Presently, several methods are familiar for casting the membrane supports into a desired shape. Amongst these methods, extrusion and uniaxial pressing methods are two important methods that can be adopted to fabricate membranes using both paste and powder inorganic precursor mixtures.

Shaping by extrusion

Extrusion is one of the important methods for ceramic membrane fabrication. The schematic of industrial extrusion apparatus is shown in Fig. 1.2. During extrusion, the paste is kept under vacuum to avoid the presence of bubbles. Eventually, through an endless screw or piston, the paste is forced through the opening of a die.

The extrusion speed can be chosen to elaborate and achieve homogeneous tubes. The geometry of the extrusion cone and die critically influence the shaping and structural density of the wet tubes. Typically mono and multichannel tube dies are available to shape the membranes into single channel and multichannel ceramic tubes, respectively.

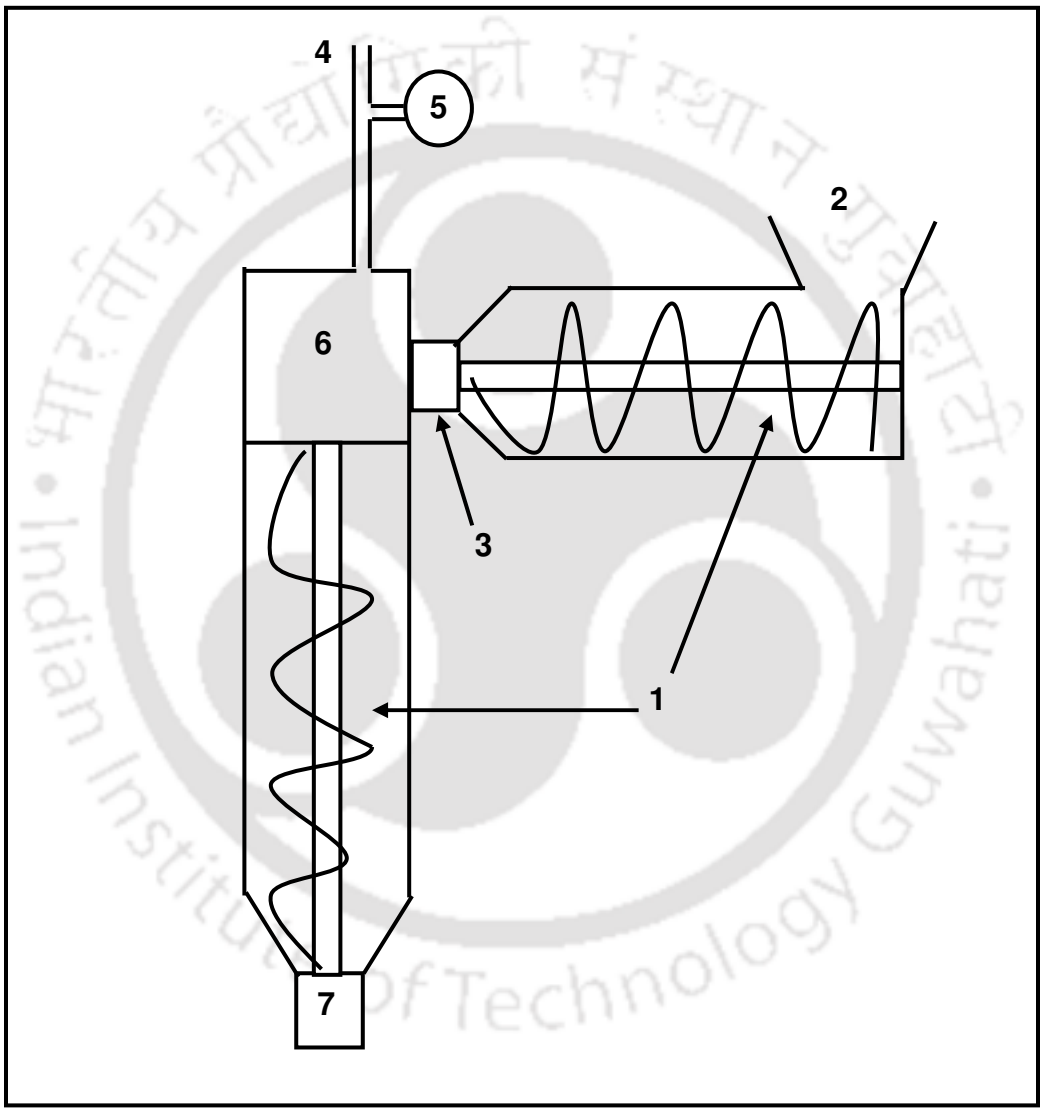

Figure 1.2: Schematic of an industrial extrusion apparatus: (1) endless screw, (2) paste inlet, (3) compression, (4) vacuum, (5) pressure gauge, (6) vacuum chamber, (7) die.

Shaping by uni-axial compaction

Uniaxial pressing method is an inexpensive and simple preparation technique for the fabrication of membrane support. Uniaxial pressing involves the preparation of the ceramic powder with a suitable binder and subsequent compaction of the powder using a suitable mould at a high pressure (30 – 50 MPa) in a single axial direction. The compaction is achieved through a rigid punch or piston. Fabrication pressure is an important parameter to influence upon the morphological properties of the membrane.

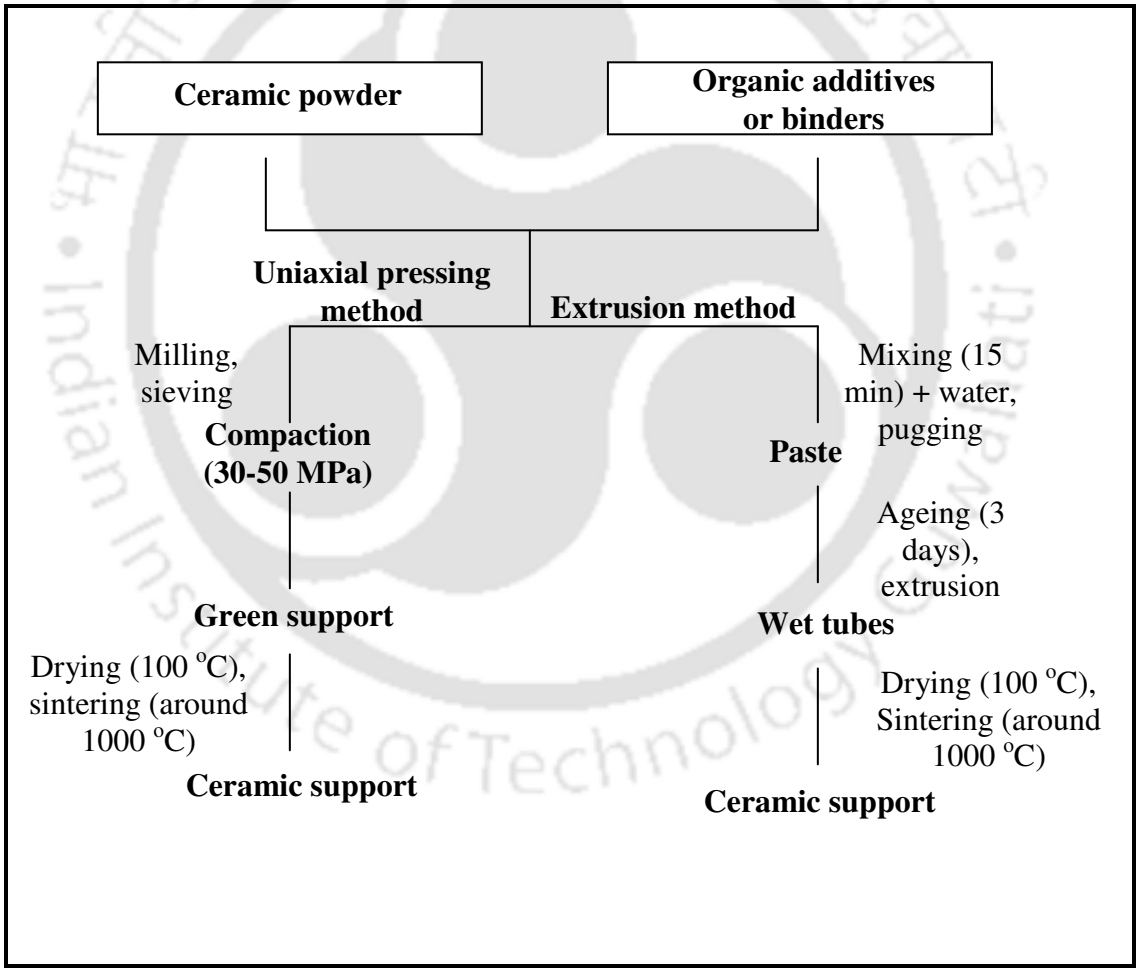

Figure 1.3: A schematic summary of various methods for ceramic membrane support fabrication.

d) Consolidation or firing (Heat treatment)

The firing treatment strengthens the green membrane support. Heat treatment enables the elimination of bonded water and organic additives to finally achieve the temperature of allotropic transitions. Therefore, to visualize upon the completion of the firing step, thermogravimetric analysis is necessary. The firing treatment can be described in two stages in which the first corresponds to the combustion of the organics, and the second allows the membrane to sinter by densification and grain growth. During sintering, membrane properties such as pore diameters, density and mechanical resistance depend on the temperature and time of sintering. A schematic that summarizes the preparation of ceramic membrane supports is presented in Fig. 1.3.

1.3.2 Top layer formation

Several coating techniques exist for the fabrication of the top/skin layer over a membrane support. Among these, dip coating and sol gel methods are the most versatile methods due to their simplicity and ease of operation.

a) Dip-coating

The dip-coating technique has been widely used to achieve asymmetric composite membranes. Dip-coating technique involves a colloidal processing technique with which coatings and layered membrane structures can be effectively fabricated. During dip coating, a porous substrate is withdrawn from the dispersion. There are two distinct approaches in dip coating namely capillary colloidal filtration and film coating.

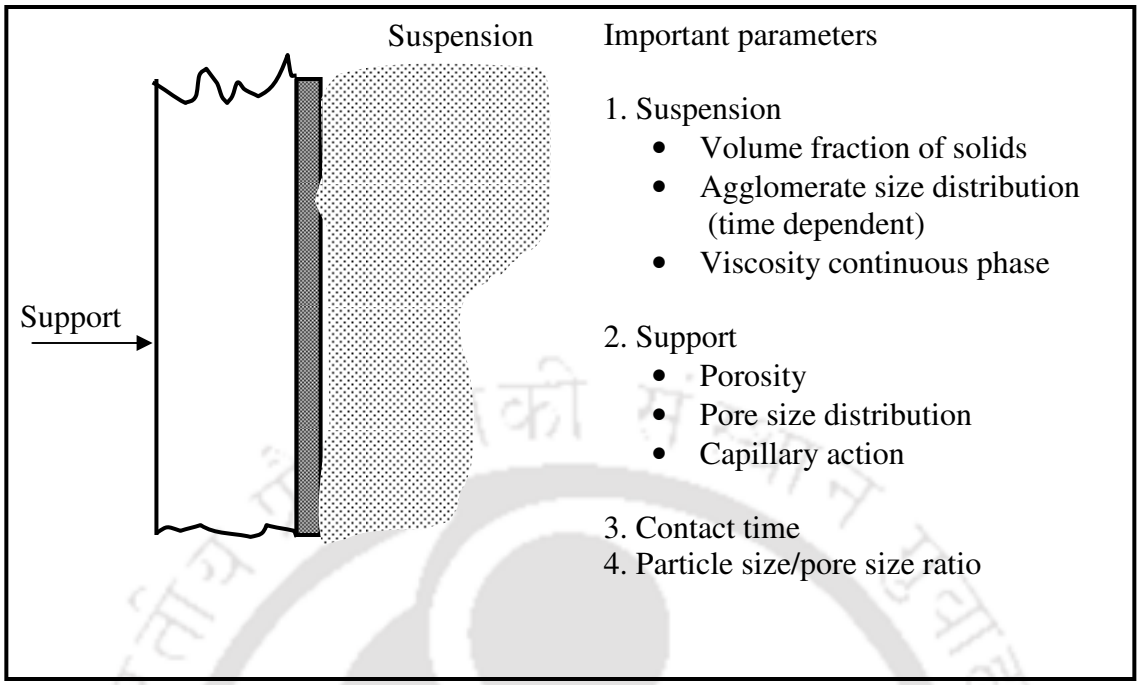

Figure 1.4: A schematic of the working principle of capillary colloidal filtration mode of dip coating process.

Capillary colloidal filtration

Capillary colloidal filtration occurs when a dry substrate comes in contact with the dispersion and the porous surface of the substrate is wetted by the dispersion liquid. Thereby, capillary suction occurs that facilitates and drives layering particles to the interface. Thereby these layered particles not being permeable through the substrate surface transform into a compact layer. For large colloidal particles, thickness of compact layer grows with time according to the square root time law until the substrate is saturated with dispersion liquid. On the other hand, for a dispersion of small colloidal particles, the thickness reaches a saturation state due to back diffusion. Fig. 1.4 illustrates the principle involved in the capillary filtration mode of dip-coating.

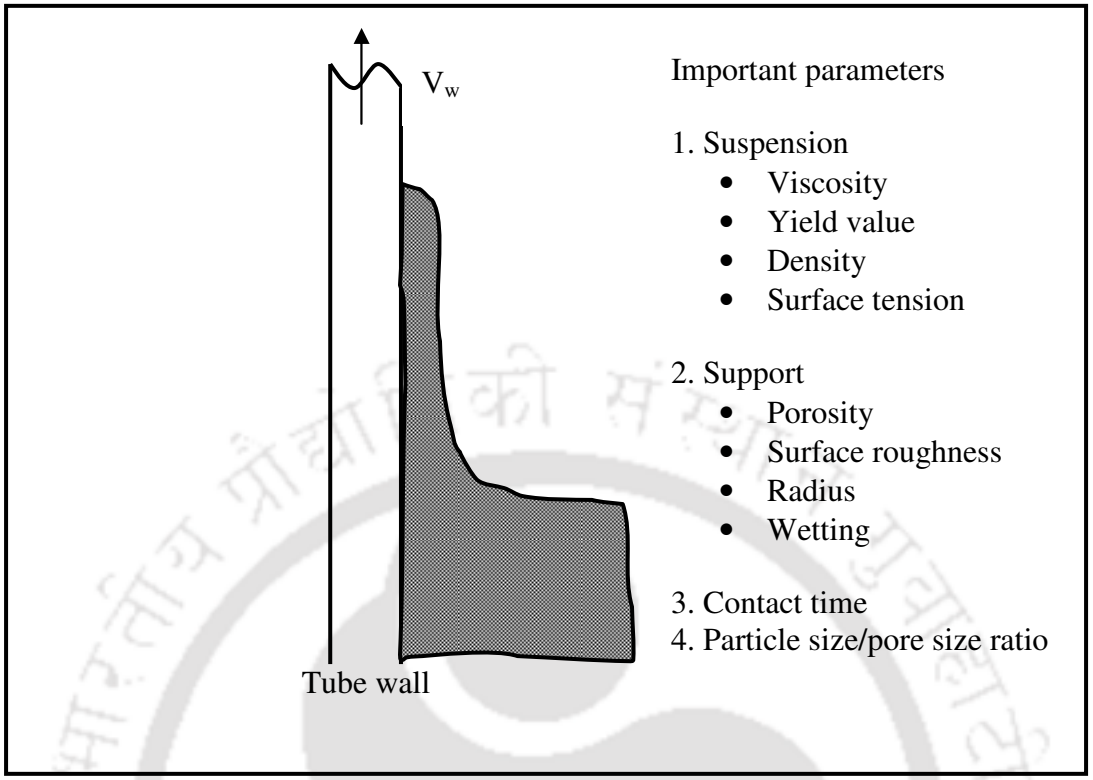

Figure 1.5: Schematic of film coating mode of dip coating process for ceramic-ceramic composite membrane preparation

Film-coating

During film-coating, the drag force exerted by the substrate during its withdrawal from the dispersion enables for formation of an adhering dispersion layer. To achieve pure film-coating, the capillary suction of the porous substrate must be suppressed. The thickness and morphology of the entrained dispersion layer is strongly influenced with withdrawal speed and dispersion viscosity. The thickness of the entrained dispersion layer increases with increasing combinations of withdrawal speed and viscosity. Further contact time does not significantly influence the film thickness. Fig. 1.5 depicts the underlying mechanism of film coating process.

b) Sol-gel method

The sol-gel process is one of the most appropriate methods to achieve a functional active top layer on a membrane support. Besides being less energy intensive, it is widely used due to its simplicity and doesn't need sophisticated instrumentation. Typically, two sol-gel routes are used for composite membrane preparation. The first corresponds to colloidal route that explores colloidal chemistry in aqueous media and the other corresponds to the polymeric route that exploits the chemistry of metal organic precursors with organic solvents. Fig. 1.6 summarizes sol-gel method for both colloidal and polymeric routes. The first stage in the sol-gel process refers to the preparation of a sol using molecular precursors which are either metal salts or metal organics. For both cases (colloidal as well as polymeric routes), condensation reactions occur at the sol stage with the formation of colloids or clusters that coalesce finally to form the gel. For the case of skin layer fabrication, it is important to note that the coating of the active layer must be carried out with the sol whose rheological behaviour is adaptable with the porous membrane substrate or support. Subsequent drying and sintering steps determine the chemical characteristics of the membrane. Drying treatment performed within an intermediate temperature range (80 – 350 ^{o}C) results in a skin layer inorganic material containing residual organics. Generally, skin layers with pure inorganic films are obtained by drying above 350 ^{o}C. The final consolidation of the composite membrane is carried out using conventional sintering procedure at elevated temperature.

The relevance of various functional materials to achieve desired morphological characteristics in inorganic composite membranes is summarized in Table 1.2. It can be

observed that alumina, clay, zirconia, zeolite etc., are common materials to achieve ceramic membranes.

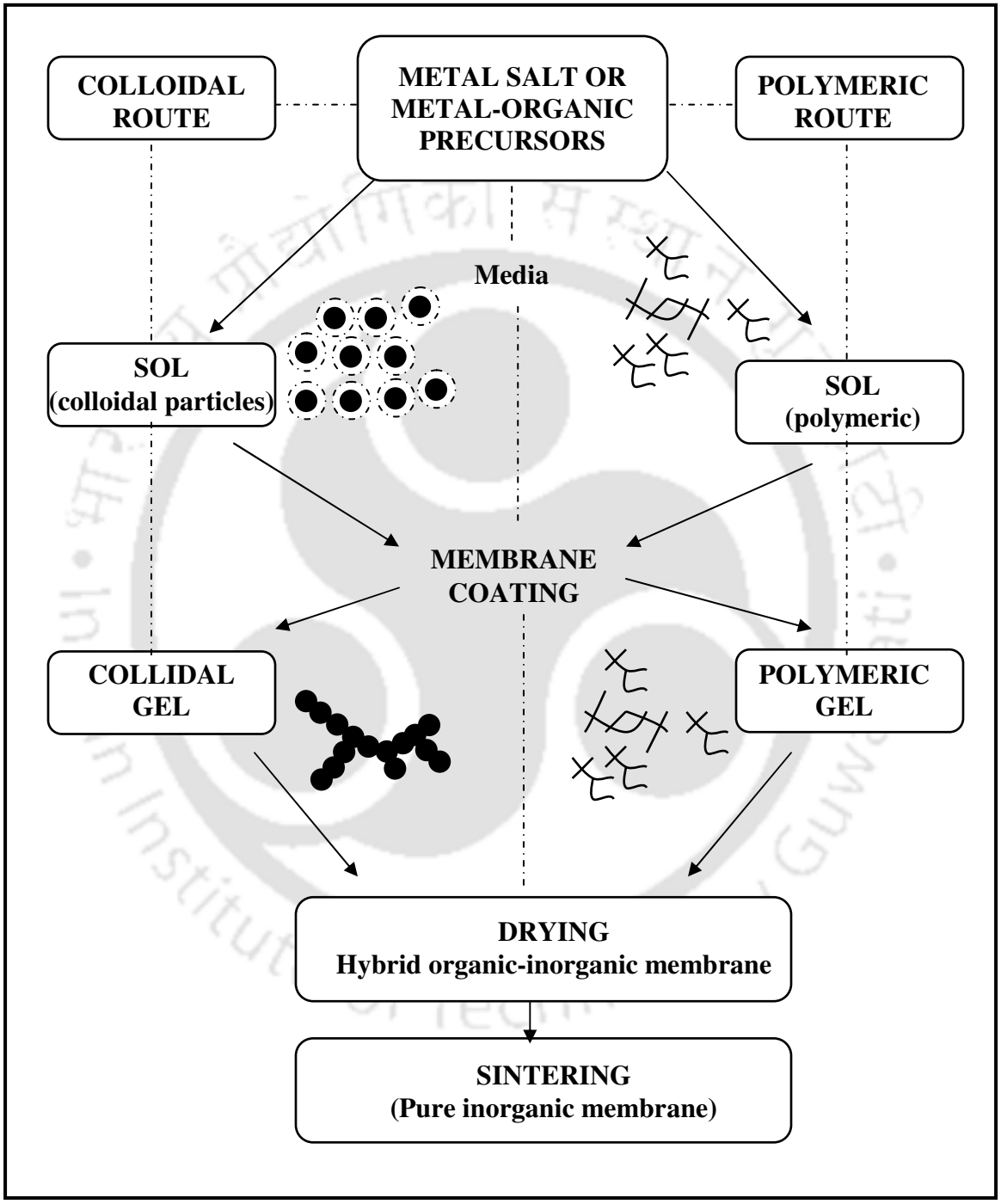

Figure 1.6: Pictorial representation of the sol-gel method to fabricate ceramic membranes.

Table 1.2: Morphological parameters for various ceramic membrane materials.

S. No.	Type of layer	Typical pore size range	Type of Separation layer	Type of materials
1	Support	0.1 to 10 µm	Macroporous	Alpha alumina, Natural clay cordierite, fly ash, apatite powder.
2	Intermediate	100 to 200 nm	Mesoporous	γ-alumina, zirconia and titania.
3	Skin layer	0.1 to 10 nm	Microporous	Zeolite, zirconia etc.

1.4 Industrial applications of ceramic membranes

Several industrial applications exist for ceramic membrane technology. These specifically refer to their applicability in

- Chemical and petrochemical industry.
- Textiles/pulp and paper industry.
- Pharmaceutical, cosmetic and biotechnology industry.
- Food, dairy and beverages industry.
- Automotive, mechanical, mineral, metal industry and surface engineering industry
- Wastewater applications.

As outlined in the literature (Mallada and Menendez 2008), specific areas of application have been outlined below for the ceramic membranes in the above industries.

a) Chemical and petrochemical industries (Mallada and Menendez 2008)

- Concentration of polymer suspensions, latex and metal hydroxide solutions.
- Catalyst recovery.
- Brine recycling.
- Recovery of dyes and pigments.
- Desalination of products such as optical brighteners, surfactants and dye stuffs.
- Cleaning, recovery and recycling of organic solvents.

b) Textiles/pulp and paper industry (Mallada and Menendez 2008)

- Lignosulfonate fractionation.
- COD reduction of bleach plant effluents.
- Whitewater recovery from paper machines.
- Paper coating recovery.
- Recovery of rinse water primary and secondary wool scouring effluent.
- Water jet loom motive water recovery.

c) Pharmaceutical, cosmetic and biotechnology industry (Mallada and Menendez 2008)

- Concentration, fractionation and isolation of pharmaceutical active agents. such as antibiotics, enzymes, proteins, amino acids and vitamins.
- Separation, concentration and dewatering of biomass and algae.
- Blood plasma filtering.
- Disposal of fat emulsions.
- Fermentation broth clarification.

- Separation of yeast.
- Concentration of bacterial suspensions.
- Vaccine production.
- Production of high purity (pyrogen and bacteria free) water.

d) Food, dairy and beverages industry (Mallada and Menendez 2008)

- Clarification and stabilization of wine, beer, cider, soy sauce, and vinegar.
- Concentration of juice.
- Removal of micro organisms from milk and whey.
- Separation and fractionation of milk and whey ingredients.
- Desalination of whey.
- Purification of spirits.
- Separation of soybean protein.
- Caramel color concentration and purification.
- Purification of drinking water.
- Recovery of product from beer and cider tank bottoms.

e) Automotive, mechanical, mineral, metal industry, surface engineering industry (Mallada and Menendez 2008)

- Recycling and disposal of degreasing and rinsing bathes.
- Treatment of oil-water emulsions.
- Recovery of heavy metals.
- Cleaning of wastewater from grinding processes.
- Treatment of wastewater from glass and glass fiber production.

f) Wastewater Applications (Mallada and Menendez 2008)

- Wastewater and potable water treatment.
- COD, BOD, and suspended solids reduction by membrane bioreactor.
- Removal of suspended solids.
- Emulsified oil removal, edible oils and waste oil treatment.
- Removal of microorganisms.
- Removal of heavy metals.
- Recycling of water form swimming pools.
- Purification of the drain of sewage plants.
- Methane digester water recovery.
- Upgrading vacuum residual oil.
- Radioactive wastewater treatment.

1.5 State of the art

With a brief overview of the contemporary research, this section summarizes the research outcome of various literatures. The objective of such review is to identify few promising areas of research that can be addressed in thesis. The state of the art has been presented for the following six sub-sections namely (a) ceramic membrane supports (b) ceramic-ceramic composite membranes (c) application of ceramic membranes for oily wastewater treatment (d) application of ceramic membranes for the removal of bacteria (e) application towards the removal of heavy metals from waste streams and (f) application of ceramic membranes towards the separation of bovine serum albumin (BSA).

1.5.1 Preparation of ceramic membrane supports

Recently, there has been significant research interest in ceramic membrane technologies due to their inherent advantages such as excellent mechanical, chemical stability, thermal stability, long shelf life, good cleaning/defouling properties and capability to withstand fouling against organic solvents (Monash and Pugazhenthi 2011). Typical applications for polymeric and ceramic membranes in industrial processing schemes include high purity water production, protein purification, gas separation and wastewater treatment. However, compared to the polymeric membrane, the cost of the ceramic membrane is significantly high due to the higher cost of raw materials. In addition, ceramic membranes require higher sintering temperature (more than 1100 ^{o}C) which additionally contributes to the fabrication cost. Due to these reasons, the utilization of ceramic membrane for industrial applications is limited. Early research in the field of ceramic membrane supports was primarily focused towards the utilization of expensive raw materials such as alumina, titania and zirconia. Several literatures report upon the preparation of ceramic membranes using expensive raw materials such as α-alumina (Van gestel *et al*., 2002; Benito *et al*., 2005; Yoshino *et al*., 2005), zirconia (Fan *et al*., 2000; Falamaki *et al*., 2004) and titania (Wang *et al*., 2006).

Van gestel *et al*., (2002) used two different techniques such as slip-casting (AKP-30) and reaction bonded Al_2O_3 (RBAO) manufacturing process to fabricate alumina membranes. The membranes were sintered at 1130 and 1300 ^{o}C for AKP-30 and RBAO, respectively to obtain membranes possessing an average pore size of 0.1 and 0.2 µm, respectively from AKP-30 and RBAO processes. Using α-alumina paste and extrusion method, Benito *et al*., (2005) prepared α-alumina ceramic tubes at a sintering temperature of 1600 ^{o}C.

The membrane possessed an average pore size and porosity of 1.2 µm and 35 %, respectively. Using α-alumina powder that possessed an average particle size of 3.5 µm, Yoshino *et al*., (2005) fabricated α-alumina tubular ceramic support substrate using extrusion method at a sintering temperature of 1400 ^{o}C. The fabricated membrane possessed an average pore size and porosity of 0.7 µm and 40 %, respectively. Fan *et al*., (2000) have prepared different types of supported zirconia composite membranes using various membrane supports such as alumina and ziconia. The authors indicated that the sintering temperature increased with an enhancement in ZrO_2 content (1100 ^{o}C for 90 % ZrO_2 and 1800 ^{o}C for 100 % ZrO_2). Falamaki *et al*., (2004) prepared disk shaped zirconia membrane using uniaxial compaction method and investigated upon the effect of sintering temperature (1200 – 1500 ^{o}C) on membrane properties such as pore diameter, porosity, shrinkage, flexural strength and permeability. The authors observed that all membrane properties varied significantly with sintering temperature. Wang *et al.,* (2006) fabricated high quality tubular titania MF membranes by dip coating techniques on an α-alumina support. The average pore size of the prepared membranes is 0.1 µm.

A critical observation of the above mentioned literatures indicates that the membranes fabricated are expensive due to the higher cost of raw materials and higher sintering temperature (more than 1000 ^{o}C). These contribute towards higher raw materials cost and furnace power cost, respectively. To overcome these issues, current research needs to utilize low cost ceramic precursors which can be effectively sintered at lower sintering temperatures (less than 1000 ^{o}C) and simple fabrication studies. Recently, numerous studies have been demonstrated for the fabrication of ceramic membranes utilizing cheaper raw materials and clays (Saffaj *et al*., 2004; Belouatek *et al*., 2005; Bouzerara *et*

al., 2006; Saffaj *et al*., 2006; Masmoudi *et al*., 2007; Jedidi *et al*., 2009; Khemakhem *et al*., 2009).

Saffaj *et al.,* (2004) used low cost cordierite powder to prepare membrane supports using extrusion method and a sintering temperature of 1275 ^{o}C. The authors obtained a membrane with an average pore size and porosity of 7 µm and 40 %, respectively. Further, the membranes also possessed adequate mechanical resistance. Belouatek *et al*., (2005) have used barbotine (Algerian clay) to prepare a ceramic support which was sintered at a higher sintering temperature of 1100 ^{o}C. The authors obtained a porosity of 14.47 % and mean pore diameter of 0.9 µm. Using extrusion method and sintering temperature of 1125 ^{o}C. Bouzerara *et al*., (2006) have used kaolin and doloma mixture to develop a porous ceramic support. The authors adopted different processing routes and prepared two different configurations namely tubular and flat shaped membranes. Their research indicated that the membrane with a uniform pore size of 28 µm and porosity of 43 % was obtained at a higher sintering temperature of 1250 ^{o}C. Saffaj *et al*., (2006) developed a low cost membrane support using Moroccan clay and extrusion method. The authors studied upon the effect of sintering temperature on the membrane properties such as porosity, average pore size and mechanical strength etc., and inferred that the optimal sintering temperature is 1225 ^{o}C. At this sintering temperature, the membrane possessed an average pore size and mechanical resistance of 10.12 µm and 10 MPa, respectively.

Using extrusion method and a sintering temperature of 1150 – 1200 ^{o}C, Masmoudi *et al*., (2007) fabricated tubular ceramic membranes using low cost apatite powder. The authors inferred that the membrane porosity reduced from 50 – 45 % with an increase in the sintering temperature from 1150 ^{o}C and 1200 ^{o}C. On the other hand, the average

membrane pore size increased from 5 – 8 µm with increasing sintering temperature. Jedidi *et al*., (2009) have developed a membrane support using low cost fly ash. The authors evaluated that the mean pore diameter and pore volume has been about 4.5 µm and 51 %, respectively. Khemakhem *at al*., (2009) have fabricated tubular configured ceramic membrane supports using Tunisian natural material. The support was sintered at 1190 ^{o}C and the fabricated membrane possessed an average pore diameter and porosity of about 9.2 µm and 49 %, respectively.

Recently, instead of using single raw material or clay, few researchers have used a mixture of raw materials in order to achieve good combinations of membrane properties such as higher mechanical strength and chemical resistance and lower average pore size. Few literatures summarize such efforts to prepare ceramic membranes using mixed raw materials (Nandi *et al*., 2008; Monash and Pugazhenthi 2011). Nandi *et al*., (2008) have fabricated disk shaped ceramic membrane supports using pasting method and inexpensive raw material (kaolin, quartz, calcium carbonate, sodium carbonate, sodium metasilicate and boric acid). They have studied upon the effect of sintering temperature and have observed that the average pore size increases from 550 to 810 nm with an increase in the sintering temperature from 850 – 1000 ^{o}C. Monash and Pugazhenthi (2011) have used low cost clays (kaolin, ball clay, feldspar, quartz, calcium carbonate and pyrophyllite) to prepare a ceramic membrane support that provided good mechanical stability and chemical stability. In addition, the support possessed an average pore diameter and porosity about 1.01 µm and 44 %, respectively at optimized sintering temperature of 950 ^{o}C.

Conventional fabrication techniques such as extrusion, tape casting and dry compaction methods provide excellent low-cost manufacturing routes for several shapes. Dry compaction method has been successfully used for the ceramic membrane fabrication and recent study shows that this method results in minimal macro-defects and dense-packed homogenous compact structure (Monash and Pugazhenthi 2011). Table 1.3 presents a summary of the research findings of various authors for the fabrication of ceramic membrane supports.

Table 1.3: Literature data summary for microfiltration range ceramic membranes.

Materials	**Average pore size (µm)**	**Sintering temperature (^oC)**	**Methods of preparation**	**References**
Alumina	0.1 and 0.2	1130 and 1300	Slip casting (AKP-30) and reaction bonded alumina (RBAO)	Van gestel *et al*., (2002)
Alumina/ zirconia	0.17 – 0.15/ 0.11 – 0.15	1300 – 1500/ 1300 – 1500	Uniaxial compaction method	Falamaki *et al*., (2004)
α-alumina	1.2	1600	Extrusion	Benito *et al*., (2005)
α-alumina	0.7	1400	Extrusion	Yoshino *et al*., (2005)

Materials	Average pore size (µm)	Sintering temperature (^oC)	Methods of preparation	References
Cordierite	7	1275	Extrusion	Saffaj *et al*., (2004)
Algerian clay	0.9	1100	-	Belouatek *et al*., (2005)
Kaolin and doloma	28	1250	-	Bouzerara *et al*., (2006)
Moroccan clay	10.12	1225	Extrusion	Saffaj *et al*., (2006)
Apatite	5 to 8	1150 to 1200	Extrusion	Masmoudi *et al*., (2007)
Fly ash	4.5	1125	Extrusion	Jedidi *et al*., (2009)
Tunisian natural material	9.2	1190	-	Khemakhem *et al*., (2009)
Mixed raw materials	0.55 to 0.810	850 to 1000	Paste method	Nandi *et al*., (2008)
Mixed raw materials	1.01	950	Uniaxial compaction method	Monash and pugazhenthi (2011)

1.5.2 Preparation of ceramic-ceramic composite membranes

Recently, different types of composite membranes were fabricated. These include polymeric-polymeric, polymeric-ceramic and ceramic-ceramic composite membranes. Due to their higher corrosive resistance, solvent resistance and applicability for wider pH range, there is an increasing interest to develop ceramic-ceramic composite membranes

instead of polymer-ceramic composite membranes. Generally, composite membranes are asymmetric membranes that constitute a dense skin layer on a macroporous support. Ceramic-ceramic composite membranes constitute a ceramic skin layer of inorganic material such as alumina, titania, zirconia and zeolite over a macroporous ceramic support. Compared to the symmetric ceramic membranes, ceramic-ceramic composite membranes possess superior combinations of structural integrity, fouling resistance, flux and selectivity. Several experimental methodologies have been addressed to prepare the selective skin layer of polymeric as well as ceramic composite membranes. These include dip-coating (Flamaki *et al*., 2005; Yoshino *et al*., 2005; Erdem *et al*., 2006), chemical vapour deposition (CVD) (Amanipour *et al*., 2012), in-situ hydrothermal synthesis and microwave assisted hydrothermal treatment (Huang *et al*., 2004; Li *et al*., 2006). In the field of ceramic-ceramic composite membranes, the fabrication methods primarily refer to dip-coating and hydrothermal synthesis.

Falamaki *et al.,* (2005) fabricated zirconia-zircon composite membranes on porous disk shaped α-Al_2O_3 supports using dip coating. The authors studied the effect of slip concentration, sintering temperature and number of coating step on the membrane characteristics. Yoshino *et al.,* (2005) developed silica based membranes and membrane modules for hydrogen separation at high temperature. In their work, tubular α-alumina substrates with 0.7 µm pore size and 40 % porosity were prepared as membrane supports with extrusion method and an intermediate α-alumina layer with a pore size of 60 nm and porosity of 39 % was deposited using dip-coating technique. Erdem *et al*., (2006) have ceramic composite membrane for the separation of whey components. The authors adopted dip-coating method for the deposition of zirconia selective layer on an alumina

ceramic support, which provided good lactose protein separation (lactose retention of 7 % with a high protein content of 80 %). Adopting a co-current CVD method, Amanipour *et al*., (2012) prepared a hydrogen-selective nano-composite ceramic membrane by depositing a dense SiO_2 and Al_2O_3 layer on an alumina ceramic support. The skin layer thickness has been evaluated to be 80 – 100 nm.

Several other research groups also targeted the fabrication of zeolite composite membranes which have been widely studied for pervaporation application due to their promising features such as good adsorption properties, uniform molecular sized pores, thermal stability, chemical and mechanical stability. The zeolite membrane exhibited very good dehydration performance for binary mixtures such as isopropanol/water, acetonitrile/water and methylethylketone/water in comparison with the commercial pervaporation polymeric membranes (Hoof *et al.*, 2006). In addition to that, compared to the polymeric membranes, zeolite membranes did not swell. The polymeric membrane swelling leads to higher permeability and lower selectively (Praptowidodo 2005). Various types of zeolite membranes such as MFI (Lai and Gavalas 1998; Bernal *et al*., 2001; Hedlund *et al*., 2002; Lai *et al*., 2003) and LTA (NaA) (Jafar *et al*., 1997; Kondo *et al*., 1997; Aoki *et al*., 1998; Morigami *et al*., 2001; Li *et al*., 2001; Huang *et al*., 2004; Pina *et al*., 2004; Li *et al*., 2006) have been prepared on different types of supports. Compared to other zeolite membranes, NaA (Linde type-A) zeolite membrane possesses excellent properties due to the achievement of low pore size (0.4 nm) and therefore, small molecules such as H_2 (0.29 nm) and N_2 (0.364 nm) can be easily separated from short-chain alkanes by molecular sieving or configurational diffusion mechanism (Aoki *et al*., 1998). Since NaA has high affinity for water, it is very effective towards the dehydration

of alcohol/water mixture by pervaporation (Jafar *et al*., 1997; Kondo *et al*., 1997). The membrane provided good combinations of fluxes and selectivities even at low feed water concentrations, which makes them applicable for the pervaporation operation of feed streams with low feed water concentrations (Hoof *et al.*, 2006). Due to these reasons, considerable research has been addressed upon the synthesis and application of NaA zeolite membrane in the last decade.

Morigami *et al*., (2001) developed a zeolite A ceramic composite membrane using porous tubular ceramic support. The Zeolite A layer was prepared by hydrothermal treatment on the seeded porous support. The authors inferred that the membrane was highly selective towards water permeation and provided high permeation flux in pervaporation (PV) and vapor permeation. Using these membranes, the first large-scale PV plant that produces 530 L/h of solvents (EtOH, IPA, MtOH, etc) at less than 0.2 wt.% of water from 90 wt.% solvent at 120 °C had been installed. Xu *et al.,* (2001) have synthesized NaA zeolite membranes on seeded α-Al_2O_3 support adopting microwave heating method. The authors indicated that compared to conventional heating, microwave heating drastically promoted the formation of NaA layer than the conventional heating due to which the synthesis time reduced significantly from 3 h (conventional heating) to 15 min (microwave heating). Tiscareno-Lechuga *et al*., (2003) prepared zeolite A membranes adopting seeded in situ hydrothermal synthesis on the lumen of asymmetric tubular supports (Inocermic) using a novel device. The prepared membranes were applied for the pervaporation of ethanol/water mixture to achieve good combinations of flux and separation factors. Huang *et al.,* (2004) synthesized A-type zeolite membranes by secondary growth method with vacuum seeding on porous alumina tubular support. The authors studied upon the

effect of seed particle size, suspension concentration, coating pressure and coating time on membrane morphology. The optimum synthesized conditions have been reported as seed particle size of 500 – 1200 nm, suspension concentration of 4 – 8 g/l, coating pressure difference of 0.0100 – 0.0250 MPa and coating time of 45 – 180 s.

Kazemimoghadam and Mohammadi (2006) have fabricated zeolite A ceramic composite membrane on mullite ceramic support prepared with kaolin. The authors fabricated NaA layers on the external surface of the mullite support hydrothermally. These membranes were used for the separation of water/UDMH mixture and showed very high selectivity of water for water/UDMH mixture. Li *et al*., (2006) developed a new fabrication method (in-situ aging–microwave synthesis) to deposit NaA layer on a porous α-Al_2O_3 support without seeding. The effects of synthesis parameters including in-situ aging temperature, time and microwave heating time on the characteristics and separation performance of the synthesized zeolite composite membranes were investigated. The authors observed that the in-situ aging temperature and microwave heating time had significant influence on the membrane morphology. Zah *et al*., (2006) synthesized zeolite A membrane on α-Al_2O_3 support by direct in-situ crystallization from a clear solution. The authors investigated upon the effect of layer development time as a synthesis parameter on the membrane properties such as morphology, growth rate and elemental composition.

Adopting hydrothermal synthesis technique, Kyotani *et al.,* (2007) prepared tubular NaA (LTA) zeolite membranes on porous alumina substrates. The authors indicated that hydrothermal synthesis refers to the seeding and regrowth method from clear solutions and the prepared membrane can be applied for the pervaporation of ethanol/water mixture. Sato and Nakane (2007) have developed a highly reproducible fabrication

method for high-flux NaA zeolite membranes. The authors fabricated zeolite membranes that were hydrothermally synthesized on the surface of a tubular α-alumina monolayer substrate and dip coating was employed for seeding. Pervaporation experiments for these membranes indicated higher permeate water flux (5.6 kg m^{-2} h^{-1}) and high water/ethanol selectivity (above 5000) for a feed mixture of ethanol (90 wt.%) and water mixture at 75 ^{o}C. Huang and Yang (2008) developed a high quality NaA zeolite membrane with uniform and small crystals on tubular α-alumina support by adding a small amount of tetramethylammonium hydroxide (TMAOH) in the clear synthesis solution. For the fabricated membrane, the zeolite particles were deposited on the membrane surface by adopting in-situ hydrothermal synthesis. The authors investigated upon the effect of TMAOH amount on membrane formation and permeation properties. Also, the author indicated that the membrane showed good separation selective properties due to the addition of TMAOH in the clear synthesis solution. Pera-Titus *et al*., (2008) prepared zeolite NaA membranes inside porous tubular titania (rutile) asymmetric supports. Adopting hydrothermal synthesis, the NaA layers were prepared with or without previous brush-seeding of the supports. The membranes provided very good separation capabilities to dehydrate ethanol/water mixtures during pervaporation. Recently, Ling *et al*., (2011) fabricated zeolite NaA membrane on porous tubular α-alumina supports using microwave hydrothermal treatment and the effect of seeding on the membrane synthesis was investigated.

In summary, several synthetic techniques have been used to fabricate zeolite membrane such as in-situ (without seeding) hydrothermal synthesis (Noble and Falconer 1995), secondary (seeded) growth (Xomeritakis *et al*., 2000), vapor phase transport (Kikuchi *et*

al., 1997) and post-treatments of zeolite membranes (Yan *et al*., 1997). Among different synthetic strategies reported, zeolite NaA membranes have been conventionally prepared with hydrothermal synthesis onto a porous support in one or several batch cycles involving either in situ or with a preliminary seeding step. Compared to other synthesis methods, in situ hydrothermal synthesis is very easy to implement from operational perspective. Table 1.4 presents an overview on various literatures for preparation of ceramic-ceramic composite membranes.

Table 1.4: State of the art in ceramic-ceramic composite membranes.

Support material	**Skin layer material**	**Routes of preparation**	**References**
α-Al_2O_3	Zirconia	Dip-coating	Falamaki *et al*., (2005)
α- alumina	α- alumina	Dip-coating	Yoshino *et al*., (2005)
Alumina	Zirconia	Dip-coating	Erdem *et al*., (2006)
Alumina	SiO_2 and Al_2O_3	Co-current chemical vapour deposition (CVD)	Amanipour *et al*., (2012)
Tubular ceramic support	Zeolite A	Hydrothermal treatment	Morigami *et al*., (2001)
α-Al_2O_3	NaA zeolite	Microwave heating	Xu *et al*., (2001)
Lumen (Inocermic)	Zeolite A	In-situ hydrothermal synthesis	Tiscareno-Lechuga *et al*., (2003)

Support material	**Skin layer material**	**Routes of preparation**	**References**
Alumina	A-type zeolite	Secondary growth method	Huang *et al*., (2004)
Mullite	Zeolite A	Hydrothermal synthesis	Kazemimoghadam and Mohammadi (2006)
α-Al_2O_3	Zeolite NaA	In-situ aging – microwave synthesis	Li *et al*., (2006)
α-Al_2O_3	Zeolite A	In-situ crystallization	Zah *et al*., (2006)
Alumina	NaA (LTA)	Hydrothermal synthesis	Kyotani *et al*., (2007)
α-alumina	NaA zeolite	Hydrothermal synthesis	Sato and Nakane (2007)
α- alumina	NaA zeolite	In-situ hydrothermal synthesis	Huang and yang (2008)
Titania (rutile)	Zeolite NaA	In-situ hydrothermal synthesis	Pera-Titus *et al*., (2008)
α-alumina	zeolite NaA	Microwave hydrothermal treatment	Ling *et al*., (2011)

1.5.3 Applications of membrane technology

To date, ceramic membranes have been found to be suitable in various separation applications such as desalination, industrial effluent treatment, food processing and drinking water production. Since this work attempts to fabricate low cost ceramic membranes, we consider four major applications such as treatment of industrial oily

wastewater, removal of bacteria, removal of chromium metal and separation of bovine serum albumin (BSA) from aqueous solutions. This is also due to the fact that these cases refer to standard applications for furthering the possibilities of ceramic membranes in industrial processing scenarios.

1.5.3.1 Oily wastewater treatment

Oily wastewater streams are produced from various industries including metallurgical, petrochemical, transportation and petroleum refineries. Typical compositions of these streams vary between 50 – 1000 mg/L of oil concentration (Arnot *et al*., 2000; Cumming *et al*., 2000; Mohammadi *et al*., 2004). Due to severe ecological hazard, these streams need to be treated before they are discharged. Existing environmental legislations impose a strict constraint for the discharge of oily waste water streams at a maximum grease/oil concentration of 10 – 15 mg/L (Hua *et al*., 2007; Zhou *et al*., 2010). In comparison with several conventional separation processes such as gravity separation and skimming, dissolved air flotation, de-emulsification, coagulation and flocculation, membrane separation technology is advantageous and effective at low feed concentrations (Hua *et al*., 2007) and is therefore recommended for the treatment of oily wastewaters with stable emulsions (Cheryan 1998). Further, membrane technology offers additional features such as high efficiency and low cost. So far, several studies reported experimental investigations involving microfiltration, ultrafiltration and reverse osmosis (Srijaroonrat *et al*., 1999; Mohmmadi *et al*., 2003; Ebrahimi *et al*., 2009).

Scott *et al*., (1994) studied the behavior of the cross-flow MF of stable dispersions (mean droplet size of 1 µm) using commercial MF membranes such as polysulfone, nylon,

polytetrafloroethylene (PTFE) membranes (all possessing a mean pore size of 0.2 µm) and mixed cellulose acetate/nitrate membranes of variant mean pore sizes (0.2, 0.45 and 1.2 µm). The authors reported that the polymeric membranes possessing an average pore size of 0.2 µm provided more than 90 % rejection for cross flow velocities of 3 – 4 m/s. Scott *et al*., (2001) also performed the cross flow microfiltration of water-in-oil emulsions using corrugated hydrophobic polytetrafloroethylene (PTFE) membranes with a mean pore size of 0.2 µm. The authors reported upon the effect of cross flow velocity, flow channel height and trans-membrane pressure on flux rate. For the membranes, the authors reported that an oil rejection of 100 % and permeate flux of 27 L/m^2h at a pressure and feed concentration of 0.8 bar and 30 % (w/w), respectively. Gorouhi *et al*., (2006) performed the cross flow microfiltration of oily wastewater using a polypropylene membrane with a pore size of 0.2 µm. They have obtained oil rejection and permeate flux of 89 % and 15 kg/m^2h, respectively at a pressure and feed concentration of 0.75 bar and 5 Wt.%, respectively. Li *et al*., (2006) developed a hydrophilic hollow fiber polymeric UF membrane with low fouling tendency that provided a rejection of 99.6 % at a pressure and feed concentration of 0.1 MPa and 800 mg/L, respectively for the treatment of oil water emulsions. Hao *et al*., (2008) developed crosslinked poly ethylene oxide fouling resistant membranes that provided 400 % higher water flux values than those obtained with an uncoated polysulfone membrane after 24 h of operation. The membranes also provided higher rejection of 98.5 % and permeate flux of 60 L/m^2h at a pressure and concentration of 10 bar and 1350 mg/L, respectively. Wu *et al*., (2008) studied the separation performance of oily water using poly (vinyl alcohol) membrane by cross flow ultrafiltration. The effects of operating conditions such as temperature, oil concentration,

trans-membrane pressure and cross flow velocity on the membrane permeate flux and oil retention were investigated. The authors reported that the membrane provided an oil rejection of 93 % with permeate flux of 330 L/m^2h at a pressure and feed concentration of 0.10 MPa and 242.25 mg/L, respectively.

Opposed to polymeric membranes, ceramic membranes are very attractive due their promising advantages such as resistance to chemical, thermal and biological attacks (Koruniewicz and Field 1996). Ceramic membranes are less susceptible to fouling and much more sensitive to control with respect to the operating conditions. Using both low cost and conventional ceramic membranes, several researchers have reported the performance characteristics of ceramic membranes for the treatment of oil-water emulsions.

Kottuniewicz and Field (1996) have investigated the separation performance of oil-in-water emulsions with cross flow microfiltration using both polymeric membranes (Millipore 0.45 µm and Gelman 0.1 µm) and ceramic membranes (ceramesh 0.1 µm and Membralox 0.1 µm). The authors found that the ceramic membranes provided better performance with higher and stable permeate flux. Yang *et al*., (1998) investigated the performance of ZrO_2/α-Al_2O_3 membrane with a pore size of 0.2 µm for the separation of oil-water emulsion and achieved 99.8 % of oil rejection and 93 L/m^2h permeate flux at a feed concentration of 5000 mg/L. Zhong *et al*., (2003) evaluated upon a combination of flocculation and microfiltration for the treatment of oily wastewaters. The authors reported an oil rejection of 99.8 % and permeate flux of 170 L/m^2h at a pressure and feed concentration of 0.1 MPa and 6000 mg/L, respectively. Using kaolin, Mohammadi *et al*., (2004) prepared a tubular ceramic membrane with a pore size of 10 µm for oil-water

emulsion separation application and studied the effect of operating conditions such as applied pressure, cross flow velocity and feed oil concentration on the membrane performance. Cui *et al*., (2008) reported that two different ceramic membranes (average pore sizes of 1.2 and 0.4 μm) provided an average oil rejection of 99 % and permeate flux of 36 L/m^{2}h at a pressure and feed concentration of 50 kPa and 100 mg/L, respectively. Ebrahimi *et al*., (2009) have used different MF/UF/NF ceramic membranes (average pore sizes ranging from 0.2 μm to 750 Da) for the treatment of water produced in crude oil-fields. Their studies indicated that the rejection and flux varied from 58 – 82 % and 200 – 55 L/m^{2}h, respectively for a feed concentration of 149 – 113 mg/L at a applied pressure of 1 bar. Nandi *et al*., (2010) have used a ceramic membrane for the treatment of oily wastewater and investigated upon the effect of feed concentration and operating pressure on the rejection performance of the membrane. The authors achieved an oil rejection and permeate flux of 98.8 % and 5.36×10^{-6} m^3/m^{2}s, respectively at a pressure of 69 kPa and feed concentration of 250 mg/L. At a trans-membrane pressure of 0.16 MPa, Zhou *et al*., (2010) inferred that hydrophilic nano-sized ZrO_2/Al_2O_3 composite membranes provide a very high rejection and flux of 97.8 % and 441 L/m^{2}h, respectively during the microfiltration of oily wastewater feed streams at a concentration of 1000 mg/L. Abadi *et al*., (2011) evaluated the cross flow performance of tubular ceramic microfiltration membranes with an average pore size of 0.2 μm for the MF of oily wastewaters. Their study involved the effect of operating parameters such as trans-membrane pressure, cross flow velocity and temperature on the permeate flux, total organic carbon removal efficiency and fouling resistance. The authors reported that a rejection of 85 % and permeate flux of 250 L/m^{2}h at a pressure and feed concentration of 1.25 bar and 26 mg/L,

respectively. Pan *et al*., (2012) prepared titanium dioxide dynamic membranes for the cross flow microfiltration of oil-in-water emulsions. The authors reported that the rejection of 99 % and permeate flux of 858 L/m^{2}h at a pressure and feed concentration of 0.125 MPa and 500 mg/L, respectively.

Amongst several research perspectives for the development and application of ceramic membranes for oil water separation, the development and utilization of ceramic membranes using mixed clays is attractive owing to their low cost. Table 1.5 summarizes data obtained for the membrane based treatment of oil water emulsions.

Table 1.5: A summary of the literature reported membrane performance characteristics for the treatment of oil-water emulsions.

Membrane	**Feed concentration (mg/L)**	**Rejection (%)**	**Flux (L/m^{2}h)**	**Pressure (bar)**	**Reference**
Polysulfone, nylon, polytetrafloroethylene (PTFE)	-	90	-	-	Scott *et al*., (1994)
Hollow fiber cellulose UF membrane	800	99.6	-	1	Li *et al*., (2006)
Poly ethylene oxide	1350	98.5	60	10	Hao *et al*., (2008)
poly (vinyl alcohol) membrane	242.25	93	330	1	Wu *et al*., (2008)
ZrO_2/Al_2O_3	1000	97.8	441	1.6	Zhou *et al*., (2010)

Membrane	**Feed concentration (mg/L)**	**Rejection (%)**	**Flux (L/m^2h)**	**Pressure (bar)**	**Reference**
γ-Al_2O_3/α-Al_2O_3	5000	99.8	18	1	Yang *et al.*, (1998)
α-Al_2O_3/α-Al_2O_3	5000	99.9	22	1	Yang *et al.*, (1998)
α-Al_2O_3/α-Al_2O_3	5000	94.3	27	1	Yang *et al.*, (1998)
ZrO_2/α-Al_2O_3	5000	99.8	93	1	Yang *et al.*, (1998)
ZrO_2	6000	99.8	170	1	Zhong *et al.*, (2003)
Kaolin	3000	-	-	2	Mohammadi *et al.*, (2004)
NaA/α-Al_2O_3	100	98.8	36	0.5	Cui *et al.*, (2008)
NaA/α-Al_2O_3	500	99.5	31	0.5	Cui *et al.*, (2008)
Al_2O_3	179	59	200	1	Ebrahimi *et al.*, (2009)
Al_2O_3	149	58	200	1	Ebrahimi *et al.*, (2009)
Mixed clay ceramic membrane	250	98.8	19.3	0.69	Nandi *et al.*, (2010)
α-Al_2O_3	26	85	250	1.25	Abadi *et al.*, (2011)
Carbon/ titania	500	99	858	1.25	Pan *et al.*, (2012)

1.5.3.2 Removal of bacteria (*E. coli*)

In the past decade, membrane technologies have been identified to be important for the production of potable water and treated wastewater streams. Bacteria contamination either in food or drinking water is very dangerous from health perspective. Henceforth, the elimination/removal of microorganisms such as algae, fungus, bacteria and virus are of major concern for the production of high quality medical and drinking water. Membrane separation processes including microfiltration (MF) and ultrafiltration (UF), have been addressed by few authors for the removal of microbes (Ghayeni *et al*., 1999; Judd and Till 2000). The increasing use of membrane technology for water and wastewater treatment might be due to stringent water quality regulations that cannot be effectively achieved by conventional treatment processes. Further, lower processing costs offered by membrane technology due to rapid technological advances in both membrane materials and configurations is promising. Conventional treatment processes for water treatment include chemical addition (aluminium sulphate, lime, and polymers), coagulation, sedimentation, filtration and disinfection. These processes are based on the principles of physical separation and chemical effect. However, they do not ensure higher confidence levels with respect to the separation efficiency or removal of microbes from water streams. On the other hand, microfiltration/ultrafiltration can provide a complete removal of most bacteria and all protozoan cysts as long as the membrane and associated system components are intact and operating efficiently. Virus removal is also achievable using ultrafiltration (Arkhangelsky and Gitis 2008).

An Escherichia coli (*E. coli*) is a famous bacterium that lives in all lower digestive tracts of human beings. However, problems arise when humans ingest antibiotic resistant

E. coli into their upper digestive tract. It can cause a deadly infection. The average cell *E. coli* is about 2 µm long. Microscopic bacteria are sometimes round, sometimes rod-shaped and sometimes spiral and they are in the size range of 2 – 3 µm. Few articles demonstrate the removal of *E. coli* using membrane filtration. Kobayashi *et al*., (1998) have reported the complete removal efficiency (100 %) of *E. coli* using polyacrylonitrile (PAN) ultrafiltration membranes at a feed concentration of 10^7 CFU/mL. Judd and Till (2000) performed the cross-flow microfiltration of sewage for bacteria (*E. coli*) removal using low cost-polypropylene microfiltration membranes. The authors reported LRV of 0.5 at a feed concentration of 6.03×10^6 cells/mL. The role of cell-wall structure for the retention of bacteria using polycarbonate track-etched microfiltration membranes (pore size of 0.4 µm) was investigated by Lebleu *et al*., (2009). Their result indicated that the removal of *E. coli* is 3.2 LRV at a feed concentration of 10^4 CFU/mL. In another work, Lebleu *et al*. (2010) studied bacterial retention of *E. coli* using cellulose ultrafiltration membrane. They achieved around 7 LRV with a feed concentration of 10^4 CFU/mL. Their work also demonstrated the respective roles of skin and support layers of an ultrafiltration membrane in the retention mechanisms of bacteria. In contrast to polymeric membranes ceramic membranes have a stronger application potential because of their higher chemical, thermal and mechanical stability. Based on these excellent membrane characteristics back-flushing methods can be used to regenerate the fouled membrane without affecting the membrane surface. In addition, ceramic materials do not show any swelling behaviour as observed for few polymers. Till date, only few literatures are available for the removal of bacteria using ceramic membranes.

Table 1.6: Literature data for the separation of bacteria (*E. coli*) using polymeric and ceramic membranes.

Membrane/ pore size	Strain	Feed concentration	Removal	Reference
Polyacrylonitrile ultrafiltration membrane (PAN)	*E. coli*	10^7 CFU/mL	100 %	Kobayashi *et al*. (1998)
Polypropylene / 0.45 µm	*E. coli*	6.03×10^6 cells/mL	0.5 LRV	Judd and till (2000)
Polycarbonate track-etched membrane	*E. coli*	10^4 CFU/mL	3.2 LRV	Lebleu *et al*., (2009)
Cellulose ultrafiltration membrane	*E. coli*	10^4 CFU/mL	~ 7 LRV	Lebleu *et al*., (2010)
Titanate nanotube	*E. coli*	4×10^6 CFU/mL	100 %	Zhang *et al*., (2009)

Kroll *et al*. (2010) prepared zirconia ceramic microtubes by extrusion method for bacteria filtration. Their studies indicated that the obtained microporous ZrO_2 microtubes with antibacterial functionalisation are highly promising candidates for the design of sustainable bacteria filtration processes. Zhang *et al*., (2009) prepared the titanate nanotube filtration membrane for the removal of waterborne pathogens using *E. coli* as test species at a feed concentration of 4×10^6 CFU/mL to obtain 100 % removal of *E. coli* for all experimental investigations. Table 1.6 summarizes the results obtained by various authors for the separation of bacteria with polymeric and ceramic membranes. The existence of very few literatures in the field of bacteria removal using ceramic

membranes indicates that emphasis shall be towards the development and application of ceramic membranes for the separation of microbes.

1.5.3.3 Removal of chromium metal

The presence of heavy metals such as chromium, copper, lead, nickel etc., in wastewater is hazardous to the human health and environment. Large quantities of chromium containing wastewater generated from various processes industries such as leather tanning, pigment and metallurgical industries need to be treated before discharge into the natural water bodies. In the tanning industry, chromium (III) salts are employed for tanning the raw hides and skins. Thereby, significant quantity of the unused metal is discharged in the waste streams containing chromium metals. The existence of chromium metal in wastewaters is well known for its toxicity to living organisms. Further, it also causes allergies, eczema, irritations and respiratory track disorders (Katz and Salem 1993; Kotas and Stasicka 2000). Generally, chromium element exists mainly in two oxidation states, Cr (III) and Cr (VI). Between the two forms, Cr (VI) is the most toxic. The World Health Organization recommended that the maximum allowable concentration in drinking water for total chromium should be 0.05 mg/L. The discharge of Cr (VI) to surface water is regulated to below 0.05 mg/L by USEPA and European Union, while total Cr, Cr (III), Cr (VI) and other forms are usually regulated to below 2 mg/L.

Conventional treatment technologies for the removal of heavy metals and chromium ions from waste streams including coagulation, adsorption, electrochemical treatment and ion exchange are often uneconomical with difficulties in operational feasibilities. Moreover,

the final metal recovery requires additional treatments, which complicate the process. During the past decade, the application of membrane filtration for chromium removal has been constantly increasing due to its inherent separation capabilities for the removal of heavy metal. Membrane filtration processes such as ultrafiltration and nanofiltration have been widely studied for the removal of chromium metal.

Hafiarle *et al*., (2000) investigated the removal of hexavalent chromium by nanofiltration and the process was investigated as a function of ionic force and pH. The authors concluded that the nanofiltration is a very promising method for wastewater charged with hexavalent chromium and achieved 80 % of rejection at a feed concentration of 1 mM. Cengeloglu *et al*., (2003) investigated the transport of hexavalent chromium through ion-exchange membranes. The effect of salt solutions on the transport of chromium (VI) was investigated. Their results inferred that the chromium (V1) transport through anion exchange membranes depends on the nature of the electrolyte solution. The authors obtained a removal of 99 % at a feed concentration of 0.01M. Arthanareeswaran *et al*., (2007) conducted ultrafiltration process for the removal of chromium metal from aqueous solution using cellulose acetate and sulfonated poly(ether ether ketone) ultrafiltration membranes. Their study demonstrated the role of various factors that affect the percentage rejection and permeate flux. These include pH, concentration of solute, concentration of PVA, transmembrane pressure and composition of blend membranes. The authors obtained a rejection of 93 % at a feed concentration of 200 mg/L. Ren *et al*., (2010) performed nanofiltration for the removal of chromium (VI) from wastewater using asymmetric poly (*m*-phenylene isophthalamide) membranes.

Table 1.7: Performance characteristics of membrane technology for chromium removal from synthetic wastewater solutions.

Membrane	**Method of filtration**	**Feed concentration (mg/L)**	**Rejection (%)**	**References**
CA/SPEEK	Dead-end UF	200	93	Arthanareeswaran *et al*., (2007)
Poly (m-phenylene isophthalamide) (PMIA)	NF	5	98	Ren *et al*., (2010)
polysulfone	Polymer enhanced UF	10	100	Aroua *et al*., (2007)
γ-Al_2O_3	Combined adsorption-permeation process	0.5	99.9	Pagana *et al*., (2008)
polyacrylonitrile	Polyelectrolyte enhanced UF	5 and 50	100	Korus and Loska (2009)
α-Al_2O_3/γ-Al_2O_3	Combined adsorption-permeation process	0.5	90	Pagana *et al*., (2011)

The authors conducted the separation experiments on chromium (VI) solution at variant operating conditions of feed concentration, applied pressure and pH and. The authors reported the removal of above 98 % at a feed concentration of 5 mg/L. On the other hand, microfiltration has been applied in several studies for the removal of chromium ions in

integrated processes. Aroua *et al*., (2007) employed a polymer-enhanced UF system to remove Cr (III) and Cr (VI) from aqueous solution using polysulfone ultrafiltration membranes. The authors evaluated 100 % chromium removal for a concentration of 10 mg/L. Pagana *et al*., (2008) proposed a novel scheme of combined adsorption-ultrafiltration (AUF) process for the removal of chromium from water using nano-sized Fe_2O_3 adsorbent and γ-Al_2O_3 ultrafiltration membranes (average pore diameter of ~3 – 4 nm) and achieved 99.9 % rejection for a feed concentration of 0.5 mg/L. Korus and Loska (2009) used a polyelectrolyte-assisted UF system to study the removal of chromium ions from aqueous solution and observed very high Cr (VI) (100 %) removal efficiency at a pH of 6 for feed concentrations of 5 and 50 mg/L, respectively. In another work, the authors Pagana *et al*., (2011) studied an innovative adsorption-membrane process for the removal of chromium ions and achieved 90 % removal efficiency at a feed concentration of 0.5 mg/L.

On the other hand, the use of biosorbent or biomass has been reported to be cost effective for the removal of heavy metals due to the fact that biomass can be obtained and recycled from various fermentation industries (Volskey 1990). The utilization of non-living biomass has many advantages in comparison to the living biomass. These refer to greater binding capacities of dead biomass with toxic metals and ease of availability from numerous fermentation industries. It is well known that the yeast cells can uptake heavy metals from aqueous solution in various operating conditions and can be successfully applied for the removal of heavy metals from wastewater streams (Norris and Kelly 1977; Huang *et al*., 1990)

Brady *et al*., (1976) investigated the removal of heavy metals bound with yeast cells using hollow fiber cross-flow microfiltration. Recently, Bayhan *et al*., (2001) reported the removal of divalent heavy metal mixtures (Ni^{2+}, Cu^{2+}, Pb^{2+}) using yeast (*saccharomyces cerevisiae*) and membrane filtration (anisotropic cellulose acetate membrane with an average pore size of 0.2 µm). The authors achieved higher rejection and flux for Pb in comparison with other metals (Cu and Ni).

1.5.3.4 Separation of bovine serum albumin (BSA)

Protein purification is a topic of profound significance in the field of bioseparation engineering, food and medical applications. Protein separation from fermentation broth or tissue extract is a challenging task. Conventional separation processes such as centrifugation, precipitation, chromatography and electrophoresis are labor-intensive processes. For this application, with recent developments in the field of separation technology, membrane filtration is attractive and promising due to its high separation efficiency and less operating cost. Ultrafiltration using membranes is one of the commonly used processes for the purification of proteins. Various membranes such as polymeric, ceramic and polymeric ceramic composite membranes have been used for the separation of protein particularly bovine serum albumin using ultrafiltration. Gosh and Cui (1998) studied the separation of bovine serum albumin (BSA) using polysulfone polymeric membrane (50 kDa MWCO) by ultrafiltration. The membrane has been evaluated to provide a rejection and flux of 99.5 % and 3.34×10^{-3} kg/m^{2}s, respectively at a feed concentration and pH of 500 mg/L and 8.8, respectively. Becht *et al*., (2008) conducted the ultrafiltration experiment using polysulfone (50 kDa MWCO) membrane

in both dead-end and cross flow mode for the separation of bovine serum albumin (BSA). The experiments were carried out with a feed concentration of 500 mg/L at a trans-membrane pressure of 25 kPa. The authors obtained a maximum rejection and permeate flux of 90 % and 60 L/m^{2}h, respectively at a pH of 4.9 for dead-end ultrafiltration. During cross flow MF, the membrane provided 100 % rejection and permeate flux of 70 L/m^{2}h at a pH of 8.4. Few other researchers have studied ceramic membranes for BSA separation.

Table 1.8: State of the art for membrane based separation of bovine serum albumin (BSA).

Membrane	**Feed concentration (mg/L)**	**Permeate flux (m^3/m^2s)**	**Rejection (%)**	**References**
Polysulfone	500	1.66×10^{-5}	90	Becht *et al.*, (2008)
Polysulfone	500	1.94×10^{-5}	100	Becht *et al.*, (2008)
Ceramic membrane	100	-	100	Almecija *et al.*, (2007)
cellulose acetate-ceramic composite membrane	1000	12.2×10^{-3}	50	Nandi *et al.*, (2009)
Silica membrane	500	-	98.64	Fakhfakh *et al.*, (2010)
Silica membrane	500	-	78.33	Fakhfakh *et al.*, (2010)

Almecija *et al*., (2007) used ceramic tubular membrane (300 kDa) for the fractionation of whey protein solution that contained 100 mg/L of BSA. The authors conducted cross flow ultrafiltration experiments for varied pH values and have evaluated that the bovine serum albumin was completely retained by the membrane. Nandi *et al*., (2009) prepared cellulose acetate-ceramic composite membranes for the dead-end ultrafiltration of bovine serum albumin (BSA). They obtained a maximum rejection and permeate flux of 50 % and 12.2×10^{-3} m^3/m^2s, respectively at a pressure and feed concentration of 345 kPa and 1000 mg/L, respectively. Fakhfakh *et al*., (2010) prepared two different silica ceramic membranes for the separation of BSA from its synthetic solution. The filtration experiments were carried out in a cross flow mode with feed concentration of 500 mg/L. The obtained results indicated that a maximum rejection of 78.33 % and 98.64 % for the membranes.

Table 1.8 summarizes the data presented in literatures for the separation of bovine serum albumin (BSA) using membrane filtration.

1.6 Scope for further research

A critical insight into various summarized applications for ceramic membranes presented in section 1.4 infers that ceramic membranes have been widely utilized for microfiltration and ultrafiltration applications and also as supports for the fabrication of polymer-ceramic composite membranes for reverse osmosis applications. Based on the existing trends in the literature, the following areas of research have been identified to be of immense relevance for promoting the industrialization of low cost ceramic membranes.

1.6.1 Preparation and characterization of low cost ceramic membranes

Table 1.3 summarizes various important research findings in the area of low cost ceramic membrane preparation and characterization. It can be observed that ceramic membrane research has been primarily addressing the fabrication of α-alumina membranes that are expensive due to higher cost of the inorganic precursors and sintering temperature. Using alumina precursors, the average pore size of various fabricated membranes is in the range of 0.1 – 0.7 µm. Moreover, the sintering temperature used for fabricating alumina membrane is in the range of 1100 – 1600 ^{o}C. Further, the literature data indicates that membrane fabrication research was also carried out using low cost clay based raw materials such as cordierite, apatite, moroccan clay, kaolin and doloma, algerian clay, fly ash and tunisian natural material. Even though, these raw materials are inexpensive, the sintering temperature and pore size of fabricated membranes are 0.9 – 28 µm and 1100 – 1275 ^{o}C, respectively. Therefore, ongoing research should target the fabrication of low cost ceramic membranes using (a) low cost precursors such as kaolin (b) lower sintering temperature (below 1000 ^{o}C) and (c) simple fabrication technique (such as uniaxial dry compaction method). Similarly, MF membrane possessing submicron range average pore size (0.1 – 0.5 µm) using low cost precursors and sintering temperature lower than 1000 ^{o}C also needs to be addressed. The larger (1 – 5 µm) and smaller (0.1 – 1 µm) pore size possessing low cost MF membranes could potentially serve as inexpensive supports for MF and UF applications.

1.6.2 Preparation of ceramic-ceramic composite membranes

Table 1.4 presents the summary of literature survey for the preparation of ceramic-ceramic composite membranes. It can be noted that several literatures addressed the fabrication of ceramic-ceramic composite membranes using expensive α-alumina as a support material. Moreover, most of the work indicates that alumina, silica, titania and zirconia were used as a skin layer material. Except titania, skin layer materials such as alumina, silica and zirconia are not the preferred choice for the preparation of low cost composite membranes due to their higher cost. Under these circumstances, future research for the fabrication of inexpensive ceramic-ceramic composite membrane should target (a) utilization of kaolin based low cost ceramic support instead of alumina based support to reduce the cost of the composite membrane. (b) Use of low cost skin layer materials such as kaolin, zeolite and fly ash etc., (c) simpler membrane preparation methods for manufacturing to minimize the cost. These approaches could identify potential pathways to furthering the industrial competitiveness of the ceramic-ceramic composite membranes.

1.6.3 Applications of low cost ceramic membranes

For low cost ceramic membranes, microfiltration and ultrafiltration processes targeting wastewater treatment are promising. Amongst various wastewater treatment processes, low cost ceramic membranes have the edge to treat oil-water emulsions, separate chromium from synthetic solutions, separate bacteria from its solution and separate bovine serum albumin from aqueous solution. Thus, these potential applications adopt microfiltration application due to higher average pore size of the ceramic membrane.

Below a brief overview of the possible scope for further research is presented in these three fields of wastewater treatment.

1.6.3.1 Treatment of oil-water emulsions

Most of the research work addresses the treatment of oily wastewater using polymeric membranes such as poly vinyl alcohol, polyvinylidene fluoride, PTFE, polypropylene, poly ethylene oxide, polysulfone, nylon and polytetrafloroethylene (Table 1.5). Later, ceramic membranes have been as well studied for the treatment of oily wastewater using expensive membranes such as alumina and zirconia. In this context, the use of low cost ceramic membranes for the treatment of oily wastewater would be beneficial for industrial applications. Moreover, most of the literatures addressed the treatment of oily wastewaters for feed oil concentrations in the range of 500 – 6000 mg/L. The higher feed concentrations refer to unstable oil droplets. In these emulsions, droplets with sizes higher than 50 µm can be easily removed. However, lower droplet sizes (less than 50 µm) exist for feed with oil concentrations below 100 mg/L which are highly stable. Therefore, the separation of stable oil droplets a challenging task. For such a complicating scenario, ceramic membrane technology could be beneficial. To the best of our knowledge, the applicability of low cost membranes made from inexpensive raw materials to treat the oily wastewater consisting of oil concentrations less than 250 mg/L has not been studied till date. This work aims at studying the treatment of oily wastewater using kaolin based low cost ceramic membranes. For the treatment of oily wastewater, both dead end and cross flow microfiltration studies need to be targeted in this work to further the applicability of inexpensive membrane technology for wastewater treatment.

1.6.3.2 Removal of bacteria (*E. coli*)

A critical insight into the literatures presented in Table 1.6 infers that mainly polymeric membranes have been used for the removal of bacteria. This is due to the fact that polymeric membranes are inexpensive in comparison with the ceramic membranes. However, the polymeric membranes are susceptible to biological attacks. To best of our knowledge, the applicability of ceramic membranes for the removal of bacteria has not been studied so far. For these circumstances, the usage of low cost ceramic membranes for the removal of bacteria (*E. coli*) shall be beneficial for the production of bacteria free drinking and medical water. With the objective of bacteria filtration using low cost ceramic membranes, this work aims to identify the separation potential and fouling characteristics of low cost ceramic membranes.

1.6.3.3 Removal of chromium (VI)

Table 1.7 summarizes various literatures for the removal of chromium metal from waste streams. A critical insight into these literatures infers that mainly membrane filtration such as ultrafiltration (UF) and nanofiltration (NF) have been studied during experimental investigations. However, UF/NF provides lower permeate flux and higher fouling in comparison with the microfiltration (MF) process. Therefore, microfiltration shall be beneficial in terms permeate flux and longer shelf life for industrial application. In general, the microfiltration for the removal chromium metals is typical carried out using various processes such as polymer enhanced microfiltration, micelle enhanced microfiltration and combination of adsorption and membrane permeation process. However, the cost of the polymer or polyelectrolyte is very high. Therefore, alternative

low cost binding agent needs to be addressed to reduce the cost of operation. In our work, we intend to carry out the microfiltration of chromium metal using baker's yeast as a binding agent in order to get good performance (permeate flux and rejection) and reduce the cost of microfiltration.

1.6.3.4 Separation of BSA using low cost ceramic-ceramic composite membranes

While several applications have been proposed for ceramic-ceramic composite membranes, the separation of BSA from its synthetic solution is a typical task that is investigated to evaluate the separation capabilities of ceramic-ceramic composite membranes. Table 1.8 summarizes various literatures for the separation of bovine serum albumin (BSA) by membrane filtration. The table indicates that the applicability of ceramic-ceramic composite membranes has not been studied so far. This is due to the reason that developed ceramic-ceramic composite membranes with narrow pore-size distributions could make protein separation a feasible choice. Therefore, this work attempts to study the applicability of LTA zeolite ceramic composite membranes for the separation of bovine serum albumin (BSA).

1.7 Objectives of the thesis

Based on the state of the art presented in sections 1.5, the thesis addresses the following major objectives that have been identified in the earlier section:

1. Preparation and characterization of low cost ceramic supports with in the average pore size range of 1 – 5 µm.
2. Preparation and characterization of micron range microfiltration membranes.

3. Dead end microfiltration of oil-water emulsions using fabricated low cost ceramic membranes.
4. Dead end microfiltration of bacterial solutions.
5. Development of microfiltration based process for the removal of chromium from its synthetic solution.
6. Cross-flow microfiltration of oil-in-water emulsions using low cost ceramic membranes.
7. Preparation, characterization and applications of LTA zeolite composite membranes. These membranes need to be fabricated with the developed inexpensive ceramic supports.
8. Dead end microfiltration of bovine serum albumin (BSA).

1.8 Organization of the thesis

Chapter 2 presents a detailed account of the preparation and characterization of low cost ceramic support using inexpensive raw materials. The functional attributes of raw materials, support preparation method are summarized. Subsequently, the influence of sintering temperature on various support properties such as average pore size, porosity, flexural strength, corrosion resistance and hydraulic permeability have also been addressed.

Chapter 3 addresses the preparation and characterization of micron range microfiltration membranes. The effect of sintering temperature on the membrane properties such as porosity, average pore size, flexural strength, corrosion resistance and hydraulic permeability have been studied. In addition to these characterization efforts, the

separation efficiency of the prepared membrane was tested for the treatment of oil-water emulsions, bacteria filtration and chromium metal separation applications.

Chapter 4 summarizes the preparation and characterization of microfiltration membranes using three different compositions of raw materials which are obtained by the addition/removal of TiO_2/$CaCO_3$ to the previously identified compositions. The effect of compositions of raw materials on the membrane properties was tested. Subsequently, the fabricated membranes were applied for the treatment of oil-water emulsions in dead-end filtration mode.

Chapter 5 elaborates upon the cross flow microfiltration of oil-water emulsions using fabricated kaolin based low cost membranes. Subsequently, the flux decline phenomena along with the identification of suitable membrane fouling mechanism have been targeted.

Chapter 6 addresses the preparation and characterization of LTA zeolite membrane by in-situ hydrothermal crystallization. The prepared membrane was investigated for its separation efficiency for bovine serum albumin (BSA).

Chapter 7 presents a summary of conclusions of the addressed research work. Finally, the scope for further research in the future has been outlined.

Chapter 2:

Preparation and Characterization Of Low Cost Ceramic Membrane Supports

Chapter 2

Preparation and Characterization of Low Cost Ceramic Membrane Supports

This chapter addresses the fabrication of low cost ceramic membrane supports (A1 – A3) using inexpensive inorganic precursors. A trial and error based approach was adopted to identify new composition of raw materials. These compositions were used to fabricate ceramic membrane supports by following uniaxial compaction method. Lower sintering temperature range (900 – 1000 ^{o}C) was used to fabricate the support. The optimal sintering temperature was identified based on best combinations of various membrane properties. The characteristics of the prepared support were evaluated by performing structural and morphological studies. Pure water permeation experiments were carried out to evaluate the membrane performance. Corrosion resistance and flexural strength tests were conducted to identify the chemical and mechanical stability of the supports. Eventually, the cost analysis of the fabricated support was carried out to compare its cost with the data available in the literature.

2.1 Experimental

2.1.1 Inorganic precursors

The choice of raw materials and their relative composition is very important to achieve defect free membranes. The structural and morphological properties of a membrane are largely dependent upon the raw materials used and hence the selection of raw materials and their composition is very important.

Table 2.1: Summary of identified inorganic raw material compositions for (A1 – A3) ceramic membranes fabrication.

Raw Materials	**Composition (wt. %)**
Kaolin	40
Quartz	15
Calcium carbonate	25
Sodium carbonate	10
Boric acid	5
Sodium metasilicate	5

In this work, several low cost raw materials were selected to fabricate membrane supports and. A summary of selected raw materials and their composition is presented in Table 2.1. Kaolin and sodium metasilicate were obtained from CDH India; quartz was procured from Research Lab Fine Chem. Industry, India; calcium carbonate, boric acid and sodium carbonate were obtained from Merck (I) Ltd. All these raw materials were used without further purification. Different raw materials used in this work for the preparation of ceramic supports serve for different functional attributes. While kaolin provides low plasticity and high refractory properties for the support, quartz increases mechanical and thermal stability of the supports. On the other hand, calcium carbonate and sodium carbonate contribute to the pore texture in the ceramic supports. Further, boric acid acts as a colloidal agent and improves dispersion properties of the inorganic raw materials. Similarly, sodium metasilicate acts as a binding agent and enables achieving higher mechanical strength in the ceramic membrane supports. The final composition reported in this work is obtained with a trial and error based approach using various ratios of

inorganic raw materials. The reported precursor formulations in Table 2.1 enabled the fabrication of defect free membranes with good permeation, pore size distribution and porosity characteristics.

2.1.2 Fabrication of membrane supports

The procedure for support fabrication is depicted in Fig. 2.1. The raw materials (Table 2.1) at their specified compositions were mixed with 4 mL of 2 wt.% aqueous polyvinyl alcohol (PVA, Mol.wt. 72,000, Loba chemicals Ltd., India) in a ball mill at 40 rpm for 20 min. The resulting powder was then sieved using 30 mesh standard screen. Eventually, the requisite amount was compacted at a pressure of 50 MPa using a stainless steel mould that was designed for single ended pressing. The obtained circular disk-shaped green supports having 62 mm diameter and 5 mm thickness were subjected to two step drying processes. The supports were first dried at 100 ^{o}C for 24 h and then dried at 200 ^{o}C for 24 h in a hot air oven. The above controlled drying process ensures maximum removal of moisture and also reduces possibilities for thermal stress. Subsequently, the supports were sintered at different temperatures (900 – 1000 ^{o}C) for 6 h with a heating rate of 2 ^{o}C/min in a muffle furnace. During sintering, the supports were placed vertically over the grooves of an insulated brick to ensure uniform sintering. The rate of heating in muffle furnace was kept low to minimize the possibility of bending due to radiation shock waves. After sintering, the supports dimensions (thickness, diameter, and volume) were measured to calculate the shrinkage. The rigid and porous sintered supports were finally polished on both sides using silicon carbide abrasive paper (No. C – 220) to obtain ceramic supports possessing a uniform smooth surface.

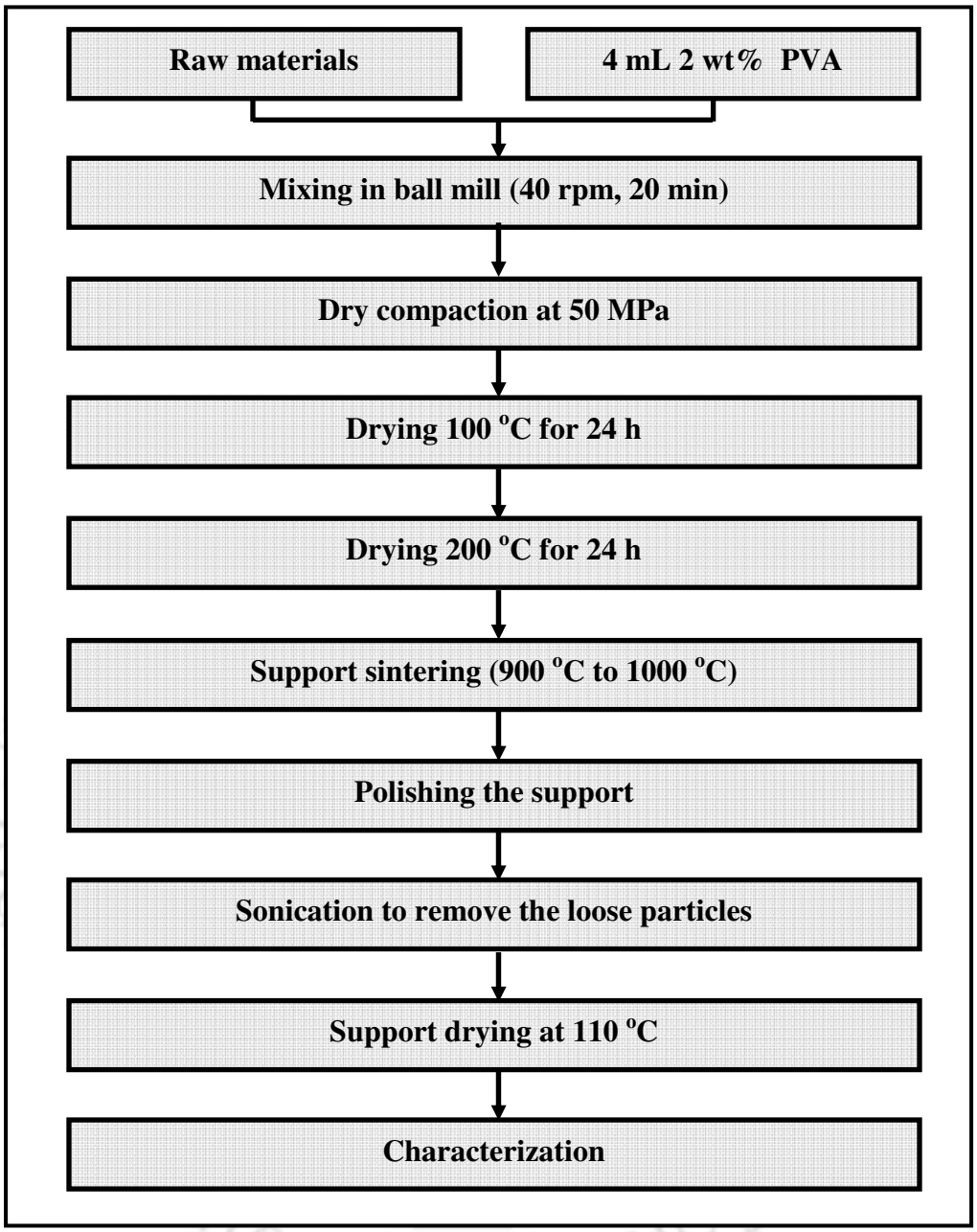

Figure 2.1: Schematic for the preparation of low cost ceramic membrane supports (A1 – A3).

Subsequently, the ceramic supports were cleaned with Millipore water in an ultrasonic bath [Model: T460; Make: Elma (India)] for 15 min to remove loose particles created during polishing.

In summary, membrane supports A1, A2 and A3 were fabricated using sintering temperatures of 900, 950 and 1000 ^{o}C, respectively.

2.1.3 Characterization techniques

The characterization procedures for raw materials and prepared supports include particle size distribution (PSD), thermogravimetric analysis (TGA), X-ray diffraction analysis (XRD), surface morphology using scanning electron microscope (SEM) and field emission SEM (FE-SEM), shrinkage determination, porosity and pore density evaluation, mechanical and chemical stability and pure water permeation test.

2.1.3.1 Particle size distribution of the raw materials

The size distribution of raw materials significantly influence membrane properties such as porosity and pore size. Therefore, the particle size distribution (PSD) of the raw materials was carried out using particle size analyzer (Model: APA 5005® hydro MU, Malvern Mastersizer 2000; Make: Malvern Instruments, Worcestershire, U.K.) in wet dispersion mode.

2.1.3.2 Thermogravimetric analysis

Thermogravimetric analysis was carried out to identify the thermal degradation behavior of raw materials and minimum sintering temperature required for support fabrication. The thermogravimetric analysis (TGA) was carried out from 25 – 950 ^{o}C using thermogravimetric analyzer (Model: TGA/SDTA 851®; Make: Mettler Toledo, Schwerzenbach, Switzerland) under N_2 atmosphere at a heating rate of 10 ^{o}C/min.

2.1.3.3 XRD analysis

The XRD analysis of the ceramic supports was conducted to evaluate the extent of phase transformations and crystallinity. The analysis was performed with XRD instrument (Model: Bruker AXS instrument, Make: Karlsruhe, Germany) using CuKα (1.5406 Å) radiation. The instrument was operated at 40 kV and 40 mA. The patterns were acquired for 2θ range of 5^{o} – 75^{o} with a scan speed of 0.05 ^{o}/s.

2.1.3.4 SEM analysis

The morphological study of membrane supports was performed using variable pressure digital scanning electron microscope (Model: LEO 1430VP®, Make: Oxford). The primary objective of the SEM analysis was to identify the morphology of the membrane surface and evaluate the surface pore size and pore density of the membrane. The pore size distribution and average pore diameter of the sintered supports was estimated from SEM micrographs using ImageJ software (open source software provided by National Institute of Health (NIH), Internet Link: http://rsbweb.nih.gov/ij/download.html). Individual pore diameters were measured for about 500 pores from SEM images. Subsequently, the average pore diameter (d_s) has been calculated using following expression:

$$d_s = \left[\frac{\sum_{i=0}^{n} n_i d_i^2}{\sum_{i=0}^{n} n_i} \right]^{0.5} \qquad (2.1)$$

where n is the number of pores, d_i is the pore diameter (μm) of i^{th} pore.

2.1.3.5 Porosity

The average membrane porosity was determined using Archimedes' principle, in which the membrane was first dried in hot air oven at 110 ^{o}C for 6 h to remove moisture and its dry weight (W_1) was determined. It was then immersed and kept in water for 24 h. After that, the membrane support was taken out from water and water on the outer surface was removed using tissue paper. Finally the wet weight of the membrane (W_2) was measured. The porosity of the support was determined using the expression

$$\varepsilon(\%) = \left[\frac{W_2 - W_1}{\rho_{water}}\right] \times \frac{100}{v_{mem}} \tag{2.2}$$

where W_2 & W_1 are the wet and dry weight of supports, ρ_{water} is the density of water and v_{mem} is the volume of the membrane support

2.1.3.6 Shrinkage Measurement

The shrinkage of the membrane support was evaluated using the dimensions (diameter, thickness) of the support before and after sintering. The dimensions were measured using a vernier caliper and a screw gauge.

2.1.3.7 Mechanical stability

The mechanical stability of the support was evaluated by measuring its flexural strength. The flexural strength of the support was measured with three point bending method on 55 mm × 5 mm × 5 mm rectangular bars using Universal Testing Machine (Model: DUTT-101, Make: M/s Deepak Polyplast, Mumbai, India). A span length of 50 mm and cross

head speed of 0.5 mm/min was used. The flexural strength of the supports sintered at various temperatures has been estimated using the expression.

$$\sigma_{fl} = \frac{3FL}{2bt_s^{\,2}} \tag{2.3}$$

where σ_{fl} is the flexural strength (MPa), F is the load at the fracture point (kN), L is the span length (mm), b is the width of the sample (mm), and t_s is the thickness of the sample (mm).

2.1.3.8 Chemical stability

The chemical stability of the membrane was evaluated by placing the support individually in acidic (HCl; pH = 1) and alkaline solutions (NaOH; pH = 14). The chemical stability was measured in terms of mass loss before and after corrosion. To do so, the membranes were placed in acid and alkali solution for 24 h at atmospheric condition. Subsequently, the supports were taken out from the solution, washed with double distilled water and dried at 110 ^{o}C for 6 h. The mass loss of the supports characterizes the chemical stability. The chemical stability of the support was also evaluated with the permeation method (Fig. 2.2) using HCl (pH=1) and NaOH (pH=14) solutions individually. For this purpose, after measuring the pure water flux, the initial dry weight of the support was measured. Subsequently, acid and alkali solutions were passed through the support separately at a pressure of 69 kPa for ten consecutive runs. After these experiments, the support was taken out, washed and dried to measure the weight of the support. Eventually, the pure water flux of the support was measured to evaluate the enhancement in the membrane hydraulic permeability.

2.1.3.9 Pure water permeation test

A workshop fabricated dead end filtration setup made up of stainless steel (capacity 250 mL) was used for the determination of water flux and hydraulic permeability. The experimental setup (Fig. 2.2) used for pure water permeation test consists a cylindrical top part and a base plate with a provision to host the membrane. The membrane was placed on a perforated casing and placed in the bottom compartment. Subsequently, both compartments were sealed to conduct permeation experiment. For this purpose, the upper compartment of the batch cell was pressurized using N_2 gas at a set desired pressure using the regulator connected to the nitrogen cylinder. Before permeation studies, the supports were compacted at high pressure using Millipore water to remove any loose particles present in the pore path. Eventually, the water flux was measured at different applied pressures 69, 138, 207, 276 and 345 kPa. At each applied pressure, the collection of first 50 mL was discarded and time taken for collection of second 50 mL of water was measured to calculate the water flux. The hydraulic permeability (L_h) and average pore radius (r_l) of the support were determined according to the following expression (Almandoza *et al*., 2004)

$$J_v = \frac{\varepsilon r^2 \Delta P}{8\mu\tau l} = L_h \Delta P \qquad (2.4)$$

where J_v ($m^3\ m^{-2}\ s^{-1}$) is the liquid flux through the membrane, ΔP (kPa) is the trans-membrane pressure drop across the membrane, μ is the viscosity of water, τ is the tortuosity factor, *l* is pore length, ε is the porosity of the support. The reported water flux values were average of four different readings and the time dependent flux data was regressed as a straight line to obtain hydraulic permeability. All these quantitative

experiments were conducted for at least four different membrane samples to evaluate the pure water flux characteristics.

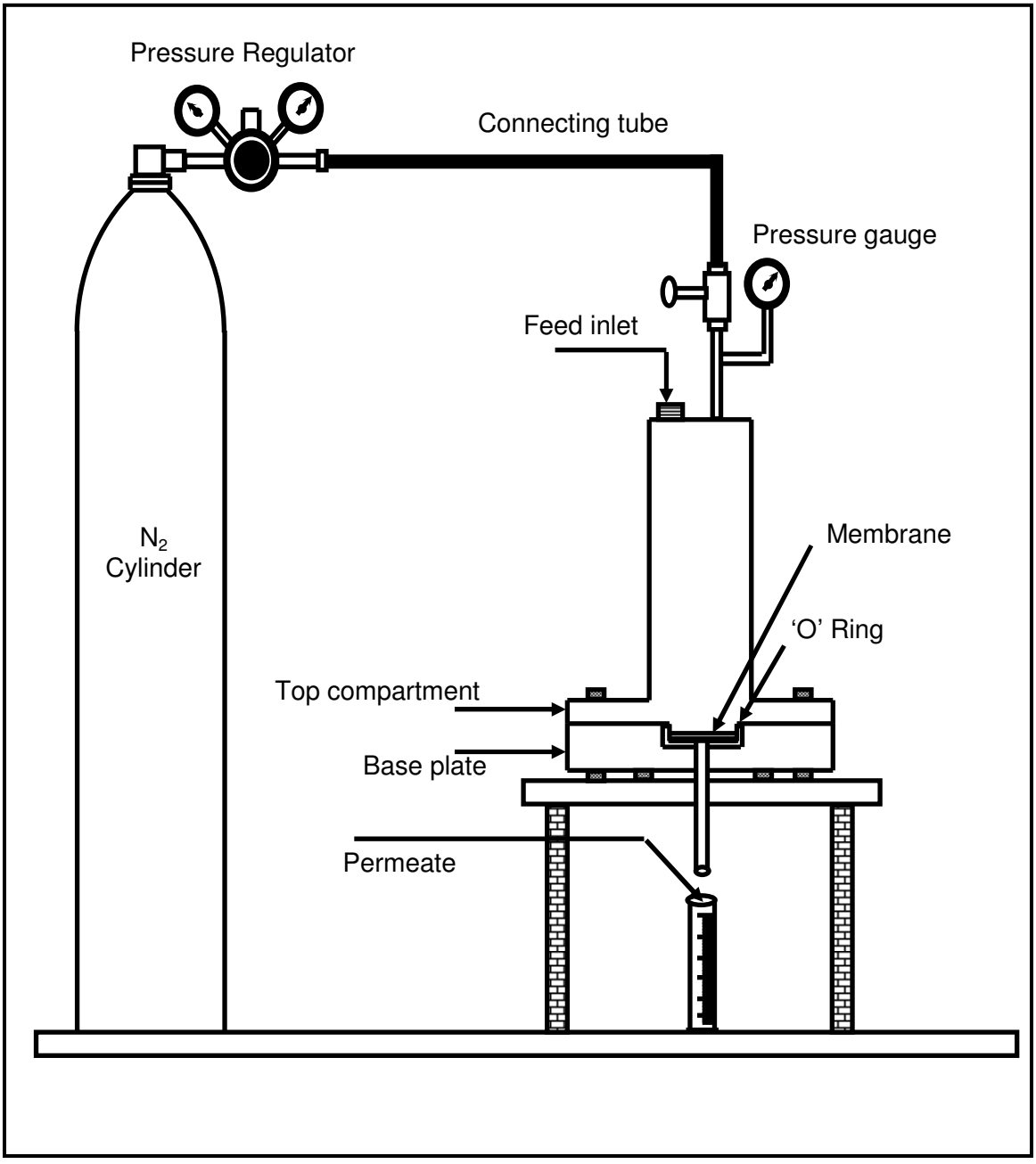

Figure 2.2: Experimental setup for pure water permeation and dead-end microfiltration tests.

2.2 Results and discussion

2.2.1 Characterization of raw materials

The raw materials were characterized for particle size distribution (PSD) and thermogravimetric analysis (TGA). These characterizations were carried out to evaluate the particle size distribution and uniformity of particles and minimum sintering temperature required to achieve a good quality support. The particle size distribution of the raw materials determines the porosity and average pore size of the support. Also, pore growth mainly depends on the initial particle size of the raw materials and compaction pressure (Falamaki *et al*., 2004). The major raw materials used for the fabrication of membrane support are kaolin, calcium carbonate and quartz and their particle size distributions are shown in Fig. 2.3a. It can be observed that majority particles are in the range of 5 – 30 μm and around 60 % of the particles are having diameter below 10 μm. Also, the average particle size of kaolin, calcium carbonate and quartz have been evaluated to be 5.85, 6.47 and 30.41 μm, respectively.

The thermogravimetric analysis of various raw materials and the powder mixture (used for making ceramic support) are shown in Fig. 2.3b. From the figure, it can be observed that the total weight loss of the powder mixture is 26 %. The weight loss at a temperature below 150 ^{o}C is due to the removal of weakly adhered water molecules in the powder mixture. The weight loss of kaolin between 100 – 400 ^{o}C is around 1 %, which can be correlated with pre-dehydration process of kaolin. The pre-dehydration process of kaolin takes place as a result of the reorganization of the octahedral layer which occurred first at the surface (Balek and Murat 1996). The major weight loss occurred in the temperature range of 550 – 730 ^{o}C is due to the thermal decomposition of $CaCO_3$ into CaO and CO_2.

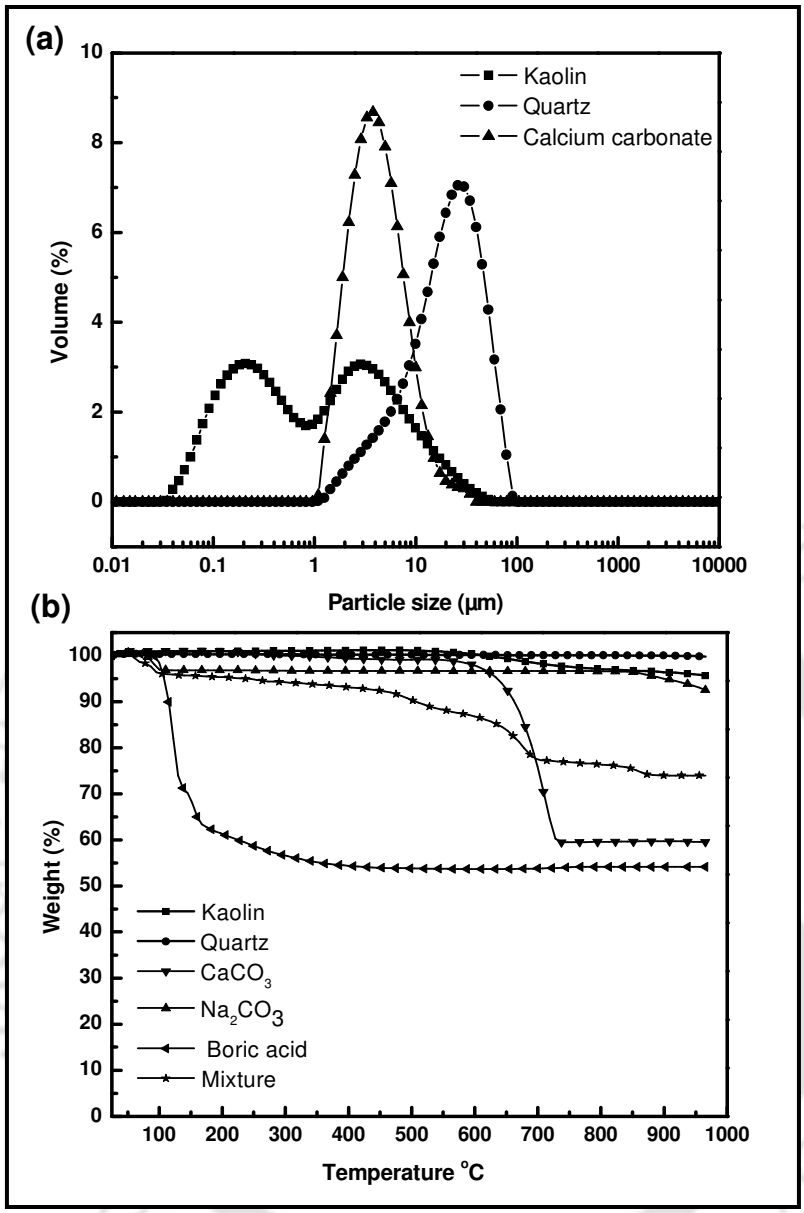

Figure 2.3: Characterization results for raw materials used to fabricate ceramic membranes (A1 – A3) (a) Particle size distribution (PSD) (b) Thermogravimetric analysis (TGA).

The generation of CO_2 enhances the porosity of the support due to the path taken by the evolved gas. The second major weight loss occurred due to the boric acid driven dehydration of crystal water at 100 – 175 ^{o}C. The mixture sample shows a very

insignificant weight loss above 850 °C. This infers that the minimum sintering temperature for the membrane fabrication should be 850 °C.

2.2.2 Characterization of ceramic membranes

2.2.2.1 XRD analysis

The main objective of the XRD analysis is to identify the phase transformation behavior of the membrane during sintering. The XRD patterns of the membranes (A1 – A3) sintered at three different temperatures are illustrated in Fig. 2.4. The main phases that appear in the raw powder mixture are kaolinite, quartz and inyoite. The observation of XRD peaks for the support sintered at 900 ^{o}C indicates that the peak corresponding to kaolinite disappeared due to the conversion of kaolinite to metakaolinite. The other phases that appear are nepheline and quartz. Nepheline (Na_2O, Al_2O_3, $2SiO_2$) has been produced due to the reaction of sodium oxide (Na_2O) and metakaolinite at a temperature of 850 °C (Wang *et al*., 1994). The peaks corresponding to quartz have not changed in the entire XRD pattern. This confirms that quartz is not affected by the sintering temperature. In this regard, it could be observed in the TGA curve (Fig. 2.3b) that there is no significant weight loss at temperature above 700 ^{o}C. The XRD pattern also portrays that there is no other considerable phase transformation at 900 ^{o}C. Thus, it is apparent that the sintering temperature of 900 ^{o}C is sufficient for the fabrication of stable ceramic membrane supports. The crystal size of the membranes at different sintering temperature was evaluated using Scherrer's formula

$$d_{XRD} = \frac{K\lambda}{\beta \cos\theta} \tag{2.5}$$

where *K* is the shape constant (0.9), λ is the wavelength (1.5406 Å) of CuKα radiation, β is the full-width at half-maximum, and θ is the diffraction angle (deg.). The crystal sizes for membranes A1 – A3 were evaluated from quartz peak and were 46 (A1), 43 (A2) and 41 nm (A3) for the supports sintered at 900 °C, 950 °C and 1000 °C, respectively. Similar data was also obtained for other peaks. It is evident that the crystal size decreases with increasing sintering temperature.

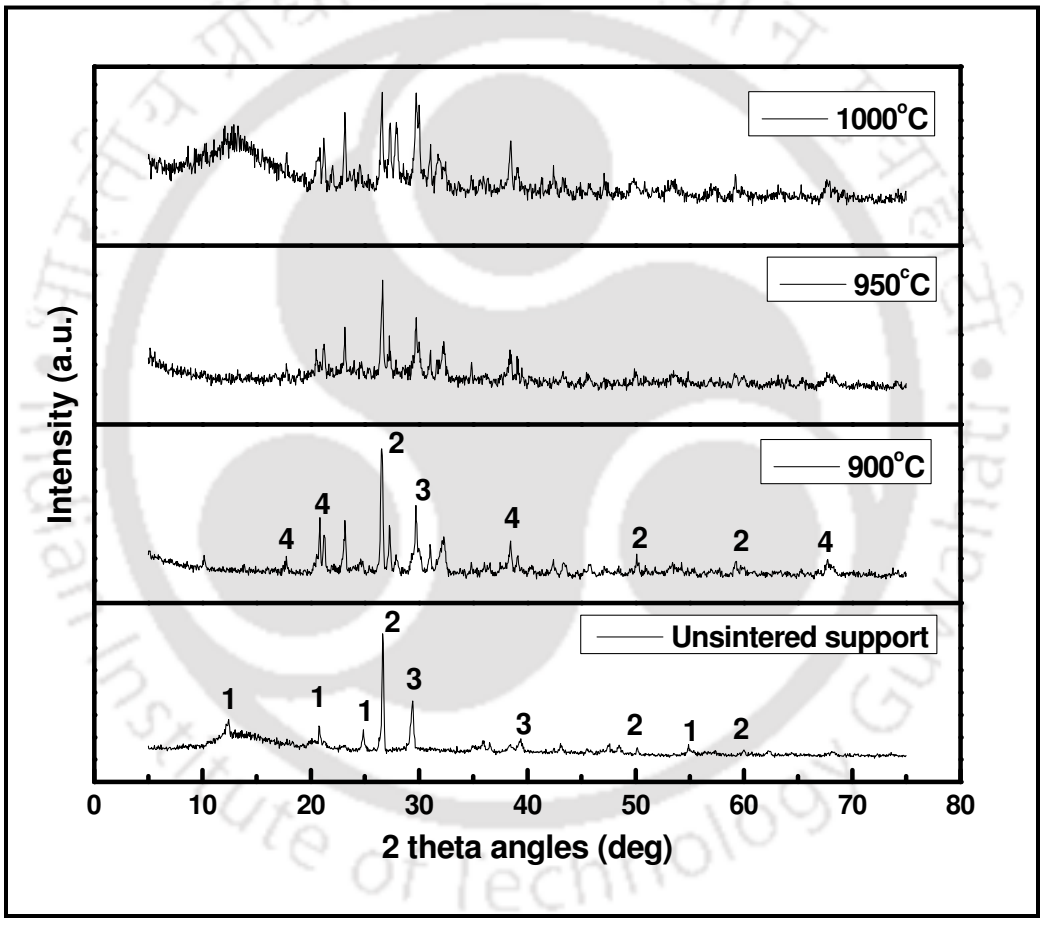

Figure 2.4: X-ray diffraction patterns of the ceramic membranes (A1 – A3) sintered at various temperatures (900 – 1000 °C). Numbered peaks (relevant database presented in parenthesis) in the patterns correspond to 1. kaolinite (PDF-78-2109), 2. quartz (PDF-86-1630), 3. inyoite (PDF-06-0361), 4. nepheline (PDF-19-1176).

This indicates that a higher degree of particle interlocking at sintering temperature would have lead to the densification of the membrane support. Similar trends were also reported in the literature for ceramic membrane structure (Monash and Pugazhenthi 2011).

2.2.2.2 SEM analysis

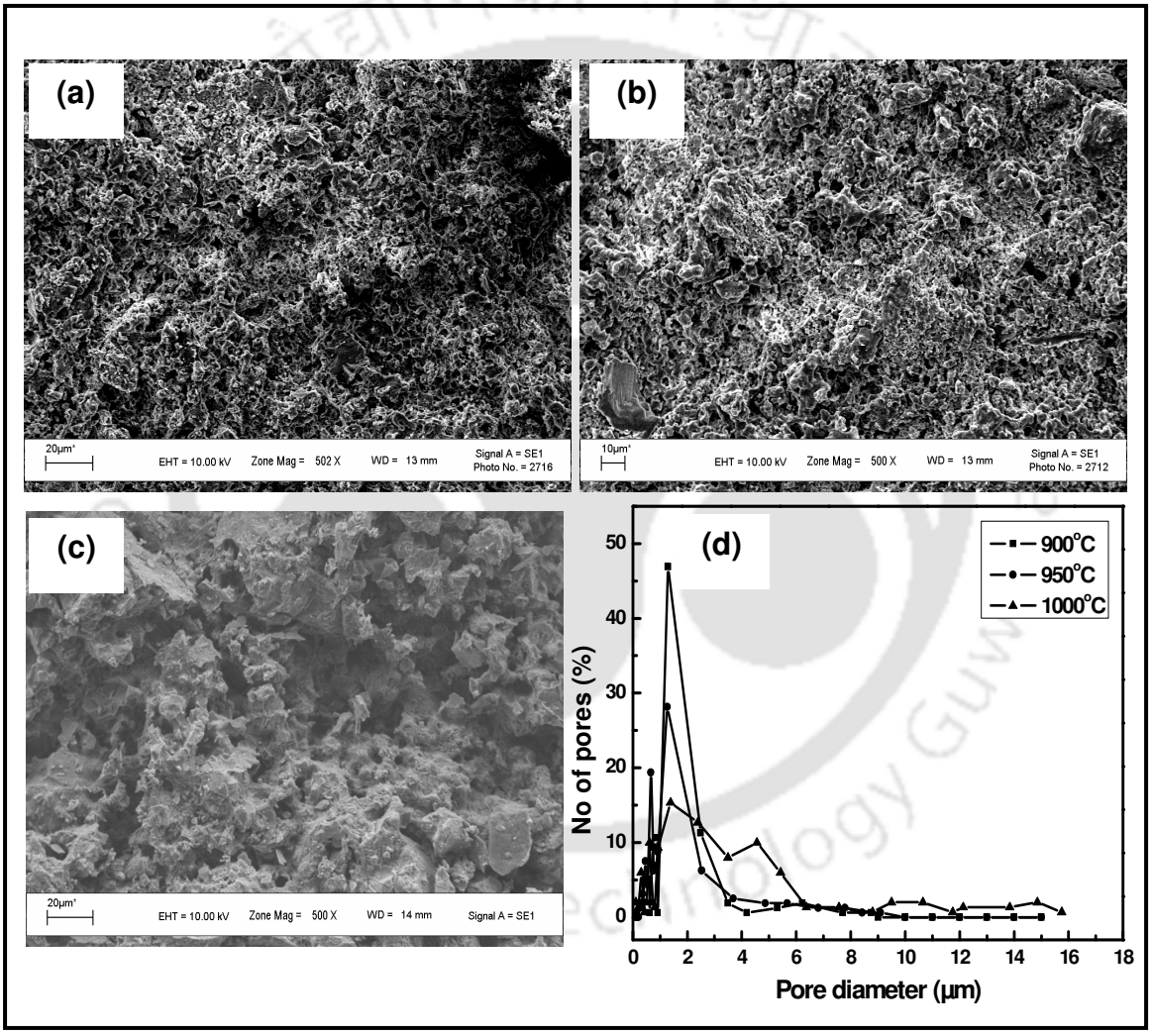

Figure 2.5: (a – c) SEM images and (d) pore size distribution of ceramic membranes sintered at various temperatures (a) 900 ^{o}C (A1) (b) 950 ^{o}C (A2) (c) 1000 ^{o}C (A3) (d) A1 – A3.

Figure 2.5 (a – c) illustrates the SEM images of the membrane A1 – A3 that were sintered at three different temperatures. It can be seen that all membranes possessed rough morphological structure, which is dependent mainly upon the sintering temperature. The supports sintered at 950 ^{o}C and 1000 ^{o}C are more consolidated than those sintered at 900 ^{o}C. This is due to the fact that higher temperature gives more densification for the support. The pore size distribution and average pore diameter of the sintered supports have been estimated from SEM micrographs (Fig. 2.5d). The graph also indicates that the pore sizes increases with increasing sintering temperature. Moreover, maximum number of pores (70 – 80 %) are in the range of 0.1 – 5 µm for all sintering temperatures.

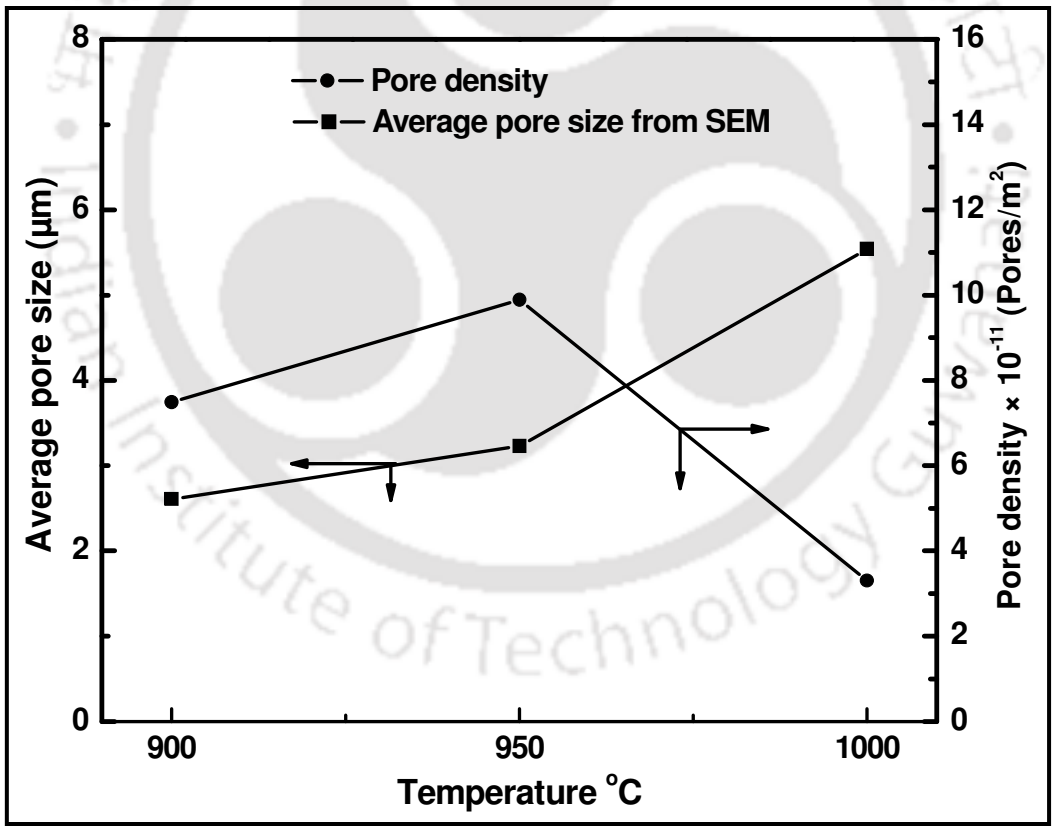

Figure 2.6: Variation of average pore size and density of the ceramic membranes (A1–A3) with sintering temperatures.

Figure 2.6 depict the average pore size and pore density of the membranes A1 – A3 that were sintered at various temperatures. It can be seen that the average pore size enhanced with an increase in the sintering temperature. This is due to the growth of grains that enabled the formation of large pores at higher temperature. The average pore diameter is estimated as 2.61, 3.65 and 5.54 μm for the supports sintered at 900, 950 and 1000 ^{o}C, respectively. The pore density is found to be 7.49×10^{11}, 9.89×10^{11} and 3.3×10^{11} pores/m^2 for the supports sintered at 900, 950 and 1000 ^{o}C, respectively. It is to be noted that the pore density increased with increasing sintering temperature from 900 to 950 ^{o}C, after which it decreased for the support sintered at 1000 ^{o}C. This is due to the formation of large sized pores at higher sintering temperature.

2.2.2.3 Porosity and shrinkage measurements

The porosity (ε) of the ceramic membrane supports A1 – A3 was estimated using Archimedes's method with water as the wetting liquid. Fig. 2.7 illustrates the variation of porosity with variation in sintering temperature. It can be observed that the porosity decreased from 44 to 27 % with an increase in sintering temperature from 900 – 1000 ^{o}C. This is due to the densification of membrane support structure at higher temperature. At higher temperature, the particle grains tend to agglomerate with each other to generate a further consolidated ceramic structure. These results are in good agreement with the trends reported in the literature for other types of clay based ceramic supports (Saffaj *et al*., 2006). The shrinkage of the ceramic membrane supports A1 – A3 was determined using dimensions of the support before and after sintering. Fig. 2.7 depicts the percentage shrinkage in diameter, thickness and volume for the membranes sintered at different temperatures (900 – 1000 ^{o}C).

It can be observed that the shrinkage of the membrane structure increased with increasing sintering temperature. The maximum shrinkage of diameter, thickness and volume for the membrane has been obtained at 1000 ^{o}C is about 4.4, 4.8 and 12.7 %, respectively. This is due to the internal rearrangement (densification process) of the ceramic membrane at higher temperature. Similar trends were reported for alumina and zirconia supports (Falamaki *et al*., 2004).

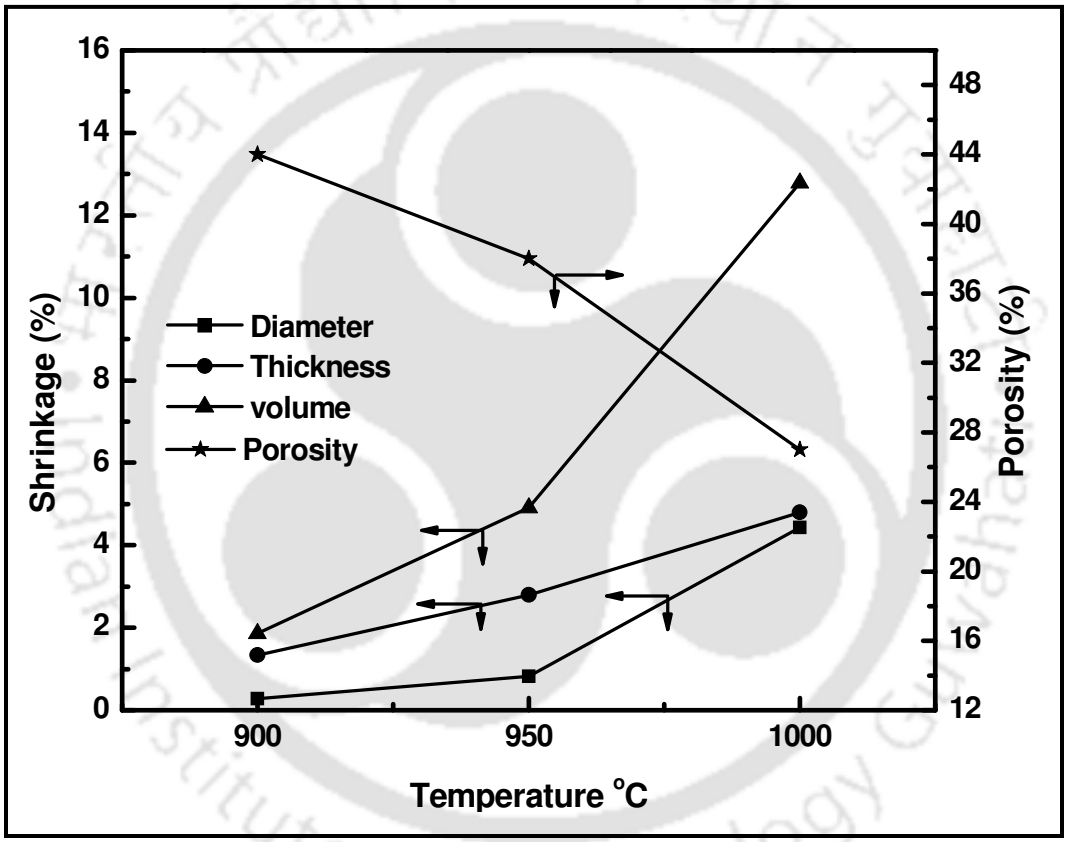

Figure 2.7: Variation of average porosity and shrinkage of ceramic membranes (A1 – A3) with sintering temperature.

2.2.2.4 Chemical stability

The chemical stability of the supports was estimated in terms of mass loss after keeping them in contact with HCl (pH = 1) and NaOH (pH = 14) solution individually for 24 h at

atmospheric condition. The weight loss due to the acidic corrosion has been depicted in Fig. 2.8. The weight loss is evaluated to be less than 2 % for all membranes sintered at various temperatures. On the other hand, the weight loss of the membranes in alkali solution (pH = 14) is found to be unaltered. The obtained results indicate that the supports exhibit a good corrosion resistance in both acidic and basic media. The pure water flux of the membrane before alkali and acid solution permeation tests was 2.76×10^{-3} m^3/m^2s. The pure water flux of the support after acid and alkali permeation tests was 2.85×10^{-3} and 2.78×10^{-3} m^3/m^2s, respectively. Therefore, it is inferred that the enhancement in pure water flux after passing acidic or alkaline solution has been minimal. In addition, the weight loss of the support after acid treatment is 4 % and alkali treatment is negligible.

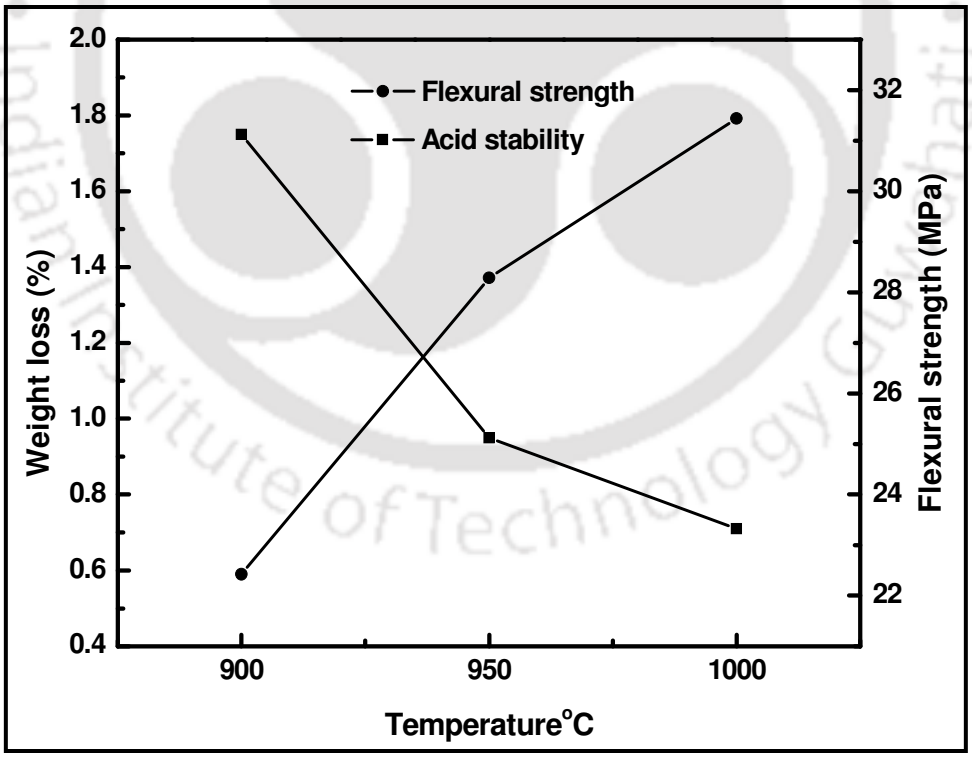

Figure 2.8: Effect of sintering temperature on acid stability and flexural strength of ceramic membranes (A1 – A3).

2.2.2.5 Mechanical Strength

Figure 2.8 depicts the flexural strength of ceramic membranes A1 – A3 sintered at different temperatures. The flexural strength increased with an increase in the sintering temperature. This is primarily due to the densification and growth of the grain boundaries. The supports sintered at 1000 ^{o}C possessed a maximum strength of 31 MPa. Similar trends for flexural strength were reported for moroccan and kaolin based ceramic membranes (Saffaj *et al*., 2006; Bouzerara *et al*., 2006)

2.2.2.6 Pure water permeation test

Figure 2.9a depicts the pure water flux data of ceramic membranes A1 – A3 sintered at various temperatures (900 – 1000 ^{o}C). The data confirms that the pure water flux increased with an increase in the applied pressure. This confirms that the membranes are defect free and the water flux depends on the applied pressure. Moreover, it has been observed that the water flux increases linearly with applied pressure. This is in accordance with Darcy's law. Fig. 2.9b depicts the pure water permeability and average pore diameter of the ceramic membranes A1 – A3 sintered at different temperature (900-1000 ^{o}C). It can be observed that the water permeability of supports increased with an increase in the sintering temperature. This is due to an increase in the membrane pore size. Similar trends were also reported in the literature for clay based inorganic membranes (Saffaj *et al*., 2005; Bouzerara *et al*., 2006). From figure 2.9b, it is confirmed that the average hydraulic pore diameter also increased with an increase in the sintering temperature. The average pore size has been evaluated to be 2.48, 3.07 and 4.46 μm for supports sintered at 900 ^{o}C, 950 ^{o}C and 1000 ^{o}C, respectively. The average pore size

obtained from the permeation study matches well with the average pore size obtained from SEM analysis for the supports sintered at 900 and 950 ^{o}C. However, it differs a little for the support sintered at 1000 ^{o}C. This could be due to the presence of dead end pores.

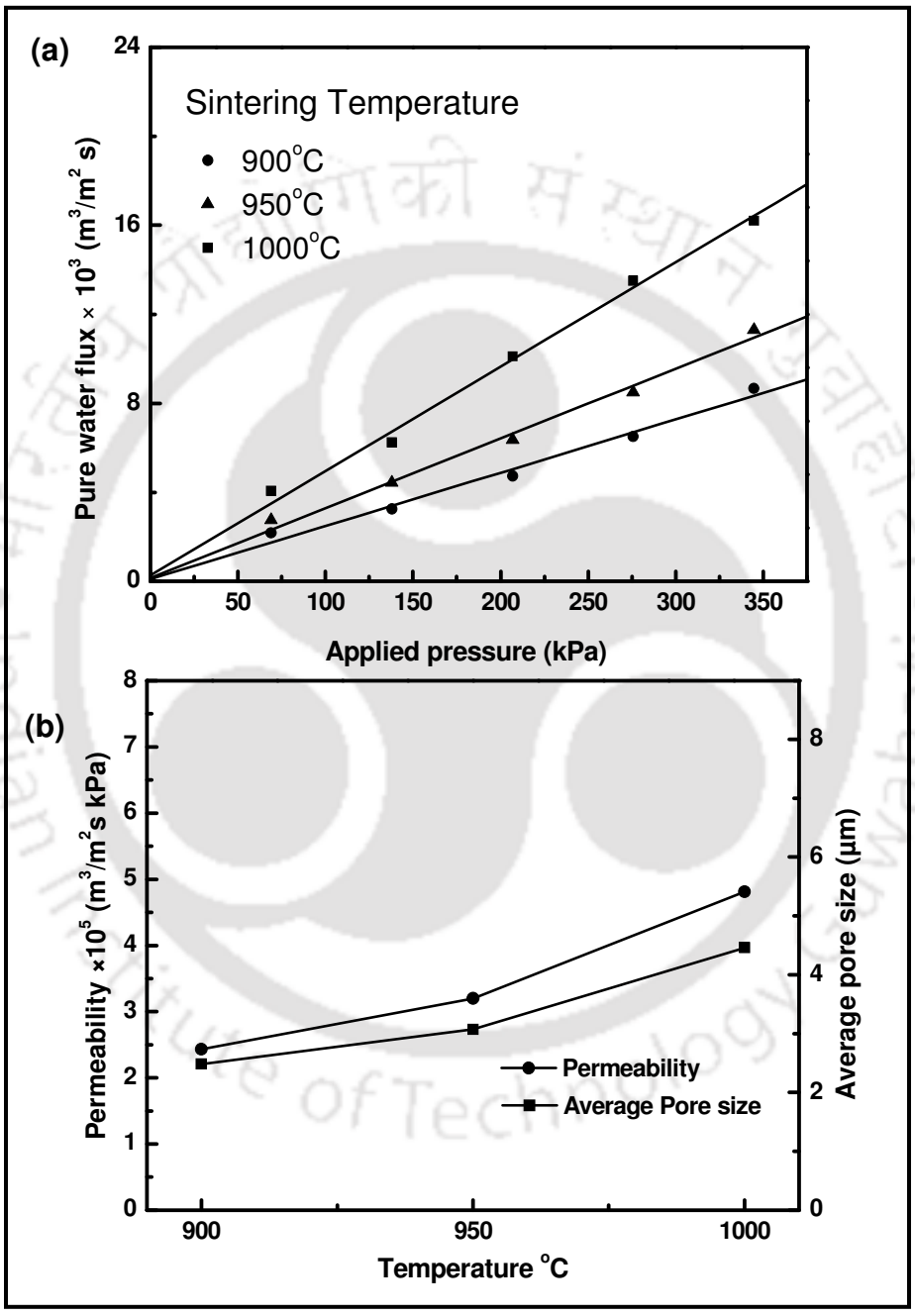

Figure 2.9: Effect of (a) applied pressure on pure water flux and (b) sintering temperature on pure water permeability and average pore size for membranes (A1 – A3).

Table 2.2: Characterization parameters obtained for (A1 – A3) ceramic membranes.

Membrane supports	Sintering temperature (^oC)	Porosity (%)	Average pore size (µm)	Average pore size (SEM) (µm)	Water permeability (m^3/m^2s kPa)	Flexural strength (MPa)
A1	900	44	2.48	2.61	2.43×10^{-5}	22
A2	950	38	3.07	3.65	3.20×10^{-5}	28
A3	1000	27	4.46	5.54	4.81×10^{-5}	31

Table 2.2 summarizes the overall characterization results obtained for various membranes fabricated at different sintering temperatures.

2.2.3 Cost estimation

The applicability of ceramic membranes in industrial applications is limited due to their high cost compared to polymeric membranes. Conventional polymeric membranes used for industrial application have a cost of 960 – 9600 Rs./m^2 (20 – 200 \$/m^2) (Bhide and stern 1991). On the other hand, inorganic membranes have been estimated to be about ten times expensive than polymeric membrane and their cost has been evaluated to be about 24000 – 48000 Rs/m^2 (500 – 1000 \$/m^2) (Cheryan 1998; Koros and mahajan 2000). Based on the retail cost of the raw materials used to prepare ceramic membrane supports in this work, the production cost of a single inorganic support has been estimated to be Rs. 3050 /m^2 (equivalent to 49.4 \$/m^2 for a foreign exchange rate of 1\$ = Rs. 61.65) (Table 2.3).

Table 2.3: Cost parameters for (A1 – A3) ceramic membranes based on retail raw material costs.

Raw Materials	Unit price (Rs./kg)	Amount of Raw material used for Preparation of one Support (kg)	Cost of one support
Kaolin	390	10.4×10^{-3}	4.056
Quartz	200	3.9×10^{-3}	0.78
Calcium carbonate	330	6.5×10^{-3}	2.145
Sodium carbonate	342	2.6×10^{-3}	0.8892
Boric acid	500	1.3×10^{-3}	0.65
Sodium metasilicate	530	1.3×10^{-3}	0.689
		Total Cost / Support	Rs. 9.20
		(Round off value)	Rs. 9.50

For the fabrication of circular disk-shaped ceramic support of 5 mm thickness and 62 mm diameter = Rs. 9.50 / Support. Raw material cost of the support/ unit area = Rs.3050/ m^2

Including the pumping cost, labor cost and maintenance cost, the average cost of low cost inorganic membrane for industrial applications would be similar to that of polymeric membrane. In comparison, the ceramic symmetric membranes made with α-alumina cost about \$ 500/m^2 and stainless steel asymmetric membranes cost around \$ 3000/m^2 (Mott Metallurgical Corporation, USA, 2007). Therefore, it can be inferred from the cost analysis that the fabricated ceramic membrane supports are significantly inexpensive than alumina supports reported in the literature (Falamaki *et al*., 2004).

2.3 Summary

Porous ceramic membrane supports A1 – A3 have been successfully prepared by uniaxial dry compaction method using low cost precursors. The particle size of the raw materials has been found in the range of 5 – 30 µm. Thermal characterization and XRD analysis infer that the appropriate sintering temperature for the chosen composition of materials is around 900 °C. The maximum shrinkage of the support structure has been estimated to be 12.7 %. The porosity of the membrane reduced with increasing sintering temperature (44 – 27 %). The SEM analysis reveals that the average pore diameter increased with increasing sintering temperature. The prepared supports possess good mechanical strength (22 to 31 MPa flexural strength) and chemical stability (< 2 % weight loss in acidic media and no weight loss in basic media) characteristics. Further, it can be concluded that the membrane A2 sintered at 950 ^{o}C is optimum support for membrane applications due to its optimal combinations of mechanical strength (28 MPa), average pore size (3.07 µm) and porosity of 38 %. Based on the raw materials used for preparing inorganic membrane supports in this work, the production cost of a single inorganic membrane has been estimated to be Rs. 3050 /m^2 (equivalent to 49.4 \$/m^2 for a foreign exchange rate of 1\$ = Rs. 61.65).

Chapter 3:

Preparation, Characterization and Application of Micron Range Microfiltration Membranes

Chapter 3

Preparation, Characterization and Application of Micron Range Microfiltration Membranes

This chapter presents results obtained for the fabrication, characterization and application of low cost ceramic microfiltration membranes B1 – B3. The membranes were prepared with identified new compositions of low cost raw materials. The effect of sintering temperature on membrane properties such as porosity, average pore size, chemical and mechanical stability, pure water permeability and surface morphology was investigated. Solvent permeation studies were also conducted to identify the solvent resistance of the B1 membrane. In addition to that, the prepared membrane B1 was subjected to microfiltration experiments for the removal of oil, bacteria and chromium (VI) from synthetic solution. The oil and bacteria removal experiments were targeted to examine the effect of feed concentration and applied pressure on the permeate flux and rejection of the membrane. Similarly, biomass assisted chromium separation experiments were conducted to elaborate upon the effect of applied pressure, solution pH, feed concentration and biomass concentration on permeate flux and rejection. Finally, the cost analysis of the fabricated membranes was carried out to compare the membrane cost with other membranes available in the literature.

Table 3.1: Identified inorganic precursor compositions for (B1 – B3) ceramic membranes fabrication.

Raw Materials	**Composition (wt. %)**
Kaolin	50
Quartz	25
Calcium carbonate	25

3.1 Experimental

In the previous chapter, the reported inorganic compositions enabled to achieve A1 – A3 membranes with average pore sizes of 2.48 – 4.46 µm. The achieved average pore sizes of these membranes are significantly high in comparison to those that are typically applied for microfiltration applications. Typically, micron and sub-micron range microfiltration membranes have been reported in the literature to be effective for various wastewater treatment applications. Thereby, it is important to identify few additional compositions with which the average pore size of the membranes could be targeted to the desired range. In this sub-section, the identified raw material compositions and membrane fabrication/characterization procedures have been presented. Amongst these details, the raw material compositions have been identified on a trail and error basis.

3.1.1 Raw materials

Table 3.1 presents the identified composition of low cost raw materials for the fabrication of micron range ceramic membranes. The composition was obtained from trial and error

experimental approaches. Kaolin was obtained from CDH India. Quartz was procured from Research Lab Fine Chem. Industry, India and calcium carbonate was procured from Merck India. All these raw materials were used without any further purification. Different raw materials used in this work for the membrane fabrication provided distinct functional attributes. Kaolin provides low plasticity and high refractory properties to the membrane. Quartz increases the mechanical strength and thermal stability of the membrane. Calcium carbonate serves as a pore forming agent and sintering aid. The membrane preparation procedure is similar to that presented in section 2.1.2 of the thesis. Thus, membranes B1, B2 and B3 were fabricated at sintering temperatures of 900, 950 and 1000 ^{o}C, respectively.

3.1.2 Membrane characterization

The membrane characterization studies include particle size distribution analysis (PSD), thermogravimetric analysis (TGA), X-ray diffraction analysis (XRD), scanning electron microscopic analysis (SEM), porosity, mechanical stability and pure water permeation test. Procedures for these studies have been presented in section 2.1.3 of the thesis. Other tests have been briefly presented in the following sub-section

3.1.2.1 Chemical stability test

The chemical stability of membranes B1 – B3 was evaluated by soaking the membrane in acidic (HCl, pH = 1) and alkaline (NaOH, pH = 14) solutions individually for one week at atmospheric condition. The chemical stability was evaluated in terms of percent mass lost after corrosion test.

3.1.2.2 Solvent permeation experiment

The solvent permeation experiment was carried out using various solvents whose physical properties have been summarized in Table 3.2. Both polar (alcohols) and non-polar (alkanes) solvents were used for the experiments. All solvents used in this work were of analytical grade quality. The experiments were conducted continuously with methanol first and n-heptane in the last. While opting for the solvents during an experiment, the membrane was loaded and flushed with the next solvent to remove the existing solvent. The solvent flux was then determined at various applied pressures in the range of 69 – 345 kPa. For the solvent flux measurement, the first 50 mL permeate sample was discarded at each applied pressure and the time taken for the collection of second 50 mL was recorded. The solvent permeability of the membrane was evaluated by linear regression of the flux versus applied pressure data. These quantitative experiments were conducted for at least four different membrane samples for evaluating the general solvent permeability characteristics.

3.1.3 Preparation of oil-in-water emulsions

Crude oil obtained from Guwahati Refinery, Indian Oil Corporation Limited (IOCL), India, was used without any pretreatment for emulsion preparation. The emulsion was prepared by mixing of the crude oil of specified composition with Millipore water in a sonicator bath [Model: T460; Make: Elma (India)]. Depending upon the oil concentration, the mixing was facilitated for about 5 – 15 h. The emulsion preparation was carried out at room temperature without addition of any surfactant as natural surfactants present in the crude oil stabilized the emulsion sufficiently to conduct the

experiments. The emulsion concentration refers to 125 and 250 mg/L for all microfiltration experiments.

3.1.4 Preparation of bacterial solution

The microbial strain used in this study was *E. coli* (DH5α), which is a non-pathogenic bacterium and easy to cultivate microbe. Stock cultures of *E. coli* were maintained on agar slants (containing peptone (5 g/L), beef extract (5 g/L), sodium chloride (5 g/L) and requisite amount of agar-agar) at 4 °C. For the preparation of bacterial solution, the bacteria were incubated on agar plates at 37 ^{o}C for two consecutive days. Bacteria colonies of the second 24 h culture were harvested and suspended in NaCl aqueous solution (concentration of 9 g/L corresponding to an ionic strength of 150 mmol/L) to obtain desired concentration of microbes in synthetic solution. The isotonic solution was used to avoid osmotic shock and control the bacteria size in the feed solution. The bacterial solution with two different concentrations (6×10^4 and 6×10^5 CFU/mL) was prepared and used for microfiltration experiments.

3.1.5 Preparation of yeast biomass and feed solution

Baker's yeast (*saccharomyces cerevisiae*) was procured from SAF yeast Co. Ltd., Chembur, Mumbai, India. The yeast cells were washed three times with Millipore water and were subsequently centrifuged and dried at 80 ^{o}C for 24 h in a hot air oven to deactivate the cells (Schiewer and Volesky 1995). The stock solution of chromium (VI) was prepared by dissolving appropriate amount of analytical grade potassium dichromate (Merck India Ltd) in Millipore water.

Table 3.2: Physical properties of various solvents used for B1 membrane solvent permeation experiments.

Solvent	MW (g/mol)	Density (g/ml)	Viscosity (cP)	Molar volume (cm^3/mol)	Surface tension, σ (mN/m)	Dielectric constant	Molar volume/viscosity (cm^3/mol cP)
Water	18	0.998	1.02	18	72.0	80.3	17.7
Methanol	32	0.7917	0.59	40.7	22.6	32.6	69.0
Ethanol	46	0.7893	1.20	58.5	22.32	24.3	48.8
Isopropyl alcohol	60	0.7854	2.245	76.9	23.78	20.1	34.3
Acetone	58	0.792	0.3	74	23.32	20.7	247
Butanol	74	0.810	2.95	91.5	24.6	17.8	31
n-pentane	72	0.626	0.234	116.2	16	1.8	496
n-hexane	86	0.659	0.32	131.6	17.9	1.9	411.3
n-heptane	100	0.684	0.40	146.2	19.7	1.93	366
Toluene	92	0.8669	0.56	25.4	28	2.38	184.4

To prepare the feed solution, specific amount of the dried yeast biomass was added to 100 mL of Cr (VI) solution in 250 mL Erlenmeyer flasks. Before adding biomass, the pH of the solution was adjusted either with 1N HNO_3 or 1N NaOH solution. The suspension was then thoroughly mixed at a constant temperature (25 ^oC) in an incubator shaker at 200 rpm for 24 h, which was sufficiently long time for ensuring equilibrium. After substantial shaking, the feed solution was subjected to microfiltration experiments.

3.1.6 Microfiltration of oil-in-water emulsion

The microfiltration experiment was conducted with synthetic oil-in-water (o/w) emulsions of two different oil concentrations (125 and 250 mg/L) at various applied pressures. At each applied pressure, the first 10 mL permeate sample was discarded and the time taken for the collection of second 10 mL of permeate was measured for the evaluation of permeate flux. All the experiments were conducted at room temperature (25 ^oC) and the rejection (*R)* was evaluated using the expression

$$R(\%) = \frac{C_f - C_p}{C_f} \times 100 \qquad (3.1)$$

where C_f and C_p are the oil concentrations in feed and permeate, respectively. The oil concentration in feed and permeate were evaluated using a UV–vis spectrophotometer (Model: UV 2300; Make: Spectrascan) at a wave length of 235 nm, where the maximum absorbance was observed (Chakrabarty *et al*., 2008). Appendix A presents the calibration chart for oil-water emulsions that was developed for the estimation of unknown sample concentration. After conducting the MF experiment at each pressure, the membrane was systematically cleaned and regenerated. The following procedures were sequentially

adopted to clean membrane: (1) soaking the membrane in hot water at 90 ^{o}C for 20 min. (2) soaking the membrane into surf detergent water solution (concentration of 2 g/L) for 30 min. (3) rinsing the membrane thoroughly with Millipore water to remove residual detergent from the membrane surface and (4) sonication of membrane for 15 minutes with Millipore water. To ensure efficient cleaning and regeneration, the membrane pure water flux was evaluated before and after cleaning.

3.1.7 Microfiltration of synthetic bacteria (*E. coli*) solutions

The bacteria filtration experiment was conducted with a feed bacteria concentration of 6×10^4 and 6×10^5 (CFU/mL) at various applied pressures. Initially, the membrane and the filtration setup were disinfected by soaking them in sodium hypochlorite solutions (200 ppm) for 30 min and then thoroughly rinsing with sterile distilled water to prevent any contamination. After this step, the dead-end MF setup was loaded with the bacterial solution to carry out the MF experiments.

All experiments were conducted at room temperature (25 ^{o}C). The permeate flux was evaluated by measuring the time required for the collection of 10 mL of permeate at each applied pressure. The bacteria rejection (R) was also evaluated using equation 3.1, where C_f and C_p refer to bacteria concentration in the feed and permeate. The bacteria concentration in the feed and permeate solutions were determined using a UV–vis spectrophotometer (Model: UV 2300; Make: Spectrascan). The bacterial solution was initially calibrated for different known bacteria concentration in terms of absorbance measured at a wavelength of 600 nm. The prepared calibration chart has been presented in Appendix B. To evaluate a sample concentration (CFU/mL, colony forming unit per

unit volume), tenfold dilution series of the sample was carried out and the dilutions were put into the agar plate. Subsequently the colony forming units (CFU) were evaluated after overnight incubation of the plates at 37 ^{o}C. The relation between absorbance vs. bacteria concentration (CFU/mL) has been found to be a linear one. The same relation has been used to measure the bacteria concentration of the unknown sample. After conducting the experiments at each applied pressure, the membrane was cleaned by passing sterile water through it at higher pressure until original pure water flux was regained.

3.1.8 Microfiltration of chromium (VI)

The microfiltration experiments were performed in a dead-end filtration setup. All experiments were conducted at room temperature (25 ^{o}C). For all experiments, 100 mL feed solution was filled in the filtration setup. During MF experiments, the first 10 mL of permeate was discarded and the time taken for the collection of second 10 mL permeate sample was measured for the evaluation of permeate flux. The percent removal (R) was evaluated using equation 3.1, where C_f is the concentration of Cr (VI) in the feed and C_p is the concentration of Cr (VI) in the permeate. The concentration of Cr (VI) ion in the permeate was determined by 1,5-diphenyl carbazide (DPC) method using UV-vis spectrophotometer (Model: UV 2300; Make: Spectrascan) at a wavelength of 540 nm (Ozer and Ozer 2003). Appendix C presents the calibration chart for chromium (VI) that was developed for the estimation of unknown sample concentration. After each experiment, the membrane was cleaned using Millipore water to remove the gel or cake layer formed on the membrane surface and the water flux of the cleaned membrane was measured to ensure that the membrane has been efficiently cleaned. To investigate upon

the effect of operating parameters such as applied pressure, solution pH, chromium concentration and biomass dosage on the permeate flux and removal efficiency, the effect of applied pressure on the removal of Cr (VI) and biomass was first carried out at various applied pressures (69 – 345 kPa) with feed chromium concentration of 100 mg/L, solution pH of 6 and biomass dosage of 10 g/L. Subsequently, the effect of initial pH, Cr (VI) concentration and biomass dosage were performed with optimized applied pressure at which maximum flux was observed (207 kPa). Thus only one parameter was changed at any time while all other parameters were maintained constant. The effect of initial pH on the removal of Cr (VI) was performed at various pH ranges (1 – 7) with initial Cr (VI) concentration of 100 mg/L and biomass dosage of 10 g/L. Further, the effect of Cr (VI) concentration was investigated by varying the feed concentration in the range of 100 – 250 mg/L at a fixed biomass dosage of 10 g/L with optimized pH (1) and applied pressure (207 kPa). Finally, the effect of biomass dosage on the removal of Cr (VI) was studied using variant biomass concentrations (6 – 16 g/L) while other optimized parameters were maintained constant. All these experiments were conducted thrice and the average results were used for the evaluation of general membrane characteristics

3.2 Results and discussion

3.2.1 Membrane characterization

The particle size distribution of the raw materials contributes to both porosity and average pore size of the membrane. Further, it has been mentioned that the pore growth mainly depends on the initial particle size of the raw materials (Falamaki *et al*., 2004). The raw materials used to fabricate membranes B1 – B3 were analyzed for their particle

size distribution (PSD). The obtained results have been illustrated in Fig. 3.1. The PSD of kaolin and calcium carbonate shows a narrow size distribution in the range of 0.1 – 10 μm. However, for quartz, the size distribution is in the range of 1 – 100 μm. An overall observation conveys that majority of particles are in between 5 – 30 μm and around 60 % of the particles have sizes below 10 μm. Furthermore, the average particle size of kaolin, calcium carbonate and quartz has been evaluated as 5.85, 6.47 and 30.41 μm, respectively.

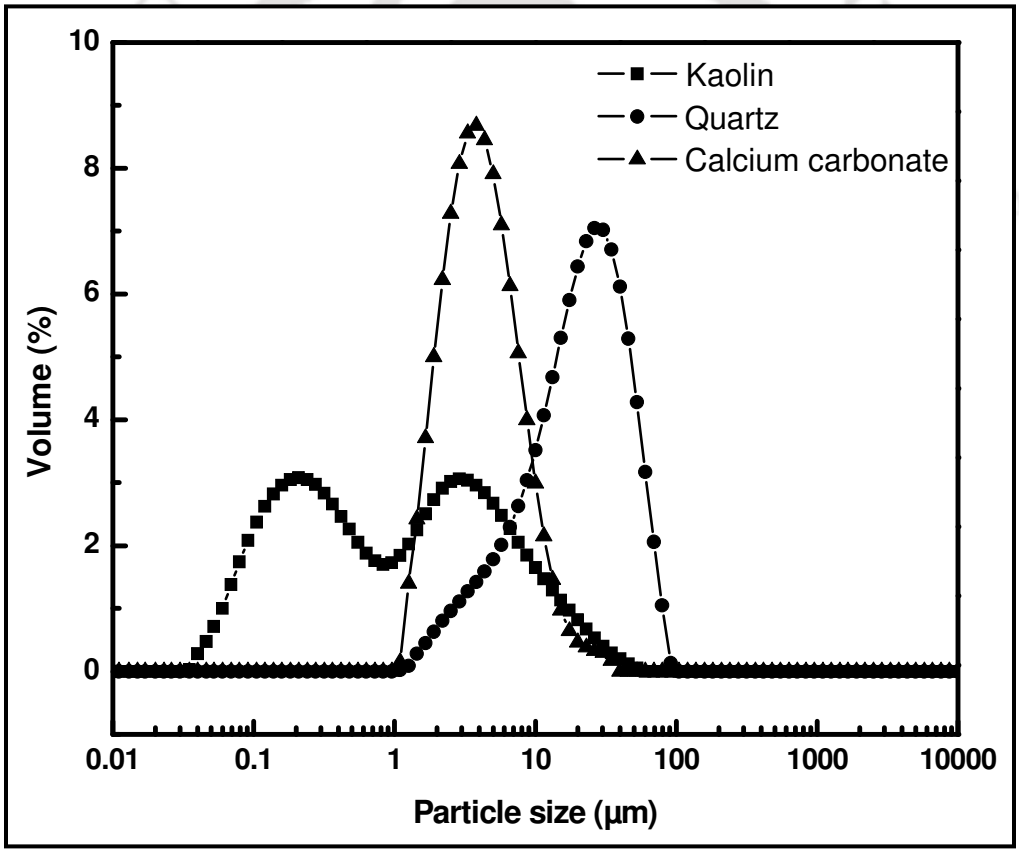

Figure 3.1: Particle size distribution profiles of various inorganic raw materials used to fabricate (B1 – B3) ceramic membranes.

The thermogravimetric analysis (TGA) enabled to indicate upon the minimum sintering temperature required to achieve a good membrane. It is well known that sintering temperature strongly controls the pore size, porosity and mechanical stability of a membrane. The thermogravimetric analysis of the individual raw materials and the powder mixture to fabricate B1 – B3 ceramic membranes is shown in Fig. 3.2. It can be observed in the figure that major weight loss occurred due to the thermal decomposition of $CaCO_3$ into CaO and CO_2 at 550 – 730 ^oC. The formation of CO_2 enhances the porosity of the membrane which is dependent upon the path taken by the evolved CO_2 gas. The total weight loss of the powder mixture has been found to be around 21 %.

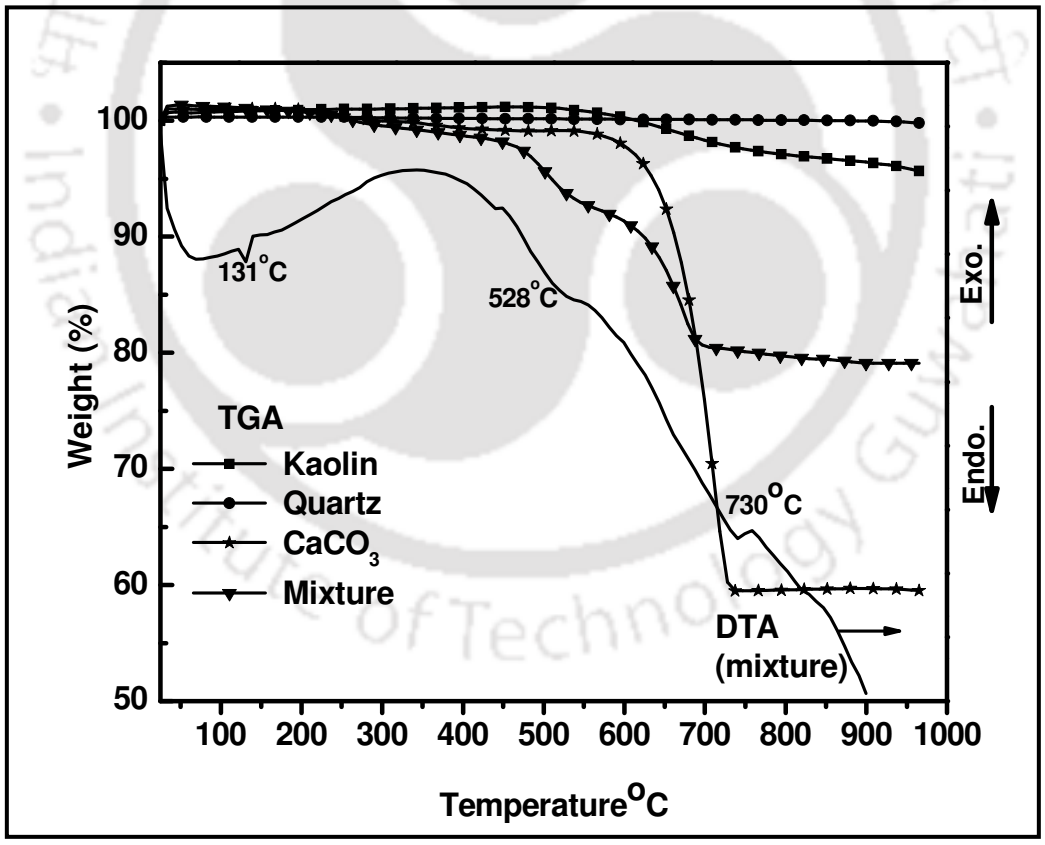

Figure 3.2: TGA-DTA curves for kaolin, quartz, $CaCO_3$ and raw material mixture used to fabricate (B1 – B3) ceramic membranes.

The weight loss in the raw material mixture below 150 ^{o}C is due to the removal of weakly adhered water molecules in the powder mixture. The DTA curve characterizes specific water loss for the corresponding first endothermic peak at 131 ^{o}C. The second endothermic peak in the DTA curve corresponds to the loss of structural hydroxyl groups at 528°C. This is due to the transformation of kaolinite to metakaolinite as presented below (Chen *et al*., 2004):

$$Al_2O_3\,2SiO_2\,2H_2O \rightarrow Al_2O_3\,2SiO_2 + 2H_2O$$

Kaolinite Metakaolinite

The third endothermic peak at 730 ^{o}C in the curve is due to the formation of CO_2 by the thermal decomposition of calcium carbonate. The mixture sample shows a very insignificant weight loss above 730 °C as conveyed by the TGA curve. From the TGA result, it can be inferred that a minimum sintering temperature of 730 ^{o}C is enough to fabricate the ceramic membrane.

The XRD patterns enable the identification of various phases in the membrane during sintering. Fig. 3.3 shows the XRD patterns of the membranes B1 – B3 sintered at various temperatures. The main phases that appear in the raw material mixture refer to kaolin, quartz and calcium carbonate. After sintering, the peaks corresponding to kaolin disappeared due to the transformation of kaolinite to metakaolinite. On the contrary, the peaks corresponding to the quartz have not changed in the XRD patterns after sintering. This confirms upon the thermal stability of the quartz phase. In this regard, it could be noted that there is no significant weight loss for quartz as depicted by the TGA curve (see Fig. 3.2). The peaks of calcium carbonate have also disappeared in the sintered samples due to the thermal decomposition. The new phases that appear after sintering are

anorthite ($CaO.Al_2O_3.2SiO_2$), mullite ($3Al_2O_3.2SiO_2$), and wollastonite ($CaSiO_3$). The formation of mullite is due to the transformation of metakaolinite in the temperature range of 800 – 1000 ^oC (Guo *et al.*, 2007). The XRD patterns for membranes sintered at higher temperatures confirm that significant phase transformations occur below 900 ^oC and therefore, the minimum sintering temperature of about 900 ^oC taken in this work is justified.

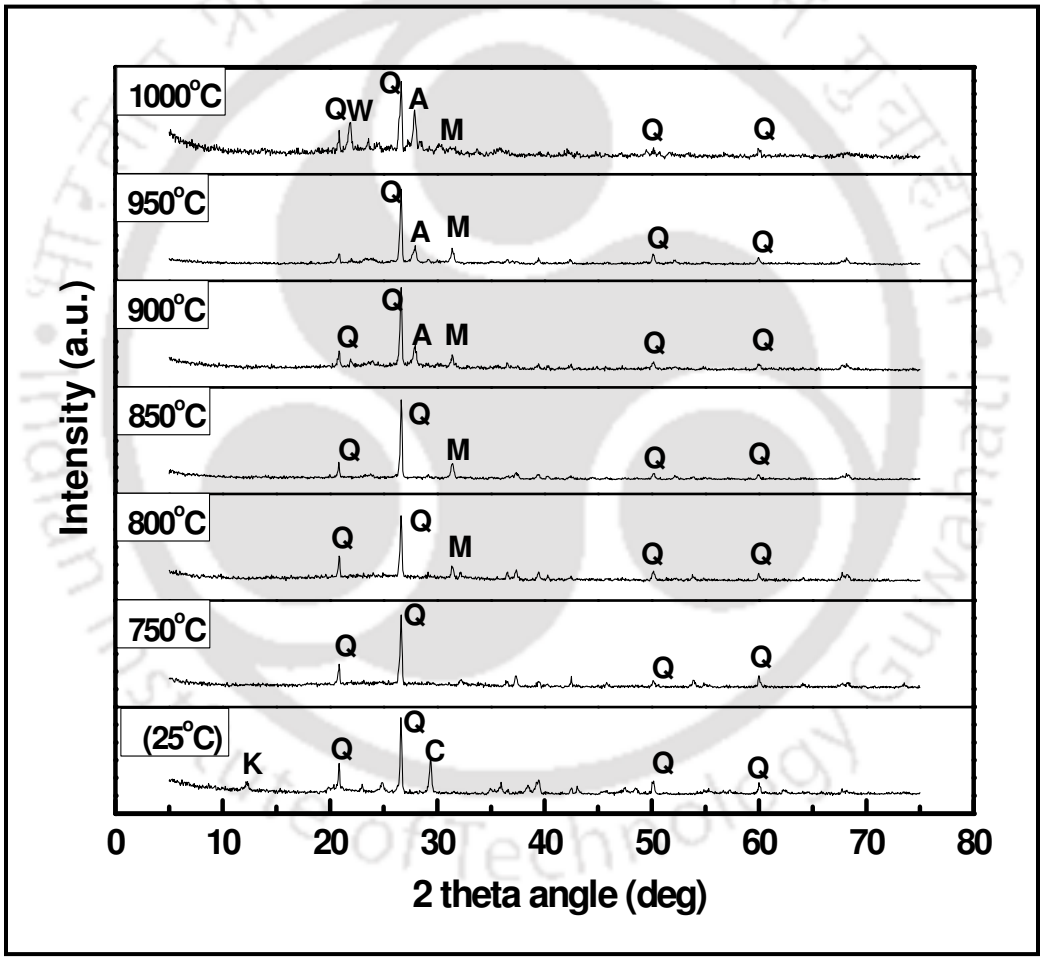

Figure 3.3: XRD patterns of the membranes (B1 – B3) fabricated at various sintering temperatures. Peaks in the patterns correspond to (K) Kaolin, (Q) Quartz, (C) Calcium carbonate, (A) Anorthite, (M) Mullite, (W) Wollastonite.

The shrinkage of the membranes B1 – B3 was evaluated using dimensions of the membrane before and after sintering. As shown in Fig. 3.4, increasing sintering temperature enable an increase in the membrane shrinkage. It has been evaluated that after sintering the variation in the membrane thickness is negligible whereas the change in the diameter is noticeable. The maximum shrinkage of diameter and volume for the membrane sintered at 1000 ^{o}C is found to be 5 and 11 %, respectively. This is due to the internal rearrangement (densification process) of the membrane at higher sintering temperature. Similar trends were reported for alumina and zirconia membranes (Falamaki *et al.*, 2004).

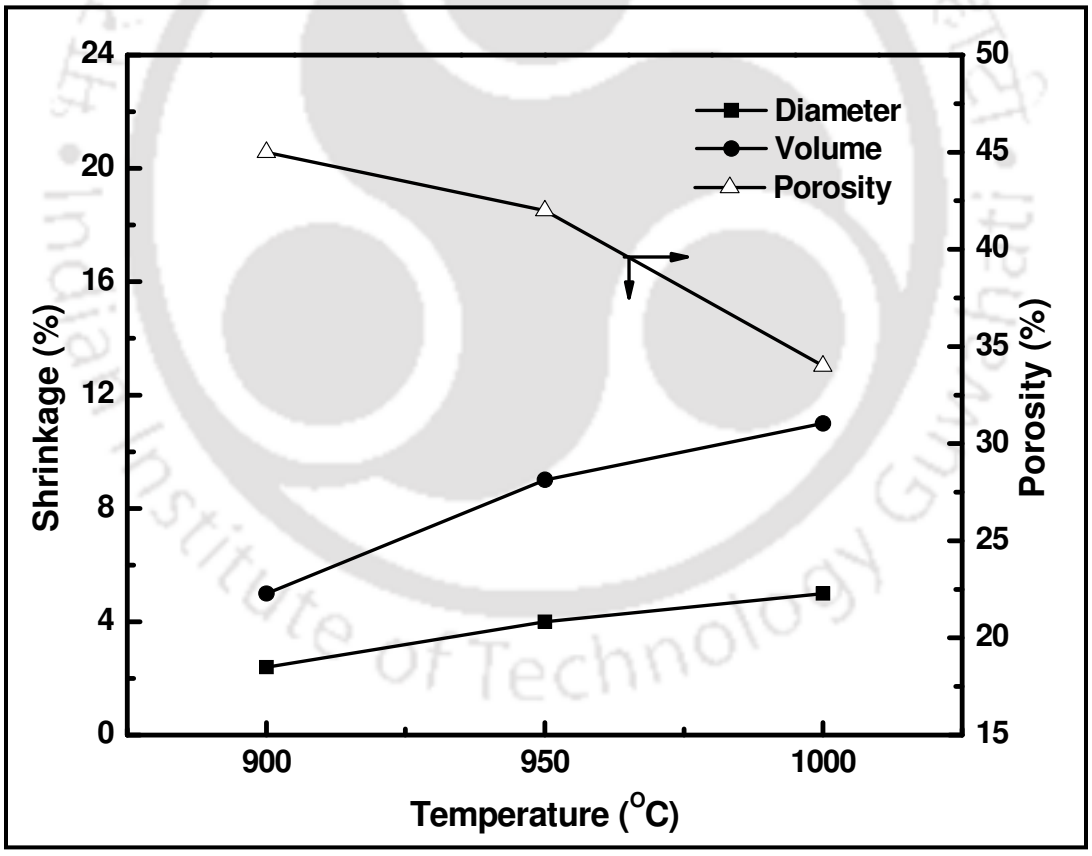

Figure 3.4: Effect of sintering temperature on the shrinkage and porosity of ceramic membranes (B1 – B3).

Figure 3.4 also presents the variation of membrane porosity with sintering temperature. The membrane porosity reduced from 45 to 34 % for an increase in the sintering temperature from 900 to 1000 ^{o}C. Also, it can be observed that the porosity reduced insignificantly from 900 to 950 ^{o}C but sharply from 950 to 1000 ^{o}C. The latter is due to the densification of the membrane at higher temperature. This is due to the fact that, at higher temperature, the particles tend to agglomerate with each other to achieve a more consolidated ceramic structure. The obtained porosity trends are in good agreement with the trends reported in the literature (Dong *et al*., 2007).

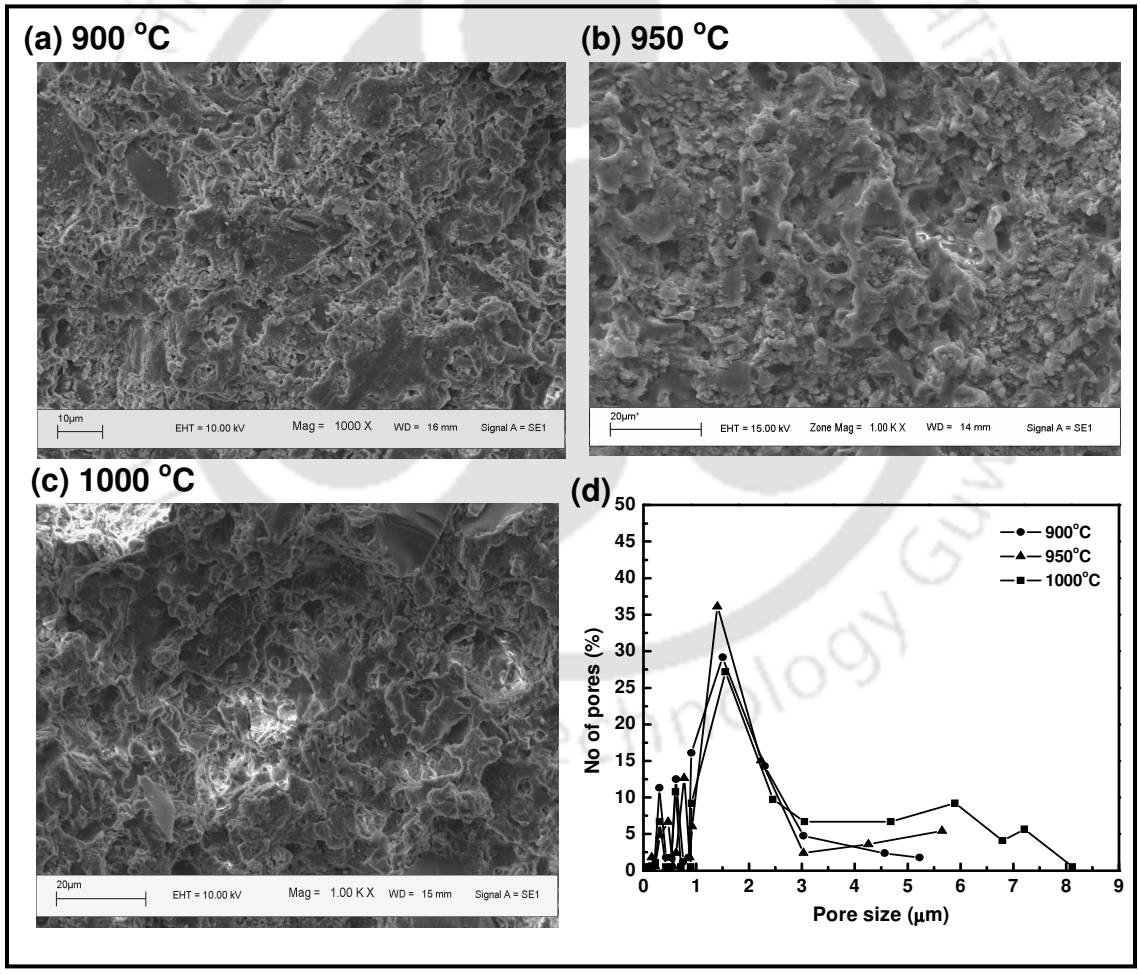

Figure 3.5: (a – c) SEM images and (d) pore size distribution of various ceramic membranes (a) B1 (900 ^{o}C) (b) B2 (950 ^{o}C) (c) B3 (1000 ^{o}C) (d) B1 – B3 membranes.

Figure 3.5 (a – c) respectively illustrate the SEM images of the membranes B1 – B3 that were sintered at three different temperatures namely 900, 950, 1000 ^{o}C. It has been analyzed from SEM images that the morphology of the membrane depends significantly on the sintering temperature. Moreover, it is clearly evident that the pore sizes have significantly changed with increasing sintering temperature. The pore size distribution and average pore diameter of sintered membranes B1 – B3 were estimated from SEM micrographs (Fig. 3.5d) using ImageJ software (open source software provided by National Institute of Health (NIH), weblink: http://rsbweb.nih.gov/ij/download.html). The evaluated trends refer to unimodel pore size distribution for all sintering temperatures. The average pore size of the membrane increased with increasing sintering temperature. This is due to the growth of grains that facilitate towards the formation of large pores at higher temperature. Also, 65 – 70 % of pores are in the range of 0.5 – 2 µm for all sintering temperatures. The average pore diameter for the membranes B1 – B3 has been estimated as 1.42, 1.60 and 2.72 µm, respectively.

The chemical stability of membranes B1 – B3 was evaluated in terms of mass loss after keeping them in contact with acidic and alkaline solutions individually. The weight loss due to acidic corrosion has been depicted in Fig. 3.6. The weight loss has been found to be less than 6 % for all membranes (B1 – B3). However, the weight loss of the membrane due to alkali has been found to be unaltered. Thus, the results indicate that the membrane exhibits good corrosion resistance in both acidic and basic media. These results are comparable with the corrosion resistance of cordierite membrane (prepared by Dong *et al*., 2007) in basic medium. The flexural strength of membranes B1 – B3 was evaluated using three point bending method. Fig. 3.6 presents the variation of the flexural strength

with sintering temperature. As shown, the flexural strength increases from 34 to 46 MPa with an increase in sintering temperature from 900 to 1000 ^{o}C. The increase in flexural strength is primarily due to the membrane structural densification at higher sintering temperature. The membrane sintered at 1000 ^{o}C possessed a maximum strength of 46 MPa. These evaluations are in good agreement with the literature data provided for Moroccan clay (Saffaj *et al*., 2006).

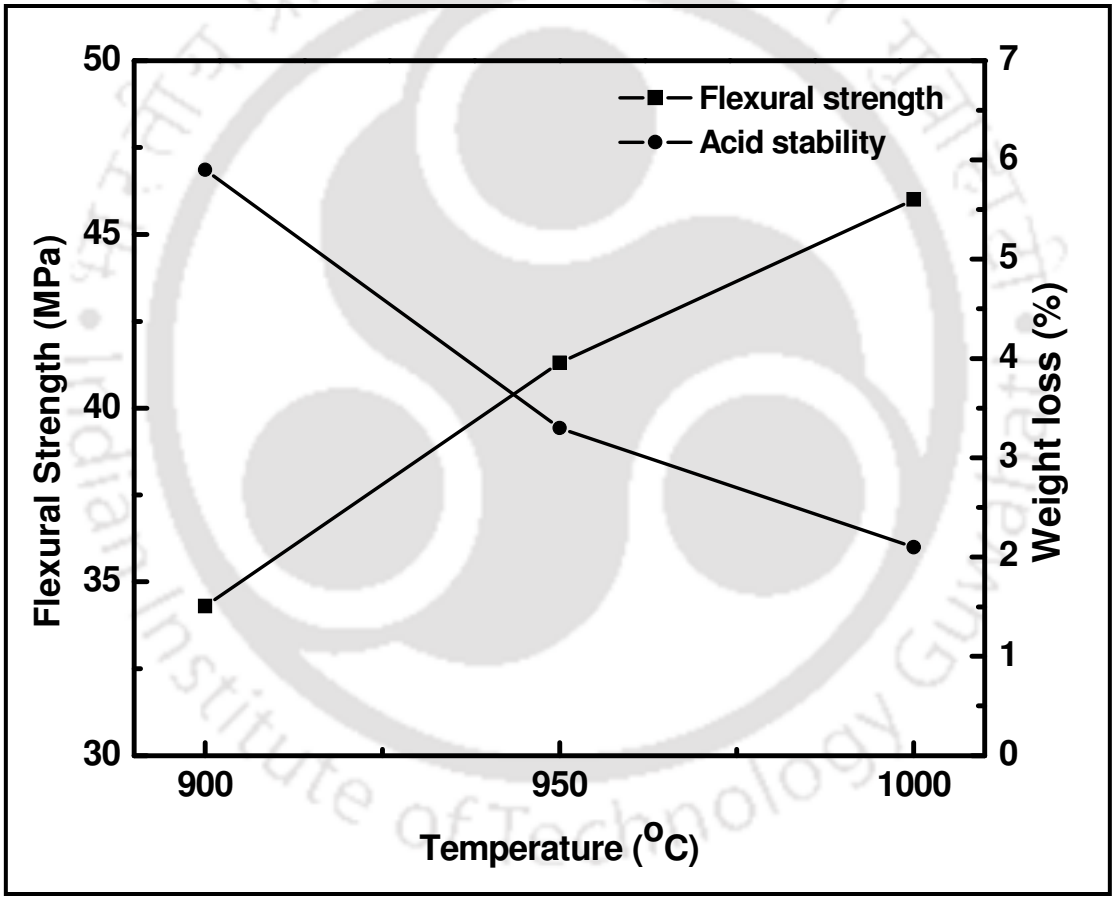

Figure 3.6: Effect of sintering temperature on the flexural strength and acid stability of (B1 – B3) ceramic membranes.

Figure 3.7a depicts the pure water permeability and average pore diameter of the membranes B1 – B3 that were sintered at different temperatures (900 – 1000 ^{o}C). It has been observed that the water permeability and average pore diameter increases with an increase in the sintering temperature. The average pore diameter has been found to be 1.06, 1.33 and 2.22 µm for the membrane sintered at 900, 950 and 1000 ^{o}C, respectively. Also, it can be observed in Fig 3.7b that the water flux increases linearly with pressure. i.e., it follows the Darcy's law. The average pore diameter obtained from the permeation study closely matches with the average pore size obtained from SEM analysis. Similar trends were also reported for other clay based inorganic membranes (Bouzerara *et al*., 2006). Table 3.3 summarizes results obtained for the membranes B1 – B3. From the Table, it can be concluded that the membrane B1 sintered at 900 ^{o}C is the optimum membrane as it possessed good combinations of membrane properties (porosity of 45 %, average pore size of 1.06 µm and mechanical strength of 34 MPa). Thus, B1 membrane has been considered for further MF experimentation.

3.2.2 Solvent permeation studies

Figure 3.8a shows the membrane flux and permeability of various solvents through the B1 membrane. The relation between the flux and applied pressure has been found to be linear, which indicates that pressure difference is the only driving force for the solvent permeation. Moreover, higher permeability has been obtained for non-polar solvents. This confirms that B1 membrane is hydrophobic in nature. It can also be seen that in the alcohol series, the methanol permeability is about two times higher than that of ethanol permeability and about five times higher than that of the butanol permeability.

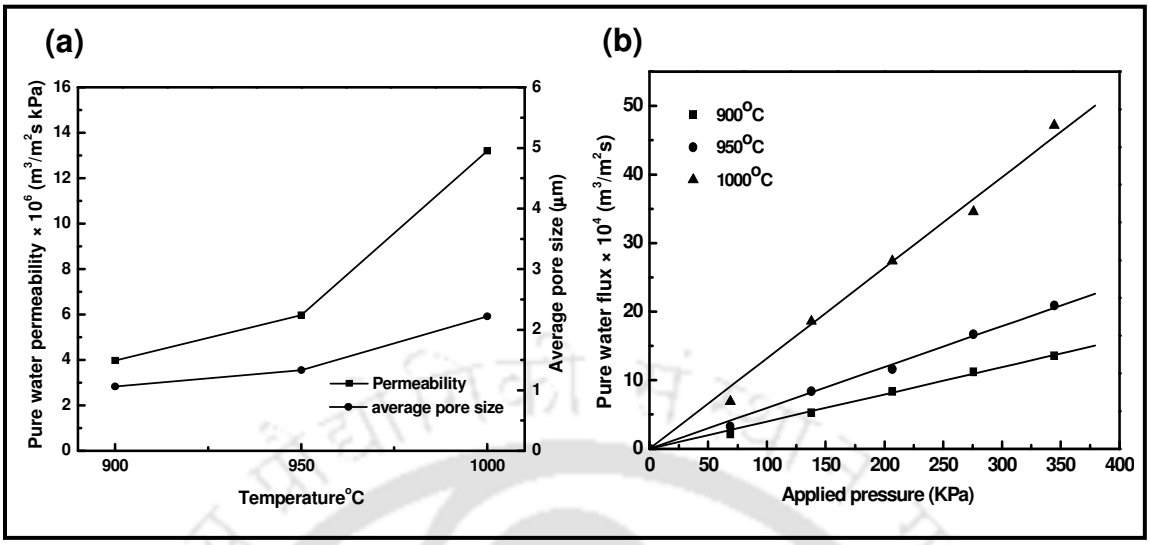

Figure 3.7: (a) Effect of sintering temperature on hydraulic permeability and average pore size of (B1 – B3) membranes (b) Effect of applied pressure on the pure water flux of (B1 – B3) membranes.

Table 3.3: Characterization parameters for ceramic membranes B1 – B3.

Membrane	Sintering temperature (°C)	Porosity (%)	Average pore size (μm)	Average pore size (μm) from SEM	Water permeability (m^3/m^2s kPa)	Flexural strength (MPa)
B1	900	45	1.06	1.42	3.97×10^{-6}	34
B2	950	42	1.33	1.60	5.97×10^{-6}	41
B3	1000	34	2.22	2.72	13.2×10^{-6}	46

In the alkane series, the pentane permeability is about two times greater than that of heptane. These results indicate that the solvent permeability increases with decreasing viscosity of the solvent. Fig. 3.8b confirms this inference as the figure indicates a good correlation between solvent permeability and inverse of the solvent viscosity.

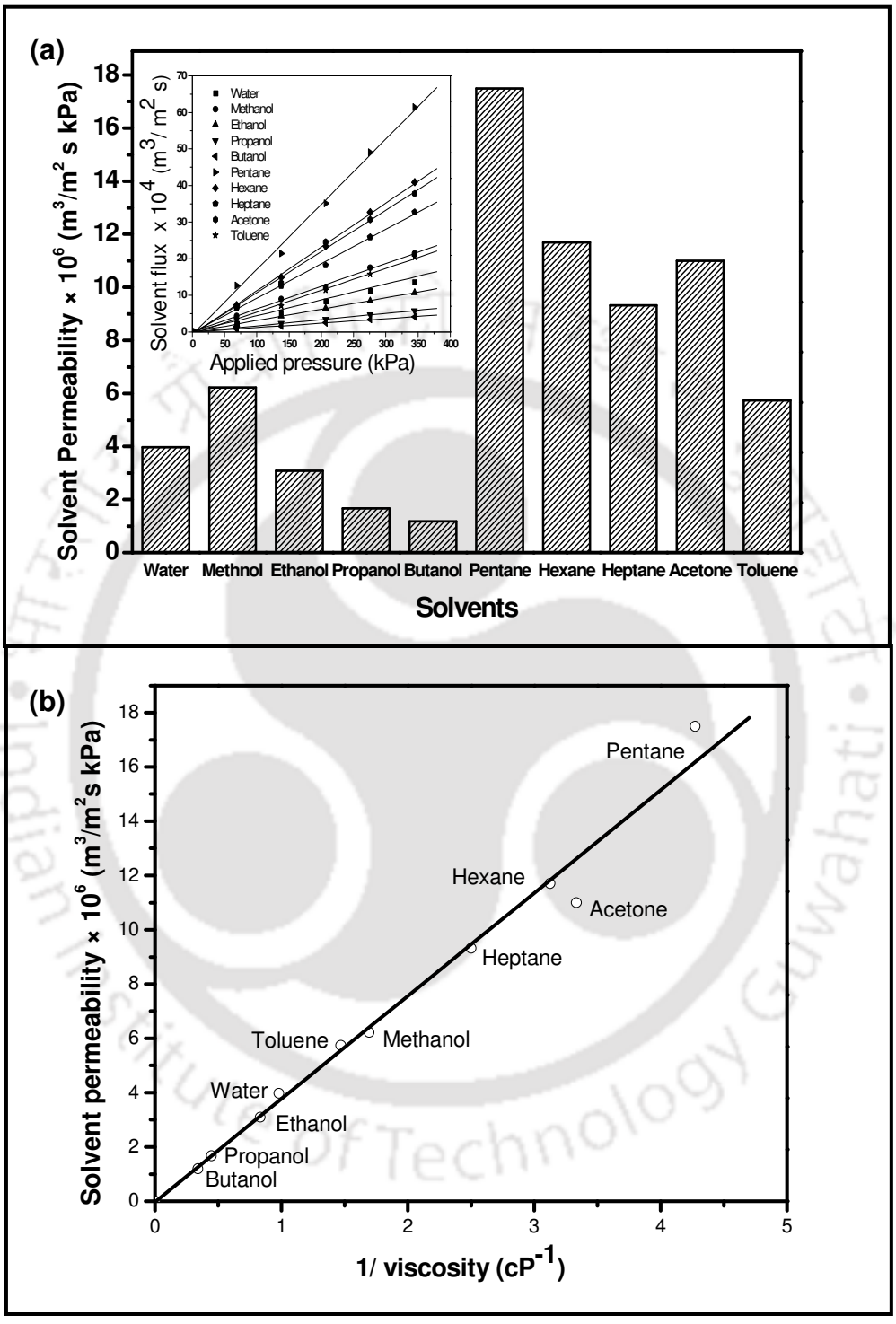

Figure 3.8: (a) Evaluated permeability of various solvents for B1 membrane (b) Plot of B1 membrane solvent permeability Vs. inverse viscosity of the solvent.

However, it can be also observed in the figures that the acetone flux is noticeably less than the hexane flux. If the viscosity of the solvent would be the controlling factor then the acetone flux should have been more than hexane flux. This implies that the surface tension also affects the flux in addition to viscosity. Even though, the acetone has a low viscosity (0.3 cP) than hexane (0.32 cP), it has a higher surface tension (23.3 mN/m) than hexane (17.9 mN/m). Due to this reason, acetone permeates slowly through the hydrophobic membrane. Similarly, pentane flux has been higher than that predictable with viscosity. This is due to its lower surface tension. It has been reported in the literature (Bhanushali *et al*., 2001) that the surface tension of the solvent is inversely proportional to the flux for a hydrophobic membrane. Based on these results, it is evident that the transport of solvent through membrane is mainly influenced by applied pressure, solvent viscosity and surface tension. Bhanushali *et al*, (2001) have reported similar observation with a hydrophobic polymeric membrane.

3.2.3 Microfiltration of oil-in-water emulsion

Figure 3.9 shows the variation of permeate flux and observed rejection with applied pressures (69 – 276 kPa) for the feed oil concentration of 125 mg/L and 250 mg/L. It is apparent that the permeate flux increases with an increase in the applied pressure. It can be observed in Fig. 3.9 that the permeate flux increased from 1.26 to 6.3 × 10^{-4} m^3/m^2s for an increase in applied pressure of 69 to 276 kPa at a feed concentration of 125 mg/L. This is due to an increase in the driving force across the membrane with applied pressure. The rejection value decreases with an increase in the pressure.

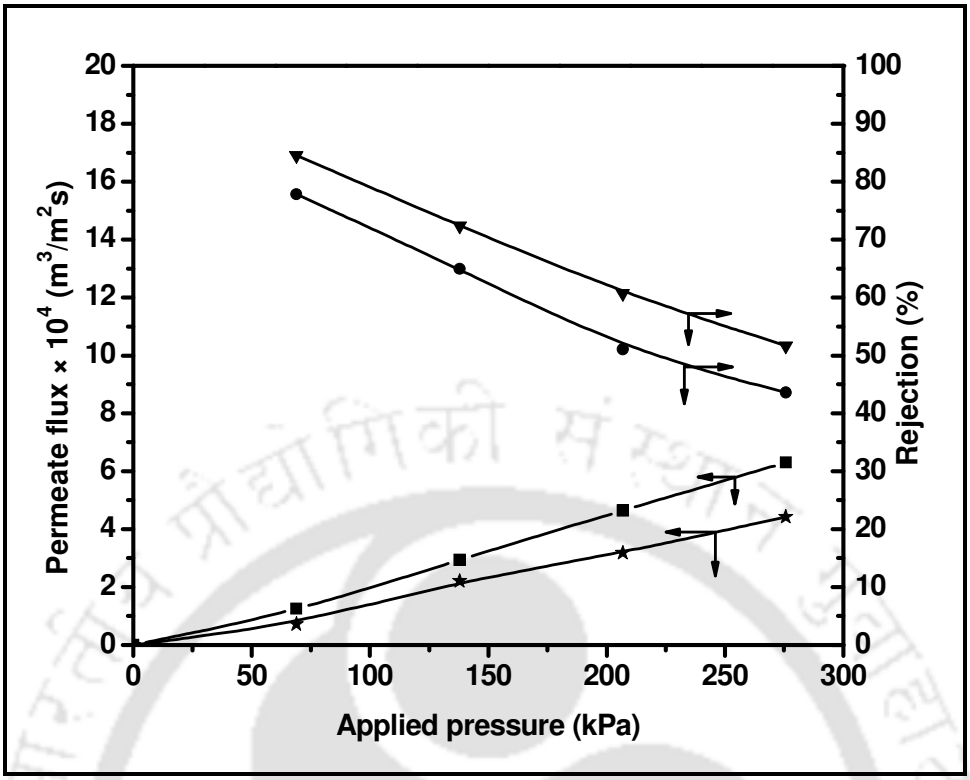

Figure 3.9: Variation of permeate flux and rejection of oil with applied pressure for B1 ceramic membrane for initial feed concentrations of 125 mg/L (■ Flux, ● Rejection) and 250 mg/L (★ Flux, ▼ Rejection).

It has been observed that, the observed rejection decreases from 78 to 44 % for an increase in applied pressure of 69 to 276 kPa at feed concentration of 125 mg/L. This is due to the fact that higher pressure enhances the wetting and coalescence of oil droplets and this would enable the greater passage of oil droplets to pass through the membrane and reach the permeate stream. Similar trend of permeate flux and rejection is also observed for oil concentration of 250 mg/L. For a higher feed concentration of 250 mg/L, the rejection value is in the range of 52 – 85 % (Fig. 3.9). An overall observation is that the permeate flux decreases with increasing feed oil concentration. This is due to the reason that higher feed concentration facilitates enhancement in concentration

polarization. It may also be observed from the figure that the percentage of oil rejection increases from 78 – 85 % for an increase in feed oil concentration from 125 to 250 mg/L at 69 kPa. The increase in oil rejection with an increase in feed oil concentration is due to the larger droplet size of the emulsions (Chakrabarty *et al*., 2008). It has been reported that the average droplet size of the oil used in this work (crude oil obtained from Guwahati refinery) was found to be 0.78 and 0.92 µm for the oil concentration of 125 mg/L and 250 mg/L, respectively (Nandi *et al*., 2010).

The rejection value (85 % at 69 kPa at a feed oil concentration of 250 mg/L) reported in this work is comparable with those reported in the literature (Abbasi *et al*., 2010; Nandi *et al*., 2010; Salahi *et al*., 2010; Abadi *et al*., 2011). Abbasi *et al*., (2010) have reported 85.4 % of oil rejection (permeate flux of ~8.333×10^{-6} m^3/m^2s at 300 kPa) for the feed oil concentration of 250 mg/L using mullite ceramic membrane (average pore size of 0.289 µm). Nandi *et al*., (2010) evaluated that the ceramic membrane having an average pore size of 0.51 µm provided a maximum oil rejection of 98.8 % and a permeate flux of 5.36×10^{-6} m^3/m^2s at 69 kPa and feed oil concentration of 250 mg/L. About 66.3 % of oil rejection (permeate flux of ~1.667×10^{-5} m^3/m^2s) was achieved using polysulfone membrane (average pore size of 0.2 µm) for the initial feed oil concentration of 80 mg/L and applied pressure of 300 kPa (Salahi *et al*., 2010). Also, commercial α-Al_2O_3 membrane provided 85 % of oil rejection (permeate flux of ~6.38×10^{-5} m^3/m^2s) for a feed oil concentration of 30 mg/L at 100 kPa (Abadi *et al*., 2011). A comparison of the obtained results with those presented in the literature convey that the membrane permeate flux (average pore size = 1.06 µm) reported in this work (7.23×10^{-5} m^3/m^2s) is higher. Comparatively, good rejection has been obtained (85 %) at a lower applied pressure of 69

kPa. Based on such comparison, it can be concluded that the low cost membrane reported in this work is comparable or even better than the membranes reported in the literature.

Also, adsorption of oil droplet on the membrane structure was evaluated. To do so, the membrane was first soaked in feed oil emulsions (concentrations of 125 mg/L and 250 mg/L) for 30 min. Eventually, the membrane was taken out and the pure water flux was measured at a pressure of 69 kPa. The adsorption effect was evaluated in terms of flux decline after keeping it in contact with oil emulsion. It has observed that the change in flux of the membrane is insignificant. Henceforth, the membrane reported in this work with higher flux is expected to be less susceptible to fouling. Thus, the developed membrane is characterized with good combinations of flux, rejection and fouling for the MF of oil-water emulsions.

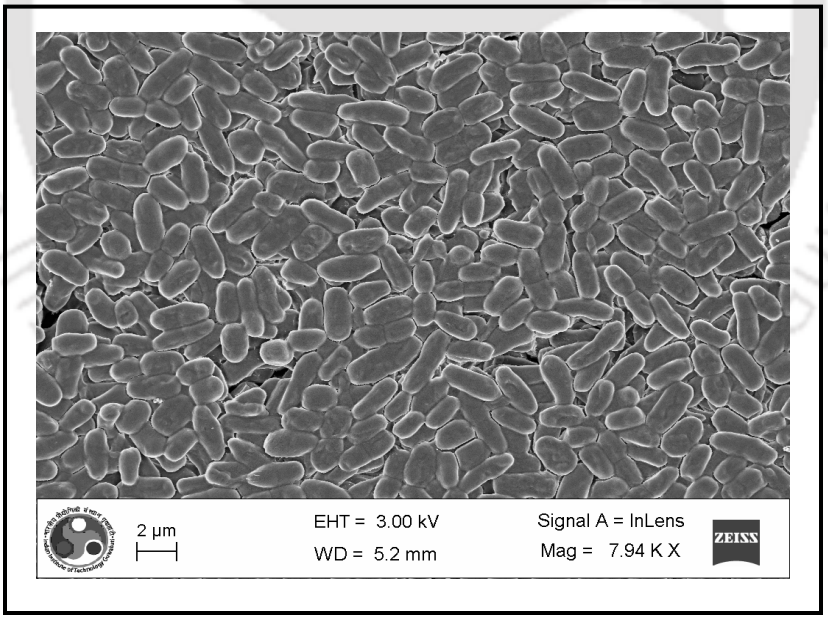

Figure 3.10: SEM image of *E. coli* bacteria.

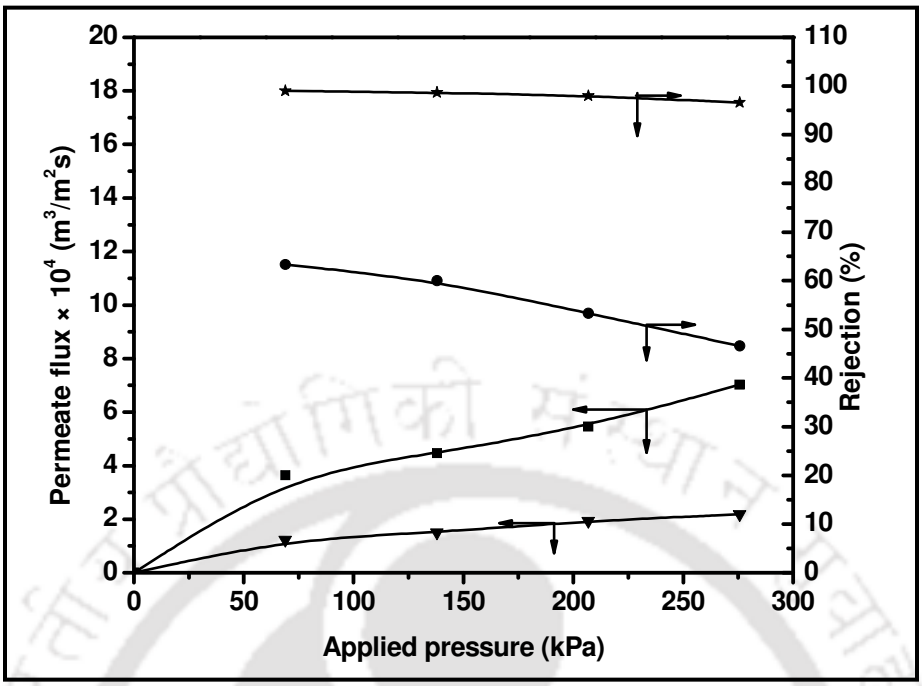

Figure 3.11: Variation of B1 membrane permeate flux and bacteria rejection with applied pressure for initial bacteria concentrations of 6×10^4 CFU/mL (■ Flux, ● Rejection) and 6×10^5 CFU/mL (▼ Flux, ★ Rejection).

3.2.4 Microfiltration of bacteria (*E. coli*)

Figure 3.10 depicts the SEM image of bacteria (*E. coli*). It can be observed from the figure that all bacteria cells are rod shaped entities. Moreover it has been evaluated that almost all bacteria cells have similar size of about 2×1.5 µm.

The bacteria MF experiments were performed with bacterial solutions (concentration of 6×10^4 and 6×10^5 CFU/mL) at various applied pressures (69 – 276 kPa). The obtained results for variation in permeate flux and rejection with variation in applied pressure and concentration has been shown in Fig. 3.11. As shown, the permeate flux increases with an increase in the applied pressure. This is due to an increase in driving force across the membrane with increasing pressure. However, the increase in flux with applied pressure

did not follow a linear trend. This indicates that there are additional transport resistances (i.e. resistance due to adsorption and partial pore blocking). While increasing the pressure, the microbial cells in the solution travel very fastly towards the membrane surface and reach it very rapidly. As a result, a layer containing large number of microbial cells forms on the membrane surface. This layer gets compacted at higher applied pressure due to which significant pore blocking occurs. For a feed bacteria concentration of 6×10^4 CFU/mL, at an applied pressure of 69 kPa, figure 3.11 indicates that the maximum observed rejection and permeate flux refer to 63 % and 3.64×10^{-4} m^3/m^2s, respectively. For feed concentration of 6×10^5 CFU/mL, the rejection of above 96 % has been obtained for the entire applied pressure range (Fig. 3.11). This confirms that at higher feed concentration, rejection increases. This is due to the fact that at higher concentration, the interaction among the microbial cells increases and large sized microbial cells could get formed. The MF based separation of bacteria mainly occurred due to sieving mechanism, where the solute size larger than the membrane pore size enabled effective separation. It is well known that the E. *coli* are rod shaped bacterium of well defined dimensions (2 µm × 1 µm) (Arkhangelsky and Gitis 2008). These cells have comparatively bigger size than the average pore size (1.06 µm) of membrane. On the other hand, the unexpected bacteria leakage was found at even lower concentration despite considering the fact that the average pore of the membrane is smaller than the size of the bacterium. This is due to few large pores in the membrane morphology. Similar observation of *E. coli* leakage with polymeric membrane (tract-etched membrane with an average pore size of 0.4 µm) was also reported in the literature (Lebleu *et al*., 2009).

In addition, the interaction between membrane and *E. coli* was evaluated by soaking the membrane in bacteria solutions individually at feed concentrations of 6×10^4 and 6×10^5 CFU/mL. For these experiments, the membrane was soaked at 25 °C for 2 h. Eventually, the concentration of the bacteria solution before and after membrane soaking was evaluated. It has been observed that around 9 % of the bacteria adsorbed on the membrane surface for the bacteria feed concentration of 6×10^5 CFU/mL. The adsorption of bacteria at a lower feed concentration of 6×10^4 CFU/mL has been found to be negligible.

3.2.5 Microfiltration of chromium (VI)

3.2.5.1 Effect of applied pressure

The effect of applied pressure on the permeate flux and removal of Cr (VI) bound with biomass was investigated in the range of 69 – 345 kPa. Fig. 3.12 depicts the variation of permeate flux and Cr (VI) removal as a function of applied pressure. In general, it has been observed that the permeate flux is lower than the pure water flux. Also, it has been observed that the permeate flux increases ($1.55 – 2.07 \times 10^{-5}$ m^3/m^2s) with increasing applied pressure (69 – 345 kPa), which is due to the enhancement in the driving force across the membrane. However, the increase in the flux with applied pressure did not follow a linear trend, indicating that there are additional resistances (i.e. resistance due to adsorption and partial pore blocking). While increasing the pressure, the yeast cells in the solution travel very fastly towards the membrane surface to reach it very rapidly. As a result, a layer containing large number of yeast cells forms on the membrane surface. This layer could get compacted at higher applied pressures to eventually enhanced pore

blocking rate. Also it has been observed that, the removal of Cr (VI) remains almost same over the entire range of applied pressure. This confirms that the removal of Cr (VI) complex with biomass is almost unaffected by the applied pressure. At a pressure of 207 kPa, the observed Cr (VI) removal and the permeate flux are 20 % and 2.07×10^{-5} m^3/m^2s, respectively. In general, the shape and size of the yeast cells have a major effect on the removal of metal ions. It is well documented in the literature that the size of the yeast cells is around 2 – 5 µm (Bayhan *et al*., 2001).

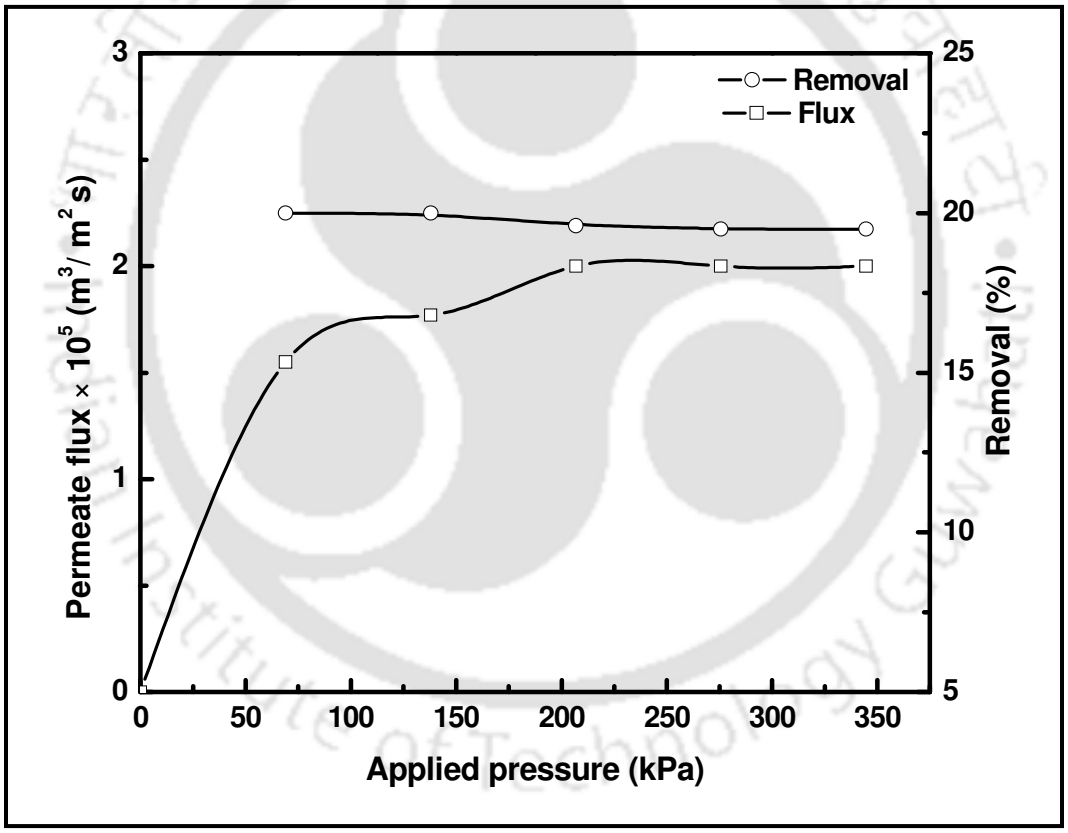

Figure 3.12: Effect of applied pressure on the B1 membrane permeate flux and Cr (VI) removal efficiency. Corresponding feed concentration, biomass dosage and pH refer to 100 mg/L, 10 g/L and 6, respectively.

Since pore size of the membrane (1.06 µm) is smaller than the yeast cells, the rejection of the yeast has been evaluated to be 100 % for the applied pressure. Based on obtained trends in permeate flux and rejection, an applied pressure of 207 kPa is the optimal choice to achieve good membrane performance. Thus, further investigations and analysis have been carried out only at 207 kPa.

3.2.5.2 Effect of initial pH

The effect of initial pH on the Cr (VI) removal efficiency and permeate flux were examined in the initial pH range of 1 – 7 and obtained results have been presented in Fig. 3.13. The results indicate that the Cr (VI) removal is higher at pH 1 and thereafter decreases (94 – 20 %) further as the pH increases. The removal of Cr (VI) strongly depends on the pH due to the higher binding of metal ion with biomass cell wall ligands at lower pH. Depending upon Cr (VI) concentration and solution pH, chromium (VI) can exist in the aqueous solution in different ionic forms such as $HCrO_4^-$, CrO_4^{2-}, $Cr_2O_7^{2-}$ (Bai and Abraham 2001). At pH 1 – 2, $HCrO_4^-$ is the dominant species (Sar and Tuzen 2008). The $HCrO_4^-$ species are most easily exchanged with OH^- ions at active surfaces under acidic conditions. Moreover, at very low pH, the surface of biomass cells would also be surrounded by the hydronium ions, which enhance the Cr (VI) interaction with binding sites of the biomass. However, as the pH increases, the overall surface charges on the cell become negative and hence the binding capacity decreases. The higher removal (94 %) of Cr (VI) complexes with biomass has been evaluated at a lower pH of 1. The permeate flux is found to be independent over the entire pH range (1 – 7) and remained constant at 2.07×10^{-5} m^3/m^2s.

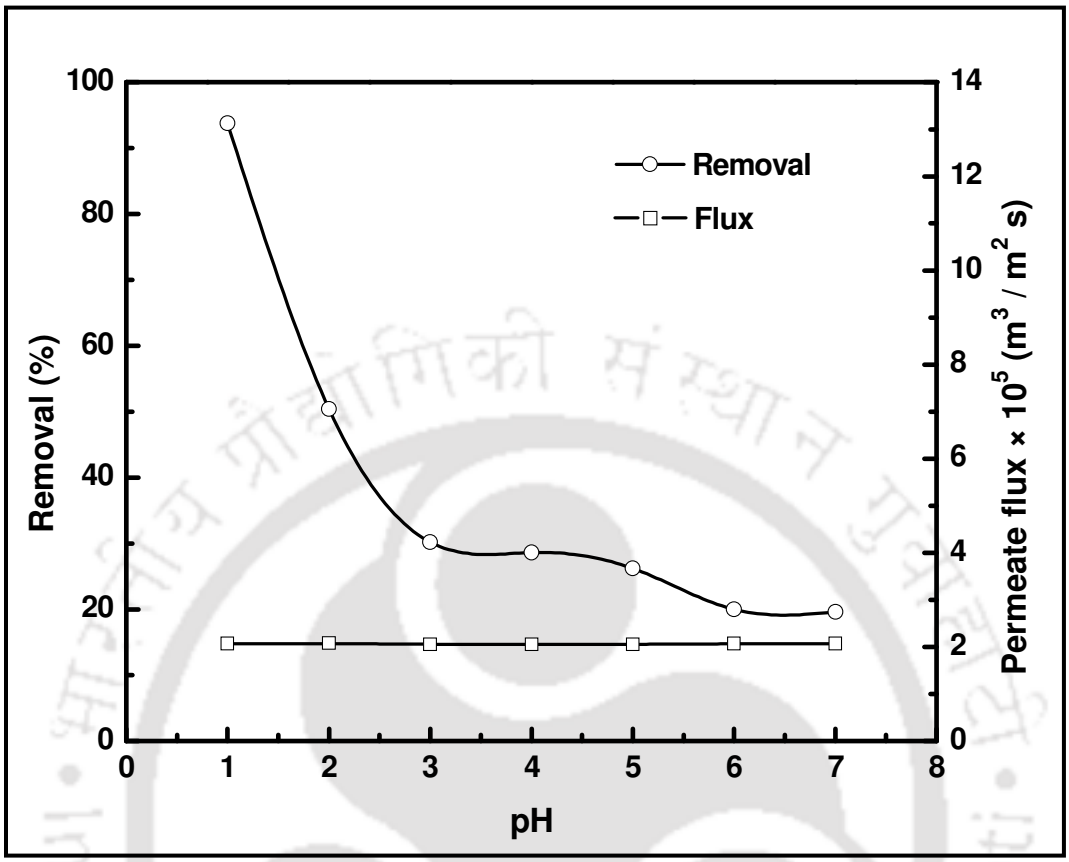

Figure 3.13: Variation of B1 membrane permeate flux and Cr (VI) removal efficiency with initial pH at a feed concentration, biomass dosage and applied pressure of 100 mg/L, 10 g/L and 207 kPa, respectively.

This confirms that the size of the yeast cells is not affected by the pH of solution. The effect of pH on the biosorption of Cr (VI) has been examined by various investigators using different types of biomass (Bai and Abraham 2001; Ozer and Ozer 2003). Optimum biosorptive removal of Cr (VI) at low pH (2) was reported for *Rhizopus nigricans* (Bai and Abraham 2001). At a pH of 1, the maximum removal of Cr (VI) was also reported for *saccharomyces cerevisiae* (Ozer and Ozer 2003).

3.2.5.3 Effect of initial Cr (VI) ion concentration

The effect of Cr (VI) concentration on the permeate flux and removal was investigated for variant feed concentration of Cr (VI) (100 – 250 mg/L). The obtained results are presented in Fig. 3.14. Fig. 3.14 illustrates that initial Cr (VI) concentration did not significantly alter metal ion removal percentage. The removal of Cr (VI) decreased (94 – 85 %) slightly with an increase in the metal ion concentration. This is due to the saturation of the binding sites on the biomass.

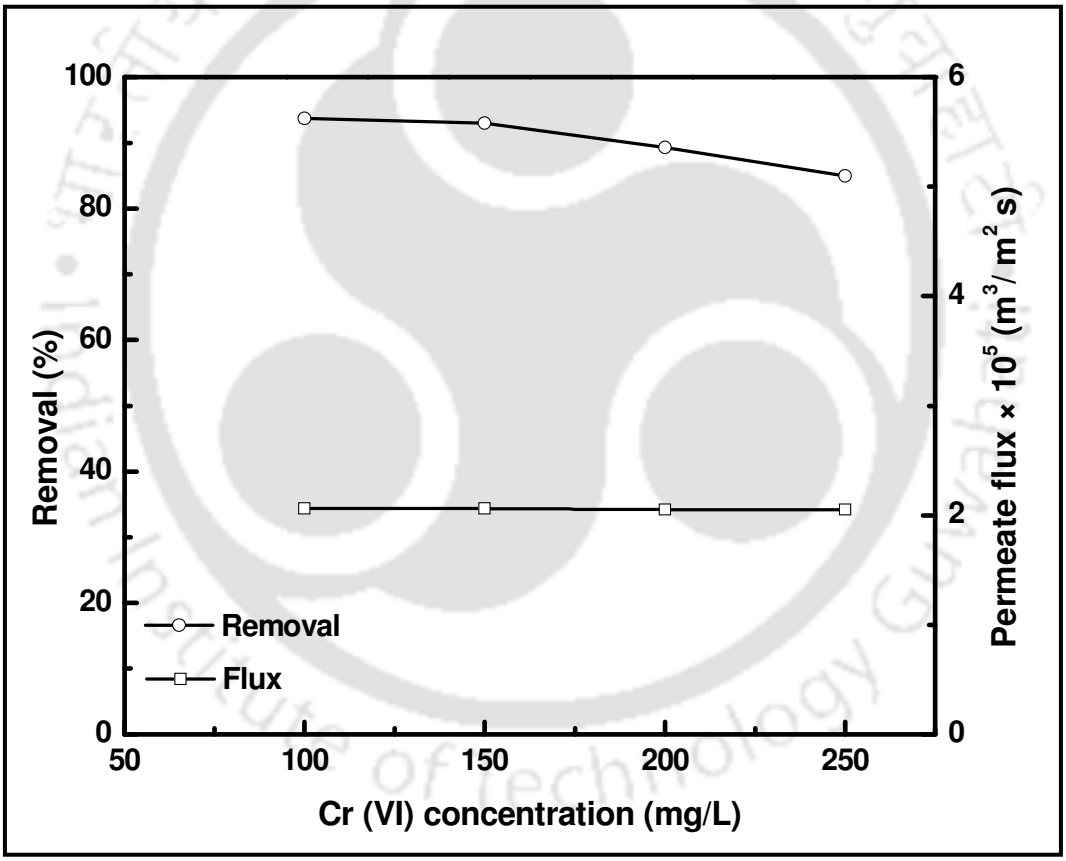

Figure 3.14: Effect of Cr (VI) feed concentration on the B1 membrane permeate flux and Cr (VI) removal efficiency at pH, biomass dosage and applied pressure of 1, 10 g/L and 207 kPa, respectively.

It has been hypothesized in the literature that the initial metal ion concentration acts as an important driving force to overcome mass transfer resistances of metal ions between aqueous and solid phases (Vimala and Nilanjana 2009). A similar type of the removal trend was also reported for divalent metal ion mixtures using *saccharomyces cerevisiae* (Bayhan *et al*., 2001). The maximum removal (94 %) of Cr (VI) was observed at a metal concentration of 100 mg/L. The permeate flux remained almost constant for all the studied initial Cr (VI) concentrations, indicating that the permeate flux is not affected by the initial Cr (VI) concentration values. This confirmed that the permeate flux is mainly dependent upon the concentration of yeast cells but not on the metal solution concentration.

3.2.5.4 Effect of biomass dosage

Figure 3.15 illustrates the variation of Cr (VI) percentage removal with biomass dosage. It can be observed that the removal of Cr (VI) ion largely depends on the concentration of biomass used for binding the Cr (VI) in the medium. The removal of Cr (VI) increases (65 – 99 %) with an increase in the biomass concentration. This trend is obvious as increasing biomass concentration provides greater availability of exchangeable sites to bind the metal ions. The maximum removal of Cr (VI) (99 %) is observed at a higher biomass concentration of 16 g/L. Corresponding permeate flux is about 1.16×10^{-5} m^3/m^2s. It can be also seen that the permeate flux decreases with increasing biomass concentration. The reduction in the permeate flux at higher biomass concentration could be explained as a consequence of enhancement in number of yeast cells in the medium. An increase in biomass concentration enable enhancement in both adsorptive and

concentration polarization resistances. Similar flux trend was reported in the literature for the other type separation of heavy metal mixture (Bayhan *et al*., 2001).

Till date, several approaches have been tested for the removal of Cr (VI) from its solution. These include adsorption-ultrafiltration (AUF) (Pagana *et al*., 2008), polyelectrolyte-enhanced UF (PEUF) (Korus and Loska 2009), polymer-enhanced UF (PUF) (Aroua *et al*., 2007) and nanofiltration (NF) (Ren *et al*., 2010). UF and NF membranes offer low membrane flux and are more susceptible for fouling.

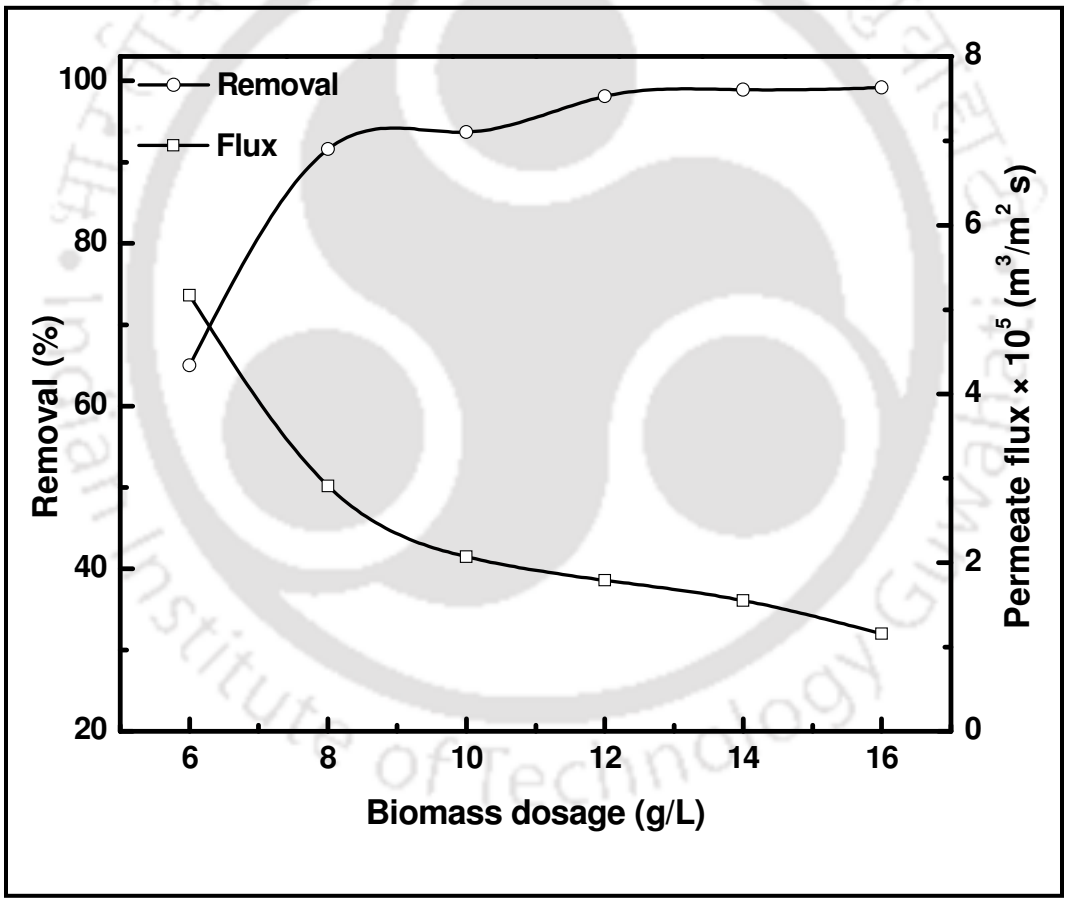

Figure 3.15: Variation of the B1 ceramic membrane permeate flux and Cr (VI) removal efficiency with biomass dosage for a feed concentration, pH and applied pressure of 100 mg/L, 1 and 207 kPa, respectively.

Furthermore, polymers and surfactants used as carrier in PEUP/PUF/SUF are expensive. Therefore, biomass assisted microfiltration would be economically beneficial for the removal of Cr (VI). Amongst several biomasses, the yeast is widely available, inexpensive and can be obtained from various fermentation industries. Moreover, the usage of microfiltration membrane enables larger flux and therefore the suggested combination is promising for industrial applications.

The obtained ceramic membrane performance indices (94 % removal efficiency and 2.07×10^{-5} m^3/m^2s permeate flux at 207 kPa and feed Cr (VI) concentration of 100 mg/L) are comparable with those reported in the literature (Neelakandan and Pugazhenthi 2003; Pugazhenthi *et al*., 2005; Ren *et al*., 2010). About 60 % removal efficiency and 2.777×10^{-6} m^3/m^2s permeate flux were obtained at 275 kPa using nitrated PMMA-EGDM composite membrane by adopting ultrafiltration of Cr (VI) solution (1000 mg/L) (Neelakandan and pugazhenthi 2003). Pugazhenthi *et al*. (2005) achieved 50 % Cr (VI) removal using unmodified carbon membrane (permeate flux of 2.22×10^{-7} m^3/m^2s) and 58 % removal with modified carbon membrane (permeate flux of $6.38 \times 10^{-7} m^3/m^2s$) at 275 kPa with ultrafiltration process. Ren *et al*., (2010) reported 90 % removal and 1.055×10^{-5} m^3/m^2s permeate flux at 700 kPa at a feed Cr (VI) concentration of 130 mg/L using PMIA nanofiltration membrane. Upon comparison of the obtained results with the above literature data, it can be inferred that, both permeate flux (2.07×10^{-5} m^3/m^2s) and removal value (94 %) reported in this work are higher than those reported even at a lower applied pressure of 207 kPa. Therefore, it is concluded that the research reported in this work is further promising for the separation of Cr (VI) from its synthetic solution.

3.2.6 Membrane cost

Based on the retail cost of various raw materials used for preparing ceramic membrane in this work, the fabrication cost of ceramic membrane has been evaluated to be Rs. 2821/m^2 (45.75 \$/m^2) (Table 3.4). In comparison, the symmetric ceramic membranes made with α-alumina cost around \$ 500/m^2 and stainless steel asymmetric membranes cost about \$ 3000/m^2 (Mott Metallurgical Corporation, USA, 2007). Therefore, it can be inferred from the cost analysis that the fabricated membrane is highly inexpensive than the alumina membrane (Mavrov *et al*., 1998) due to the chosen inexpensive raw materials and lower sintering temperature for the membranes.

Table 3.4: Raw material unit cost based cost parameters of (B1 – B3) ceramic membranes.

Raw materials	**Unit price (Rs./ kg)**	**Amount of raw material used for preparation of one membrane (kg)**	**Cost of one membrane (Rs.)**
Kaolin	390	13×10^{-3}	5.07
Quartz	200	6.5×10^{-3}	1.3
$CaCO_3$	330	6.5×10^{-3}	2.145
		Total cost of membrane	Rs. 8.51
		(Round off value)	Rs. 9.00

For the fabrication of circular disk-shaped ceramic membrane of 5 mm thickness and 62 mm diameter = Rs. 9.00 / membrane.

Raw material cost of the membrane/unit area= Rs.2821 / m^2

3.3 Summary

Low cost ceramic membranes (B1 – B3) have been successfully prepared by uniaxial dry compaction method using inexpensive raw materials. Thermal characterization confirmed that the appropriate sintering temperature for the chosen composition of materials is around 900 °C. XRD analysis also provided significantly insights for various phase transformations during sintering and quartz has been found to be the major phase for all sintered membranes. The maximum shrinkage of the membranes is about 11 % for the studied temperature range. The SEM analysis shows that the average pore diameter of the membranes increases with an increase in the sintering temperature. The porosity of the membranes decreases with increasing sintering temperature and is found to be about 34 – 45 %. The prepared membranes possessed good mechanical strength (34 to 46 MPa flexural strength) and chemical stability (< 6 % weight loss in acidic media and no weight loss in basic media). It has been concluded that the membrane (B1) sintered at 900 ^{o}C is the optimum membrane for industrial applications due to its good mechanical strength (34 MPa), better porosity (45 %) and lower average pore size (1.06 µm). The organic solvent permeation study confirms that the membrane reported in this work is hydrophobic in nature.

Moreover, the membrane B1 sintered at 900 ^{o}C performed well for the separation of oil-water emulsions, *E. coli* and biomass assisted MF separation of chromium (VI) from aqueous solution. The results confirm that the observed rejection is decreased with an increase in the applied pressure and increased with an increase in the concentration of oil-water emulsion and *E. coli*. A maximum rejection of 85 % and 99 % has been obtained through the membrane for oil-water emulsion and *E. coli*, respectively. Results for

chromium MF experiments indicate that the removal of Cr (VI) strongly depends on the pH of the solution and highest Cr (VI) removal 94 % has been achieved at a pH of 1. The removal of Cr (VI) is found to increase with increasing biomass concentration and decreases insignificantly with increasing Cr (VI) ion concentration. The adsorption-MF scheme provided an optimal removal (94 %) and membrane flux (2.07×10^{-5} m^3/m^2s) at 207 kPa for a feed Cr (VI) concentration of 100 mg/L. Based on the raw materials used to prepare ceramic membrane in this work, the fabrication cost of ceramic membrane has been evaluated to be Rs. 2821/m^2 (45.75 \$/m^2).

Chapter 4:

Ceramic Membrane Fabrication for the Microfiltration of Oil-in-Water Emulsions

Ceramic Membrane Fabrication for the Microfiltration of Oil-in-Water Emulsions

This chapter addresses further optimization of identified raw materials composition to fabricate membranes of variant morphological properties. TiO_2/$CaCO_3$ addition/removal has been carried out to target the necessary variations. Two new compositions were identified to reduce the pore size of the membrane. The main objective of this chapter is to evaluate upon the role of TiO_2 addition on various membrane properties such as porosity, average pore size, flexural strength and pure water permeability. The prepared membranes (B1, C1 & C2) were subjected to dead-end MF of oil-water emulsions. These experiments were conducted to evaluate upon the effect of applied pressure and oil concentration on the permeate flux and oil removal efficiency.

4.1 Experimental

In chapter 3, membranes B1, B2 and B3 were reported, whose average pore size is about 1.06, 1.33 and 2.22 μm, respectively. Amongst these, the B1 membrane has been identified as the optimal choice due to its good performance characteristics. However, higher pore size of the membranes is not favourable for the effective treatment of oil-water emulsions in the range of 50 – 200 mg/L. Thus, further engineering is targeted to achieve sub-micron range MF membranes. To do so, further reduction in membrane pore size is anticipated by altering the identified raw materials composition.

4.1.1 Starting materials

Table 4.1 summarizes various precursor formulations that were identified for the fabrication of various microfiltration membranes namely B1, C1 and C2. Kaolin, quartz, calcium carbonate, titanium dioxide were obtained from CDH India, Research Lab Fine Chem. Industries, India, Merck, Mumbai, India, Rankem India Ltd., respectively. All these raw-materials were used without any further purification procedures. Amongst the raw materials, kaolin is the major raw material in terms of composition and is one of the cheapest raw materials readily available in India. Moreover, other raw materials have been selected to serve for various functional attributes. Kaolin provides low plasticity and high refractory properties to the membrane. Quartz enables higher mechanical strength and thermal stability to the membrane. Calcium carbonate serves as a pore forming agent and sintering aid. Titanium dioxide provides additional mechanical strength to the membrane.

Table 4.1: Identified compositions of raw materials for (B1, C1 and C2) membranes preparation.

Raw materials	**Membrane B1 (wt. %)**	**Membrane C1 (wt. %)**	**Membrane C2 (wt. %)**
Kaolin	50	50	50
Quartz	25	25	25
Calcium carbonate	25	22	15
Titanium dioxide	-	3	10

4.1.2 Membrane preparation and characterization

Chapters 2 and 3 presented a detailed account with respect to the membrane preparation and characterization. Similar procedures were followed to fabricate C1 and C2 membranes. Targeted characterization techniques include particle size distribution (PSD), thermogravimetric analysis (TGA), X-ray diffraction analysis (XRD), scanning electron microscopic analysis (SEM), porosity, mechanical stability, chemical stability test and pure water permeation test.

4.1.3 Treatment of oil-in-water emulsions

The crude oil was obtained from Indian Oil Corporation Limited (IOCL) petroleum refinery located at Guwahati. The oil-water emulsions were prepared by the emulsification of crude oil with Millipore water (Make: Millipore, Model: ELIX-3) in an ultrasonic cleaning bath (Make: Elma (India); Model: T460) for about 5 – 15 h. For microfiltration studies, four different concentrations (50, 100, 150 and 200 mg/L) of oil-in-water emulsion were prepared. Microfiltration tests at various applied pressures (69 – 345 kPa) were carried out using dead-end filtration setup. At each applied pressure, 10 mL of permeate collected initially during the MF run was discarded and the average permeate flux was evaluated by measuring the time taken to collect the second sample of 10 mL permeate solution. The permeate flux was evaluated by evaluating the ratio of permeate volume to membrane area and sampling time. The average rejection (*R)* was determined using the expression

$$R(\%) = \frac{C_f - C_p}{C_f} \times 100 \qquad (4.1)$$

where C_f and C_p are the oil concentration in the feed and permeate, respectively. The concentrations of feed and permeate solution samples have been obtained using a calibration chart (Appendix A) that has been prepared using standard known concentrations of synthetic oil-water emulsions. The calibration chart has been prepared by measuring the absorbance of the emulsion solutions at a wave-length of 235 nm (Chakrabarty *et al*., 2008) using a UV–vis spectrophotometer (Make: Spectrascan; Model: UV 2300). Using the calibration chart correlation, the unknown oil concentrations were obtained by measuring the absorbance of various feed and permeate samples. After carrying out a MF test, the membrane cleaning was carried out using a detergent solution (commercial surf excel detergent at an aqueous solution concentration of 2 g/L) to remove the crude oil adhering to the membrane surface. Eventually, high pressure (414 kPa) flushing with Millipore water for a period of 1 h was performed to regain the original pure water flux.

4.2 Results and discussion

4.2.1 Characterization of membranes

The particle size distribution and average particle size of the raw materials significantly influences the pore size and sintering temperature of the membrane. A general rule of thumb is that the finer particles require lower sintering temperatures and yield a membrane with lower average pore size and narrow pore size distributions. On the other hand, coarser particles require higher sintering temperature and enhance the average pore size of the membrane (Wang *et al*., 2007).

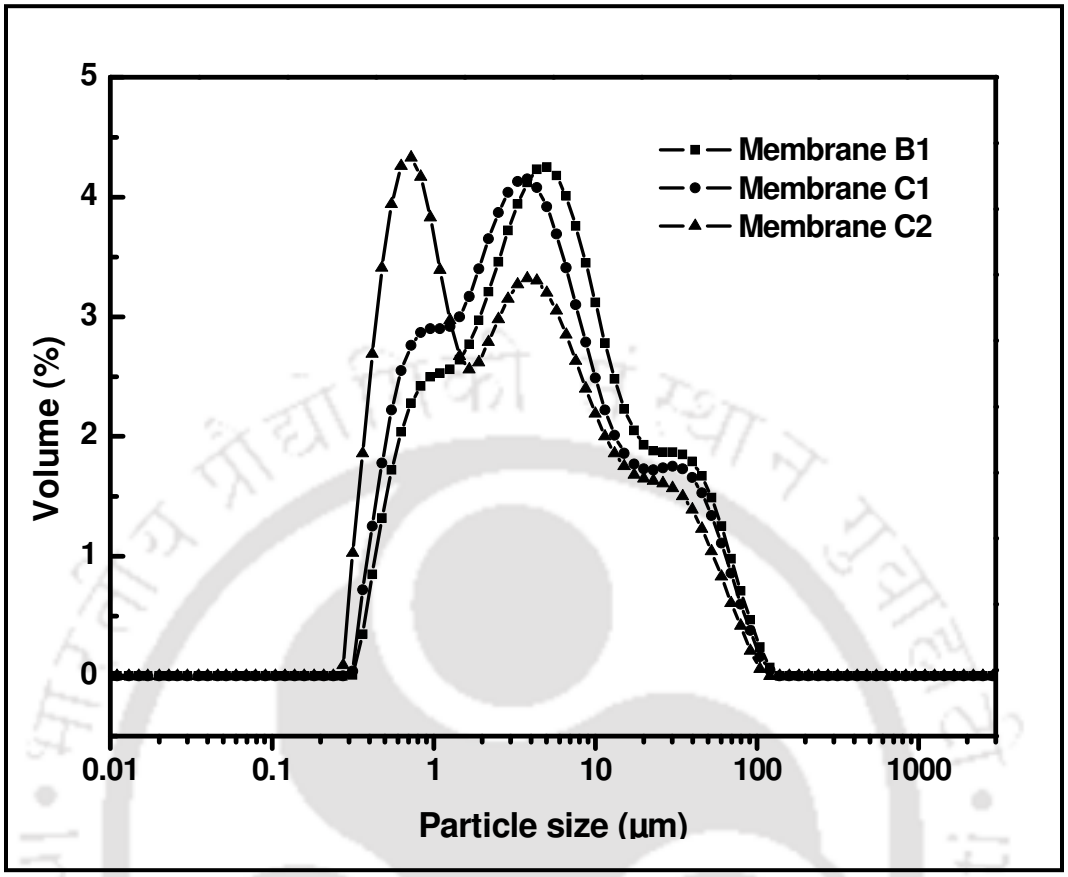

Figure 4.1: Particle size distribution of the raw material mixtures used for B1, C1 and C2 membrane fabrication.

Particle size distribution (PSD) of the raw materials for corresponding compositions of membranes B1, C1 and C2 were obtained from particle size analyzer and are illustrated in Fig. 4.1. The figure conveys that the particle size of each composition varies between 0.3 to 120 µm and the average particle size of the powder mixtures corresponding to B1, C1 and C2 membranes is about 19.1, 17.8 and 15.3 µm, respectively.

Figure 4.2 presents the TGA analysis of the raw material mixture used for the membranes. From the figure, it has been evaluated that the weight loss of the powder mixture is about 21, 18 and 14 % for membrane B1, C1 and C2, respectively.

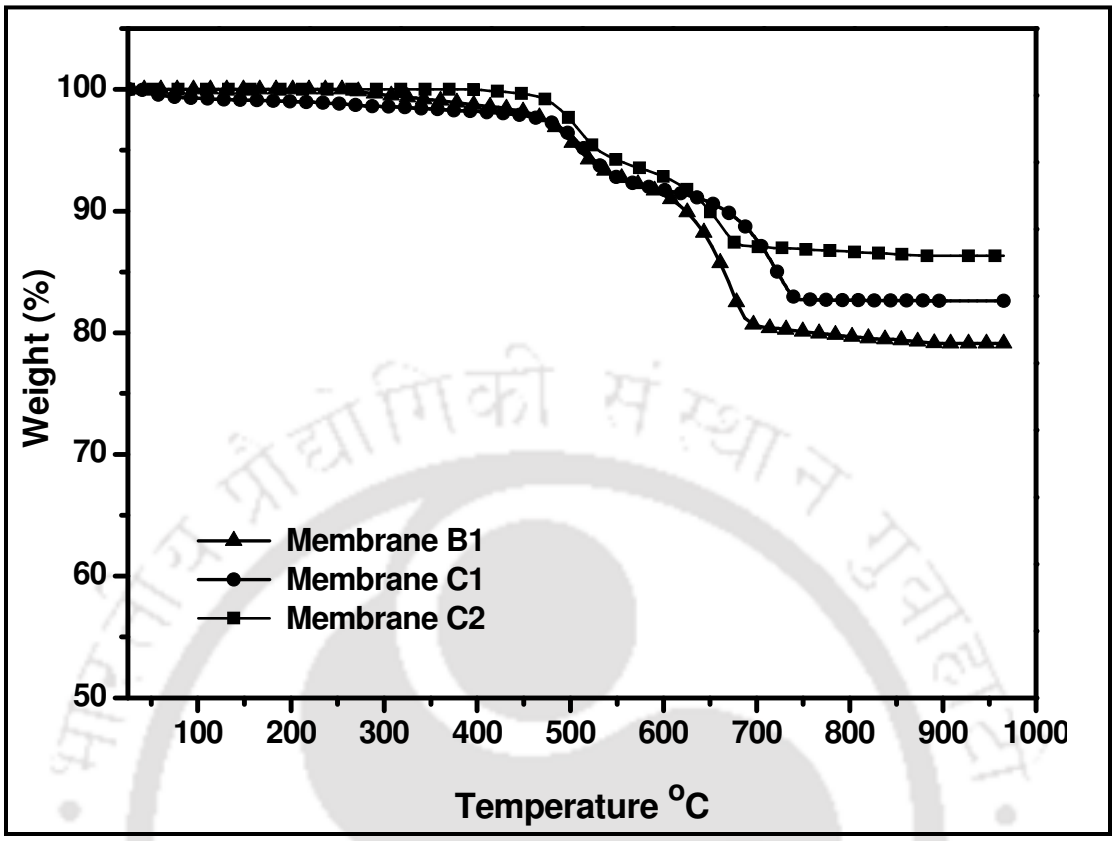

Figure 4.2: TGA curves for the B1, C1 and C2 membrane raw material mixtures.

The weight loss of the sample can be explained as follows: firstly, moisture content in the powder sample is removed at temperatures below 150 ^{o}C. Secondly, thermal decomposition of $CaCO_3$ in the mixture occurs and this results in the conversion of $CaCO_3$ to CaO and CO_2. The generated CO_2 contributes to the porous structure of the membrane whose morphology is dependent upon the path taken by the evolved gas. At higher temperatures, the weight loss of the sample further decreases. Therefore, it is apparent that the weight loss of the sample is directly related to the quantity of calcium carbonate present in the sample. Moreover, it can be observed in the figure that there is no significant weight loss above 750 ^{o}C and hence the minimal sintering temperature shall be above 750 ^{o}C and the chosen sintering temperature of 900 ^{o}C is justified.

XRD analysis of the microfiltration membranes was carried out to identify the phase transformations during sintering. Fig. 4.3 presents the results obtained from XRD analysis of the membranes before and after sintering. Generally, sintering process allows the membrane to undergo phase transformation and therefore new phases are formed. It can be observed in the figure that the peaks of kaolin, quartz and calcium carbonate exist in the membranes before sintering and after sintering the peaks corresponding to kaolin has disappeared. This is due to the conversion of kaolinite to mullite via metakaolinite. Furthermore, it can be observed that quartz peak did not change in the sintered membranes. This confirms upon the thermal stability of the phase. Two new phases are also observed, namely, anorthite ($CaO{\cdot}Al_2O_3{\cdot}2SiO_2$) and wollastonite ($CaSiO_3$). This is probably due to the reaction between CaO and amorphous silica. The presence of TiO_2 in the C1 and C2 membranes is confirmed by the rutile phase in the XRD patterns for these membranes in both cases namely samples before and after sintering. Moreover, it is also apparent that TiO_2 addition did not enable significant phase transformations in both C1 and C2 membranes.

The average membrane porosity was experimentally determined using Archimedes's principle. It was found that the average porosity of the membranes is 30, 26 and 23 % for membranes B1, C1 and C2, respectively. These data clearly indicate that the obtained porosity reduced with reducing porosifier ($CaCO_3$) concentration in the precursor formulations. The observations are in good agreement with the presented trends in the literature that also indicate that the porosity of the membrane increased with increased concentration of porosifier in the precursor formulations (Falamaki *et al*., 2004; Boudaira *et al*., 2009).

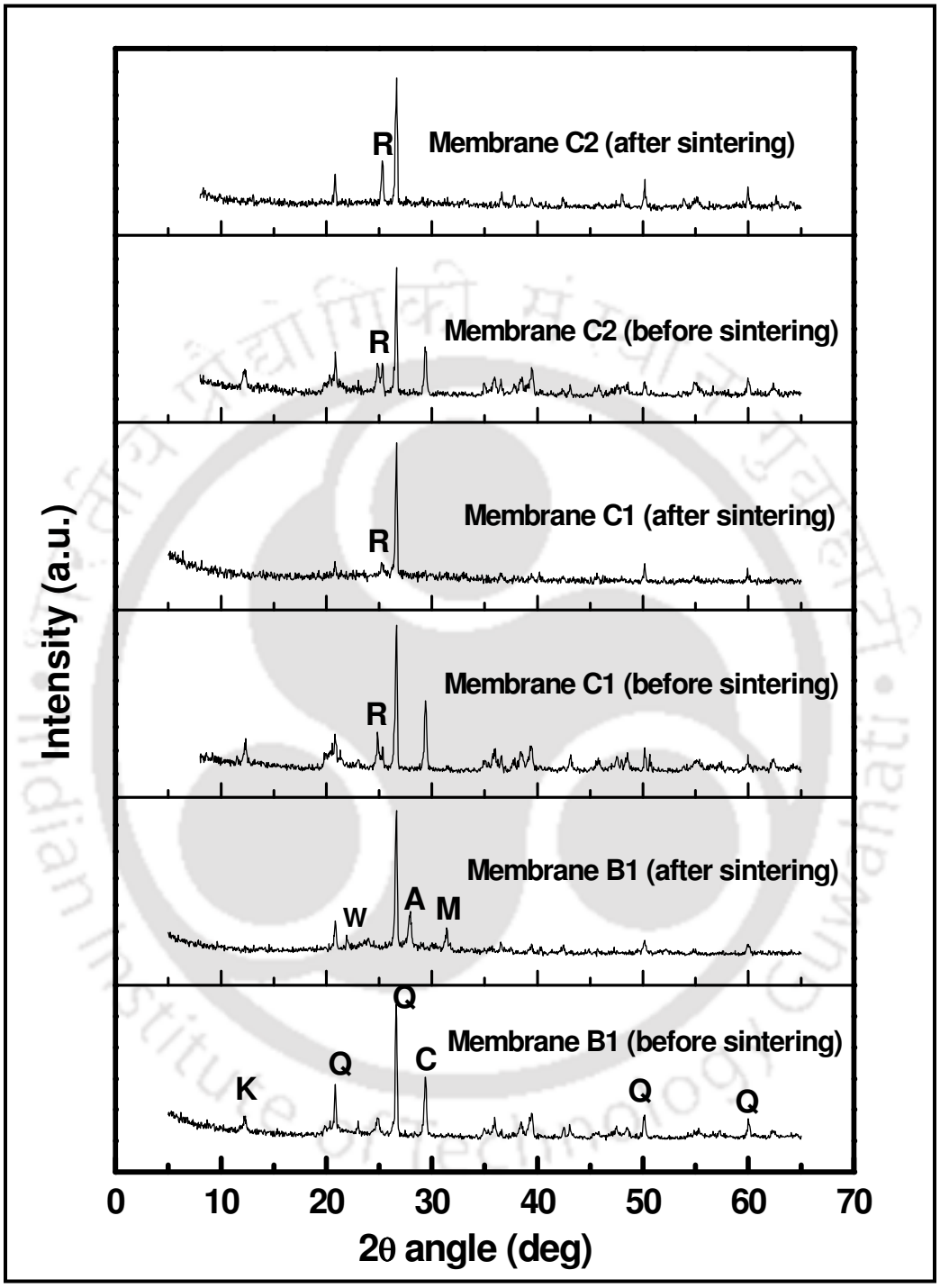

Figure 4.3: XRD patterns of (B1, C1 and C2) membranes before and after sintering Peaks in the patterns correspond to: K-Kaoiln, Q-Quartz, C-Calcium carbonate, M- Mullite, A- Anorthite, W- Wollastonite and R-Rutile.

The SEM images were used to analyze the morphology of the membranes. Fig. 4.4 (a – c) illustrates the SEM images of the fabricated membranes. These images clearly indicate that the membranes have distinct morphological structure and surface pore sizes. Therefore, it can be understood that the composition of the raw materials significantly influences the membrane surface morphology. In addition, the surface pore size of membranes was estimated from SEM micrographs using ImageJ software and the average pore diameter of the membranes B1, C1 and C2 has been evaluated to be 1.42, 1.21 and 0.56 µm, respectively.

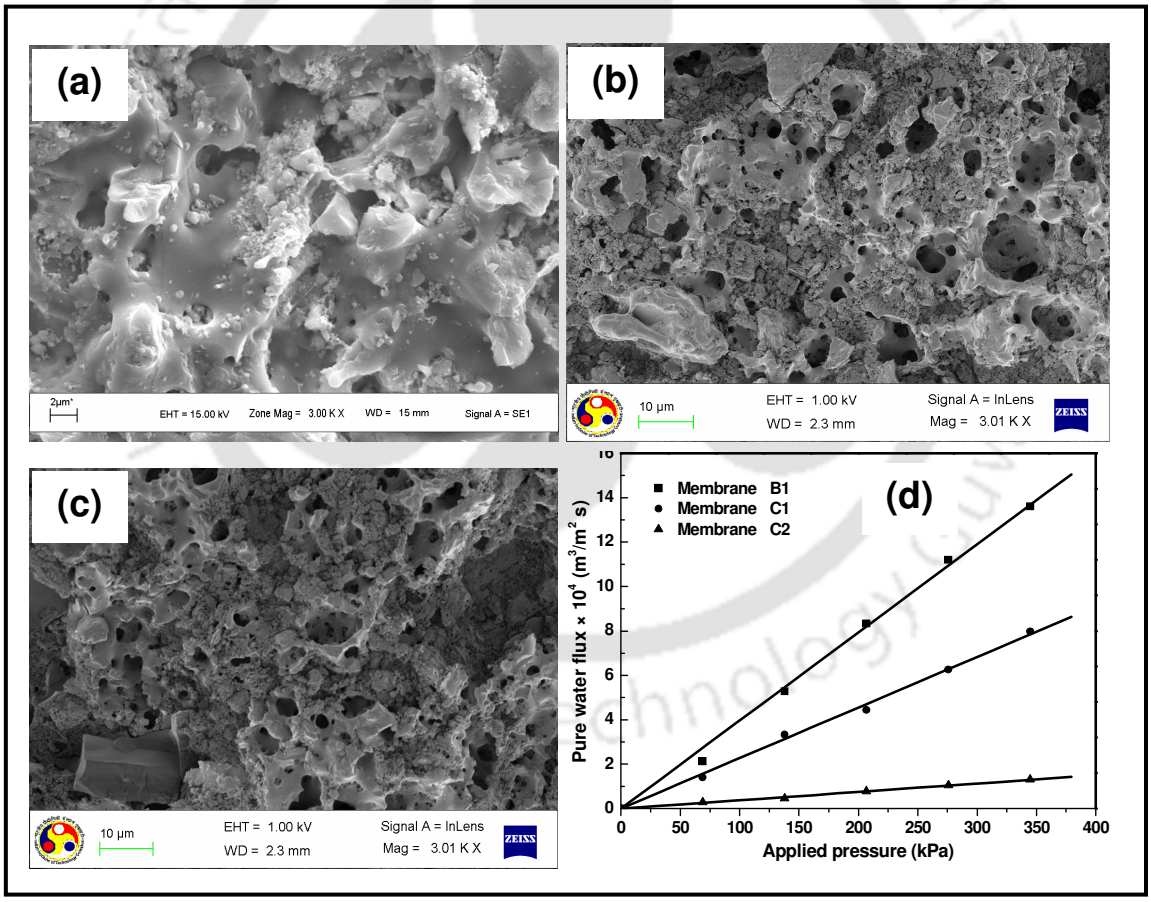

Figure 4.4: SEM images of (a) B1 (b) C1 and (c) C2 membranes. (d) Pure water flux plot for B1, C1 and C2 membranes.

Figure 4.4d presents the variation of pure water flux with applied pressures for the membranes (B1, C1 and C2). From fundamental theory of porous membranes, the hydraulic permeability is estimated to be 3.97×10^{-6}, 2.34×10^{-6} and 3.7×10^{-7} m^3/m^2s kPa for the membranes B1, C1 and C2, respectively. Further, the average pore radius of the membrane has been evaluated by assuming cylindrical pores using the equation derived from Hagen-Poiseuille equation (Almandoza *et al*., 2004).

$$r_l = \left[\frac{8\mu l L_h}{\varepsilon}\right]^{0.5} \tag{4.2}$$

where L_h is the hydraulic permeability of the membrane, μ is the viscosity of water, *l* is the pore length and ε is the porosity of the membrane (obtained from Archimedes principle). Thereby, the hydraulic average pore diameter of the membranes (based on pure water permeation experiments) has been evaluated to be 1.06, 0.99 and 0.35 μm for the membranes B1, C1 and C2, respectively. The reduction in average membrane pore size with reduction in porosifier ($CaCO_3$) concentration is in agreement with the trends presented in the literature (Falamaki *et al*., 2004; Boudaira *et al*., 2009).

The chemical stability tests for various membranes indicated that all membranes have satisfactory chemical stability in both acidic and basic media. For the case of acid media tests, it has been found that the weight loss of the membranes is 6, 4, and 1 % for membranes B1, C1 and C2, respectively. For C1 and C2 membranes, the increasing trend in acid stability is due to the enhancement of TiO_2 concentration in their formulations. On the other hand, for base chemical stability tests, the weight loss has been found to be negligible for all membranes and therefore, the membranes are more stable for alkali range cleaning in comparison to acid based cleaning procedures.

The measurement for flexural strength was carried out using the three point bending method. The flexural strength of the membranes was found to be 34, 12 and 10 MPa for B1, C1 and C2, respectively. These values indicate that the membranes have greater mechanical stability and the flexural strength of the membranes reduced with reducing $CaCO_3$ in the raw material palette. These observations are in agreement with the conception that $CaCO_3$ contributes dually to the inorganic membrane and acts both as a porosifer as well as sintering aid (Falamaki *et al*., 2004). The membrane structural densification is highly dependent on the sintering aid. Consequently, the membrane densification decreased with a reduction in the sintering aid concentration and this contributed to a reduction in flexural strength. The observed trends are in good agreement with the reported enhancement in structural densification with increasing $CaCO_3$ concentration for aluminium nitride in the literature (Molisani *et al*., 2006). Therefore, it can be opined that the composition of raw materials significantly affects membrane properties namely porosity, pore size, flexural strength and hydraulic permeability.

Table 4.2: Characterization parameters for B1, C1 and C2 low cost ceramic membranes.

Properties	Membrane B1	Membrane C1	Membrane C2
Pore size (SEM)	1.42 µm	1.21 µm	0.56 µm
Pore size (from water flux)	1.06 µm	0.90 µm	0.35 µm
Porosity (%)	45	41	39
Hydraulic permeability (m^3/m^2s kPa)	3.97×10^{-6}	2.34×10^{-6}	3.7×10^{-7}
Chemical stability			
Acid – Weight loss (%)	6	4	1
Base – Weight loss (%)	Nil	Nil	Nil
Flexural strength (MPa)	34	12	10

Table 4.2 presents the summary of characterization results of the membranes prepared with different compositions. A comparative summary of these results with the characterization results of membranes presented in various literatures is presented in Table 4.3. From both Tables 4.2 and 4.3, it can be inferred that the fabricated low cost ceramic membranes compare well with those reported in the literatures (Bouzerara *et al*., 2006; Saffaj *et al*., 2006; Dong *et al*., 2007; Masmoudi *et al*., 2007).

4.2.2 Treatment of oil-in-water emulsions

Synthetic oily wastewater solutions prepared at four different concentrations (50, 100, 150 and 200 mg/L) were characterized for their droplet size distributions using a particle size analyzer (Model: APA 5005; Make: Malvern Mastersizer 2000). The obtained crude oil droplet size distributions have been presented in Fig. 4.5. It is evident from the figure that the droplet sizes of emulsion varied from 0.05 – 100 µm for all oil concentrations. The average diameter of emulsions droplet has been evaluated to be 0.770, 0.991, 6.025 and 6.928 µm for feed oil emulsion concentrations of 50, 100, 150 and 200 mg/L, respectively.

Figure 4.6 presents the variation of membrane permeate flux and oil rejection for the membranes B1, C1 and C2. In comparison with the pure water flux, the permeate flux of the emulsions are low. The permeate flux is dependent on the applied pressure and increased with increasing pressure (Fig. 4.6 a – c). This is due to the enhancement in driving force across the membrane at higher trans-membrane pressure differentials. The permeate flux obtained for membrane C2 is lower than the flux obtained with membranes B1 and C1.

Table 4.3: A comparative summary of (B1, C1 and C2) membrane characterization parameters with those reported in the literature.

Membrane Materials	Sintering temperature (^{o}C)	Average pore size (µm)	Porosity (%)	Mechanical strength (MPa)	Chemical stability (Wt.%)	References
Kaolin+Dolama	1200	3.77	40.99	6 (Tensile strength)	-	Bouzerara *et al.*, (2006)
Kaolin+Dolama	1250	11.09	40.81	15 (Tensile strength)	-	Bouzerara *et al.*, (2006)
Moroccan clay	1175	10.75	43	3	-	Saffaj *et al.*, (2006)
cordierite	1380	8.66	36.20	31	Acid -17 Base -12	Dong *et al.*, (2007)
Apatite	1150	5	48	14	Acid -25 Base - 5	Masmoudi *et al.*, (2007)
Membrane B1	900	1.06	45	34	Acid - 6 Base - Nil	Present work
Membrane C1	900	0.90	41	12	Acid - 4 Base - Nil	Present work
Membrane C2	900	0.35	39	10	Acid - 1 Base - Nil	Present work

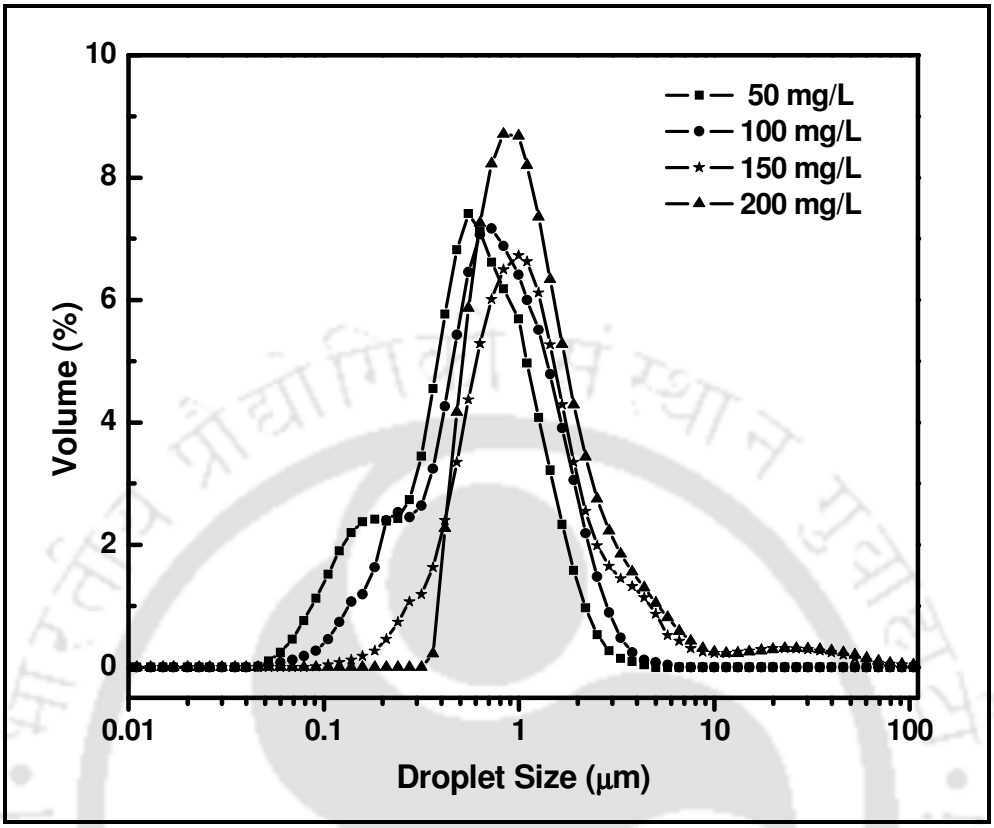

Figure 4.5: Droplet size distributions of oil-in-water emulsions in the concentration range of 50 – 200 mg/L.

For the membranes, the permeate flux is in the order of B1 > C1 > C2. This trend is in agreement with the significant variation in the average pore diameter of the membranes (1.06, 0.99 and 0.35 μm for B1, C1 and C2, respectively). Moreover, the permeate flux also varied with feed concentration and reduced with increasing concentration. Such a trend is obvious with the fact that increasing feed concentration enhanced oil droplet sizes, which thereby enhanced pore blocking. The maximum permeate flux has been evaluated to be 6.5×10^{-4}, 6.16×10^{-4} and 9.8×10^{-5} m^3/m^2s for membrane B1, C1 and C2, respectively at higher pressure (345 kPa).

The average rejection of various membranes for microfiltration of oil-water emulsions is depicted in Fig. 4.6 (d, e and f). The maximum rejection of 90.8, 96.3 and 98.4 % was obtained for the membranes, B1, C1 and C2, respectively at higher concentration (200 mg/L). It can be observed that the rejection value reduced with an increase in the applied pressures. This is due to the effect of wetting and coalescence of oil droplets at higher pressures that enhance the passage of oil droplets through the membrane and enter the permeate stream. On the other hand, the average rejection increases with increasing oil concentration in the feed which is probably due to the increase in oil droplet size and emulsion density. Also, the obtained results indicate that the oil rejection as well is dependent upon the pore diameter of the membrane. The literature data (Chakrabarty *et al*., 2008) also indicates that at higher pressures (increasing from 69 to 172 kPa), the rejection reduced from 95.7 to 90 % for a feed concentration of 100 mg/L. Further, at a constant trans-membrane pressure differential of 103 kPa and higher concentrations (75 – 200 mg/L), the rejection increased from 88.8 % to 98.5 %. Table 4.4 summarizes the comparative performance of B1, C1 and C2 membranes with the membranes reported in the literatures (Yang *et al*., 1998; Cui *et al*., 2008; Ebrahimi *et al*., 2010). It can be observed that all membranes performed satisfactory in terms of their permeability and rejection. Since the membranes provided good flux and have been able to satisfy the regulatory constraint for oil concentration in the permeate stream (Hua *et al*., 2007; Zhou *et al*., 2010), the fabricated low cost ceramic membranes are opined to be effective in removing oil from oil-water emulsions. With respect to the literature data, the performance of the membrane C1 (~96 % rejection with permeability of

94.2 × 10^{-8} m^3/m^2s kPa) reported in this work is comparable with those reported in literatures (Abbasi *et al*., 2010; Abadi *et al*., 2011).

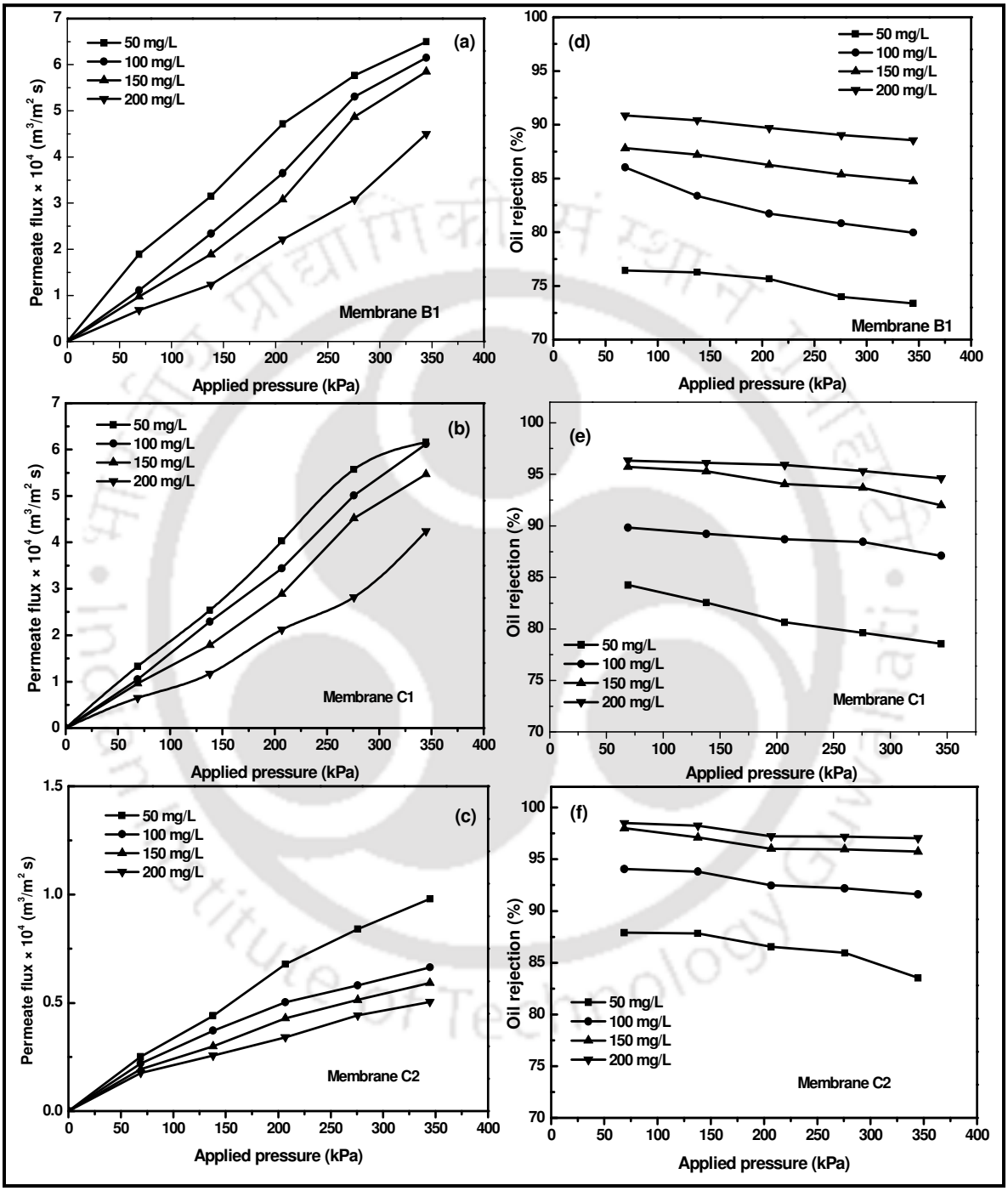

Figure 4.6: Variation of permeate flux (a – c) and oil rejection (d – f) with applied pressure for B1 (a, d); C1 (b, e) and C2 (d, f) membranes.

Abbasi *et al*., (2010) obtained 85.4 % of oil rejection and permeability of 2.78 × 10^{-8} m^3/m^2s kPa for a feed oil concentration of 250 mg/L using mullite ceramic membranes (average pore size of 0.289 µm). The membrane made from α-Al_2O_3 provided about 85 % of oil rejection and permeability of ~63.8 × 10^{-8} m^3/m^2s kPa for a feed oil concentration of 30 mg/L (Abadi *et al*., 2011). When compared with the literature data, the reported values for permeability (94.2 × 10^{-8} m^3/m^2s kPa) and rejection value (~96 %) is comparable or even better. A further comparison of membranes B1, C1 and C2 indicates that the membrane C1, in comparison with B1 and C2 provides good combinations of permeability and observed rejection coefficient (Table 4.5). Therefore, it is concluded that the low cost ceramic membrane C1 is the optimal choice for consideration towards the industrial application of oil-water emulsions and further studies need to dovetail towards module design, deployment and scale up issues.

4.2.3 Cost analysis of the membranes

In general, the high cost of ceramic membrane is compensated by their higher permeability and longer lifetime, which reduces the operating and maintenance cost. Table 4.6 presents the results obtained after a conceptual cost analysis of the fabricated membranes that considered raw materials and sintering/fabrication costs. Inclusive of all costs, the estimated membrane cost varied between 49 and 52 $/m^2$. On the other hand, the ceramic α-alumina symmetric membranes have a cost of $ 500/m^2 and stainless steel asymmetric membranes cost about $ 3000/m^2 (Mott Metallurgical Corporation, USA, 2007. http://www.mottcorp.com). Therefore, in comparison, it can be concluded that the

fabricated membrane is highly inexpensive than other commercial membranes from materials cost and sintering temperature perspectives.

Table 4.4: Comparative performance characteristics (permeability and rejection) of B1, C1, C2 and literature membranes for the treatment of oil-water emulsions.

Membrane/ support materials	**Mean pore size (µm)**	**Feed concentration (mg/L)**	**Permeability ($m^3/m^2 s$ kPa)**	**Rejection (%)**	**References**
α-Al_2O_3 / α-Al_2O_3	0.2	5000	6.1×10^{-8}	99.99	Yang *et al.*, (1998)
α-Al_2O_3 / α-Al_2O_3	1.0	5000	7.5×10^{-8}	94.3	Yang *et al.*, (1998)
ZrO_2 /α-Al_2O_3	0.2	5000	25.8×10^{-8}	99.8	Yang *et al.*, (1998)
NaA zeolite / α-Al_2O_3	1.2	100	16.7×10^{-8}	98.8	Cui *et al.*, (2008)
NaA zeolite / α-Al_2O_3	0.4	100	1.38×10^{-8}	99.4	Cui *et al.*, (2008)
α-Al_2O_3	2.1	100	13.9×10^{-8}	55.0	Cui *et al.*, (2008)
α-Al_2O_3	0.1	150	88.6×10^{-8}	61.4	Ebrahimi *et al.*, (2010)
Membrane B1	1.06	200	98.5×10^{-8}	90.8	Present work
Membrane C1	0.99	200	94.2×10^{-8}	96.3	Present work
Membrane C2	0.35	200	25.65×10^{-8}	98.4	Present work

Table 4.5: Flux and separation efficiencies of B1, C1 and C2 membranes for the separation of oil-water emulsions.

Membranes	Pore size (µm)	Feed concentration (mg/L)	Flux (m^3/m^2s)	Applied Pressure (kPa)	Rejection (%)
Membrane B1	1.06	200	6.80×10^{-5}	69	90.8
Membrane C1	0.99	200	6.5×10^{-5}	69	96.3
Membrane C2	0.35	200	1.77×10^{-5}	69	98.4

Table 4.6: Cost parameters of (B1, C1 and C2) membranes.

Raw materials used for the fabrication of membrane	Unit price (Rs./Kg)	Amount of raw materials required for the fabrication of one membrane (g) (diameter = 62 mm and thickness = 5 mm)		
		Membrane B1	Membrane C1	Membrane C2
Kaolin	390	13	13	13
Quartz	200	6.5	6.5	6.5
Calcium carbonate	330	6.5	5.72	3.9
Titanium dioxide	520	-	0.78	2.6
Raw materials cost per membrane (Rs.)		8.51	8.66	9.00
Raw materials cost per unit area of the membrane (Rs./m^2)		2819	2869	2981
Raw materials cost per unit area of the membrane ($/$m^2$)		45.7	46.5	48.3
Total fabrication cost (including pressing and sintering cost) of the membrane ($/$m^2$)		49.2	50	51.8

4.3 Summary

This work addressed the effect of low cost ceramic membrane precursor formulation on their morphology and microfiltration performance. Ceramic disk shaped microfiltration membranes with three distinct precursor compositions have been successfully prepared with the uniaxial compaction method. The results indicate that the properties of membrane (pore size, porosity, hydraulic permeability, flexural strength and chemical stability) are strongly influenced with varying composition of the raw materials. For membranes B1, C1 and C2, the average porosity and pore size have been evaluated to be 45, 41 and 39 % and 1.06, 0.90 and 0.35 μm, respectively. The flexural strength of the membranes varied between 10 – 34 MPa. With good performance characteristics from chemical stability tests, the microfiltration tests for oil-water emulsions indicated that the membranes provided a good rejection value (73 – 98 %). Based on the obtained results from microfiltration tests, C1 is inferred to be the best membrane for oily wastewater treatment application. For a feed oil concentration of 200 mg/L, C1 membrane provided an oil rejection and permeate flux of 96 % and 6.5×10^{-5} m^3/m^2s, respectively, at a lower applied pressure of 69 kPa. Inclusive of all costs, the cost of the membranes has been estimated to be 49, 50 and 52 $\$/m^2$ for membranes B1, C1 and C2, respectively.

Chapter 5:

Cross-flow Microfiltration of Oil-in-Water Emulsions using Low Cost Ceramic Membranes

Chapter 5

Cross-flow Microfiltration of Oil-in-Water Emulsions using Low Cost Ceramic Membranes

This chapter presents studies upon the application of prepared ceramic membranes (B1, C1 and C2) for the treatment of oil-in-water emulsions. Synthetic oil-in-water emulsions were subjected to microfiltration in cross-flow mode of operation. The aim of these experiments was to evaluate upon the effect of applied pressure as well as cross flow rate on the permeate flux and oil rejection of the membranes. Subsequently, the flux decline were analyzed using different pore blocking models such as complete pore blocking, standard pore blocking, intermediate pore blocking and cake filtration to gain insights into the nature of membrane fouling during permeation.

5.1 Experimental

In chapter 4, the results obtained from the dead end microfiltration of oil-water emulsions have been reported for various ceramic membranes (B1, C1 and C2). While dead-end microfiltration provides significantly stringent conditions of fouling for the membranes, they are not often practiced in the industrial scale operating systems. Typically, cross flow microfiltration is practiced on a pilot plant and industrial scale operation. Therefore, the flux and separation characteristics obtained from dead end microfiltration are not directly relevant to infer upon the confidence levels associated to the application of the developed membranes. Thus, cross flow microfiltration study has been targeted in this

chapter for the developed membranes and would be elaborated in the subsequent sub-sections.

5.1.1 Membranes

Cross-flow microfiltration of oil-in-water emulsions was performed using different ceramic membranes (B1, C1 and C2). Chapter 4 presented a detailed account upon the properties of the membranes. A summary of various properties of the membranes (B1, C1 and C2) is presented in Table 4.2.

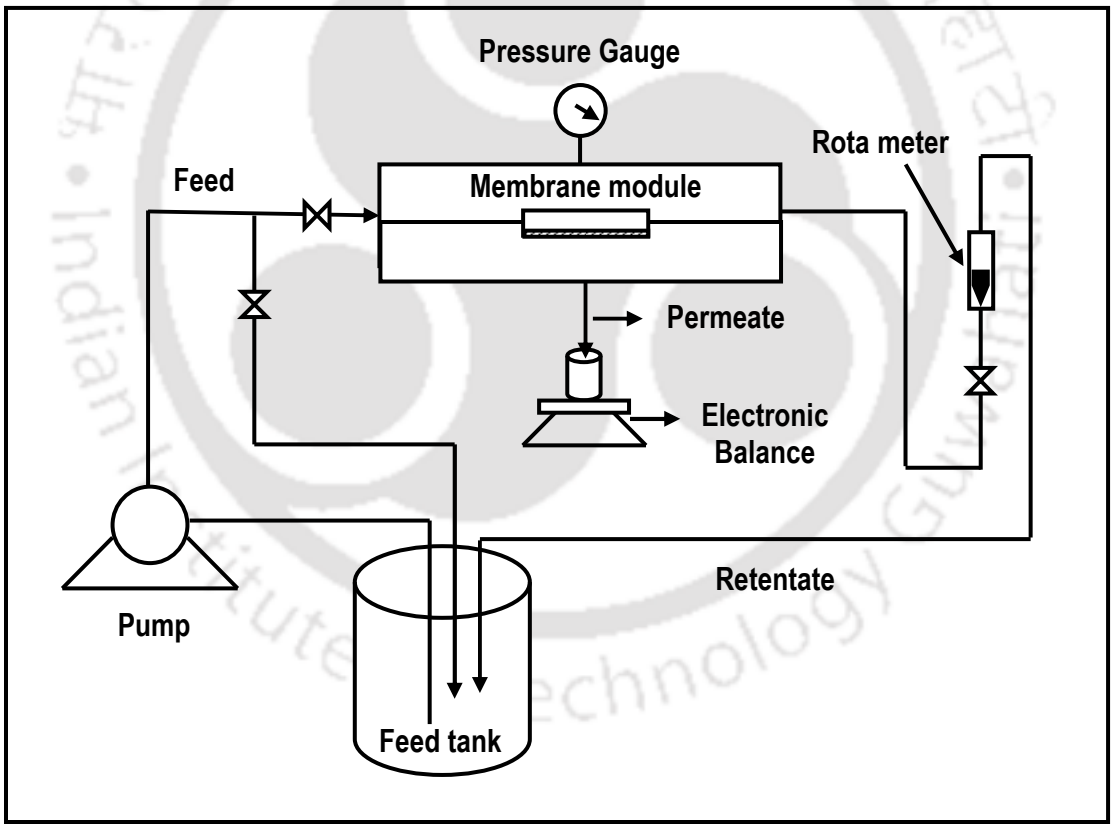

Figure 5.1: Schematic of the cross flow microfiltration setup.

5.1.2 Cross-flow microfiltration setup

Figure 5.1 shows a schematic diagram of the cross flow microfiltration setup. The setup consists of a feed tank, higher pressure plunger pump, assembled membrane module, rotameter (1 – 5 L/h), pressure gauge and three control valves (needle valves).

The membrane was sealed in a perforated casing and fixed in the membrane module. The feed was pumped from the feed tank through the membrane module and the retentate was returned to the feed tank. The permeate side was kept open to the atmosphere and the permeate obtained was measured using an electronic balance. The pressure was regulated manually using the valves located in the retentate and bypass pipe lines. All experiments were conducted at room temperature (~25 ^{o}C).

5.1.3 Determination of pure water flux

The cross flow filtration setup (shown in Fig. 5.1) was used to measure pure water flux of the membranes. For each membrane, the water fluxes were measured at different applied pressures (69 – 345 kPa) at a fixed cross flow rate (2.78×10^{-7} m^3/s) for 30 minutes.

5.1.4 Cross- flow microfiltration of oil-in-water emulsions

Synthetic oily wastewater was prepared using crude oil procured from Indian Oil Corporation Limited (IOCL), Guwahati. The preparation procedure involved the emulsification of the crude oil with Millipore water (Model: ELIX-3; Make: Millipore) in an ultrasonic cleaning bath [Model: T460; Make: Elma (India)] for about 15 h with a feed concentration of 100 mg/L. Thus, no additional emulsifiers have been added during the emulsification process. The emulsion droplet size in the feed was measured using laser

particle size analyzer (Model: Malvern Mastersizer 2000 APA 5005® hydro MU; Make: Malvern Instruments, Worcestershire, U.K.). Based on obtained droplet size distributions illustrated in Fig. 5.2, the average droplet size has been evaluated to be about 0.99 µm. Cross-flow microfiltration experiments were carried out using the setup shown in Fig. 5.1 for a time period of 1 h at five different pressure differentials (69 – 345 kPa) and three different cross flow rates (2.78 –13.9 $\times 10^{-7}$ m^3/s).

5.1.5 Analytical methods

The permeate flux (J) was evaluated as the ratio of permeate volume with the product of membrane area and sampling time

$$J = \frac{V}{A \times t} \tag{5.1}$$

where V, A ant t correspond to the sample volume collected, area of membrane and filtration time, respectively.

The oil rejection (R) was evaluated using the following expression.

$$R(\%) = \frac{C_f - C_p}{C_f} \times 100 \tag{5.2}$$

where C_f and C_p are the oil concentrations in the feed and permeate, respectively.

After carrying out a preliminary calibration procedure, the precise concentrations of feed and permeate samples have been evaluated by measuring the absorbance of the oil water emulsion samples at a wavelength of 235 nm using a UV-vis spectrophotometer (Model: UV 2300; Make: Spectrascan). The calibration procedure involved measuring the absorbance of various emulsion samples with known concentration of oil in the prepared emulsion. Appendix A presents the obtained calibration curve for oil-water emulsions.

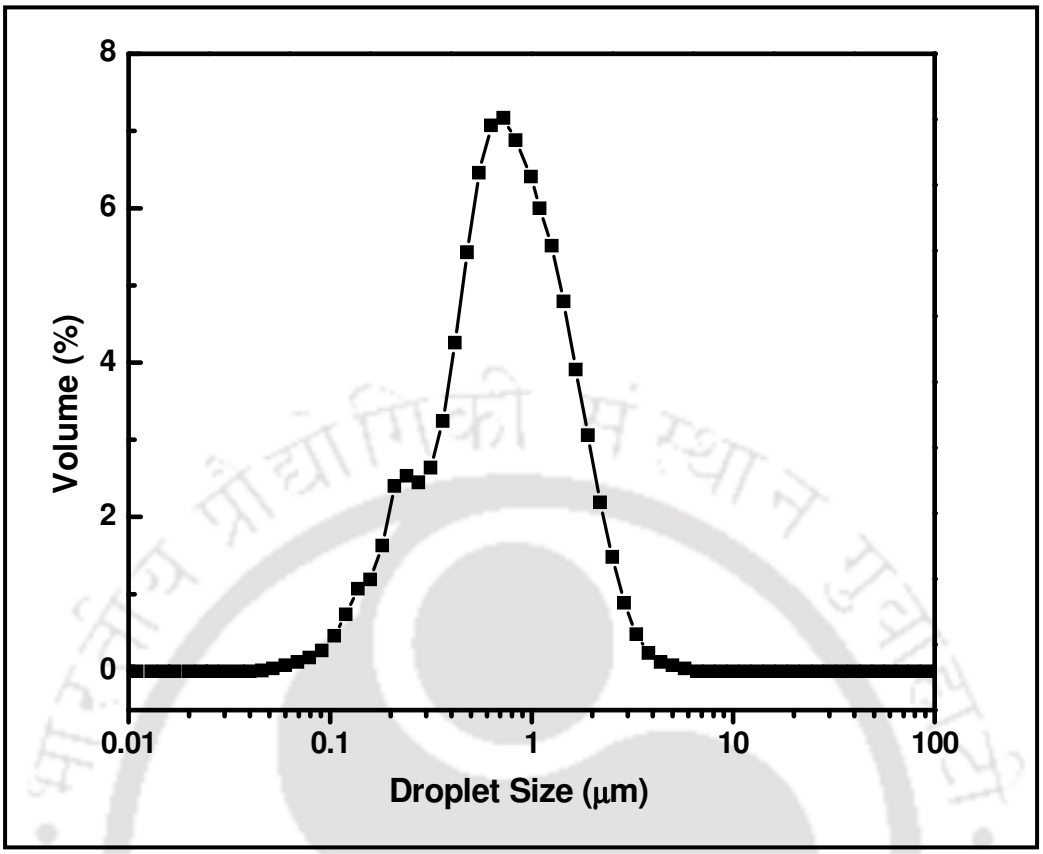

Figure 5.2: Droplet size distribution of oil-water emulsions prepared at 100 mg/L oil concentration.

5.1.6 Membrane cleaning

After each run, the membrane was cleaned and regenerated. Initially the membrane was cleaned using a detergent (commercial surf excel detergent) at a solution concentration of 2 g/L to remove the adsorbed oil from the membrane sample. Then the membrane was subjected to the sonication in an ultrasonicator [Model: T460; Make: Elma (India)] to remove the oil droplets adhering in the porous structure of the membrane. After regenerating the membrane completely, the membrane was used for the next microfiltration run.

5.1.7 Analysis of membrane fouling

The pertinent fouling mechanisms during cross-flow microfiltration have been analyzed using cake filtration, intermediate pore blocking, standard pore blocking and complete pore blocking models (Koltuniewicz *et al*., 1995; Wang *et al*., 2008).

5.1.7.1 Complete pore blocking

During complete pore blocking, it is assumed that the particle/oil arriving at the membrane surface completely block the membrane pores without any superposition and the blocked surface area is proportional to the permeate volume. Thereby, the variation of permeate flux (J) with time (t) is expressed as

$$\ln(J^{-1}) = \ln(J_0^{-1}) + k_b t \tag{5.3}$$

5.1.7.2 Standard pore blocking

During standard pore blocking, the permeating particles are much smaller than the pore size of the membrane and therefore enter into the membrane pores and adhere on the internal pore walls. Due to this reason, the membrane pore volume decreases proportionally with the permeate volume. Assuming standard pore blocking, the time dependent permeate flux is expressed as:

$$J^{-0.5} = J_0^{-0.5} + k_s t \tag{5.4}$$

5.1.7.3 Intermediate pore blocking

During intermediate pore blocking, it is assumed that the permeating particles arriving to the membrane surface can either settle on the membrane surface or on previously

adhering solute to eventually seal the membrane pore. Therefore, the permeate flux is regarded to be proportional to permeate volume but is restrictive than the proportionality corresponding to complete pore blocking. The following expression refers to the permeate flux dependence on time during intermediate pore blocking

$$J^{-1} = J_0^{-1} + k_i t \tag{5.5}$$

5.1.7.4 Cake filtration

During cake filtration, bigger particles or macromolecules, colloids or aggregates deposit over the membrane surface, and thus form a cake or fouling layer that provides resistance to the permeate flow or flux. The variation of permeate flux with time is evaluated using the expression

$$J^{-2} = J_0^{-2} + k_c t \tag{5.6}$$

The fitness of the experimentally obtained flux decline data with any of the above four flux decline models is confirmed by comparing the coefficient of correlation (R^2) values obtained from linear regression analysis using the models expressed in eqns. (5.3 – 5.6). Eventually, the model that represents experimental data with best fit R^2 value (close to 1) has been regarded to indicate upon the pertinent fouling mechanism during cross-flow microfiltration.

5.2 Results and discussion

5.2.1 Pure water flux

Figure 5.3 depicts the pure water of flux of membranes (B1, C1 and C2) measured at different applied pressures. For all membranes, the pure water flux was observed to be

constant during the entire filtration time (Fig. 5.3). Also, the pure water flux increased linearly with increasing pressure which indicates that it follows Darcy's law.

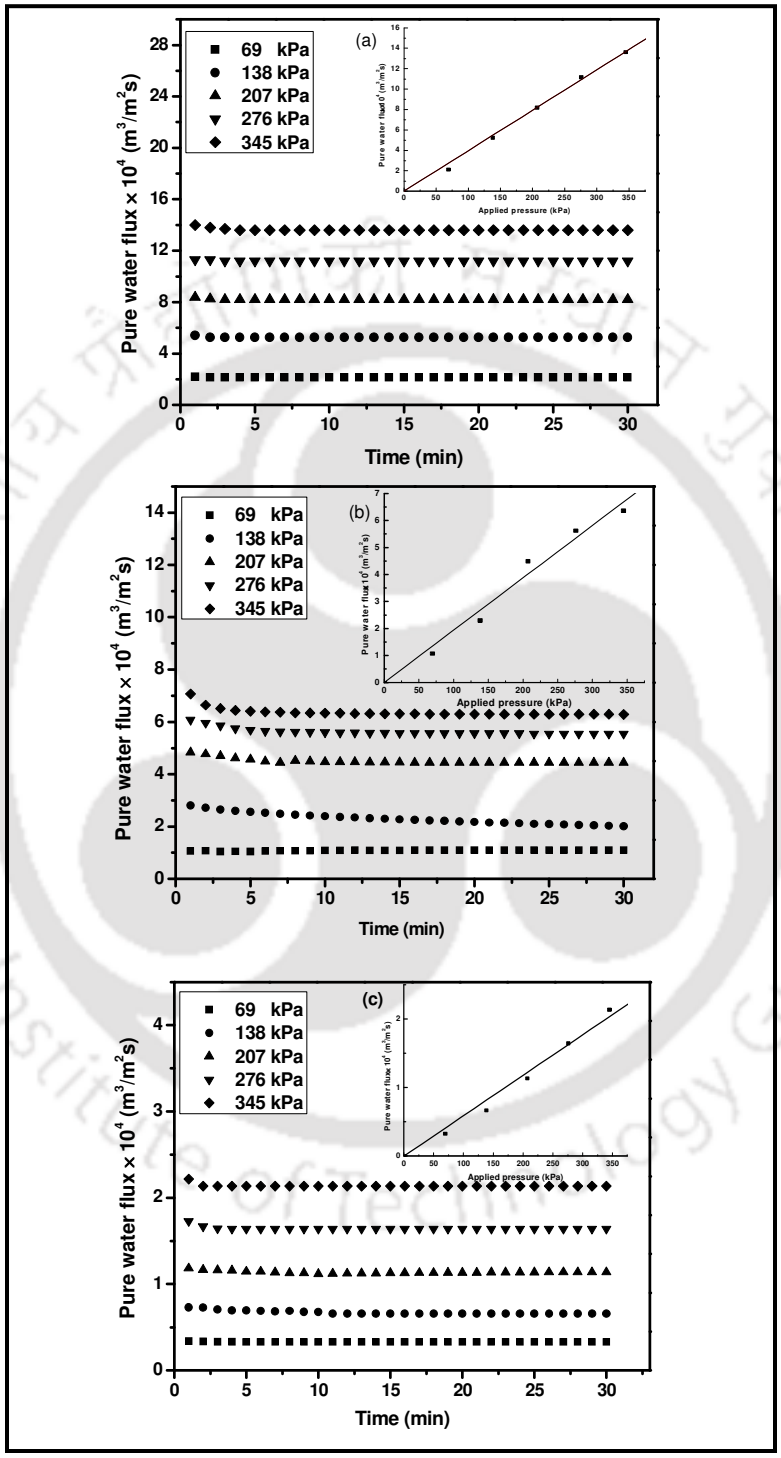

Figure 5.3: Variation of pure water flux with time at different applied pressures for (a) B1 (b) C1 and (c) C2 ceramic membranes.

5.2.2 Cross- flow microfiltration of oil-in-water emulsions

5.2.2.1 Effect of applied pressure

Fig. 5.4 (a – c) depicts the permeate flux decline as a function of time with different applied pressures for all membranes at a cross flow rate of 2.78×10^{-7} m^3/s. As indicated theoretically, the membrane flux can be observed to increase with applied pressure differentials, which is due to an enhancement in the driving force with increasing pressure. However, the permeate flux variation with applied pressure did not follow a linear trend (Fig. 5.4 (inset)) and this is possibly due to the contribution of additional transport resistances from adsorption and concentration polarization (Chakrabarty *et al*., 2008).

With respect to the flux decline trends, it can be observed that during first 10 min, the flux declines rapidly and eventually the flux declines gradually to achieve an almost constant value after 50 minutes of microfiltration run. It can be also observed in the figure that the rate of flux decline is greater at higher pressure differential across the membrane. This is explained with the reason that when the applied pressure increases, the oil layer rapidly forms at the surface and enables faster membrane fouling. The rapid flux decline during the early stages of microfiltration can also be explained to follow pore blocking phenomenon in the early stages of permeation. The second phenomenon that also takes place during microfiltration is the concentration polarization which significantly contributes to the flux decline during the later stages of the experiment. As time proceeds, pore blocking process gradually becomes insignificant and the oil layer formed on the membrane surface causes the flux decline. In general, concentration polarization is a slow process and therefore the corresponding flux decline rate is reduced

at a later stage. It can be also analyzed from the figure that the rate of flux decline is significant for the B1 membrane in comparison with the C1 and C2 membranes (Fig. 5.4, a – c). Among the membranes, the lowest flux decline rate is observed for the C2 membrane. For the three membranes, the rate of fouling is in the order of B1 > C1 > C2. This trend indicates that the fouling rate is greater for membranes with larger pore. At an applied pressure of 345 kPa, the maximum permeate flux after 1 h operation is found to be 4.82×10^{-5}, 5.75×10^{-5} and 2.96×10^{-5} m^3/m^2s for the membranes B1, C1 and C2, respectively. For all the membranes (B1, C1 and C2), C1 membrane provided a maximum permeate flux.

The variation of oil rejection as a function of time with applied pressure is presented in Fig. 5.4 (d – f). The rejection value reduced (89 – 83 %, 93 – 89 % and 97 – 91 % for B1, C1 and C2, respectively) with increasing pressure (69 – 345 kPa) and this is due to the effect of higher degree of wetting and coalescence of oil droplets at higher pressures. Thereby, oil droplets are facilitated to pass through the membrane and enter the permeate stream. It is also observed from the figure that the rejection value slightly increased with increasing time, which is due to the effect of pore blocking phenomenon after a certain time. According to the results shown in Fig. 5.4, the prepared membranes provided good oil rejection values. The membranes B1, C1, and C2 provided the maximum rejection of 89 – 97 % at a lower applied pressure of 69 kPa. The obtained results show that the oil rejection has been significantly influenced with the pore size of the membranes. From this study, considering permeate flux, flux decline rate and oil rejection, the applied pressure of 207 kPa has been identified to be the best choice and further investigations and analysis has been addressed at this applied pressure value.

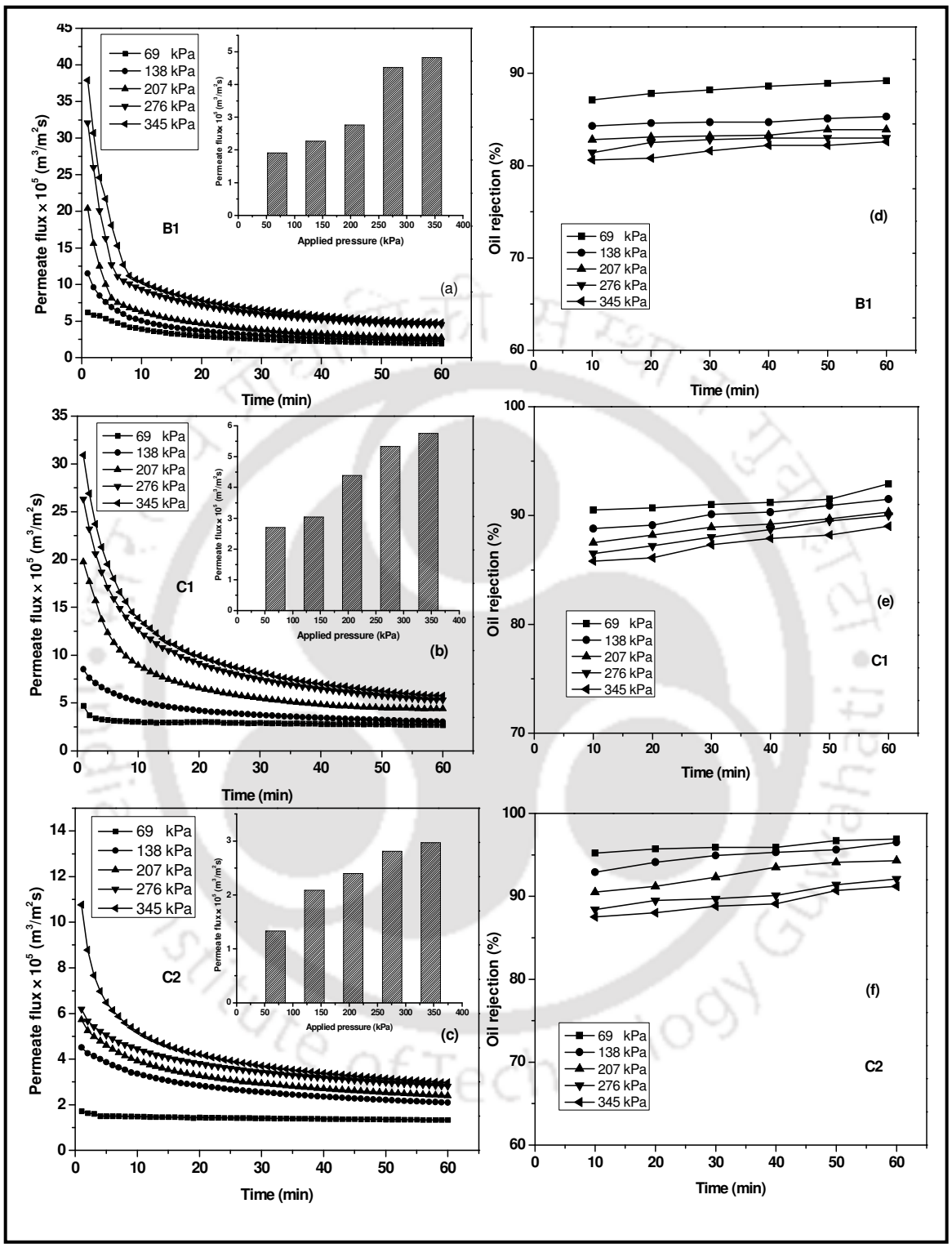

Figure 5.4: Effect of applied pressure on the cross-flow MF permeate flux (a – c) and oil rejection efficiency (d – f) for the membranes (B1, C1 and C2).

5.2.2.2 Effect of cross flow rate

The effect of cross flow rate was investigated at three different cross flow rates ($2.78 – 13.9 \times 10^{-7}$ m^3/s) at an applied pressure of 207 kPa and the obtained results are presented in Fig. 5.5. It can be observed that an improvement in cross flow rate enhanced the permeate flux. This is due to the reduction in concentration polarization with an increase in the cross flow rate. The enhancement in the cross flow rate enhanced shear stress on the membrane surface. Due to this reason, a reduction occurs in the thickness of the adsorbed oil layer on the membrane surface. Further, the rate of flux decline is found to decrease with increasing cross flow rate (Fig. 5.5, a – c). This is due to the fact that an increase in cross flow rate reduces the formation of cake layer on the membrane surface. Therefore, the permeation resistance to the permeate flow decreases with increasing cross flow rate. For all membranes, the maximum permeate flux ($2.78 – 3.70 \times 10^{-5}$ m^3/m^2s) was observed with higher cross flow rate of 13.9×10^{-7} m^3/s at the studied applied pressure (207 kPa).

The membrane rejection has been found to decrease insignificantly (84 – 82 %, 90 – 87 % and 94 – 93.7 % for B1, C1 and C2, respectively) with increasing cross flow rate ($2.78 – 13.9 \times 10^{-7}$ m^3/s) (Fig. 5.5, d – f). As discussed earlier, increasing cross flow rate leads to a reduction in the thickness of the cake layer that forms on the membrane surface. Since cake layer contributes to enhancement in oil rejection as a secondary filter on the membrane surface, higher cross flow velocity reduces the contribution of cake layer towards the oil rejection. Also, higher cross flow rates could enable a reduction in the size of oil droplets and finer droplets thereby enter the permeate product stream. Therefore, oil rejection decreases with an increase in cross flow rates. For all membranes,

at an applied pressure of 207 kPa, the maximum oil rejection (84 – 94 %) has been obtained at a lower cross flow rate of 2.78×10^{-7} m^3/s. Even though, the rejection value is less at higher cross flow rate, the permeate flux is high. Considering permeate flux, the higher flow rate of 13.9×10^{-7} m^3/s has been selected as optimum cross flow rate. The performance of all membranes at optimal process conditions is presented in Table 5.1. When compared with B1 and C2 membranes, the performance of C1 membrane is found to be promising. Even though the rejection value of C1 membrane is slightly lower than the C2 membrane, its permeate flux values are higher than that of the C2 membrane. Further, it is worth mentioning that the B1 membrane provides lower values of permeate flux, despite considering the fact that B1 membrane has a higher average pore size (1.06 µm). The membrane C1 provided about 87 % of oil rejection and permeate flux of 5.54×10^{-5} m^3/m^2s at a pressure of 207 kPa and a cross flow rate of 13.9×10^{-7} m^3/s. In general, ceramic membranes for application towards industrial scale separation should provide higher combination of rejection efficiency and permeate flux.

Table 5.1: Comparative performance data for membranes B1, C1 and C2 at a feed oil concentration, applied pressure and cross flow rate of 100 mg/L, 207 kPa and 13.9×10^{-7} m^3/s, respectively.

Membranes	**Rejection (%)**	**Permeate flux (m^3/m^2s)**	**Flux declination (%)**
Membrane B1	82	3.70×10^{-5}	83.2
Membrane C1	87	5.54×10^{-5}	74.9
Membrane C2	94	2.78×10^{-5}	52.2

Therefore, it can be concluded that the membrane C1 is the best choice for consideration towards industrial application.

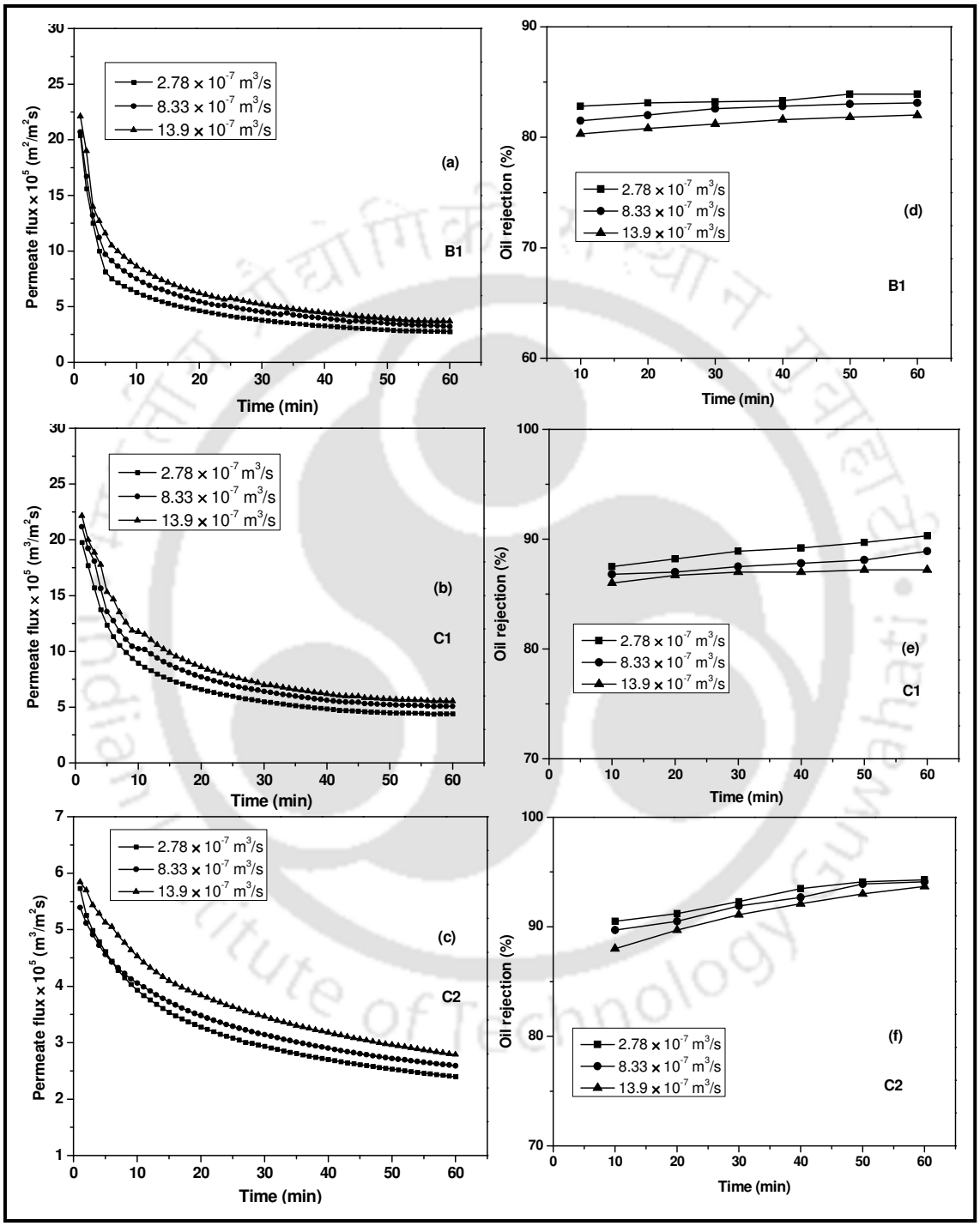

Figure 5.5: Effect of circulation rate on the permeate flux (a – c) and oil rejection (d – f) for various membranes (B1, C1 and C2) during cross flow MF.

5.2.3 Analysis of membrane fouling

Four different filtration models have been used to investigate mechanism of flux decline in the cross flow microfiltration of oil-in-water emulsions. The fitness of fouling models towards evaluated flux decline enables to infer whether the flux decline is controlled by cake filtration or pore blocking. While cake filtration corresponds to reversible fouling mechanisms, pore blocking does affect membrane morphologies significantly and therefore refers to irreversible fouling mechanism. Therefore, it is anticipated that the onset of cake filtration during microfiltration is promising to enhance the shelf life of the membranes.

Figure 5.6 illustrates the fitness of various pore blocking models for all membranes at an applied pressure of 207 kPa and cross flow rate of 13.9×10^{-7} m^3/s. It can be observed from the figures that, amongst all models, cake filtration model has best fitness with the experimental data. The model parameters such as correlation coefficient (R^2), slope and initial permeate flux values (J_0 at t = 0) obtained with different pore blocking models for the membranes (B1, C1 and C2) are presented in Table 5.2. From the table, it is clear that the cake filtration model offers highest R^2 value for all the membranes. Therefore it can be concluded that the cake filtration model describes well the fouling mechanism. Similar results have been reported by Vela *et al*., (2008), who confirmed that highest values of R^2 were obtained for the cake filtration model to represent the flux decline of polyethylene glycol (PEG). Also, Salahi *et al*., (2010) inferred that the cake filtration model provides the best fitness to represent the experimental flux decline data obtained during the MF of industrial oily wastewater using polymeric membranes.

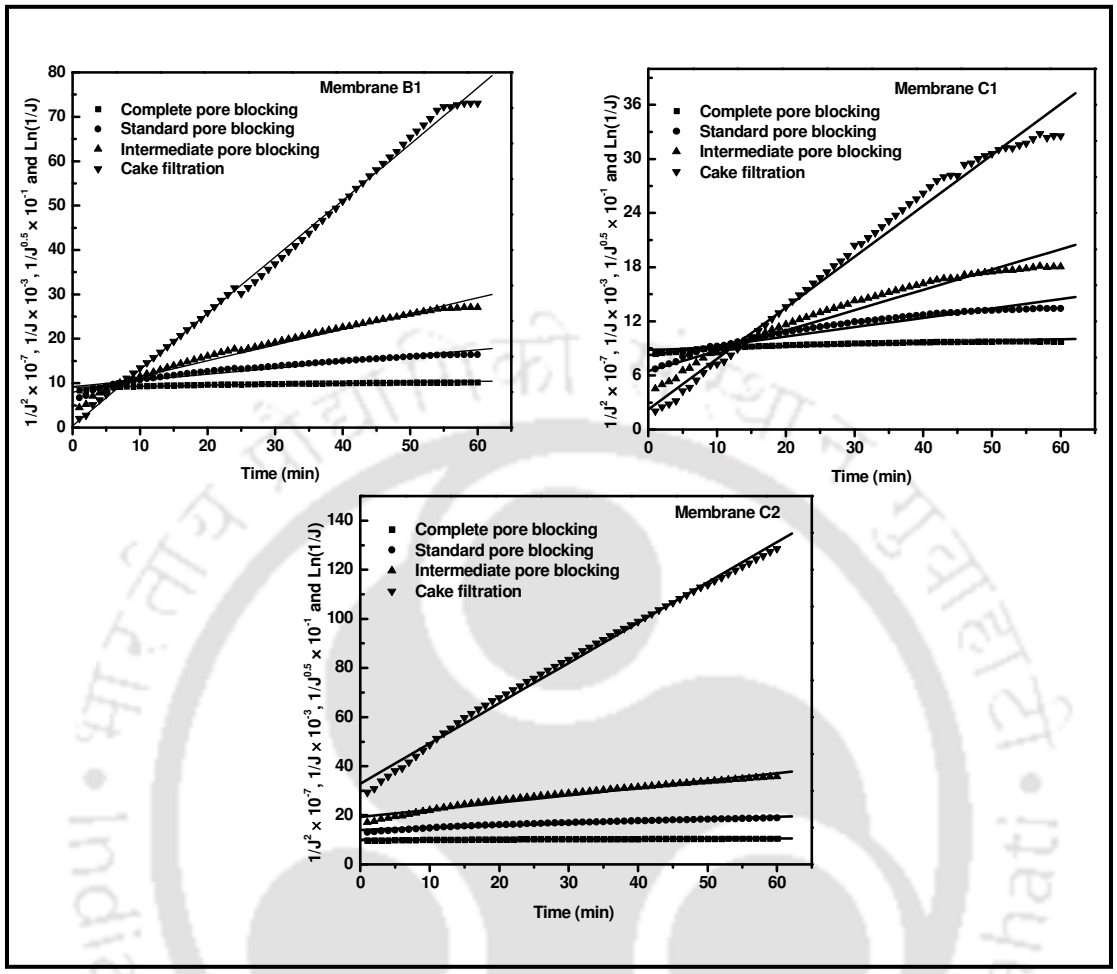

Figure 5.6: Fitness plots for various pore blocking models to represent measured cross flow MF flux decline of B1, C1 and C2 membranes. Operating conditions: Applied pressure and cross flow rate of 207 kPa and 13.9 $\times 10^{-7}$ m^3/s, respectively.

Table 5.2 also presents the model parameter (k) values that were evaluated from various filtration models for all the membranes. According to the definition and physical meaning of Hermia's model parameters, the magnitude of k refers to the severity of fouling. It can be observed from Table 5.2 that the value of 'k' is higher for the B1 membrane (except cake filtration model) suggesting that the fouling is significant for the B1 membrane. This is due to larger membrane pore size which enabled higher rate of membrane pore

blocking. It can be also noted from the table that the initial permeate flux values (J_o) obtained from intercept of different filtration models are lower than the initial permeate flux of experimental data and therefore, each model tends to underestimate the initial flux. Moreover, large deviation is observed for the complete pore blocking, standard pore blocking and intermediate pore blocking models, but the cake filtration model provided good fitness with respect to the experimental flux decline data. Overall, it can be concluded that the cake filtration model provides best fitness with the experimental data. The observation of cake filtration model to fit well with the experimental data during cross flow microfiltration is promising towards the shelf life of the membranes, as cake filtration enables significant external fouling which need not contribute significantly towards the irreversible fouling of the membranes.

Table 5.2: Summary of pore blocking model parameters (correlation coefficient (R^2), Slopes (k) and initial permeate flux (J_0) for membranes B1, C1 and C2.

Models	Membrane B1			Membrane C1			Membrane C2		
	Correlation coefficient (R^2)	Slope (k)	Initial permeate flux J_0 $m.s^{-1}$	Correlation coefficient (R^2)	Slope (k)	Initial permeate flux J_0 $m.s^{-1}$	Correlation coefficient (R^2)	Slope (k)	Initial permeate flux J_0 $m.s^{-1}$
Complete pore blocking	0.8506	0.0004 s^{-1}	1.12×10^{-4}	0.8549	0.0003 s^{-1}	1.44×10^{-4}	0.9325	0.0002 s^{-1}	5.05×10^{-5}
Standard pore blocking	0.9269	0.023 $s^{0.5}\ m^{-0.5}$	1.16×10^{-4}	0.9091	0.0173 $s^{0.5}\ m^{-0.5}$	1.47×10^{-4}	0.9553	0.0151 $s^{0.5}\ m^{-0.5}$	5.11×10^{-5}
Intermediate pore blocking	0.9727	5.9096 m^{-1}	1.26×10^{-4}	0.9481	3.7548 m^{-1}	1.54×10^{-4}	0.9733	4.9643 m^{-1}	5.20×10^{-5}
Cake filtration	0.9973	211478 $s.m^{-2}$	5.15×10^{-4}	0.9869	94088 $s.m^{-2}$	2.13×10^{-4}	0.9949	273544 $s.m^{-2}$	5.52×10^{-5}

5.3 Summary

Cross flow microfiltration was successfully carried out for the separation of oil from oil-in-water emulsion with three ceramic membranes (B1, C1 & C2) that were prepared with three different compositions of inexpensive inorganic precursors. Cross flow microfiltration experiments indicated that the permeate flux increases and rejection decreases with applied pressure and cross flow rate, while rejection reduced with increasing applied pressure and cross flow rate. For all membranes (B1, C1 and C2) considered in this work, the membrane C1 provided an optimal combination of rejection (87 %) and permeate flux (5.54×10^{-5} m^3/m^2s), respectively at a pressure and cross flow rate of 207 kPa and 13.9×10^{-7} m^3/s respectively. From all investigations, it can be concluded that the membrane C1 is the best choice for oil-in-water emulsion separation application. The analysis of pertinent fouling mechanism with different pore blocking models indicates that the cake filtration model is the best fit to represent the experimental data for all membranes. In summary, the present work indicates upon the competence of the prepared membranes for the treatment of oil-water emulsions.

Chapter 6:

Preparation, Characterization and Application of LTA Zeolite Composite Membranes

Chapter 6

Preparation, Characterization and Application of LTA Zeolite Composite Membranes

This chapter presents details with respect to the preparation, characterization and application of LTA zeolite ceramic composite membranes. Zeolite composite membranes D1, D2, D3 and D4 were prepared on low cost ceramic support B1 using in-situ hydrothermal crystallization technique. Various characterization techniques such as thermogravimetric analysis (TGA), particle size distribution (PSD), X-ray diffraction analysis (XRD) and field emission scanning electron microscopic analysis (FESEM) were carried out to characterize the zeolite composite membranes. Also, the porosity, average pore size, water permeation data were as well evaluated. Finally, ultrafiltration experiments with aqueous bovine serum albumin (BSA) solutions were conducted using D4 membrane to evaluate its flux and separation performance.

6.1 Experimental

In the earlier chapters, (Chapters 2 – 5), membranes with diverse membrane morphologies have been presented. The membrane with lowest average pore size refers to C2 membrane whose average pore size is 0.35 µm. A further reduction in the average pore size of the membrane is required to target ultrafiltration applications. Therefore, it is apparent that additional materials need to be targeted as skin layer materials for the fabrication of ultrafiltration asymmetric low cost ceramic membranes. Amongst various

available materials, zeolite is one of the most favoured choice due to its low cost. Thereby, further research has been initiated in this work to target and achieve ultrafiltration range ceramic membranes. For this purpose, the efficacy of the in-situ hydrothermal method is also targeted. Typically, asymmetric membranes are developed on a macroporous support with moderately higher average pore size. This is primarily due to the fact that a macroporous support with lower average pore size offers significant hydraulic resistance, which is not beneficial. Thus, considering all these issues, membrane B1 has been used as the macroporous support to fabricate zeolite composite membranes.

6.1.1 Membrane support

LTA zeolite membranes were prepared on low cost ceramic support that was prepared and characterized previously. Membrane B1 has been used as the ceramic support due to its optimal combinations of pore size, porosity, flexural strength etc. Chapter 3 presented details on the preparation method and properties of the membrane support. Table 6.1 presents a summary of various properties of the B1 membrane support.

6.1.2 Synthesis of LTA zeolite membrane

A-type zeolite membrane was prepared on the low cost ceramic support B1 using in-situ hydrothermal crystallization. Fig. 6.1 summarizes the procedure followed to achieve a zeolite film on the ceramic support. As presented, firstly, two reactant solution (namely aluminates and silicate solution) was prepared by dissolving sodium aluminate (NaO_2: Al_2O_3: 3 H_2O) and sodium metasilicate (Na_2SiO_3: 5 H_2O) in sodium hydroxide solution.

Table 6.1: A summary of characterization parameters for the B1 membrane support. The B1 membrane support has been used to fabricate D1 – D4 membranes.

Properties	**Value**
Thickness (mm)	4.5
Porosity (%)	45
Pore size (µm)	1.06
Permeability (m^3/m^2s kPa)	3.97×10^{-6}
Flexural strength (MPa)	34
Cost (Rs/m^2)	2821 (61 $\$/m^2$)

To do so, the sodium hydroxide solution was prepared by dissolving 0.723 g of sodium hydroxide in 80 mL of water. Then the solution was divided into two equal volumes. The aluminate solution was prepared by adding 8.258 g of sodium aluminate into one portion of sodium hydroxide solution. Similarly, the silicate solution was prepared by dissolving 15.48 g of sodium metasilicate in the other portion of sodium hydroxide solution. Finally, the silicate solution was poured into aluminate solution and mixed gently to achieve a homogenous solution. The molar composition of resulting solution was 3.165 Na_2O Al_2O_3 1.926 SiO_2 128 H_2O. The synthesis solution was then transferred to Teflon-lined auto clave reactor (250 mL capacity) in which membrane support B1 was kept. The crystallization was carried out a in hot-air oven facilitated with appropriate temperature controller. The synthesis solution was heated up quickly to 99 $^oC \pm 1$ ^oC in 5 min and was kept for 4 h at 100 ^oC. After crystallization process, the membrane was recovered and washed several times with Millipore water to remove loosely adhering crystals. Subsequently, the washed membrane was then dried at 100 ^oC for 24 h and sintered at 600 ^oC for 6 h. The same procedure was repeated to achieve multiple coating steps,

wherein the procedure of crystallization, washing, drying and sintering steps were repeated in sequence.

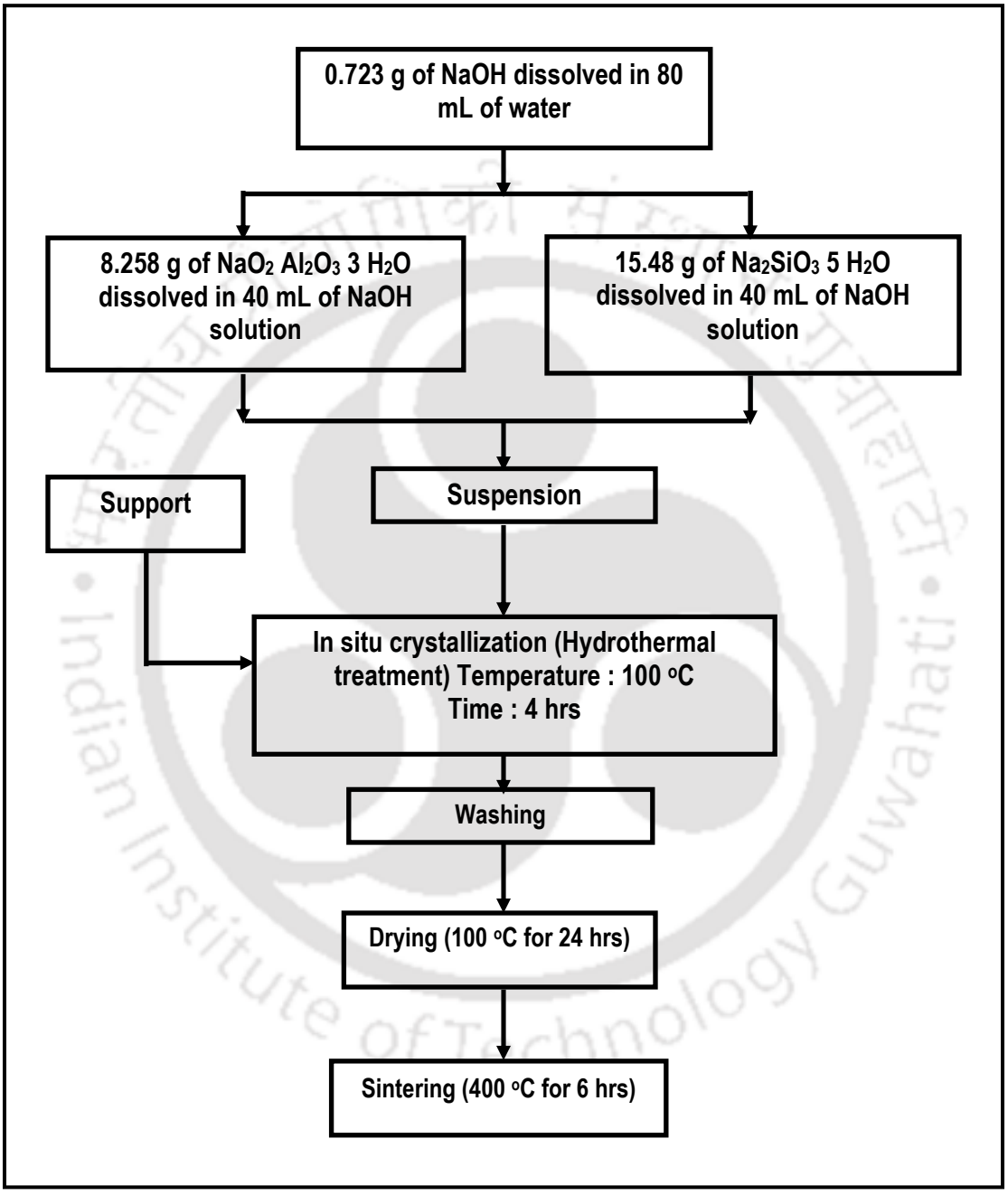

Figure 6.1: Schematic of LTA zeolite composite membrane preparation method.

6.1.3 Characterization of zeolite powder and membrane

The zeolite particles and zeolite membranes were characterized using various techniques such as thermogravimetric analysis (TGA), particle size distribution (PSD), X-ray diffraction analysis (XRD) and field emission scanning electron microscopic analysis (FE-SEM). The thermogravimetric analysis of the synthesized zeolite seeds was carried out using a thermogravimetric analyzer (Model: TGA/SDTA 851®; Make: Mettler Toledo, Schwerzenbach, Switzerland). The particle size and particle size distributions (PSD) of synthesized zeolite particles before and after sintering were measured using particle size analyzer (Malvern Mastersizer 2000, APA 5005® hydro MU, Malvern Instruments, Worcestershire, U.K.) in wet dispersion mode. X-ray diffraction (XRD) analysis was conducted to identify the existence of several phases including zeolite on the membrane surface using Bruker AXS instrument (Karlsruhe, Germany). The XRD measurement provided CuKα (1.5406 Å) radiation and was operated at 40 kV and 40 mA. The XRD patterns were acquired for 2θ range of 5^o – 75^o at a scan speed of 0.05 ^{o}/s. The morphology of membranes D1 – D4 was measured using field emission scanning electron microscope (FESEM). In addition to the above characterization, the pure water flux of the synthesized membranes D1 – D4 was measured at different applied pressures (207 – 483 kPa). The procedure to measure pure water flux has been presented in section 2.1.3.9 of the thesis.

6.1.4 Separation of bovine serum albumin (BSA)

Aqueous BSA feed solution (1000 mg/L) was prepared by dissolving 1 g of BSA in 1 L of Millipore water with continuous stirring for 1 h. The separation experiment was

carried out in dead-end filtration mode using dead-end filtration setup whose details have been presented in section 2.1.3.9 of the thesis. In order to evaluate upon the effect of operating conditions such as pH and applied pressure, the first set of experiments were carried out at a fixed pressure of 207 kPa and varied pH of 2.5 – 8. Thereby, the optimized pH was identified with which the second set of experiments was carried out with variant applied pressures (207 – 345 kPa). For all experiments, 100 mL BSA feed solution was used in the filtration setup. During MF experiment, the first 10 mL permeate collected was discarded and the time required to collect the second 10 mL permeate sample was noted for the evaluation of membrane flux. The membrane BSA rejection was determined using the expression

$$R(\%) = \frac{C_f - C_p}{C_f} \times 100 \tag{6.1}$$

where C_f and C_p are the concentration of feed and permeate samples. The concentration of BSA in the permeate sample has been determined using UV-vis spectrophotometer (Model: UV 2300; Make: Spectrascan) at a wavelength of 275 nm. For this, initially, the calibration curve was prepared by measuring the absorbance of samples with known concentrations of BSA. The calibration curve presented in Appendix D was found to be linear. Subsequently, the calibration chart has been used to evaluate the concentration of unknown samples by measuring their absorbance.

6.1.5 Membrane cleaning

In order to regenerate a fouled membrane, the membrane was initially rinsed with hot water for 30 min. Subsequently, the membrane was cleaned using sodium dodecyl sulphate (SDS) solution for 30 min. Finally, pure water was passed through the

membrane at higher pressure to remove the SDS adsorbed to the membrane surface. After completing the cleaning process, the pure water flux was measured to confirm upon the complete restoration of pure water permeability

6.2 Results and discussion

6.2.1 Characterization of membranes

6.2.1.1 Thermogravimetric analysis

The thermogravimetric analysis aims to obtain details with respect to the thermal stability of synthesized LTA zeolite and thereby identify the minimum temperature required for sintering. Fig. 6.2 depicts the TGA curve obtained for the synthesized zeolite. It can be analyzed that sharp weight loss occurred below 200 ^{o}C.

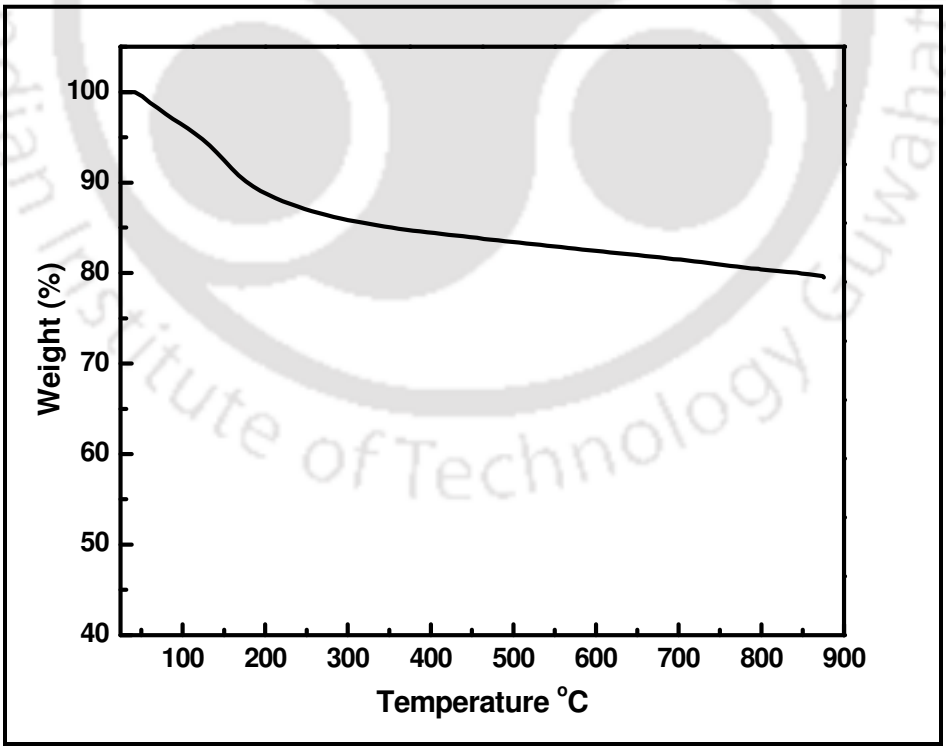

Figure 6.2: TGA curve for LTA zeolite particles.

This is due to the removal of water molecules from the sample. The total weight loss of the sample has been evaluated to be about 20 %. After 200 ^{o}C, the sample weight loss has been insignificant and this confirms that the zeolite is thermally stable. Hence the zeolite membrane can be used for high temperature applications. Furthermore, it can be concluded that a sintering temperature of 400 ^{o}C is sufficient to obtain zeolite skin layer on the membrane support. Similar TGA profile has been reported in the literature (Ling *et al*., 2011).

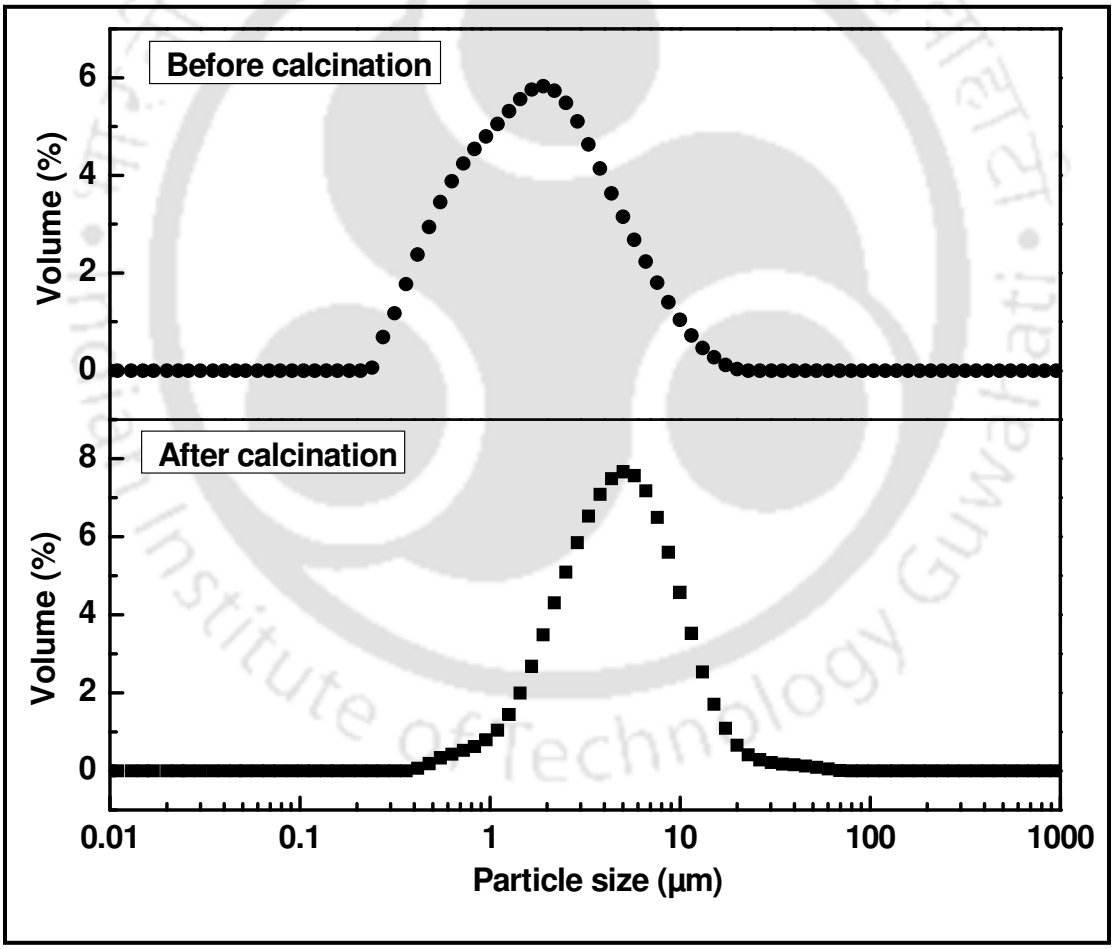

Figure 6.3: Particle size distributions of LTA zeolite particles.

6.2.1.2 Particle size distribution

For the evaluation of particle size and particle size distribution (PSD) of the zeolite membrane, the powder formed in the autoclave reactor during the membrane synthesis was subjected to particle size analysis. Particle size distribution of both uncalcined and calcined zeolite has been presented in Fig. 6.3. The PSD profiles confirm that unimodel PSD exists for both uncalcined and calcined zeolite samples. Further, it can be observed that narrow PSD exists for the uncalcined sample. This indicates that sintering enhanced the range of the PSD. Furthermore, it can be noted that, for uncalined sample, the particle size varied from 0.24 – 20 µm, which increased to 0.4 – 70 µm for the calcined sample. The volume weight mean particle size has been evaluated to be ~2.7 and ~6.4 µm for uncalcined and calcined sample, respectively. The variation in average particle size for calcined sample is possibly due to the growth in zeolite particles during sintering.

6.2.1.3 XRD analysis

X-ray diffraction analysis (XRD) was performed to identify various phases (including zeolite) in the membrane. To do so, XRD analysis was conducted for zeolite powder that was collected from the bottom of the autoclave. Fig. 6.4 depicts the XRD pattern of zeolite powder for both samples that were collected before and after calcination. Major peaks corresponding to LTA zeolite structure were observed in both samples, thus confirming upon the presence of LTA structure in the sample. Further, it has been observed that no significant changes occurred in the peak position and intensity for samples obtained after calcinations.

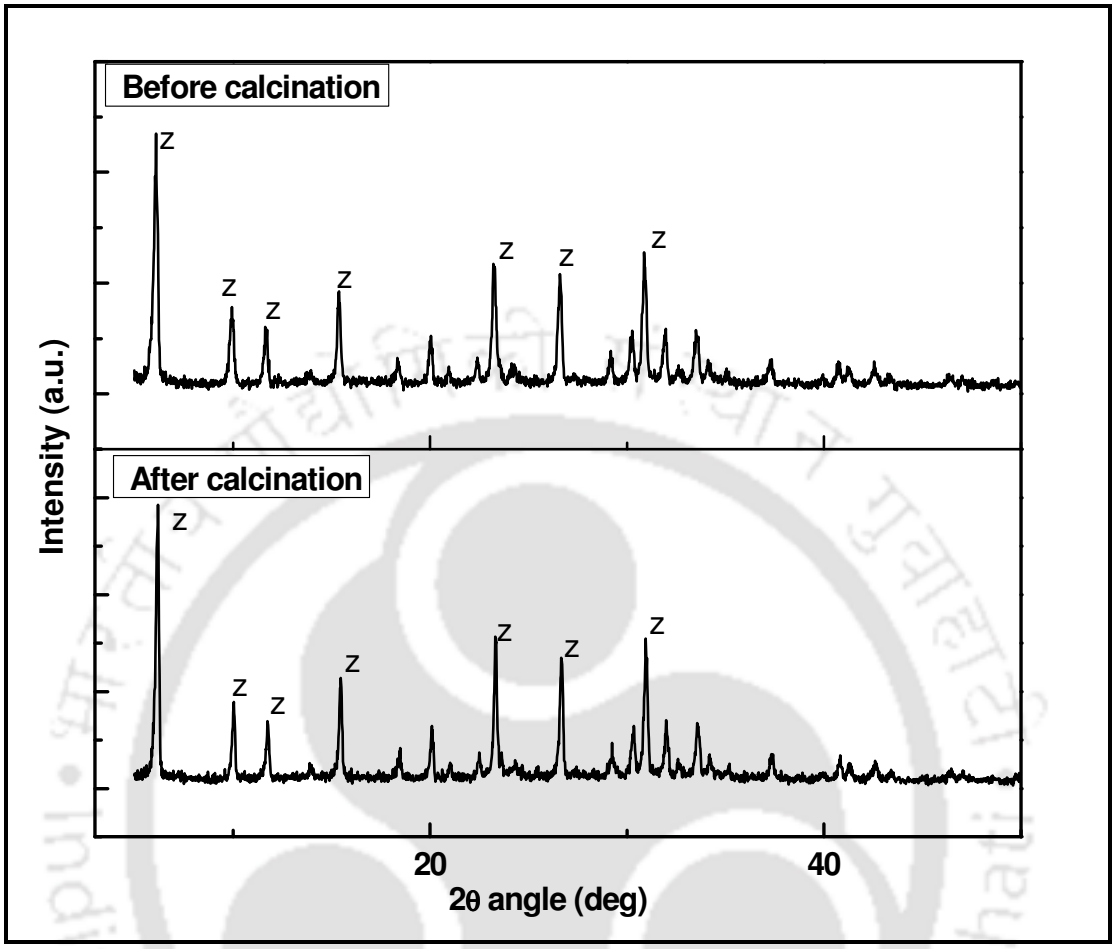

Figure 6.4: XRD patterns of LTA zeolite powder.

Also, other contaminating phases were also observed for both cases, which could not be further analyzed. In summary, the XRD study confirmed that no phase transformation occurred during the calcination process.

6.2.1.4 SEM analysis

The morphology of the LTA zeolite power and LTA membranes (D1 – D4) were analyzed using field emission scanning electron microscope (FE-SEM). Fig. 6.5 (a – f)

shows the surface morphology of the membrane support, synthesized zeolite power and coated membranes (D1 – D4), respectively.

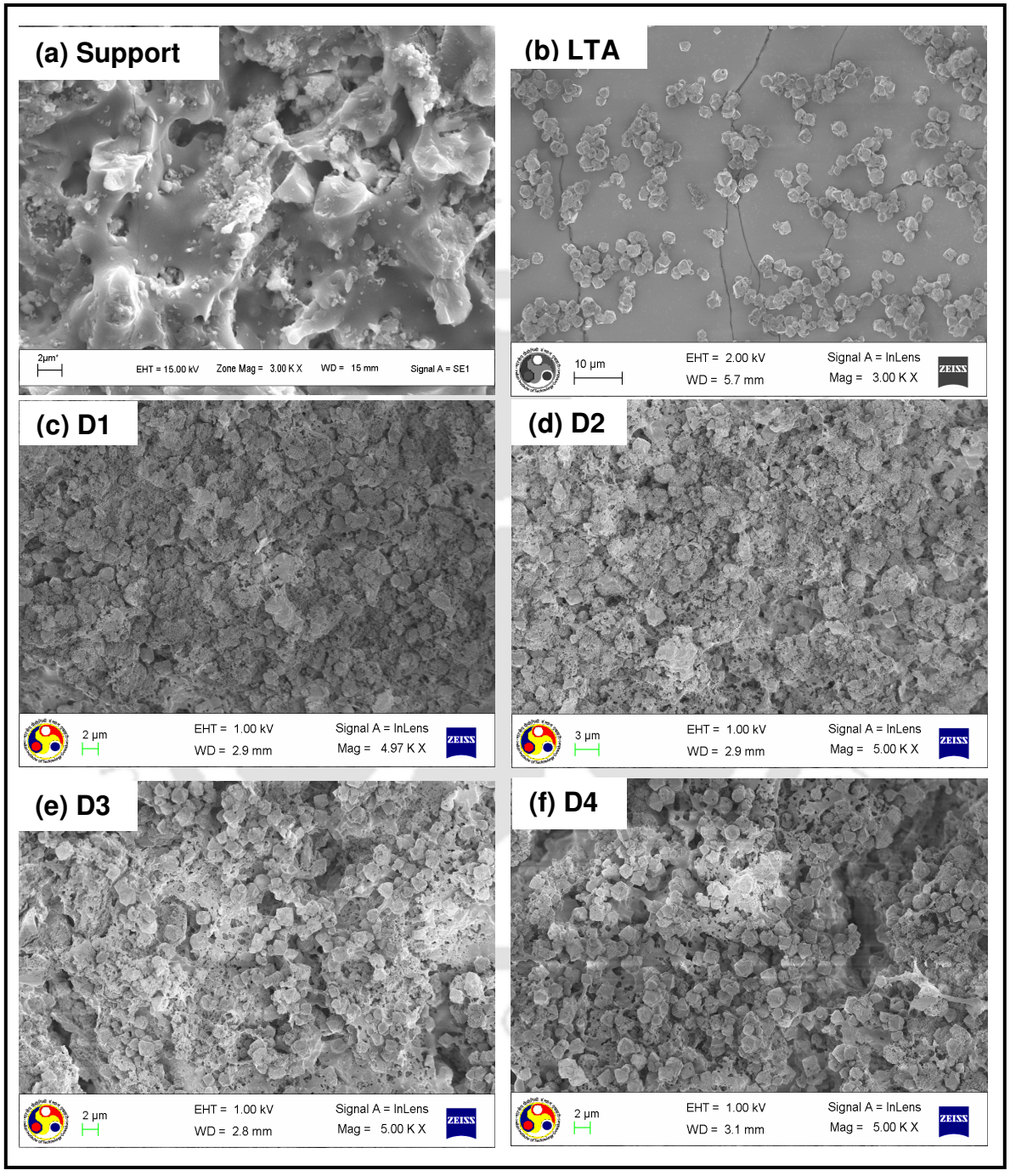

Figure 6.5: SEM images of various membranes (a) B1 membrane support (b) LTA zeolite particles (c) D1 LTA zeolite composite membrane (d) D2 membrane (e) D3 membrane (f) D4 membrane.

It has been observed that LTA crystals are uniform and cubic in shape. The size of LTA zeolite crystals is about 2 – 3 µm (Fig. 6.5 b). Moreover, it is apparent that the support was covered with irregular LTA zeolite layer and zeolite particles with similar LTA type morphology scattered on the support surface. Also, it can be observed that the particle density increases with increasing number of coating steps (Fig. 6.5 c – f).

6.2.1.5 Water flux and permeability

The LTA zeolite composite membranes D1 – D4 were evaluated for pure water permeability data in the applied pressure range of 207 – 483 kPa. Fig. 6.6 presents the variation of pure water flux with applied pressure for D1 – D4 membranes.

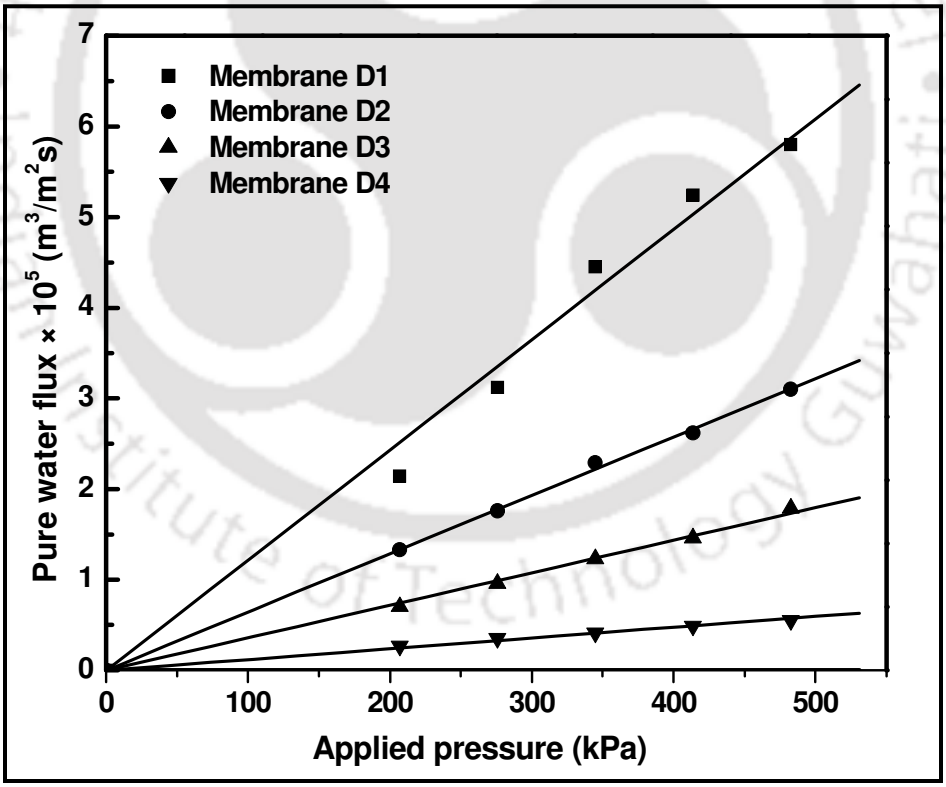

Figure 6.6: Variation of pure water flux with applied pressure for (D1 – D4) LTA zeolite composite membranes.

The results clearly indicate that the pure water flux trends followed Darcy's law and increase linearly with applied pressure for all membranes. Also, the pure water flux of the coated membranes is significantly lower than that of the uncoated B1 membrane (support). Moreover, it has been noted that the membrane pure water flux decreases with increasing number of coating steps. This is due to the fact that the pore size of the membranes reduces with increasing sequential coating steps. The hydraulic permeability (L_h) of the membranes was determined from the linear regression of water flux (J_v) versus applied pressure (ΔP) data. The permeability value has been evaluated to vary from 1.22×10^{-7} – 1.19×10^{-8} m^3/m^2s kPa for D1 – D4 zeolite composite membranes, respectively

6.2.1.6 Membrane porosity and pore size

Membrane porosity is an important parameter, as it significantly influences the evaluated average hydraulic pore size. Fig. 6.7 shows the variation of porosity and hydraulic pore size with the number of coating steps for the membranes D1 – D4. It can be observed that the membrane porosity reduced with increasing number of coating steps. This is due to the fact that as number of coating steps increase, pore volume gets reduced. The porosity of the membrane varied between 30 – 23 %. Also, it can be also observed that, the average hydraulic of the membranes decreases with increasing number of coating steps. The average pore size has been evaluated to be about 215 – 76 nm for D1 – D4 membranes.

The overall characterization results obtained for various membranes D1 – D4 with respect to various coating steps has been presented in Table 6.2. The table confirmed that

weight gain increased and porosity, average pore size and water permeability reduced with increasing number of coating steps for the zeolite membranes.

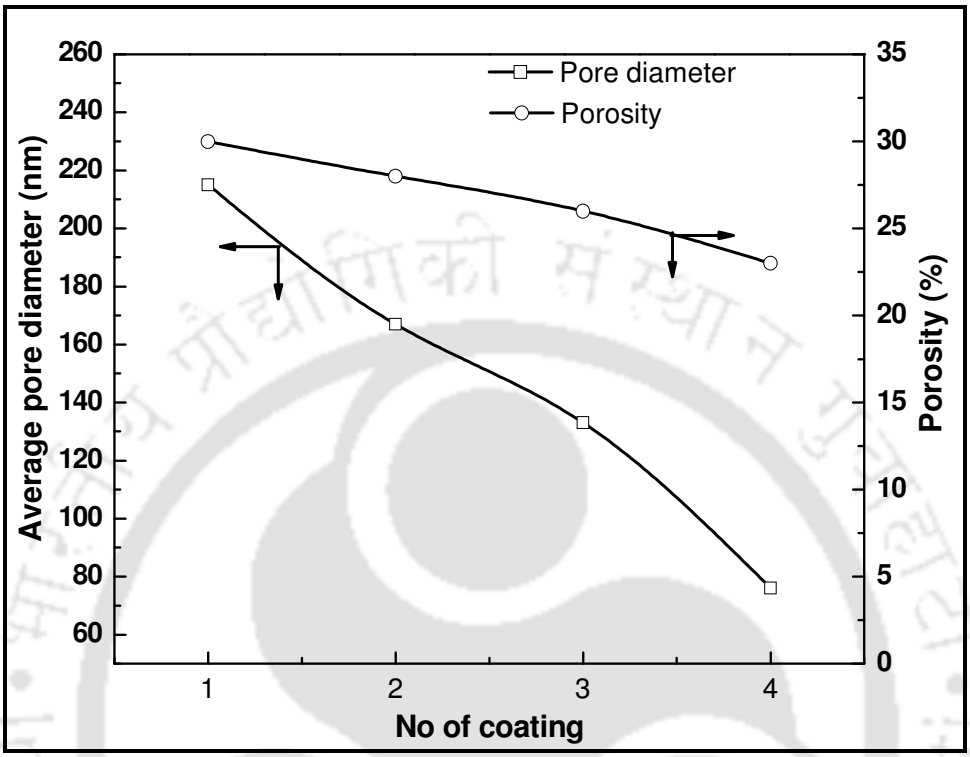

Figure 6.7: Variation in average pore size and porosity with number of coating steps for (D1 – D4) composite membranes.

Table 6.2: Characterization parameters for membranes D1 – D4 LTA zeolite composite membranes.

Membranes	**Average pore diameter (nm)**	**Porosity (%)**	**Pure water permeability (m^3/m^2s kPa)**	**Weight increment (g)**
Support	1006	45	3.97×10^{-6}	-
D1	215	30	1.22×10^{-7}	0.314
D2	167	28	6.44×10^{-8}	0.3243
D3	133	26	3.59×10^{-8}	0.4648
D4	76	23	1.19×10^{-8}	0.1079

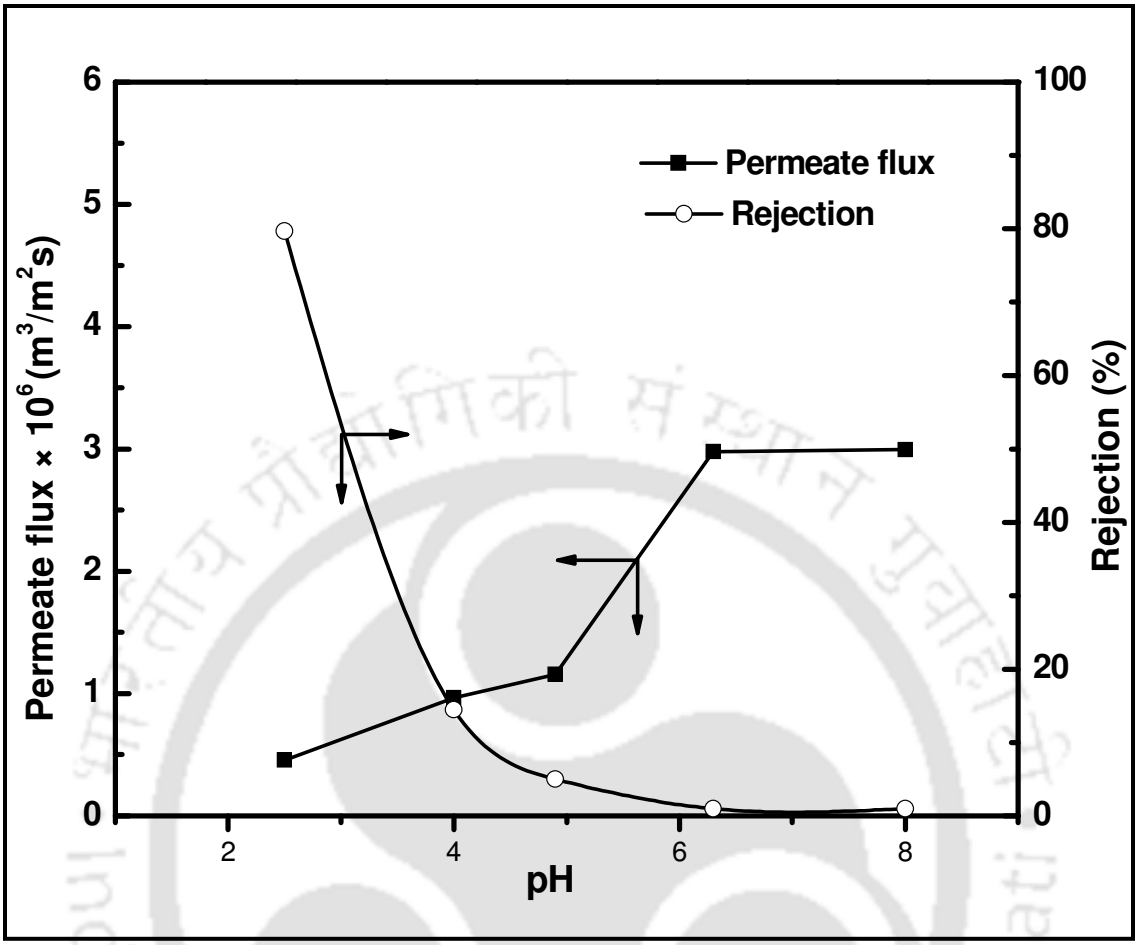

Figure 6.8: Effect of pH on permeate flux and BSA rejection of D4 zeolite composite membrane at an applied pressure and feed concentration of 207 kPa and 1000 mg/L, respectively.

6.2.2 Separation of bovine serum albumin (BSA)

6.2.2.1 Effect of initial pH

Figure 6.8 illustrates the variation of D4 membrane flux and BSA rejection as a function of pH at a pressure of 207 kPa. It can be seen that the permeate flux (4.54 – 29.9 × 10^{-7} m^3/m^2s) has been significantly influenced with pH variation. The variation in the permeate flux with pH is possibly due to the following reasons. Firstly, pH enabled

variations in the conformation (shape and size) of BSA. Secondly, electrostatic interaction between BSA and the LTA membranes occurred. This has been well documented in the literature. The solution pH can alter the size and shape of the BSA molecule. This effect can influence the permeate flux and BSA rejection (Pujar and Zydney 1998). It has been reported that BSA has three different conformations with respect to the solution pH namely, expanded (pH less than 3), fast (pH 3 – 4) and normal (pH 5 – 8) forms. In comparison with other forms, the size of BSA molecules is high in the expanded form. Also, the solution pH can alter the electric charge of the BSA molecule. For solution pH values less than 4.9, (pH less than IEP), the BSA is positively charged. At a pH of 4.9 (IEP of BSA), the BSA is not charged. At a pH greater than 4.9, BSA has a negative charge. On the other hand, it has been reported that the LTA zeolite has a permanent negative charge (Kugbe *et al*., 2009).

From the figure, it can be noted that a lower permeate flux has been obtained at the lower pH (2.5). This is primarily due to the electrostatic attraction between BSA and membrane as BSA is positively charged and membrane is negatively charged. Due to this reason, the membrane was subjected to very intense fouling. Also, it can be noted that the permeate flux increased with increasing pH. This is due to a reduction in the attraction between BSA and zeolite membrane at higher pH. Moreover, the permeate flux improved above a pH of 4.9. This can be explained due to the enhancement in the repulsion effect, which has been due to same negative charges for both BSA and membrane. Further, the rejection has been found to decrease with increasing pH (Fig. 6.8). At a lower pH of 2.5, the membrane shows higher rejection of BSA (80 %). This can be explained with the variation in BSA molecule conformation. For a lower pH value less than 3, the BSA

exists in the expanded form where the size of BSA molecules is high. This reduces the transport of BSA and enables higher rejection. Moreover, the rejection has been found to be insignificant (around 1 %) at higher pH (6.3 – 8). BSA exists in normal form at moderate pH range of (5 – 8). Under these conditions, the BSA molecule can easily penetrate through the membrane and hence rejection values have been low. A maximum rejection of around 80 % was evaluated at a pH of 2.5. Corresponding permeate flux has been evaluated to be 4.54×10^{-7} m^3/m^2 s. From pH studies, a pH of 2.5 has been identified as the optimal pH. Hence, pressure variation effect was studied at a pH of 2.5.

6.2.2.2 Effect of applied pressure

Figure 6.9 depicts the variation of permeate flux and rejection of BSA as a function of applied pressure (207 – 345 kPa). It has been observed that the permeate flux (4.54 – 5.95×10^{-7} m^3/m^2s) increases with increasing applied pressure and this is due to the enhancement in driving force with applied pressure. However, the rate of flux enhancement is not significant. This is due to the effect of charge which provides additional resistance to the permeate flow. The maximum permeate flux of 5.95×10^{-7} m^3/m^2s has been evaluated at a higher pressure of 345 kPa. Further, it has been observed that the rejection of BSA decreased with increasing applied pressure. This indicates that at higher pressure, the membrane allows the BSA molecule to pass through. The rejection has been reduced from 80 to 54 % for an increase in applied pressure from 207 to 345 kPa. Due to the ineffective enhancement in permeate flux at higher applied pressure, the lower applied pressure of 207 kPa and pH of 2.5 have been regarded to the optimal operating MF conditions.

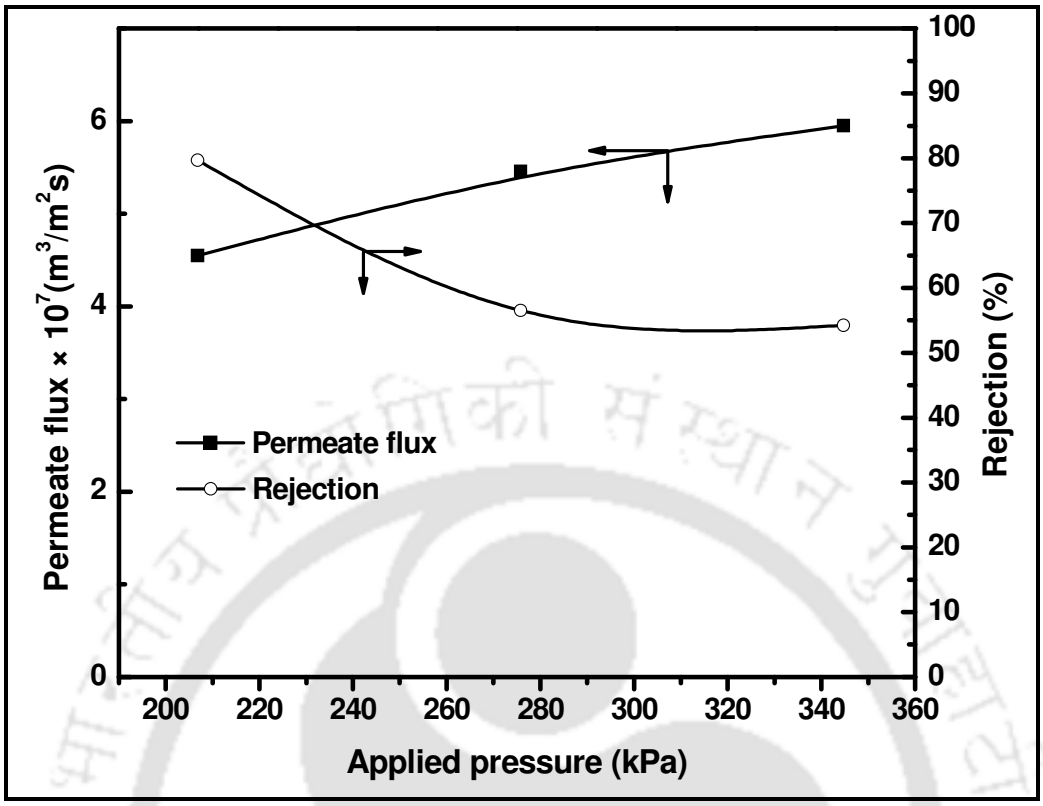

Figure 6.9: Variation of D4 membrane of permeate flux and BSA rejection with applied pressure at a pH and feed concentration of 2.5 and 1000 mg/L, respectively.

Further, a comparative study of the membrane D4 with other membranes reported in the literature is presented in Table 6.3. It can be observed that the polymeric membranes reported in the literature provided significantly higher flux in comparison with the zeolite composite membranes. However, it shall be noted that till date no other work has carried out BSA separation study using inorganic composite membranes and the performance characteristics reported in this work are anticipated to serve as benchmark data. Using this data, further, refinement in the research activity is expected in the near future to fabricate inexpensive inorganic membranes that provide superior combinations of flux and rejection.

Table 6.3: Flux and separation characteristics of D4 and literature reported membranes for UF based BSA separation.

Membrane	Feed concentration (mg/L)	Permeate flux (m^3/m^2s)	Rejection (%)	References
Polyethersulfone (PES)	500	1.75×10^{-5}	59	Tung *et al*., 2007
Polysulfone	500	1.66×10^{-5}	90	Becht *et al*., (2008)
Polysulfone	500	1.94×10^{-5}	100	Becht *et al*., (2008)
cellulose acetate-ceramic composite membrane	1000	12.2×10^{-3}	50	Nandi *et al*., (2009)
Membrane D4	1000	4.54×10^{-7}	80	Present work

This is especially true for the cases where research innovation in fabrication methodology could reduce the thickness of zeolite films and enable higher combinations of flux and rejection.

6.3 Summary

LTA zeolite ceramic composite membranes D1 – D4 have been successfully prepared on a low cost ceramic support using in-situ hydrothermal crystallization technique. TGA analysis confirmed that the LTA zeolite membranes are thermally stable upto 900 ^{o}C. The XRD analysis confirmed that the composite membranes have LTA zeolite crystalline

structure. The SEM micrographs also confirmed showed that the zeolite particles have grown well on the membrane support and the density of zeolite particles increased with an increase in the number of coating steps. The water permeability, porosity and average pore of the membranes have been found to be decreasing with increasing number of coating steps. Ultrafiltration of bovine serum albumin (BSA) solutions confirmed that the solution pH significantly affects the permeate flux and rejection. For the D4 membrane, the optimal flux and rejection values of 4.54×10^{-7} m^3/m^2 s and 80 %, respectively were obtained at a pH and pressure of 2.5 and 207 kPa, respectively.

Chapter 7:

Conclusions and Scope For Future Work

Conclusions and Scope for Future Work

This chapter summarizes various conclusions and scope for further research in the near future. The primary objective of thesis is to fabricate low cost ceramic membranes and LTA zeolite composite membranes. New inexpensive compositions were identified by trial and error based approach to prepare ceramic support (2 – 6µm) and sub micron range microfiltration (0.35 – 1.06 µm) membranes. Morphological and structural characterization has indicated that the prepared membranes possessed desired properties for various applications. The prepared membranes were studied for the removal of oil, bacteria and chromium (VI) from their aqueous solution. The LTA zeolite composite membranes were prepared using in-situ hydrothermal crystallization technique. The performance of the zeolite composite membranes was carried out by conducting separation studies on bovine serum albumin (BSA) from aqueous solution.

7.1 Conclusions

- In the sintering temperature range of 900 – 1000 ^{o}C, three MF range membrane supports (A1 – A3) have been successfully prepared using uniaxial dry compaction method developing inexpensive precursors.
- The A2 membrane sintered at 950 ^{o}C was found to be optimum for membrane applications due to its superior combinations of mechanical strength (28 MPa), and average pore size (3.07 µm) and porosity (38 %).

- Micron range MF membranes (B1 – B3) were fabricated with identified newer compositions of raw materials and sintering temperature (900 – 1000 ^{o}C).
- Based on the better characteristics (flexural strength of 34 MPa, better porosity of 45 % and lower average pore size of 1.06 µm), the membrane (B1) sintered at 900 ^{o}C was identified as the best membrane for the separation of oil and bacteria and chromium (VI) from aqueous solution.
- The membrane B1, demonstrated a maximum rejection of 85 % and 99 % at a applied pressure of 69 kPa for oil-water emulsions and *E. coli*, respectively.
- For the B1 membrane, at a applied pressure of 207 kPa, the adsorption-MF hybrid system provided a maximum Cr (VI) removal of 94 % and a permeate flux of 2.07×10^{-5} m^3/m^2s during baker's yeast assisted microfiltration studies.
- In order to further reduce the pore size, two new compositions were formulated with the addition/removal of $TiO_2/CaCO_3$ in the identified raw material composition of membrane B1. Three membranes, namely, B1, C1 and C2 were prepared and subjected to microfiltration of oil-in-water emulsions.
- For membranes B1, C1 and C2, the average porosity and pore diameter were found to be 45, 41 and 39 % and 1.06, 0.90 and 0.35 µm, respectively. The flexural strength of the membranes (B1, C1 and C2) varied between 10 – 34 MPa.
- The membrane, C1 was identified as the optimal membrane for the treatment of oil-water emulsions in dead-end mode, as it provided optimal rejection and optimal permeate flux values. For a feed oil concentration of 200 mg/L, C1 membrane provided ~96 % rejection of oil with permeate flux of 6.5×10^{-5} m^3/m^2s at a lower applied pressure of 69 kPa.

- Membranes B1, C1 and C2 were subjected to cross flow microfiltration of oil-in-water emulsions. Amongst these membranes, membrane C1 has been evaluated to provide a good combination of rejection (87 %) and permeate flux (5.54×10^{-5} m^3/m^2s) at an applied pressure of 207 kPa and cross flow rate of 13.9×10^{-7} m^3/s, respectively.
- The analysis of fouling mechanism of different pore blocking models indicates that the cake filtration model was the best fit to represent the experimental data for all membranes.
- LTA zeolite composite membranes (D1 – D4) were prepared on the low cost ceramic support B1 using in-situ hydrothermal crystallization technique. The water permeability, porosity and average pore size of the membranes were found to decrease with increasing number of coating steps.
- Ultrafiltration of bovine serum albumin (BSA) solutions confirmed that the pH of the solution significantly affected membrane (D4) permeate flux and rejection. The optimal flux and rejection values correspond to 4.54×10^{-7} m^3/m^2s and 80 %, respectively at a pH and applied pressure of 2.5 and 207 kPa, respectively.
- Based on the retail cost of the raw materials, the fabrication cost of A2, B1 and C1 membranes has been estimated to be 49.4, 49.2 and 50 $\$/m^2$, respectively.

In summary, this identified newer compositions for various low cost MF membranes whose performance is satisfactory and comparably better than those reported in the literature for various applications.

7.2 Future scope

Based on the outcome of this work, few recommendations for future research have been presented as follows

Development and characterization of inorganic membranes

- Develop multi channel tubular low cost ceramic membranes using inexpensive raw materials (clays) by extrusion method.
- Investigate upon the effect of extrusion velocity on the morphology and structural properties of membranes.
- Study the role of various binders (polyvinyl alcohol, polyethylene glycol and carboxy methyl cellulose) on the membranes properties.
- Evaluate pore size distribution and average membrane pore size using mercury porosimetry approach and molecular weight cutoff (MWCO) studies.
- Develop bi-layered tubular ceramic composite membranes using low cost skin layer materials such as zirconia and zeolite.

Microfiltration applications of low cost tubular and multichannel ceramic membranes

- Separation of toxic metals (Cr, Pb, Cd) using zeolite composite membranes with cross flow mode MF.
- Treatment of industrial oily wastewater streams to obtain confidence levels for the commercial application of low cost ceramic membranes.
- Pilot plant study for chromium and bovine serum albumin (BSA) separation with the low cost ceramic MF and UF.

References

References

Abadi, S.R.H., Sebzari, M.R., Hemati, M., Rekabdar, F. and Mohammadi, T., 2011. Ceramic Membrane Performance in Microfiltration of Oily Wastewater, *Desalination*, 265, 222 – 228.

Abbasi, M., Mirfendereski, M., Nikbakht, M., Golshenas, M. and Mohammadi, T., 2010. Performance Study of Mullite and Mullite–Alumina Ceramic MF Membranes for Oily Wastewaters Treatment, *Desalination,* 259, 169 – 178.

Almandoza, M.C., Marchese, J., Pradanos, P., Palacio, L. and Hernandez, A., 2004. Preparation and Characterization of Non-supported Micro-filtration Membranes from Aluminosilicates, *Journal of Membrane Science,* 241, 95 – 103.

Almecija, M. C., Ibanez, R., Guadix, A. and Guadix, E. M., 2007. Effect of pH on the Fractionation of Whey Proteins with a Ceramic Ultrafiltration Membrane, *Journal of Membrane Science,* 288, 28 – 35.

Amanipour, M., Safekordi, A., Babakhani, E.G., Zamaniyan, A. and Heidari. M., 2012. Effect of Synthesis Conditions on Performance of a Hydrogen Selective Nano-composite Ceramic Membrane, *International Journal of Hydrogen Energy*, 37, 15359 – 15366.

Aoki, K., Kusakabe, K. and Morooka, S., 1998. Gas Permeation Properties of A-type Zeolite Membrane Formed on Porous Substrate by Hydrothermal Synthesis, *Journal of Membrane Science,* 141, 197 – 205.

Arkhangelsky, E. and Gitis, V., 2008. Effect of Transmembrane Pressure on Rejection of Viruses by Ultrafiltration Membranes, *Separation and Purification Technology* 62, 619 – 628.

Arnot, T.C., Field, R.W. and Koltuniewicz, A.B., 2000. Cross-flow and Dead-end Microfiltration of Oily-water Emulsions Part II. Mechanisms and Modelling of Flux Decline, *Journal of Membrane Science,* 169, 1 – 15.

Aroua, M. K., Zuki, F. M. and Sulaiman, N. M., 2007. Removal of Chromium Ions from Aqueous Solutions by Polymer-Enhanced Ultrafiltration, *Journal of Hazardous Materials,* 147, 752 – 758.

Arthanareeswaran, G., Thanikaivelan, P., Jaya, N., Mohan, D. and Raajenthiren, M., 2007. Removal of Chromium from Aqueous Solution using Cellulose Acetate and Sulfonated Poly(ether ether ketone) Blend Ultrafiltration Membranes, *Journal of Hazardous Materials*, B139, 44 – 49.

Bai, R.S. and Abraham, T.E., 2001. Biosorption of Cr(VI) from Aqueous Solution by *Rhizopus Nigircans*, *Bioresource Technology,* 79, 73 – 81.

Balek, V. and Murat, M., 1996. The Emanation Thermal Analysis of Kaolinite Clay Minerals, *Thermochimica Acta*, 282, 385 – 397.

Bayhan, Y.K., Keskinler, B. Cakici, A., Levent, M. and Akay, G., 2001. Removal of Divalent Heavy Metal Mixtures from Water by *Saccharomyces cerivisiae* using Crossflow Microfiltration, *Water Research*, 35, 2191 – 2200.

Becht, N.O., Malik, D.J. and Tarleton, E.S., 2008. Evaluation and Comparison of Protein Ultrafiltration Test Results: Dead-end Stirred Cell Compared with a Cross-flow System, *Separation and Purification Technology,* 62, 228 – 239.

Belouatek, A., Benderdouche, N., Addou, A., Ouagued, A. and Bettahar, N., 2005. Preparation of Inorganic Supports for Liquid Waste Treatment, *Microporous and Mesoporous Materials,* 85, 163–168.

Benito, J.M., Conesa, A., Rubio, F. and Rodriguez, M.A., 2005. Preparation and Characterization of Tubular Ceramic Membranes for Treatment of oil emulsions, *Journal of the European Ceramic Society,* 25, 1895 – 1903.

Bernal, M.P., Xomeritakis, G. and Tsapatsis, M., 2001. Tubular MFI Zeolite Membranes Made by Secondary (seeded) Growth, *Catalysis Today,* 67, 101 – 107.

Bhanushali, D., Kloos, S., Kurth, C. and Bhattacharyya, D., 2001. Performance of Solvent-Resistant Membranes for Non-Aqueous Systems: Solvent Permeation Results and Modeling, *Journal of Membrane Science,* 189, 1 – 21.

Bhide, B.D. and Stern, S.A., 1991. A New Evaluation of Membrane Processes Enrichment of Air. II. Effects of Economic Membrane Properties. *Journal of Membrane Science,* 62, 37 – 58.

Boudaira, B., Harabia, A., Bouzerara, F. and Condom, S., 2009. Preparation and Characterization of Microfiltration Membranes and their Supports using Kaolin (DD2) and $CaCO_3$, *Desalination and Water Treatment,* 9, 142 – 148.

Bouzerara, F., Harabi, A., Achour, S. and Larbot, A., 2006. Porous Ceramic Supports for Membranes Prepared from Kaolin and Doloma Mixtures, *Journal of the European Ceramic Society,* 26, 1663 – 1671.

Brady, D., Rose, D. and Duncan, J.R., 1976. The Use of Hollow Fiber Cross-flow Micro-Filtration in Bioaccumulation and Continuous Removal of Heavy Metals from Solution by *Saccharomyces cerevisiae*, *Biotechnology and Bioengineering,* 99, 1362 – 1366.

Burggraaf, A.J. and Cot, L., 1996. Fundamentals of Inorganic Membrane Science and Technology, Elsevier, Amsterdam, The Netherlands.

Cengeloglu, Y., Tor, A., kir E. and Ersoz, M., 2003. Transport of Hexavalent Chromium through Anion-Exchange Membranes, *Desalination,* 154, 239 – 246.

Chakrabarty, B., Ghoshal, A.K. and Purkait, M.K., 2008. Ultrafiltration of Stable Oil-in-Water Emulsion by Polysulfone Membrane, *Journal of Membrane Science,* 325, 427 – 437.

Chen, Y.F., Wang, M.C. and Hon, M.H., 2004. Phase Transformation and Growth of Mullite in Kaolin Ceramics, *Journal of the European Ceramic Society,* 24, 2389 – 2397.

Cheryan, M., 1998. Ultrafiltration and Microfiltration Handbook, Technomic, Lancaster, PA.

Cheryan, M., 1998. Ultrafiltration and Microfiltration Handbook, Cost and Process Economics, Technomic Publishing Company, Basel, Switzerland.

Cui, J., Zhang, X., Liu, H., Liu, S. and Yeung, K.L., 2008. Preparation and Application of Zeolite/Ceramic Microfiltration Membranes for Treatment of Oil Contaminated Water. *Journal of Membrane Science*, 325, 420 – 426.

Cumming, I.W., Holdich, R.G. and Smith, I.D., 2000. The Rejection of Oil by Microfiltration of a Stabilized Kerosene/Water Emulsion. *Journal of Membrane Science,* 169, 147 – 155.

Dong, Y., Feng, X., Dong, D., Wang, S., Yang, J., Gao, J., Liu, X. and Meng, G., 2007. Elaboration and Chemical Corrosion Resistance of Tubular Macro-porous Cordierite Ceramic Membrane Supports, *Journal of Membrane Science,* 304, 65 – 75.

Ebrahimi, M., Shams Ashaghi, K., Engel, L., Willershausen, D., Mund, P., Bolduan, P. and Czermak, P., 2009. Characterization and Application of Different Ceramic Membranes for the Oil-field Produced Water Treatment, *Desalination*, 245, 533 – 540.

Ebrahimi, M., Willershausen, D., Ashaghi, K.S., Engel, L., Placido, L., Mund, P., Bolduan, P. and Czermak, P., 2010. Investigations on the use of Different Ceramic Membranes for Efficient Oil-Field Produced Water Treatment, *Desalination,* 250, 991 – 996.

Erdem, I., Ciftcioglu, M. and Harsa, S., 2006. Separation of Whey Components by using Ceramic Composite Membranes, *Desalination,* 189, 87 – 91.

Fakhfakh, S., Baklouti, S., Baklouti, S. and Bouaziz, J., 2010. Preparation, Characterization and Application in BSA Solution of Silica Ceramic Membranes, *Desalination,* 262, 188 – 195.

Falamaki, C., Afarani, M.S. and Aghaie, A., 2004. Initial Sintering Stage Pore Growth Mechanism Applied to the Manufacture of Ceramic Membrane Supports, *Journal of the European Ceramic Society*, 24, 2285 – 2292.

Falamaki, C., Khakpour, Z. and Aghaie, A., 2005. Zirconia–zircon Composite Microfiltration Membranes Based on Porous Alumina Supports, *Journal of Membrane Science,* 263, 103 – 112.

Falamaki, C., Naimi, M. and Aghaie, A., 2004. Dual Behavior of $CaCO_3$ as a Porosifier and Sintering Aid in the Manufacture of Alumina Membrane/Catalyst Supports, *Journal of the European Ceramic Society*, 24, 3195 – 3201.

Fan, J., Ohya, H., Suga, T., Ohashi, H., Yamashita, K., Tsuchiya, S., Aihara, M., Takeuchi, T. and Negishi, Y., 2000. High Flux Zirconia Composite Membrane for Hydrogen Separation at Elevated Temperature, *Journal of Membrane Science,* 170, 113 – 125.

Ghayeni, S.B.S., Beatsona, P.J., Fanea, A.J. and Schneider, R.P., 1999. Bacterial Passage through Microfiltration Membranes in Wastewater Applications, *Journal of Membrane Science,* 153, 71 – 82.

Ghosh, R. and Cui, Z.F., 1998. Fractionation of BSA and Lysozyme using Ultrafiltration: Effect of pH and Membrane Pretreatment, *Journal of Membrane Science*, 139, 17 – 28.

Gorouhi, E., Sadrzadeh, M. and Mohammadi, T., 2006. Microfiltration of Oily Wastewater using PP Hydrophobic Membrane, *Desalination,* 200, 319 – 321.

Guo, R., Ma, X., Hu, C. and Jiang, Z., 2939. 2007 Novel PVA-Silica Nanocomposite Membrane for Pervaporative Dehydration of Ethylene Glycol Aqueous Solution, *Polymer,* 48, 2939 – 2945.

Hafiarle, A., Lemordant, D. and Dhahbi, M., 2000. Removal of Hexavalent Chromium by Nanofiltration, *Desalination,* 130, 305 – 31.

Hao, J., McCloskey, B.D., Sagle, A.C., Wu, Y.H., Kusuma, V.A. and Freeman, B.D., 2008. Crosslinked Poly(ethylene oxide) Fouling Resistant Coating Materials for Oil/Water Separation, *Journal of Membrane Science,* 307, 260 – 267.

Hedlund, J., Sterte, J., Anthonis, M., Bons, A.J., Carstensen, B., Cororan, N., Cox, D., Deckman, H., Ginst, W.M., de Moor, P.P., Lai, F., McHenry, J., Mortier, W., Reinco, J. and Peters, J., 2002. High-flux MFI Membranes, *Microporous and Mesoporous Materials,* 52, 179 – 189.

Hoof, V.V., Dotremont, C. and Buekenhoudt, A., 2006. Performance of Mitsui NaA Type Zeolite Membranes for the Dehydration of Organic Solvents in Comparison with Commercial Polymeric Pervaporation Membranes, *Separation and Purification Technology,* 48, 304 – 309.

Hua, F.L., Tsang, Y.F., Wang, Y.J., Chan, S.Y., Chuand, H. and Sin, H.N., 2007. Performance Study of Ceramic Microfiltration Membrane for Oily Wastewater Treatment. *Chemical Engineering Journal*, 128, 169 – 175.

Huang, A. and Yang, W., 2008. Enhancement of NaA Zeolite Membrane Properties through Organic Cation Addition, *Separation and Purification Technology,* 61, 175 – 181.

Huang, A., Lin, Y.S. and Yang, W., 2004. Synthesis and Properties of A-type Zeolite Membranes by Secondary Growth Method with Vacuum Seeding, *Journal of Membrane Science,* 245, 41 – 51.

Huang, C.P., Huang, C.P. and Allen, L.M., 1990. The Removal of Cu(II) from Dilute Aqueous Solutions by *Saccharomyces cerevisiae*, *Applied Microbiology and Biotechnology,* 41, 149 – 154.

Jafar, J.J. and Budd, P.M., 1997. Separation of Alcohol/Water Mixtures by Pervaporation through Zeolite A Membranes, *Microporous Materials,* 12, 305 – 311.

Jedidi, I., Khemakhem, S., Larbot, A. and Amar, R.B., 2009. Elaboration and Characterisation of Fly Ash Based Mineral Supports for Microfiltration and Ultrafiltration Membranes. *Ceramics International,* 35, 2747 – 2753.

Judd, S.J. and Till, S.W., 2000. Bacterial Rejection in Crossflow Microfiltration of Sewage, *Desalination,* 127, 251 – 260.

Katz, S.A. and Salem, H., 1993. The Toxicology of Chromium with Respect to Its Chemical Speciation: A Review, *Journal of Applied Toxicology,* 13, 217 – 24.

Kazemimoghadam, M. and Mohammadi, T., 2006. Preparation of NaA Zeolite Membranes for Separation of Water/UDMH Mixtures, *Separation and Purification Technology,* 47, 173 – 178.

Khemakhem, S., Larbot, A. and Amar, R.B., 2009. New Ceramic Microfiltration Membranes from Tunisian Natural Materials: Application for the Cuttlefish Effluents Treatment, *Ceramics International,* 35, 55 – 61.

Kikuchi, E., Yamashita, K., Ffiromoto, S., Ueyama, K. and Matsukata, M., 1997. Synthesis of a Zeolitic Thin Layer by a Vapor-phase Transport Method: Appearance of a Preferential Orientation of MFI Zeolite, *Microporous Materials,* 11, 107 – 116.

Kobayashi, T., Ono, M., Shibata, M. and Fujii, N., 1998, Cutoff Performance of *Escherichia coli* by Charged and Noncharged Polyacrylonitrile Ultrafiltration Membranes, *Journal of Membrane Science,* 140, 1 – 11.

Koltuniewicz, A.B., Field, R.W. and Arnot, T.C., 1995. Cross-Flow and Dead-End Microfiltration of Oily-Water Emulsion. Part I: Experimental Study and Analysis of Flux Decline, *Journal of Membrane Science,* 102, 193 – 207.

Kondo, M., Komori, M., Kita, H. and Okamoto, K., 1997. Tubular-type Pervaporation Module with Zeolite NaA Membrane, *Journal of Membrane Science,* 133, 133 – 141.

Koros, W.J. and Mahajan, R., 2000. Pushing the Limits on Possibilities for Large Scale Gas Separation: Which Strategies, *Journal of Membrane Science,* 175, 181 – 196.

KoRuniewicz, A.B., and Field, R.W., 1996. Process Factors During Removal of Oil-in-Water Emulsions with Cross-flow Microfiltration, *Desalination,* 105, 79 – 89.

Korus I. and Loska, K., 2009. Removal of Cr(III) and Cr(VI) Ions from Aqueous Solutions by Means of Polyelectrolyte-Enhanced Ultrafiltration, *Desalination*, 247, 390 – 395.

Kotas, J., and Stasicka, Z., 2000. Chromium Occurrence in the Environment and Methods of Its Speciation, *Environmental Pollution*, 107, 263 – 83.

Kroll, S., Treccani, L., Rezwan, K. and Grathwohl, G., 2010. Development and Characterisation of Functionalised Ceramic Microtubes for Bacteria Filtration. *Journal of Membrane Science,* 365, 447 – 455.

Kugbe, J., Matsue, N. and Henmi, T., 2009. Synthesis of Linde Type A Zeolite–Goethite Nanocomposite as an Adsorbent for Cationic and Anionic Pollutants, *Journal of Hazardous Materials,* 164, 929 – 935.

Kyotani, T., Mizuno, T., Katakura, Y., Kakui, S., Shimotsuma, N., Saito, J. and Nakane, T., 2007. Characterization of Tubular Zeolite NaA Membranes Prepared from Clear Solutions by FTIR-ATR, GIXRD and FIB-TEM-SEM, *Journal of Membrane Science,* 296, 162 – 170.

Lai, R. and Gavalas, G.R., 1998. Surface Seeding in ZSM-5 Membrane Preparation, *Industrial and Engineering Chemistry Research,* 37, 4275 – 4283.

Lai, Z., Bonilla, G., Diaz, I., Nery, J.G., Sujaoti, K., Amat, M.A., Kokkoli, E., Terasaki, O., Thompson, R.W. Tsapatis, M. and Vlachos, D.G., 2003. Microstructure Optimization of a Zeolite Membrane for Organic Vapor Separation, *Science,* 300, 456 – 460.

Lebleu, N., Roques, C., Aimar, P. and Causserand, C., 2009. Role of the Cell-wall Structure in the Retention of Bacteria by Microfiltration Membranes, *Journal of Membrane Science,* 326, 178 – 185.

Lebleu, N., Roques, C., Aimar, P. and Causserand, C., 2010. Effects of Membrane Alterations on Bacterial Retention, *Journal of Membrane Science,* 348, 56 – 65.

Li, H.J., Cao, Y.M., Qin, J.J., Jie, X.M., Wang, T.H., Liu, J.H. and Yuan, Q., 2006. Development and Characterization of Anti-fouling Cellulose Hollow Fiber UF Membranes for Oil–Water Separation, *Journal of Membrane Science,* 279, 328 – 335.

Li, S., Tuan, V.A., Noble, R.D. and Falconer, J.L., 2001. Pervaporation of Water/THF Mixtures using Zeolite Membranes. *Industrial and Engineering Chemistry Research,* 40, 4577 – 4585.

Li, Y., Chen, H., Liu, J. and Yang, W., 2006. Microwave Synthesis of LTA Zeolite Membranes without Seeding, *Journal of Membrane Science,* 277, 230 – 239.

Ling, W.S., Thian, T.C. and Bhatia, S., 2011. Synthesis, Characterization and Pervaporation Properties of Microwave Synthesized Zeolite A Membrane. *Desalination* 277, 383 – 389.

Mallada, R. and Menendez, M., 2008. Inorganic Membranes Synthesis, Characterization and Applications, Elsevier, Amsterdam, The Netherlands.

Masmoudi, S., Larbot, A., El Feki, H. and Ben Amar, R., 2007. Elaboration and Characterisation of Apatite Based Mineral Supports for Microfiltration and Ultrafiltration Membranes, *Ceramics International*, 33, 337 – 344.

Mavrov, V., Chmiel, H., Kluth, J., Meier, J., Heinrich, F., Ames, P., Backes, K. and Usner, P., 1998. Comparative Study of Different MF and UF Membranes for Drinking Water Production, *Desalination,* 117, 189 – 196.

Mohammadi, T., Pak, A., Karbassian, M. and Golshan, M., 2004. Effect of Operating Conditions on Microfiltration of an Oil–water Emulsion by a Kaolin membrane, *Desalination*, 168, 201 – 205.

Mohammadi, T., Pak, A., Karbassian, M. and Golshan, M., 2004. Effect of Operating Conditions on Microfiltration of an Oil–Water Emulsion by a Kaolin Membrane, *Desalination,* 168, 201 – 205.

Mohmmadi, T., Kazemimoghadam, M. and Saadabadi, M., 2003. Modeling of Membrane Fouling and Decline in Reverse Osmosis During Separation of Oil-in-Water Emulsions, *Desalination,* 157, 369 – 375.

Molisani, A.L., Yoshimura, H.N., Goldenstein, H. and Watari, K., 2006. Effects of $CaCO_3$ Content on the Densification of Aluminum Nitride. *Journal of the European Ceramic Society,* 26, 3431 – 3440.

Monash, P. and Pugazhenthi, G., 2011. Development of Ceramic supports Derived from Low-Cost Raw Materials for Membrane Applications and its Optimization Based on Sintering Temperature, *International Journal of Applied Ceramic Technology,* 8, 227 – 238.

Morigami, Y., Kondo, M., Abe, J., Kita, H. and Okamoto, K., 2001. The First Large-scale Pervaporation Plant using Tubular-type Module with Zeolite NaA Membrane, *Separation and Purification Technology,* 25, 251 – 260.

Mott Metallurgical Corporation, USA, 2007. http://www.mottcorp.com.

Nandi, B.K., Moparthi, A., Uppaluri, R. and Purkait, M.K., 2010. Treatment of Oily Wastewater using Low Cost Ceramic Membrane: Comparative Assessment of Pore Blocking and Artificial Neural Network Models, *Chemical Engineering Research and Design,* 88, 881 – 892.

Nandi, B.K., Uppaluri, R. and Purkait, M.K., 2008. Preparation and Characterization of Low Cost Ceramic Membranes for Micro-Filtration Applications, *Applied Clay Science* 42, 102 – 110.

Nandi, B.K., Uppaluri, R. and Purkait, M.K., 2009. Effects of Dip Coating Parameters on the Morphology and Transport Properties of Cellulose Acetate–Ceramic Composite Membranes, *Journal of Membrane Science,* 330, 246 – 258.

Neelakandan, C., Pugazhenthi, G., Kumar, A., 2003. Preparation of NOx Modified PMMA–EGDM Composite Membrane for the Recovery of Chromium (VI), *European Polymer Journal,* 39, 2383 – 2391.

Noble, R.D. and Falconer, J.L., 1995. Silicalite-1 Zeolite Composite membranes, *Catalysis Today,* 25, 209 – 212.

Norris, P.R. and Kelly, D.P., 1977. Accumulation of Cadmium and Cobalt by *Saccharomyces cerevisiae, Journal of General Microbiology,* 99, 317 – 324.

Ozer, A. and Ozer, D., 2003. Comparative Study of the Biosorption of Pb(II), Ni(II) and Cr(VI) Ions onto S. cerevisiae: Setermination of Biosorption Heats, *Journal of Hazardous Materials*, 100, 219 – 29.

Pagana, A.E., Sklari, S.D., Kikkinides, E.S. and Zaspalis, V.T., 2011. Combined Adsorption–Permeation Membrane Process for the Removal of Chromium(III) Ions from Contaminated Water, *Journal of Membrane Science*, 367, 319 – 324.

Pagana, A.E., Sklari, S.D., Kikkinides, E.S. and Zaspalis, V.T., 2008. Microporous Ceramic Membrane Technology for the Removal of Arsenic and Chromium Ions from Contaminated Water, *Microporous and Mesoporous Materials*, 110, 150 – 156.

Pan, Y., Wang, T., Sun, H. and Wang, W., 2012. Preparation and Application of Titanium Dioxide Dynamic Membranes in Microfiltration of Oil-in-Water Emulsions, *Separation and Purification Technology,* 89, 78 – 83.

Pera-Titus, M., Bausach, M., Llorens, J. and Cunill, F., 2008. Preparation of Inner-side Tubular Zeolite NaA Membranes in a Continuous Flow System. *Separation and Purification Technology*, 59, 141 – 150.

Pina, M.P., Arruebo, M., Felipe, M., Flea, F., Bernal, M.P., Coronas, J., Menendez, M. and Santamaria, J., 2004. A semi-continuous method for the synthesis of NaA zeolite membranes on tubular supports, *Journal of Membrane Science,* 244, 141 – 150.

Praptowidodo, V.S., 2005. Influence of Swelling on Water Transport Through PVA-Based Membrane. *Journal of Molecular Structure,* 739, 207 – 212.

Pugazhenthi, G., Sachan, S., Kishore, N. and Kumar, A., 2005. Separation of Chromium(VI) using Modified Ultrafiltration Charged Carbon Membrane and Its Mathematical Modeling, *Journal of Membrane Science,* 254, 229 – 239.

Pujar, N.S. and Zydney, A.l., 1998. Electrostatic Effect on Protein Partitioning in Size Exclusion Chromatography and Membrane Ultrafiltration, *Journal of chromatography A*, 796, 229 – 238.

Ren, X., Zhao, C., Du, S., Wang, T., Luan, Z., Wang, J., Hou, D., 2010. Fabrication of Asymmetric Poly (*m*-phenylene isophthalamide) Nanofiltration Membrane for Chromium(VI) Removal, *Journal of Environmental Sciences*, 22, 1335 – 1341.

Saffaj, N., Alami Younssi, S., Albizane, A., Messouadi, A., Bouhria, M., Persin, M., Cretin, M., Larbot A., (2004). Elaboration and properties of TiO_2–$ZnAl_2O_4$ ultrafiltration membranes deposited on cordierite support. *Separation and Purification Technology* 36, 107 – 114.

Saffaj, N., Persin, M., Younsi, S.A., Albizane, A., Cretin, M. and Larbot, A., 2006. Elaboration and Characterization of Microfiltration and Ultrafiltration Membranes Deposited on Raw Support Prepared from Natural Moroccan Clay: Application to Filtration of Solution Containing Dyes and Salts, *Applied Clay Science,* 31, 110 – 119.

Saffaj, N., Persin, M., Younssi, S.A., Albizan, A., Bouhria, M., Loukili, H., Dacha, H. and Larbot, A., 2005. Removal of Salts and Dyes by Low $ZnAl_2O_4$–TiO_2 Ultra-filtration Membrane Deposited on Support made from Raw Clay, *Separation and Purification Technology,* 47, 36 – 42.

Salahi, A., Gheshlaghi, A., Mohammadi, T. and Madaeni, S.S., 2010. Experimental Performance Evaluation of Polymeric Membranes for Treatment of an Industrial Oily Wastewater, *Desalination,* 262, 235 – 242.

Sar, A. and Tuzen, M., 2008. Biosorption of Total Chromium from Aqueous Solution by Red Algae (*Ceramium virgatum*): Equilibrium, Kinetic and Thermodynamic Studies, *Journal of Hazardous Materials,* 160, 349 – 355.

Sato, K. and Nakane, T., 2007. A High Reproducible Fabrication Method for Industrial Production of High Flux NaA Zeolite Membrane, *Journal of Membrane Science*, 301, 151 – 161.

Schiewer, S. and Volesky, B., 1995. Modeling of the Proton–metal Ion Exchange in Biosorption, *Environmental Science and Technology,* 29, 3049 – 3058.

Scott, K., Adhamy, A., Atteck, W. and Davidson, C., 1994. Crossflow Microfiltration of Organic/Water Suspensions, *Water Research,* 28, 137 – 145.

Scott, K., Jachuck, R.J., Hall, D., 2001. Crossflow Microfiltration of Water-in-Oil Emulsions using Corrugated Membranes. *Separation and Purification Technology* 22-23, 431 – 441.

Srijaroonrat, P., Julien, E. and Aurelle, Y., 1999. Unstable Secondary Oil/Water Emulsion Treatment using Ultrafiltration: Fouling Control by Backflushing, *Journal of Membrane Science,* 159, 11 – 20.

Tiscareno-Lechuga, F., Tellez, C., Menendez, M. and Santamaria, J., 2003. A Novel Device for Preparing Zeolite-A Membranes under a Centrifugal Force Field. *Journal of Membrane Science,* 212, 135 – 146.

Tung, K.L., Hu, C.C., Li, C.L. and Chuang, C.J, 2007. Investigating Protein Crossflow Ultrafiltration Mechanisms Using Interfacial Phenomena, *Journal of the Chinese Institute of Chemical Engineers*, 38, 303 – 311.

Van Gestel, T., Vandecasteele, C., Buekenhoudt, A., Dotremont, C., Luyten, J., Leysen, R., Bruggen, B. V. and Maes G., 2002. Alumina and Titania Multilayer Membranes for Nanofiltration: Preparation, Characterization and Chemical Stability, *Journal of Membrane Science,* 207, 73 – 89.

Vela, M.C.V., Blanco, S.A., Garcıa, J.L. and Rodrguez, E.B., 2008. Analysis of Membrane Pore Blocking Models Applied to the Ultrafiltration of PEG, Separation and Purification Technology, 62, 489 – 498.

Vimala, R. and Nilanjana, D., 2009. Biosorption of Cadmium(II) and Lead(II) from Aqueous Solutions using Mushrooms: A Comparative Study, Journal of Hazardous Materials, 168, 376 – 382.

Volesky, B., 1990. Biosorption and Biosorbent, p. 3-5. In Volesky, B. (ed.), Biosorption of heavy metals. CRC Press Inc., Boston.

Wang, J., Guan, J., Santiwong, S.R. and David Waite, T., 2008. Characterization of Floc Size and Structure under Different Monomer and Polymer Coagulants on Microfiltration Membrane Fouling, *Journal of Membrane Science,* 321, 132 – 138.

Wang, M.C., Wu, N.C. and Hon, M.H., 1994. Preparation of Nepheline Glass-Ceramics and their Application as Dental Porcelain, *Materials Chemistry and Physics,* 37, 370 – 375.

Wang, Y. H., Zhang, Y., Liu, X.Q. and Meng, G.Y., 2007. Sol-Coated Preparation and Characterization of Macroporous α-Al_2O_3 Membrane Support, *Journal of Sol–Gel Science and Technology,* 41, 267 – 275.

Wang, Y.H., Tian, T.F., Liu, X.Q. and Meng, G.Y., 2006. Titania Membrane Preparation with Chemical Stability for Very Hash Environments Applications, *Journal of Membrane Science,* 280, 261 – 269.

Wu, C., Li, A., Li, L., Zhang, L., Wang, H., Qi, X. and Zhang, Q., 2008. Treatment of Oily Water by a Poly(vinyl alcohol) Ultrafiltration Membrane, *Desalination*, 225, 312 – 321.

Xomeritakis, G., Nair, S. and Tsapatsis, M., 2000. Transport Properties of Alumina supported MFI Membranes Made by Secondary (seeded) Growth, *Microporous and Mesoporous Materials,* 38, 61 – 73.

Xu, X., Yang, W., Liu, J. and Lin, L., 2001. Synthesis of NaA Zeolite Membrane by Microwave Heating, *Separation and Purification Technology,* 25, 241 – 249.

Yan, Y.S., Davis, M.E. and Gavalas, G.R., 1997. Preparation of Highly Selective Zeolite ZSM-5 Membranes by a Post-synthetic Coking Treatment, *Journal of Membrane Science,* 123, 95 – 103.

Yang, C., Zhang, G., Xu, N. and Shi, J., 1998. Preparation and Application in Oil-Water Separation of ZrO_2/α-Al_2O_3 MF Membrane, *Journal of Membrane. Science,* 142, 235 – 243.

Yoshino, Y., Suzuki, T., Nair, B.N., Taguchi, H. and Itoh, N., 2005. Development of Tubular Substrates, Silica Based Membranes and Membrane Modules for Hydrogen Separation at High Temperature, *Journal of Membrane Science,* 267, 8 – 17.

Zah, J., Krieg, H.M. and Breytenbach, J. C., 2006. Layer Development and Growth History of Polycrystalline zeolite A Membranes Synthesised from a Clear Solution, *Microporous and Mesoporous Materials,* 93, 141 – 150.

Zhang, H., Zhao, H., Liu, P., Zhang, S. and Li, G., 2009. Direct Growth of Hierarchically Structured Titanate Nanotube Filtration Membrane for Removal of Waterborne Pathogens, *Journal of Membrane Science,* 343, 212 – 218.

Zhong, J., Sun, X. and Wang, C., 2003. Treatment of Oily Wastewater Produced from Refinery Processes using Flocculation and Ceramic Membrane Filtration, *Separation and Purification Technology*, 32, 93 – 98.

Zhou, J., Chang, Q., Wang, Y., Wang, J. and Meng, G., 2010. Separation of Stable Oil–Water Emulsion by the Hydrophilic Nano-sized ZrO_2 Modified Al_2O_3 Microfiltration Membrane. *Separation and Purification Technology,* 75, 243 – 248.

Appendix

Appendix A: Calibration chart for oil-water emulsions

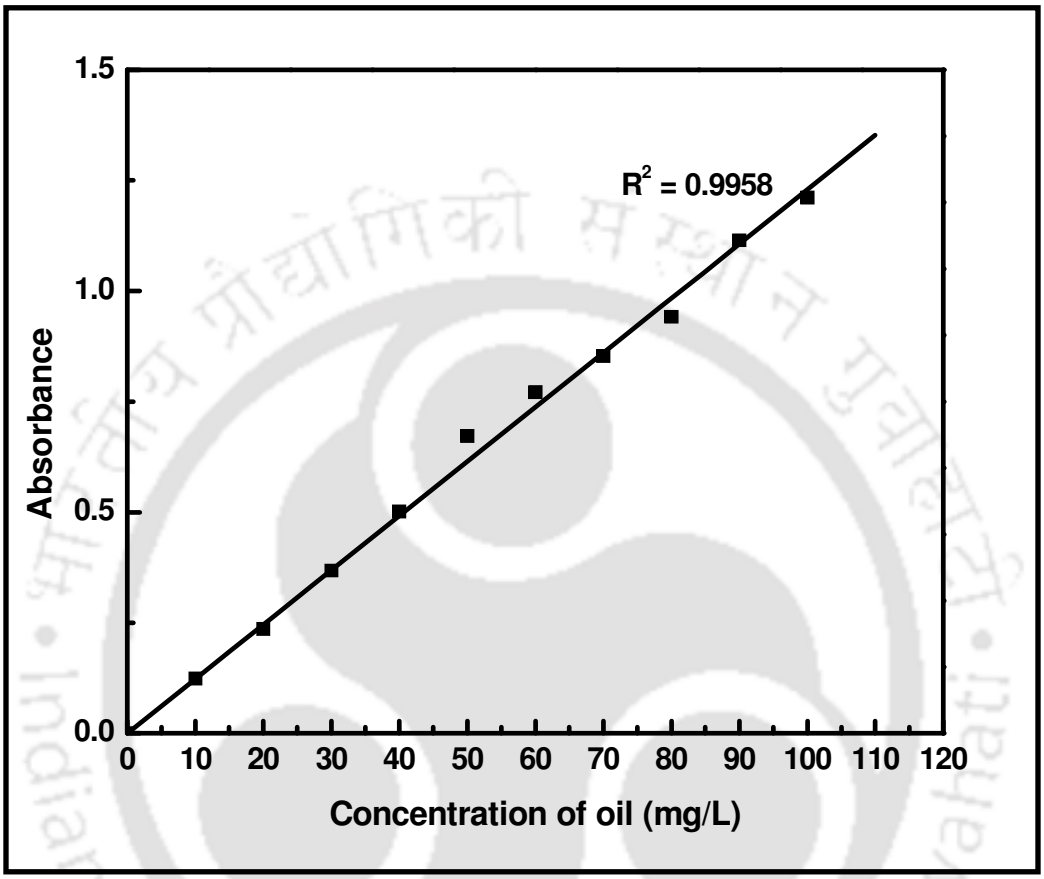

Figure A1: A calibration chart for oil-water emulsions.

The calibration chart for the measurement of concentrations of oil-water emulsions has been prepared by measuring the absorbance of the emulsion solutions with known concentrations at a wave-length of 235 nm (Chakrabarty *et al*., 2008) using a UV–vis spectrophotometer (Model: UV 2300; Make: Spectrascan). Figure A1 presents the calibration chart obtained for the oil-water emulsions in the concentration range of 0 – 100 mg/L.

Appendix B: Calibration chart for bacterial solution samples

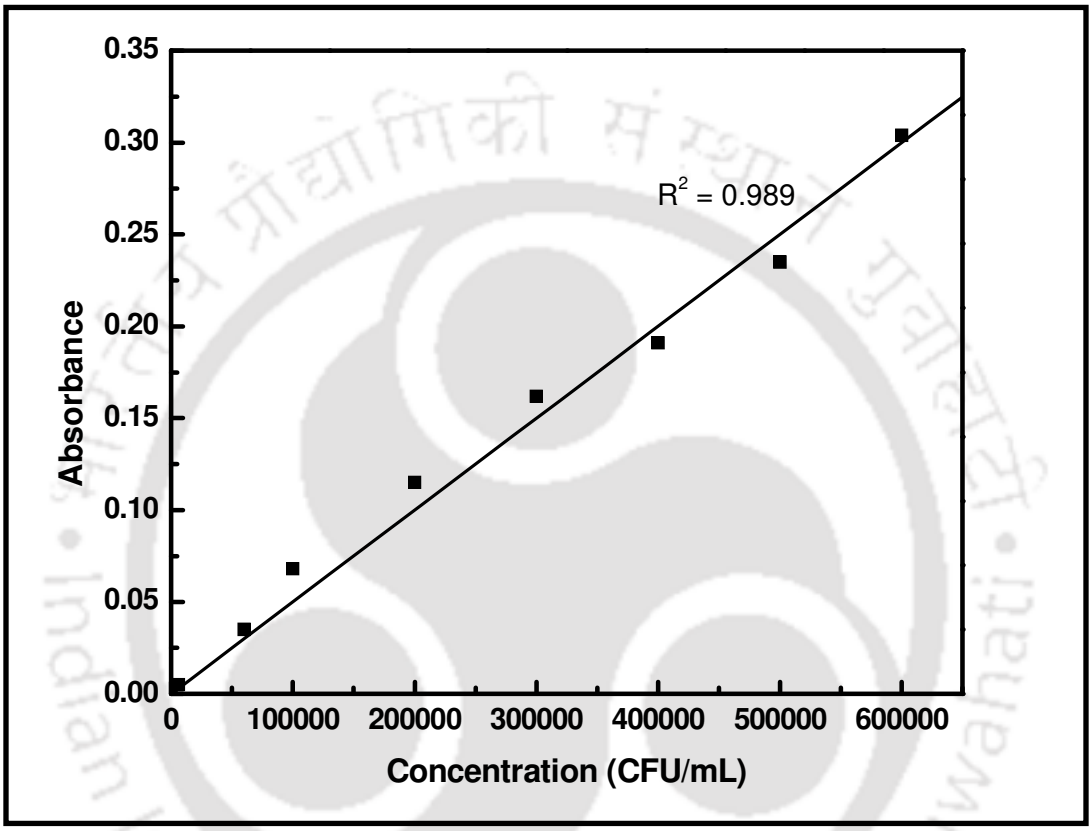

Figure B1: Calibration chart for bacterial solution samples.

Figure B1 presents the calibration chart (Absorbance Vs. Concentration in CFU/mL) that was prepared by measuring the absorbance of known concentrations of bacteria solution samples at a wave-length of 600 nm using a UV–vis spectrophotometer (Model: UV 2300; Make: Spectrascan). The calibration chart is prepared with the sample bacteria concentration range of $6 \times 10^3 - 6 \times 10^5$ CFU/mL.

Appendix C: Calibration chart for the determination of Chromium (VI) concentration in aqueous solutions

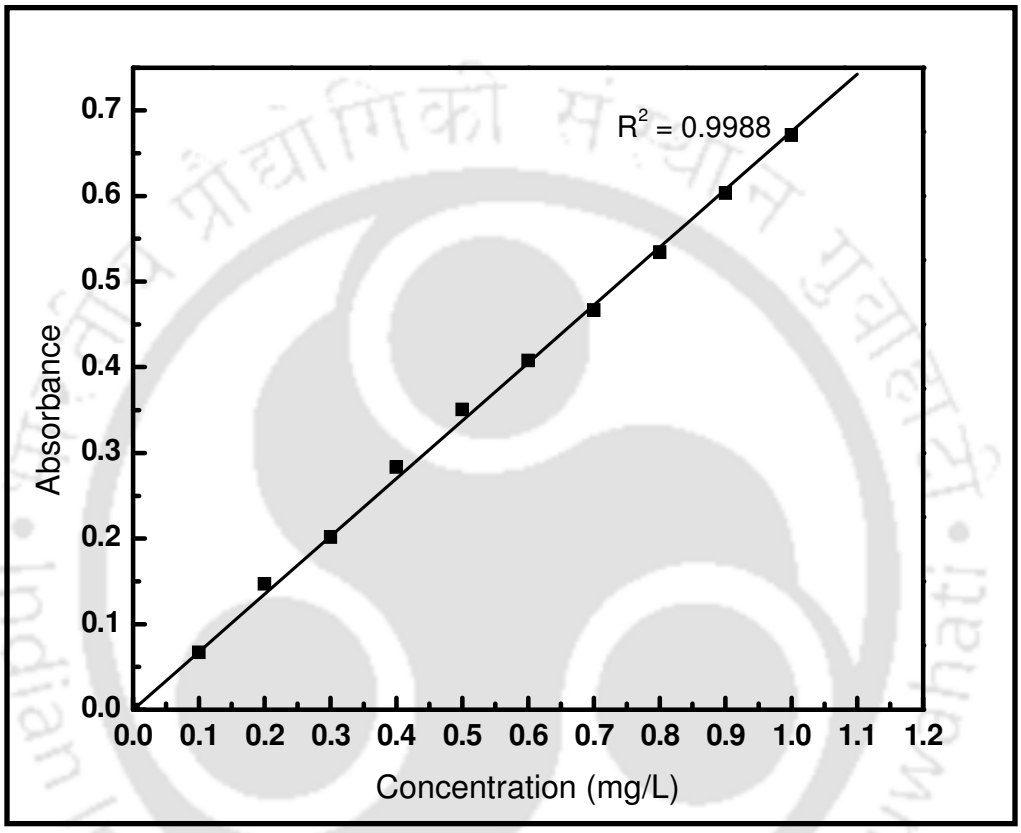

Figure C1: Calibration chart for the determination of chromium (VI) concentration in aqueous solutions.

Using 1,5-diphenyl carbazide (DPC) method, the calibration chart has been prepared by measuring the absorbance of the chromium (VI) solutions in UV-vis spectrophotometer (Model: UV 2300; Make: Spectrascan) at a wave-length of 540 nm (Ozer and Ozer 2003). Figure C1 illustrates the developed calibration chart to evaluate of unknown concentrations of chromium (VI) in permeate samples.

Appendix D: Calibration chart for the determination of bovine serum albumin

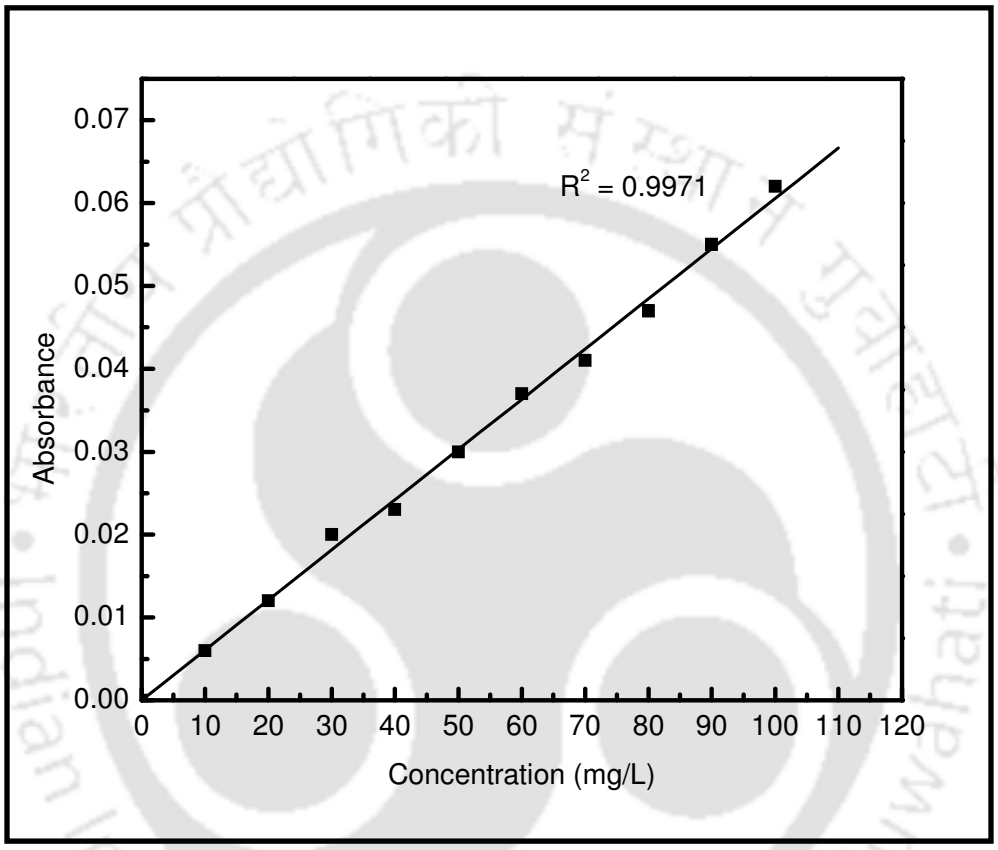

Figure D1: Calibration chart for the determination of bovine berum albumin protein concentrations in various samples.

Figure D1 presents the calibration chart developed to determine the unknown concentrations of BSA protein in various samples for the concentration range of 10 – 100 mg/L. The chart was prepared by measuring the absorbance of known concentrations of BSA solution samples at a wave length of 275 nm using a UV–vis spectrophotometer (Model: UV 2300; Make: Spectrascan).

Published Papers

List of Publications

International Journals:

1. D. Vasanth, R. Uppaluri and G. Pugazhenthi, Influence of sintering temperature on the properties of porous ceramic support prepared by uniaxial dry compaction method using low cost raw materials for membrane applications, *Separation Science and Technology*, 46 (2011) 1241 – 1249.

2. D. Vasanth, G. Pugazhenthi and R. Uppaluri, Fabrication and properties of low cost ceramic microfiltration membranes for separation of oil and bacteria from its solution, *Journal of Membrane Science*, 379 (2011) 154 – 163.

3. D. Vasanth, G. Pugazhenthi and R. Uppaluri, Biomass assisted microfiltration of chromium(VI) using backer's yeast by ceramic membrane prepared from low cost raw materials, *Desalination*, 285 (2012) 239 – 244.

4. D. Vasanth, G. Pugazhenthi and R. Uppaluri, Performance of low cost ceramic microfiltration membranes for the treatment of oil-in-water emulsions, *Separation Science and Technology*, 48 (2013) 849 – 858.

5. D. Vasanth, G. Pugazhenthi and R. Uppaluri, Cross-flow Microfiltration of oil-in-water emulsions using low cost ceramic membranes, *Desalination*, 320 (2013) 86 – 95.

6. D. Vasanth, G. Pugazhenthi and R. Uppaluri, Development of LTA zelolite composite membranes for microfiltration of bovine serum albumin (BSA), (communicated).

Conferences:

1. D. Vasanth, R. Uppaluri and G. Pugazhenthi**,** Development of porous ceramic support by uniaxial dry compaction method using low cost raw materials for membrane applications, *63rd Annual Meeting of Indian Institute of Chemical Engineers (CHEMCON 2010)*, 27-30 December 2010, Chidambaram, Tamil Nadu.

2. D. Vasanth, G. Pugazhenthi and R. Uppaluri, Development of low cost ceramic microfiltration membrane from inexpensive raw materials for bacteria removal application, *International Conference on Membranes (ICM-2011)*, 16 – 19 September 2011, Kottayam, Kerala.